

Copyright is owned by the Author of the thesis. Permission is given for a copy to be downloaded by an individual for the purpose of research and private study only. The thesis may not be reproduced elsewhere without the permission of the Author.

**Sensing and signalling mechanical stress
during intercalary growth in *Epichloë* grass
endophytes**

**A thesis presented in partial fulfilment of the
requirements for the degree of
Doctor of Philosophy (PhD) in
Genetics
at Massey University, Manawatu
New Zealand**

**Kahandawa Geeganaarachchige Sameera
Upanada Ariyawansa
2015**

Abstract

Epichloë festucae is an agronomically important seed-transmitted endophytic fungus that grows symbiotically within the intercellular spaces of temperate grass species. This fungus has previously been shown to undergo hyphal intercalary growth during host leaf colonization, a highly unusual mechanism of division and extension in non-apical compartments in vegetative hyphae, as an adaptation to colonise rapidly elongating host cells in the developing leaf. However the exact mechanism that triggers intercalary growth was not known. In this study I aimed to test the hypothesis that intercalary growth is stimulated by mechanical stretch imposed by attachment of hyphae to elongating host cells, and that this stress is sensed by mechano-sensors located on hyphal membranes.

To test this hypothesis a novel technique was designed and optimised to stretch fungal hyphae under *in vitro* conditions. Investigation of un-stretched hyphae showed that *de novo* compartmentalization occurs in sub-apical compartments of *E. festucae* hyphae according to a compartment length-dependent hierarchy. Subjecting these sub-apical compartments to mechanical stretching showed that hyphal compartment lengths can be increased while maintaining viability, provided that the stretch is within tolerable limits. It further showed that the stretched compartments undergo *de novo* compartmentalization (nuclear division and septation) similar to un-stretched hyphae but at a significantly higher rate, fulfilling the basic requirements for intercalary growth.

E. festucae WscA and MidA, which are orthologues of a yeast cell wall stress and a stretch-activated calcium channel protein respectively, were functionally characterized in order to test the possible involvement of these mechano-sensors in intercalary

growth. Their roles in general hyphal apical growth, cell wall construction and integrity maintenance during growth in culture were confirmed. The limited ability of $\Delta midA$ mutants to colonise developing leaves indicated a possible role in intercalary growth, while $\Delta wscA$ mutants showed wild-type levels of host colonization. In future, the $\Delta midA$ and $\Delta wscA$ mutants will be subjected to mechanical stretch *in vitro* to further understand their roles in mechano-sensing and intercalary growth.

Given the possible involvement of the stretch-activated calcium channel MidA in intercalary growth, a successful technique was developed to study calcium signalling and distribution in *E. festucae* using the genetically-encoded calcium sensor GCaMP5. Investigations revealed the presence of MidA-driven Ca^{2+} pulses confined to the hyphal tips with unique signatures of temporal and spatial dynamics generated by influx of Ca^{2+} . The presence of active sub-apical Ca^{2+} uptake systems were confirmed, manifested as occasional Ca^{2+} pulses in sub-apical compartments that seemed to increase in frequency with mechanical perturbation, indicating a potential crucial role in mechanical stress-driven intercalary growth.

In conclusion a prospective model for intercalary growth in the leaf expansion zone is proposed. Mechanical stretching of hyphae results in increased compartment lengths, accompanied by compartmentalization in sub-apical compartments that allows hyphae to extend along their length. Membrane distortion due to stretching activates MidA, triggering a calcium signalling cascade to stimulate cell wall synthesis and other cellular processes.

Acknowledgements

I'm incredibly grateful to my supervisors Dr Christine Voisey (AgResearch Ltd) and Prof Rosie Bradshaw (Massey University) for the remarkable supervision provided throughout my studies. Despite the very busy working schedules, both had time to discuss matters at any time and the prompt attention given to issues greatly helped me to conduct my studies smoothly. The immense academic knowledge and training I received, I believe has shaped me to become an independent researcher. I also appreciate them for being so patient and having faith in me despite the delays and encouraging me during the writing period. I thank Prof Bradshaw for making me part of her lab team, guiding and training me throughout and supporting me with all the activities at Massey University. I'm so grateful to Dr Voisey for assisting me in every possible way not just in my academic work, but also in settling down and living in New Zealand. Thank you for finding funds and encouraging me to participate in international conferences and getting me an opportunity to present in a prestigious forum.

I acknowledge Prof Nick Read (University of Manchester, UK) and Prof Neil Gow for the discussions, advice and support extended. Also I'm grateful to Prof Nick Read for kindly providing the vector pAM13-9-GCaMP5 (harbours the genetically-encoded calcium sensor GCaMP5) and Dr Alberto Muñoz for training me on calcium imaging. I acknowledge Prof. Kelly Craven's laboratory (Samuel Roberts Noble Foundation, Oklahoma, USA) for providing the plasmid pYH2A for nuclear tagging. I thank Dr Duane Harland for the support given by suggesting the fibre stretcher to stretch fungal hyphae and working through various mechanisms. I also thank Steve Gebbie (AgResearch engineering workshop, Lincoln) for making me the stretching cassettes.

I'm grateful to Dr Richard Johnson for accepting me into the team initially and advising me on my research work. Also I'm grateful to PFI team leader Dr Linda Johnson for being so supportive and providing me with opportunities. I thank Mike Christenson for sharing his expert knowledge, working along with me to help me understand the endophyte fungi. My warm gratitude goes to Jaspreet Sing for being a great friend, my lab companion and assisting me in so many ways. I'm grateful to Dr Tash forester for teaching me all the techniques, sharing experiences and always willing to help me to conduct experiments. I also thank Dr Milan Gagic and Dr Stuart Card for advice, sharing experiences and the discussions we had. Thank you also to Anouck de Bonth, Wayne Simpson, Debbie Hudson and Kelly Dunstan for teaching me techniques and for lab support. I acknowledge Dr John Koolard for providing statistical support, and AgResearch support staff for the administrative help I received. I acknowledge the team members of Prof Rosie Bradshaw's lab members for discussing my results while sharing their experiences and the staff at the Institute of Fundamental Sciences and the Graduate Research School at Massey University for all the support. Further, I'm grateful to all the present and past Heads along with the staff at the Department of Plant Sciences, University of Colombo, for giving me study leave and supporting my studies.

I'm so grateful to my wife, Thiriratni Ariyawansa, for shouldering the family responsibilities and commitments for nearly 5 years while I was away in New Zealand. Thank you for handling a huge workload on your own with the kids and giving me the freedom to conduct my studies. Without her immense support, encouragement and understanding this endeavour wouldn't have been possible at all. To my kids, Lithum and Ranuga Ariyawansa, thank you so much for being so patient until I finished the thesis to go to school, play and to do so many other postponed activities together. I am incredibly thankful to my parents for giving me everything and supporting me through

all my endeavours. I greatly appreciate my sister and her family and the parent-in-laws for their huge support extended to my wife. Finally, I am grateful to the Marsden fund, New Zealand, for funding my studies and the research project along with AgResearch Ltd for providing me this opportunity.

Table of Contents

Abstract	i
Acknowledgements	iii
Table of contents	vi
List of Figures	xiv
List of tables	xx
List of movie clips	xx
Abbreviations	xxi
1. Introduction	1
1.1 <i>Epichloë festucae</i>	2
1.1.1 Transmission	3
1.1.2 Host colonization	4
1.2 Apical hyphal growth	6
1.2.1 Mechanism of hyphal extension	7
1.3 Intercalary hyphal growth	9
1.3.1 <i>E. festucae</i> host colonization through hyphal intercalary growth	9
1.3.2 Evidence to support hyphal intercalary growth in developing leaves	10
1.3.3 Evidence of intercalary growth in other fungal species	13
1.3.4 Cellular processes associated with intercalary growth	15
1.3.4.1 Cell wall synthesis	15
1.3.4.2 Exocytosis	17
1.3.4.3 Role of the Spitzenkörper away from hyphal apex	18
1.3.5 Signalling mechanisms that may have a role in intercalary growth	19
1.4 Sensing and signalling mechanical stress in <i>E. festucae</i> hyphae	20

1.5 Calcium transporters and maintenance of calcium homeostasis in fungi	21
1.5.1 Calcium transporters in the vacuole, Golgi apparatus and endoplasmic reticulum	22
1.5.2 Calcium uptake systems in the plasma membrane	23
1.5.2.1 Structural characteristics of Mid1 and Cch1 proteins	26
1.5.2.2 Functions of the Mid1 and Cch1 complex	27
1.5.2.3 Other proteins in the calcium/calcineurin pathway	29
1.6 Cell wall integrity MAP kinase pathway	30
1.6.1 Role of the cell wall integrity MAP kinase pathway	30
1.6.2 The CWI MAP kinase pathway is highly conserved	32
1.6.3 Structure of Wsc and Mid2 proteins	33
1.6.4 Function of Wsc and Mid2 proteins	34
1.7 Hypotheses, aims and objectives	37
2. Materials and Methods	39
2.1 Biological material/ strains	40
2.2 Media preparation	43
2.2.1 Luria Bertani (LB) medium	44
2.2.2 Potato Dextrose (PD) medium	44
2.2.3 Regeneration medium (RG)	44
2.2.4 Water agar	44
2.2.5 Antibiotic selection	44
2.3 Growth conditions	45
2.3.1 <i>Escherichia coli</i>	45
2.3.2 <i>Epichloë festucae</i>	45

2.3.3	<i>Lolium perenne</i> L.	46
2.3.3.1	Surface sterilization of seeds	46
2.3.3.2	Seedling inoculation and plant growth conditions	46
2.4	DNA isolation and storage	47
2.4.1	Plasmid DNA isolation.....	47
2.4.2	Isolation of high molecular weight genomic DNA from <i>E. festucae</i>	47
2.4.3	Rapid isolation of genomic DNA from <i>E. festucae</i>	48
2.4.4	DNA Storage	48
2.5	DNA manipulation	48
2.5.1	DNA quantification	48
2.5.2	DNA concentration	49
2.5.3	Agarose gel electrophoresis	49
2.5.4	DNA recovery from agarose gels	50
2.5.5	DNA sequencing	50
2.5.6	Restriction endonuclease digestion	51
2.5.7	PCR amplification	51
2.5.7.1	Standard PCR	51
2.5.7.2	High fidelity PCR	52
2.5.8	Ligation	55
2.6	Transformation	56
2.6.1	<i>E. coli</i> transformation	56
2.6.2	<i>E. festucae</i> protoplast preparation	56
2.6.3	Transformation of <i>E. festucae</i> protoplasts	57
2.7	Plasmid Construction	59
2.7.1	Overview of the Gateway cloning system	59

2.7.2	Construction of <i>E. festucae</i> gene replacement vectors	60
2.7.2.1	Overview	60
2.7.2.2	Construction of <i>midA</i> replacement vectors	60
2.7.2.3	Construction of <i>wscA</i> replacement vectors	61
2.7.3	<i>E. festucae</i> complementation vector construction to complement $\Delta midA$ and $\Delta wscA$	61
2.7.3.1	Overview	61
2.7.3.2	Construction of <i>midA</i> complementation vector	62
2.7.3.3	Construction of <i>wscA</i> complementation vector	62
2.7.4	<i>E. festucae</i> expression vector construction	63
2.7.4.1	Construction of the <i>wscA:egfp</i> expression vector with the native promoter.....	63
2.7.4.2	Construction of <i>Ptef: wscA:egfp</i> expression vector	64
2.8	Purification of <i>E. festucae</i> F11 transformants	65
2.9	Southern blotting	65
2.10	Endophyte colonization in plants	66
2.10.1	Endophyte detection in plants by tissue print immunoassay	66
2.10.2	Endophyte detection in plants via aniline blue staining	67
2.11	Staining techniques	68
2.11.1	Calcofluor White staining	68
2.11.2	FM4-64 staining	68
2.12	Microscopy	68
2.12.1	Obtaining leaf and tiller tissue samples for microscopy	68
2.12.2	Light, DIC and florescence microscopy	69
2.12.3	Confocal laser scanning microscopy	69

2.12.3.1 Calcium imaging using confocal laser scanning microscopy	70
2.12.3.2 Visualising nuclear tagged hyphae using confocal laser scanning microscopy.....	70
2.12.3.3 Hyphal apical growth rate determination using confocal microscopy.....	71
2.13 Radial colony growth rate determination	71
2.14 Statistics	72
2.15 Bioinformatics	72
3. Characterisation of WscA of <i>E. festucae</i> and its role in intercalary growth ...	74
3.1 Identification of the <i>S. cerevisiae wscA</i> gene orthologue in <i>E. festucae</i>	75
3.2 Targeted deletion of the <i>wscA</i> gene in <i>E. festucae</i>	78
3.3 Functional characterisation of the <i>E. festucae wscA</i> gene during growth in culture	82
3.3.1 Deletion of <i>wscA</i> in <i>E. festucae</i> affects radial growth and morphology in axenic culture	82
3.3.2 Osmotic stabilization can rescue <i>E. festucae</i> $\Delta wscA$ phenotypes on the PDA culture medium	87
3.3.3 <i>E. festucae</i> $\Delta wscA$ mutants are sensitive to cell wall perturbation agents	90
3.4 WscA localization in <i>E. festucae</i> hyphae	92
3.5 Impact of <i>wscA</i> deletion on colonization of plants by <i>E. festucae</i>	96
3.5.1 Deletion of <i>wscA</i> does not influence <i>E. festucae</i> colonization of its host (<i>L. perenne</i>)	96
3.5.2 Deletion of <i>wscA</i> has no impact on the phenotype of the host	101

3.6 Discussion101

4. Characterisation of MidA of *E. festucae* and its role in intercalary growth..113

4.1 Identification of the *S. cerevisiae mid1* orthologue in *E. festucae* 114

4.2 Targeted deletion of the *midA* gene in *E. festucae* 118

4.3 Functional characterisation of the *E. festucae midA* gene during growth in culture 122

4.3.1 Deletion of *midA* in *E. festucae* affects radial growth and morphology on PDA 122

4.3.2 Osmotic stabilization can rescue *E. festucae ΔmidA* phenotypes on the PDA culture medium 128

4.3.3 Influence of calcium supplementation on the phenotype of *E. festucae ΔmidA* in culture 130

4.3.4 *E. festucae ΔmidA* mutants are sensitive to cell wall perturbation agents..... 135

4.4 Deletion of *midA* in *E. festucae* restricts hyphal entry into the host intercalary growth zone 138

4.4.1 *ΔmidA* host colonization 138

4.4.2 Deletion of *midA* has no impact on the phenotype of the host 144

4.5 Calcium distribution in *E. festucae* hyphae and the role of MidA in calcium uptake 145

4.5.1 Calcium pulses in apical compartments of *E. festucae* during growth in axenic culture 146

4.5.2 Deletion of *midA* in *E. festucae* effects dynamics of Ca²⁺ pulses 151

4.5.3	Ca ²⁺ pulses occur in intercalary compartments in <i>E. festucae</i> WT and $\Delta midA$ hyphae	156
4.5.4	Ca ²⁺ pulses in <i>E. festucae</i> are due to influx of exogenous Ca ²⁺	158
4.5.5	Intensely-labelled calcium foci visible at hyphal tips	160
4.6	Discussion	162
5.	Intercalary growth in <i>E. festucae</i> hyphae	176
5.1	Evidence of intercalary growth in sub-apical compartments of <i>E. festucae</i> hyphae	177
5.1.1	Nuclear division and septation occurs in sub-apical compartments of <i>E. festucae</i> hyphae	177
5.1.2	Sub-apical compartment division occurs according to a compartment length-dependent hierarchy	181
5.2	Nuclear shape differs in different plant regions	185
5.3	Can mechanical stretching trigger intercalary growth in <i>E. festucae</i> hyphae?	188
5.3.1	Optimization of a technique to mechanically stretch fungal hyphae under <i>in vitro</i> conditions	189
5.3.1.1	The strategy	189
5.3.1.2	Selection of a suitable membrane	190
5.3.1.3	Selection of a suitable nutrient medium	190
5.3.1.4	Stretching hyphae	192
5.3.2	Stretching <i>E. festucae</i> hyphae <i>in vitro</i>	197
5.3.3	Applied mechanical stretch can increase the length of hyphal compartments.....	198

5.4 Mechanical stretching applied in intervals can increase overall length of hyphae while maintaining viability	203
5.5 <i>E. festucae</i> hyphae increase the rate of compartmentalization as a response to sub-apical compartment elongation caused by mechanical stretching	213
5.6 A possible role for calcium in sensing mechanical stress in <i>E. festucae</i> ?	216
5.6.1 Mechanical disturbance of <i>E. festucae in vitro</i> induces Ca ²⁺ pulses	216
5.7 Discussion	218
6. Summery, conclusions and future work	232
6.1 Stimulation of intercalary growth in <i>E. festucae</i> through mechanical stress	233
6.2 Putative sensors of mechanical stress in <i>E. festucae</i>	236
6.3 General conclusion	242
7. References	244
8. Appendices	260
8.1 Appendix 1: Buffers used in this study	260
8.2 Appendix 2: PCR and restriction enzyme reaction mixtures and conditions ..	262
8.3 Appendix 3: Plasmid vector maps	263
8.4 Appendix 4: MidA and WscA protein sequences	272

List of figures

Figure 1.1: Growth zones and hyphal distribution of <i>E. festucae</i> in <i>L. perenne</i>	6
Figure 1.2: A diagrammatic representation of intercalary growth in <i>E. festucae</i> hyphae in the host (<i>L. perenne</i>) elongation zone.	13
Figure 1.3: Diagram showing the involvement of fungal calcium transporters in maintenance of calcium homeostasis and calcium signalling.	25
Figure 1.4: Diagram showing the main components and signal transduction of the Cell Wall Integrity (CWI) MAP kinase pathway of <i>S. cerevisiae</i>	32
Figure 3.1: Multiple sequence alignment between Mid1 of <i>S. cerevisiae</i> and orthologues of <i>E. festucae</i> , <i>N. crassa</i> and <i>A. fumigatus</i>	77
Figure 3.2: PCR screening to identify <i>E. festucae</i> <i>wscA</i> gene replacement mutants....	79
Figure 3.3: Southern blot analysis to confirm the <i>wscA</i> replacement locus in putative <i>wscA</i> replacement mutants.	81
Figure 3.4: Comparison of <i>E. festucae</i> WT and $\Delta wscA$ radial growth rates in culture on the PDA medium.	83
Figure 3.5: Aberrant colony morphology in <i>E. festucae</i> $\Delta wscA$ mutants.	84
Figure 3.6: Cell wall aberrations in <i>E. festucae</i> $\Delta wscA$ mutants.	86
Figure 3.7: Effect of sorbitol concentration on the growth rate, colony morphology and hyphal morphology of <i>E. festucae</i> WT and $\Delta wscA$ mutants.	89
Figure 3.8: Sorbitol mitigation of defects in radial growth rate and colony morphology caused by Calcofluor White in <i>E. festucae</i> WT and $\Delta wscA$ mutants.	91
Figure 3.9: Subcellular localization of WscA fused to EGFP.	95
Figure 3.10: Perennial ryegrass leaf sheath showing sub-cellular localization of WscA-EGFP in hyphae growing <i>in planta</i>	96

Figure 3.11: Comparison of hyphal colonization in <i>L. perenne</i> tillers infected with <i>E. festucae</i> WT and <i>wscA</i> deletion mutants expressing EGFP.	100
Figure 4.1: Multiple sequence alignment between Mid1 of <i>S. cerevisiae</i> and orthologues of <i>E. festucae</i> , <i>C. purpurea</i> , <i>N. crassa</i> and <i>G. zeae</i>	117
Figure 4.2: PCR screening to identify <i>E. festucae midA</i> gene replacement mutants...	119
Figure 4.3: Southern blot analysis to confirm <i>midA</i> replacement and absence of ectopic integration in putative <i>E. festucae midA</i> replacement mutants.	121
Figure 4.4: A comparison of the colony radial growth rate and colony morphology of <i>E. festucae ΔmidA</i> with the wild-type.	124
Figure 4.5: Hyphal tip damage in <i>E. festucae ΔmidA</i> in culture.	125
Figure 4.6: Comparison of the hyphal morphology of <i>E. festucae ΔmidA</i> mutant with the WT & complemented strain cultured on PDA.	127
Figure 4.7: Effect of sorbitol concentration on growth rate, colony morphology and hyphal morphology of <i>E. festucae</i> WT and <i>ΔmidA</i>	129
Figure 4.8: Analysis of <i>E. festucae</i> WT and <i>ΔmidA</i> radial growth rate and colony morphology on PDA with elevated Ca ²⁺ or EGTA.	133
Figure 4.9: Analysis of hyphal morphology of <i>E. festucae</i> WT and <i>ΔmidA</i> on PDA supplemented with different [Ca ²⁺].	134
Figure 4.10: Analysis of radial growth rate and colony morphology of <i>E. festucae</i> WT and <i>ΔmidA</i> on PDA in the presence of CW and CR.	137
Figure 4.11: Comparison of hyphal colonization in <i>L. perenne</i> tillers infected with WT and <i>midA</i> deletion mutants expressing EGFP.	142
Figure 4.12: Comparison of hyphal colonization in the meristem and the developing leaves by WT and <i>ΔmidA</i> expressing EGFP.	143

Figure 4.13: Transverse section from a pseudostem of a single tiller infected with <i>ΔmidA</i> showing distribution of hyphae along the length of the leaves...	143
Figure 4.14: The effect of <i>ΔmidA</i> colonisation on morphology of <i>L. perenne</i> host plants.	144
Figure 4.15: Temporal Ca ²⁺ dynamics in <i>E. festucae</i> WT hyphal tips expressing calcium sensor GCaMP5.	149
Figure 4.16: Analysis of spatial distribution of Ca ²⁺ at the <i>E. festucae</i> WT hyphal tip expressing the GCaMP5 calcium sensor.	150
Figure 4.17: Temporal Ca ²⁺ dynamics in <i>E. festucae ΔmidA</i> hyphal tips expressing calcium sensor GCaMP5.	153
Figure 4.18: Spatial distribution of Ca ²⁺ at the hyphal tip of <i>E. festucae ΔmidA</i> expressing the GCaMP5 calcium sensor.	154
Figure 4.19: Ca ²⁺ pulses in <i>E. festucae ΔmidA</i> complemented strains expressing calcium sensor GCaMP5.	155
Figure 4.20: Ca ²⁺ pulses in an intercalary compartment and in a sub-apical region of <i>E. festucae</i> hyphae.	157
Figure 4.21: Effect of elevated or depleted exogenous calcium on Ca ²⁺ pulses in <i>E. festucae</i> WT hyphal tips expressing GCaMP5.	159
Figure 4.22: Fluorescent foci in <i>E. festucae</i> hyphal tips expressing the GCaMP5 calcium sensor.	161
Figure 5.1: Phase contrast and fluorescence images of CW-stained and nuclear-labelled apical and sub-apical compartments of <i>E. festucae</i> WT hyphae.	178
Figure 5.2: Positions of nuclei relative to cell walls and septa in sub-apical compartments of nuclear-tagged <i>E. festucae</i> hyphae.	179

Figure 5.3: Comparison of compartment lengths and longitudinal nuclear lengths along WT <i>E. festucae</i> hyphae.	181
Figure 5.4: Fluorescence images of a nuclear-tagged <i>E. festucae</i> WT hyphal segment showing compartmentalization in sub-apical compartments.	183
Figure 5.5: Analysis of compartmentalization in sub-apical compartments of nuclear tagged <i>E. festucae</i> hyphae.	184
Figure 5.6: <i>E. festucae</i> nuclear shape variation in different tissues of a developing leaf.	187
Figure 5.7: Calculation of <i>E. festucae</i> longitudinal nuclear lengths in different growth zones of the developing leaf.	188
Figure 5.8: Diagrammatic representation showing the arrangement of components used to grow <i>E. festucae</i> hyphae on amino-coated silicon membranes.	191
Figure 5.9: Selection of the best medium to grow hyphae on amino-coated silicon membranes.	192
Figure 5.10: The apparatus used to stretch <i>E. festucae</i> hyphae under <i>in vitro</i> conditions.	194
Figure 5.11: Fibre stretcher used to stretch fungal hyphae growing on a silicon membrane.	196
Figure 5.12: Effects of excessive stretching on hyphal integrity.	198
Figure 5.13: Effect of mechanical stretching on compartment lengths in <i>E. festucae</i> hyphae.	201
Figure 5.14: Effect of mechanical stretching on the integrity of plasma membranes in nuclear tagged <i>E. festucae</i> hyphae.	203
Figure 5.15: Mitosis and septation in sub-apical compartments of un-stretched and stretched hyphae.	208

Figure 5.16: Change in length of each sub-apical compartment (2 nd to the 11 th) in stretched and un-stretched <i>E. festucae</i> hyphae.	212
Figure 5.17: Septation (new compartment formation) rate in sub-apical compartments of stretched and un-stretched hyphae.	215
Figure 5.18: Diagrammatic representation showing the arrangement of components used to grow <i>E. festucae</i> hyphae on amino-coated silicon membranes...	217
Figure 5.19: A model showing compartment length-dependent nuclear division and septation in sub-apical compartments of <i>E. festucae</i> hyphae.	222
Figure 5.20: A sketch of the proposed model for mechanical stretch induced intercalary growth in sub-apical compartments of <i>E. festucae</i> hyphae.	227
Figure 5.21: A representative sketch comparing nuclear division and septation at 4 time points between an un-stretched hypha and a stretched hypha.	228
Figure 8.1: Donor vectors pDONR-SML and pDONR-SMR (Invitrogen™) used to construct gene replacement vectors.	263
Figure 8.2: Replacement vectors for <i>midA</i> harbouring the 5' flank pSAM1 and 3' flank pSAM2	264
Figure 8.3: Replacement vectors for <i>wscA</i> harbouring the 5' flank pSAM3 and 3' flank pSAM4	265
Figure 8.4: Vector pII99 used for complementation vector construction.	266
Figure 8.5: Vector pSAM5 for $\Delta midA$ complementation.	266
Figure 8.6: Vector pSAM6 for $\Delta wscA$ complementation.	267
Figure 8.7: Donor vector pDONR/Zeo (Invitrogen™) used for <i>wscA:egfp</i> expression vector construction.	267

Figure 8.8: Entry vector pSAM7 harbouring <i>wscA</i> with native promoter.	268
Figure 8.9: Destination vector pFPLGh used for <i>wscA:egfp</i> expression vector construction.	268
Figure 8.10: Expression vector pSAM8 with <i>wscA:egfp</i>	269
Figure 8.11: Donor vector pDONR221 used for <i>Ptef:wscA:egfp</i> expression vector construction.	269
Figure 8.12: Entry vector pSAM7 harbouring <i>wscA</i>	270
Figure 8.13: Entry vector pDONR-TEF harbouring <i>tef2</i> promoter.	270
Figure 8.14: Entry vector pDONR-EGFP harbouring <i>egfp</i>	271
Figure 8.15: Expression vector pSAM10 harbouring <i>Ptef:wscA:egfp</i>	271

List of Tables

Table 2.1: Organisms and Plasmids used in this study.....	41
Table 2.2: Antibiotic concentrations used for transformant selection	45
Table 2.3: Primers used in this study	52
Table 5.1: A representative table showing the division of sub-apical compartments with time in a hypha from 2 nd to the 11 th compartment growing on PDA.	184
Table 5.2: Compartment length and compartmentalization in sub-apical compartments of un-stretched and stretched <i>E. festucae</i> hyphae.	210
Table 5.3: Sample calculation of the number of new sub-apical compartments formed per 100 μm of hyphae within a period of 9 h.	214

List of movie clips (in annexed CD)

1. *E. festucae* $\Delta midA$ hyphal tip lysis
2. Calcium imaging in *E. festucae*
3. Calcium imaging in *E. festucae* $\Delta midA$
4. Calcium imaging in *E. festucae* $\Delta midA$ complemented
5. Calcium imaging in sub-apical regions of *E. festucae* hyphae
6. Calcium imaging in *E. festucae* hyphae in EGTA
7. Calcium foci in *E. festucae* hyphal tips
8. Calcium pulses when disturbed

Abbreviations

aa	Amino acid
Amp ^R	Ampicillin resistant
ATP	Adenosine triphosphate
BAPTA	1,2-bis(o-aminophenoxy)ethane-N,N,N',N'-tetraacetic acid
BLAST	Basic Local Alignment Search Tool
bp	Base pair(s)
BS	Blocking solution
CaM	Calmodulin
Chlo ^R	chloramphenicol resistant
cm	Centimeter
CR	Congo red
CW	Calcofluor White
CWI	Cell wall integrity
DIC	Differential interference contrast
DIG	Digoxigenin
DNA	Deoxyribonucleic acid
dNTP	Deoxynucleotide triphosphates
E value	Expect value
EGFP	Enhanced Green Fluorescent Protein

EGTA	Ethylene glycol-bis(2aminoethylether)-N,N,N',N'-tetraacetic acid
ER	Endoplasmic reticulum
fmole	Femtomole
FRET	Förster resonance energy transfer
g	Gram
GECI	Genetically encoded calcium indicator
Gen ^R	Genitacin resistant
GS	1,3-β-glucan synthase complex
GTP	Guanosine triphosphate
h	Hour(s)
HACS	High affinity calcium system
Hyg ^R	Hygromycin resistant
Kb	Kilobase(s)
Kan ^R	Kanamycin resistant
L.S	Longitudinal section
LACS	Low-affinity calcium system
LB	Luria-Bertani
LBA	Luria-Bertani agar
M	Molar
m/s	Meters per second
MAPK	Mitogen-activated protein kinases
MAPKK	Mitogen-activated protein kinase kinase
MAPKKK	Mitogen-activated protein kinase kinase kinase

mg	Milligram
min	Minutes
mm	Millimeter
mM	Millimole
NCBI	National Center for Biotechnology Information
NCM	Nitrocellulose membrane
ng	Nanograms
nM	Nanomole
nm	Nanometers
°C	Degrees Celsius
ORF	Open reading frame
PCR	Polymerase chain reaction
PDA	Potato dextrose agar
PDB	Potato dextrose broth
PEG	Polyethylene glycol
PKC	Protein kinase C
rcf	Relative centrifugal force
RE	Restriction enzyme
RG	Regeneration
rpm	Revolutions per minute
RT	Room temperature
s	Seconds
SAM	Shoot apical meristem

SD	Standard deviation
SDS	Sodium dodecyl sulphate
SNARE	N-ethylmaleimide-sensitive factor attachment protein receptors
Sorb	Sorbitol
T.S	Transverse section
TAE	Tris-acetate-EDTA
tBLASTn	Translated nucleotide database search using a protein query
TEF	Translation elongation factor
U	Unit
USA	United States of America
v/v	Volume/volume ratio
w/v	Weight/volume ratio
WT	Wild type
YFP	Yellow fluorescent Protein
YH2A	Histone protein HH2A fused to yellow fluorescent protein
$[Ca^{2+}]_c$	Cytoplasmic calcium concentration
μg	Microgram
μL	Microliters
μm	Micrometer
μM	Micromolar

1. Introduction

1.1 *Epichloë festucae*

Epichloë festucae is an important biotrophic endophytic fungus that grows symbiotically within the intercellular spaces of cool-season grasses *Festuca* and *Koeleria* spp. within the subfamily Pooideae (Leuchtman et al., 1994; Schardl et al., 1997; Craven et al., 2001; Christensen et al., 2002). *E. festucae* and its close asexual relative *E. festucae* var. *lolii* (formally *Neotyphodium lolii*, host *Lolium perenne* L sub species *perenne*) (Glenn et al., 1996; Leuchtman et al., 2014) belong to the fungal phylum Ascomycota, order Hypocreales, family Clavicipitaceae. The family Clavicipitaceae contain mostly biotrophs that grow in plants, invertebrates or other fungi as mutualistic symbionts or pathogens (Kuldau et al., 1997; Schardl et al., 2013). Within Clavicipitaceae, *Epichloë* spp. are categorised into sub family Clavicipitoideae along with other economically important graminicolous fungi that belong to the genera *Claviceps* and *Balansia* (White Jr et al., 2000; Sung et al., 2007).

E. festucae forms mostly mutualistic symbioses with its grass hosts, although can become antagonistic during sexual reproduction. The endophyte gains nutrients while living within grass intercellular spaces and also can use the host for vertical (asexual) or horizontal (sexual) dissemination. In return, the endophyte produces alkaloidal secondary metabolites such as ergot alkaloids, indole-diterpenes, lolines and peramine that give protection against insect herbivory (Wilkinson et al., 2000; Tanaka et al., 2005; Schardl et al., 2007; Schardl et al., 2013). As *Festuca* and *Lolium* species are frequently used in pastoral agriculture, mutualistic interactions between *E. festucae* or *E. festucae* var. *lolii* and these grasses have become the subject of numerous studies. Although the natural hosts of *E. festucae* are *Festuca* or *Koeleria* spp., most studies aimed at understanding the molecular interactions between the two organisms have been

conducted using *L. perenne* as the host due to the ease of inoculation and maintenance of plants. *E. festucae* can colonise *L. perenne* and forms a stable mutualistic symbiosis similar to that which it forms with its natural host (Christensen et al., 1997; Christensen et al., 2002; Scott et al., 2012).

1.1.1 Transmission

Epichloë fungi can be vertically transmitted via direct colonization of host seeds, or horizontally transmitted between plants by entering the sexual cycle and producing infective ascospores (Schardl et al., 2004). During vertical transmission, asexual hyphae colonize the emerging inflorescence axis and then spread into the ovaries. Subsequent to fertilization the ovule develops into a seed and the hyphae colonise the developing embryo and associated tissues in the seed. As the seed germinates, the hyphae colonise the emerging shoot apical meristem and spread to newly emerging aerial tissues. This asexual form of reproduction is not antagonistic to the host (Schardl et al., 2004).

During horizontal transfer, hyphae grow epiphytically around the inflorescence axis forming a band-like stroma containing the spermatia. Conidia are transmitted via invertebrates to stromata of the opposite mating type and ascospores are produced in fruiting bodies (perithecia). The ascospores are released to the air, land on host stigmas and infect the developing ovules (Scott et al., 1993; Chung et al., 1997; Brem et al., 1999). This sexual form of reproduction is considered antagonistic as the stroma completely suppresses seed production (choke disease)(Schardl et al., 2004). Interestingly *E. festucae* can produce both infected seeds (asymptomatic inflorescences) and stroma in different tillers of the same plant having both mutualistic and antagonistic symbiosis (Schardl et al., 2004).

1.1.2 Host colonization

Epichloë fungi colonise intercellular spaces of aerial vegetative and reproductive structures of the host except the anthers and pollen (Christensen et al., 2002; Tanaka et al., 2006). Hyphae are confined to the intercellular spaces of the host, often attached to the cell walls. They rarely colonise the vascular bundles and in such a case are mainly present in the phloem and the protophloem (Christensen et al., 1997; Christensen et al., 2008). Below ground, hyphae are confined to the apical meristem of the primary root (colonised during radical formation) and do not colonise the rest of the root system (Mike Christensen pers. comm.).

Epichloë colonization is finely synchronised with the growth stages of the host. Grass leaves originate from the Shoot Apical Meristem (SAM) located at the stem apex. The stem is highly contracted and the apex is therefore located at the base of the plant. Leaf primordia form by rapid division of cells on the outermost layer of the SAM (Langer, 1979). Soon after a leaf primordium has formed, an axillary bud will develop on the opposite flank, which will eventually form a new tiller (bundle of grass leaves). A grass leaf consists of a leaf sheath and a leaf blade separated by collar tissue (Fig 1.1). The leaf primordia give rise to two meristems, each responsible for separate development of either the leaf sheath or the leaf blade. In the two meristems, cells divide and thereafter undergo rapid cell expansion displacing the older cells upwards and thus giving rise to the leaf sheath and blade. A developing grass leaf therefore consists of three broadly distinguishable zones, a meristematic zone where cell division occurs, an expansion zone where cell elongation occurs and mature zones where cell expansion ceases and cells mature (Fig 1.1).

Within a developing host leaf, most *Epichloë* hyphae show a very distinct pattern of distribution (Fig 1.1). The hyphae are very dense and highly branched in the basal meristematic regions where cell division occurs (stem, shoot apical meristem (SAM) and lateral meristems), while in the leaf expansion zone (where cell elongation occurs) and the mature leaf they are arranged parallel with the longitudinal axis of the leaf, and are seldom branched (Tan et al., 2001; Christensen et al., 2002; Christensen et al., 2008). The transition from proliferative hyphal growth in the meristematic region to controlled growth in the leaf expansion zone reflects hyphal responses to changes in host development (Fig 1.1). Hyphae appear to colonise the leaf meristematic zone largely through apical growth, and the cell expansion zone through intercalary growth (growth along the length of the filament)(Christensen et al., 2008). This is thought to result in development of long straight hyphae in the expansion zone and the mature leaf. When host cell expansion ceases and the leaf starts to mature, the hyphae too cease further colonisation (Tan et al., 2001; Christensen et al., 2008). This results in a fungal lifecycle that is finely synchronised with the host.

The intercalary growth process occurring in vegetative *Epichloë* hyphae during host colonization is defined as the expansion and septation/division of sub-apical hyphal compartments (discussed in detail in Section 1.3) (Christensen et al., 2008; Voisey, 2010). Apical hyphal growth has long been accepted as the only mode of growth in vegetative fungal hyphae, where hyphae extend/grow only at the apex and not in sub-apical/intercalary compartments (discussed in detail in Section 1.2). Thus the documentation of intercalary growth in vegetative hyphae of *E. festucae* during colonisation of grasses represents a significant departure from standard fungal growth processes and warrants further research to understand the underlying mechanisms.

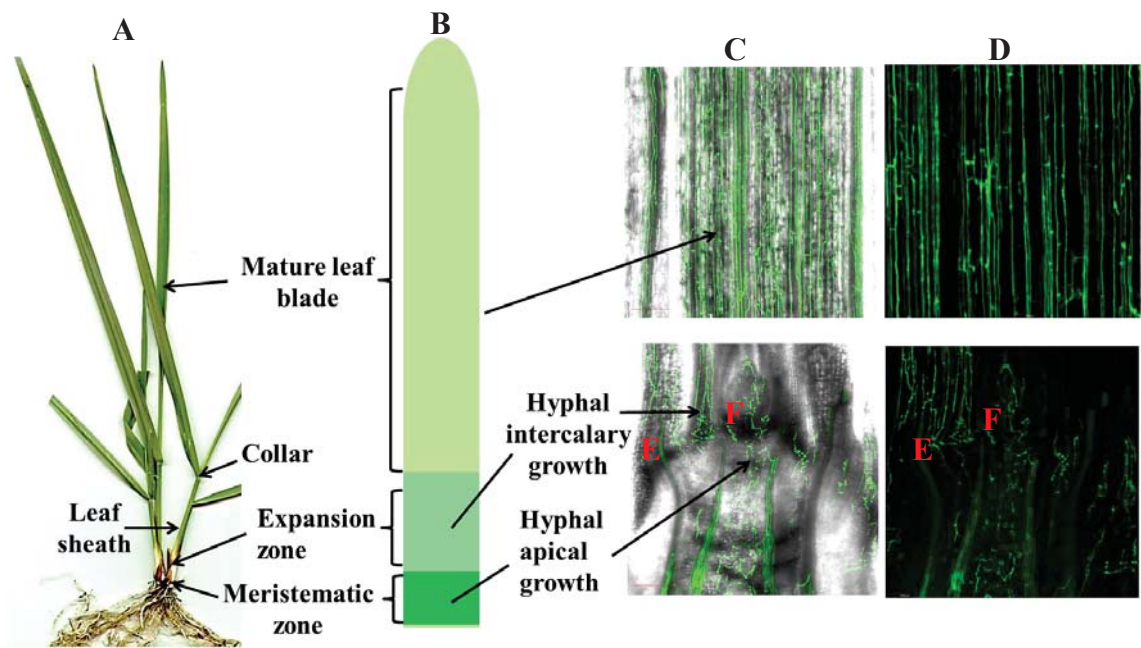


Figure 1.1: Growth zones and hyphal distribution of *E. festucae* in *L. perenne*.

The three main development zones (meristematic, expansion and mature) in a developing *L. perenne* leaf and the distribution of *E. festucae* hyphae in these zones are presented. **A & B** – Image (A) of *L. perenne* tillers and a diagram (B) of a developing leaf (not drawn to scale), Meristematic zone - endophyte colonization occurs through apical growth where host cell division occurs. Expansion zone - hyphal apical growth transitions to intercalary growth where host cell expansion occurs. Mature zone - no further host cell expansion or hyphal colonisation. **C & D** - Fluorescent and phase contrast images of wild type (WT) *E. festucae* F11 hyphae expressing EGFP in the meristematic zone, expansion zone and mature zone. **E & F** – Fluorescent and phase contrast images of WT *E. festucae* F11 hyphae expressing EGFP in developing leaves (E) and the shoot apical meristem (F).

1.2 Apical hyphal growth

Filamentous fungi are comprised of tubular hyphae that grow and extend to explore new environments to obtain nutrients or form complex specialized structures such as fruiting bodies. Hyphal extension in vegetative hyphae is believed to take place exclusively at

the apex in a polar manner (Gooday, 1995). Polarized apical extension is crucial for filamentous fungi to colonize and exploit new hosts or substrates (Gooday, 1995; Harris et al., 2004). Apical growth was proposed and later supported by evidence of deposition of cell wall material (chitins and glucans) at the apex (Ward et al., 1888; Bartnicki-Garcia et al., 1969; Gooday, 1971). Two models have been proposed to explain this phenomenon (Steinberg, 2007) ; the steady state model (Wessels, 1986; Sietsma et al., 2006) and the vesicle supply centre model (Bartnicki-Garcia et al., 1989; Bartnicki-Garcia et al., 1995). In the steady state model the cell wall of the growing apex always remains flexible, allowing extension of the hypha via cytoplasmic turgor pressure. Synthesis of cell wall material takes place at the apex (chitin and glucan chains) but these do not cross link until later to form a rigid cell wall (Sietsma et al., 2006). As the hyphae extend, chitins are covalently bound to β -1-3-glucans forming a rigid cell wall just behind the apex, while allowing hyphal extension at the extreme tip to continue to take place (Wessels, 1986; Sietsma et al., 2006). In the vesicle supply centre model, exocytic vesicles containing materials for hyphal extension accumulate at the apex forming a supply centre known as the Spitzenkörper. The Spitzenkörper moves forward during growth, providing the materials for cell wall synthesis and determining the direction and the rate of hyphal extension (Grove et al., 1970; Howard, 1981; Bartnicki-Garcia et al., 1995; Harris et al., 2005).

1.2.1 Mechanism of hyphal extension

As reviewed by Harris and Momany (2004), the major steps involved in apical extension in the vesicle supply centre model include polarity establishment (in the germ tube or the emerging branch) followed by relaying of the polarity signal, recruitment of the morphogenetic machinery, organization of the cytoskeleton, vesicle transport,

exocytosis and deposition of new cell wall material (Harris et al., 2004). Once polarity has been established it needs to be maintained continuously. In *S. cerevisiae* cortical markers composed of proteins Bud3, Bud4, Axl2, Bud8, Bud9, and Rax2 assist in deciding the polarity, reviewed by (Pringle et al., 1995; Pruyne et al., 2000; Harris et al., 2004). Once polarity has been established the next step is to relay the signal to establish the Spitzenkörper necessary for apical growth. In *S. cerevisiae* a protein called Cdc24 first moves to the site of polar growth and then activates the protein Cdc42-GDP by promoting the exchange of GDP for GTP. The activated Cdc42-GTP, together with Bem1, relays the signal to organize the cytoskeleton for apical growth (Johnson et al., 1990; Chenevert et al., 1992; Zheng et al., 1995; Pruyne et al., 2000). As a result of Cdc42 signalling, two multi protein complexes are formed in *S. cerevisiae* known as the polarisome and the Arp2/3 complex.

Organization of the actin filaments and transport of exocytic vesicles results in a collection of vesicles at the Spitzenkörper which also contains F-actins (Howard, 1981), formins (Sharpless et al., 2002), exocytic vesicles and ribosomes involved in protein synthesis (Howard et al., 1979). Microtubules and F-actins are involved in transporting vesicles to the Spitzenkörper and from there to the apex respectively (Fuchs et al., 2005). In filamentous fungi the molecular motors kinesin 1 and 3, along with dynein, are mainly involved in long distance vesicle transport along microtubules. Transport of vesicles from the Spitzenkörper to the plasma membrane at the apex is probably carried out by F-actins using class V myosin motors, which carry the vesicles toward the apex (Schuchardt et al., 2005). According to research findings so far, the hyphal extension machinery appears to be localized to the apex of the hypha due to the initial establishment of polarity. During hyphal branching the entire machinery is reorganized and a new polarity axis is established to allow the branch to develop.

1.3 Intercalary hyphal growth

As described previously (Section 1.2), growth of fungal hyphae was previously thought to occur exclusively at the apex, and this paradigm was widely accepted as the primary method of fungal growth until recently (Harold, 1997; Harris et al., 2004; Harris, 2006). Thus great emphasis has been placed on understanding the mechanism of hyphal apical growth and the extreme polarity it demonstrates. However recent studies have provided evidence that contradicts with this long-held dogma. A study on growth and colonization (Section 1.1.2) of the endophytic fungus *E. festucae* demonstrated that hyphal filaments of this fungus can grow by intercalary extension of non-apical compartments during host colonization (Christensen et al., 2008).

1.3.1 *E. festucae* host colonization through hyphal intercalary growth

As explained in Section 1.1.1, colonization of leaves by *E. festucae* occurs by invasion of the primordia as they develop on the host SAM and this process is believed to take place via apical hyphal growth. (Philipson et al., 1986; Tan et al., 2001; Schardl et al., 2004). During leaf development, cumulative host cell elongation in the expansion zone takes place at a rapid rate. Leaf tissue extends in an intercalary manner at about 1cm/day (MacAdam et al., 1989), and an individual grass epidermal cell can increase from 12-20 μm to 100-1000 μm after expansion (Schnyder et al., 1990; Schäufele et al., 2000). This growth rate is much higher than the typical apical hyphal growth rate of *E. festucae* in culture which is around 1.6 mm/day (results from this study). Hence, intercalary growth of plant cells potentially poses a challenge to fungal hyphae attempting to colonize the host tissues during the extension stage.

Early explanations for these apparently conflicting modes of growth in the host and symbiont initially included two alternative growth models based on apical hyphal

growth. In the first, colonization of developing host leaf tissues by *Epichloë* endophytes was believed to occur via hyphal apical growth. Hyphae were first proposed to grow independently of the host, with hyphae sliding between host cells within the intercellular spaces when the host cells elongated (Schmid et al., 2000; Tan et al., 2001). However evidence from microscopy investigations revealed that fungal hyphae are closely attached to the host cell walls, preventing them from sliding independently within the intercellular spaces of the host tissues (Christensen et al., 2008). The other evidence was the presence of lateral hyphal branches penetrating between files of host cells in the intercalary growth zone. If hyphae were sliding between host cells, lateral branches could not persist as they would be forcibly detached from the main hypha. As a result of these observations an alternative hypothesis was proposed. According to the second hypothesis the hyphae break when the host cells elongate and then grow apically to re-join via anastomosis (Read et al., 2006; Christensen et al., 2008). However there is no evidence of fragmented hyphae in host tissue or evidence of leakage of cytoplasm due to breaks in compartment walls (Christensen et al., 2008). It therefore became apparent that colonization of leaf tissues by *E. festucae* could not be explained by classical apical growth models. Intercalary hyphal growth was therefore proposed as the third model to explain how hyphae are able to colonize, and remain intact, in the leaf expansion zone (Christensen et al., 2008).

1.3.2 Evidence to support hyphal intercalary growth in developing leaves

Intercalary growth involves extension of hyphal compartments and the formation of new compartments along the length of the filament. This mode of growth was proposed to explain how *Epichloë* hyphae are able to grow (cumulatively) through intercalary growth at a much higher rate than through apical growth alone. Furthermore since

fungal hyphae are attached to host cells, when the host cells elongate rapidly, it is reasonable to assume that this rapid elongation imposes a mechanical stress/force on the hyphae (Fig 1.2). It has been hypothesised that this results in intercalary cell wall synthesis and new compartment formation (discussed in detail later), enabling the hyphae to grow in synchrony with the rapidly elongating host cells and along the longitudinal axis of the growing leaf. This hyphal growth model was supported by microscopic evidence (Christensen et al., 2008). TEM studies revealed that hyphae, firmly attached to host cell walls, could be observed to be stretched between cells. The presence of angled septa was further evidence to support hyphal stretching.

The study also showed that the distance between two lateral hyphal branches in the leaf elongation zone increased by about 3.7% per hour, which implied that the length of the intact hyphae in the elongation zone had increased. Conversely, no intercalary growth was observed in hyphae occupying the mature leaves. Furthermore, there was no correlation between compartment lengths and distance from the base of the leaf as would be expected if hyphal compartments simply increased in length over time. The study therefore suggested that the primary cause for hyphal extension was formation of new compartments (initiation of the cell cycle) and not solely expansion of pre-existing compartments. Moreover, the hyphae within each host developmental zone looked uniform in ultra-structure, which implied that they were of similar age and development stage, and had not entered the tissue at different times as would have been expected if hyphae were entering the tissue from the base by growing at the tip. Hyphae in the host elongation zone had a simple ultra-structure with thin cell walls, and hyphae in the mature zone of the leaf had thicker cell walls and a complex ultra-structure composed of crystalloid bodies (Christensen et al., 2008). This provided further support that cell wall synthesis/intercalary growth was taking place in the elongation zone of the leaf.

Also evident was that the hyphae grow in synchrony with the host tissues as larger, thick-walled hyphae were always found in association with mature leaf tissues (Christensen et al., 2008). Although hyphae do not extend in mature leaf tissues, they remain metabolically active and continue to synthesise cell wall resulting in thicker hyphal walls in mature parts of the leaf (Tan et al., 2001; Christensen et al., 2008). The study by Christensen, Bennett et al. 2008 proposed that mechanical stress imposed by rapidly elongating, closely attached, host cells provide the stimulus for intercalary hyphal growth, and in the absence of this stimulus intercalary growth will cease (Fig 1.2). This proposed mechanism explains why younger hyphae are only observed in the leaf elongation zone where intercalary growth occurs and mature hyphae (with thick cell walls but no extension) are present in the mature part of the leaf, where host cells do not expand (no stimulus). This hypothesis also explains why mature leaf tissues cannot be infected after they have ceased growing. Therefore, in summary, *E. festucae* hyphal colonization occurs in perfect synchrony with its host plant. In the meristematic tissues, where rapid cell division is taking place, host tissues are colonized via apical growth. In the leaf elongation zone, where host cells elongate, colonization is predominantly via intercalary growth and then hyphal extension ceases as the host cells mature and stop further growth.

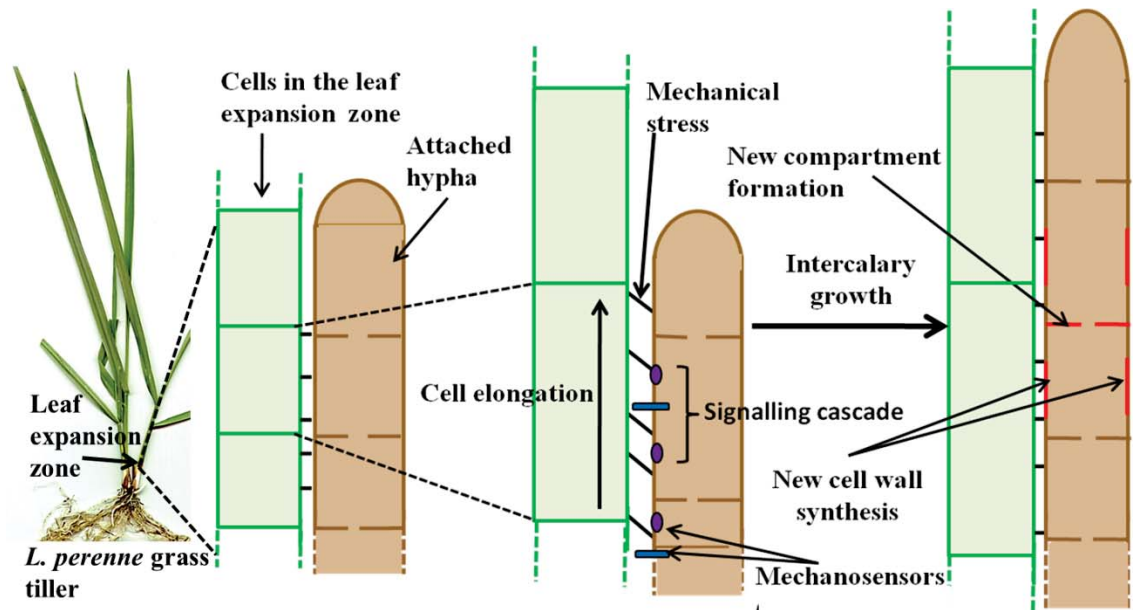


Figure 1.2: A diagrammatic representation of intercalary growth in *E. festucae* hyphae in the host (*L. perenne*) elongation zone hypothesised to be induced through mechanical stretch.

Epichloë hyphae are attached to the cell walls of the host cells. Host cell elongation exerts mechanical stretch on attached hyphae (which extend). Mechanical stress is sensed by fungal mechano-sensors located in the membranes of affected compartments. The mechano-sensors initiate a signalling cascade that activates cell wall synthesis and the cell cycle, resulting in formation of new compartments. Diagrams are not shown to scale.

1.3.3 Evidence of intercalary growth in other fungal species

It has been speculated that intercalary growth in vegetative hyphae may be more common than previously thought. Instances of intercalary growth and growth modes resembling intercalary growth in vegetative and reproductive hyphae of fungi have been reported before (Voisey, 2010). Intercalary growth during stipe development in the fruiting bodies of the Basidiomycete model fungus *Coprinus cinereus* has been well characterised (Moore, 1996; Kües, 2000; Kües et al., 2000). During *C. cinereus* fruiting body formation, vegetative dikaryotic hyphae first form knot-like structures and then

aggregate and differentiate to form a primordium (Matthews et al., 1972; Kües et al., 2000) . The primordium expands rapidly to form the basal plectenchyma, stipe and cap of the mushroom (Hammad et al., 1993). The cells in the middle section of the primordium give rise to the stipe (Kües et al., 2000), and it has been shown that rapid development and elongation of the stipe is predominantly due to hyphal intercalary growth via rapid cell elongation, and not due to cell division (although limited cell division can occur) (Eilers, 1974; Kamada et al., 1977b; Hammad et al., 1993). Rapid cell expansion is driven by cellular turgor pressure maintained throughout the expansion (Craig et al., 1977; Gooday, 1982; Moore, 1984; Kamada, 1994) and cell elongation occurs vertically in a diffuse manner while cell width remains the same (Hammad et al., 1993). To facilitate this, the cell walls need to be flexible and harder at the same time to withstand the high turgor pressure created within elongating cells. Another example of intercalary growth occurring in reproductive hyphae is seen in ascocarp formation in the Ascomycete *Trichometasphaeria turcica*. During ascocarp formation hyphae that originate from the stroma forming a paraphysis like structure is suspected to occur via intercalary growth (Voisey, 2010).

Although intercalary growth has been experimentally confirmed in reproductive hyphae, intercalary growth occurring in vegetative hyphae has not been shown experimentally thus far except in *E. festucae*. However there are some instances of vegetative hyphal growth that resemble intercalary growth. In *Allomyces macrogynus* intercalary growth can occur in vegetative aseptate hyphae originating from germinated zoospores when exposed to atmospheric oxygen concentrations. Under these conditions the hyphae start cell wall synthesis in intercalary zones increasing the overall width. Under microaerobic conditions these hyphae grow exclusively at the tip (Cleary et al., 1986; Youatt, 1986; Youatt et al., 1988). As seen in rhizomorph extension through agar, intercalary growth

is suspected to occur in the vegetative hyphae comprising the rhizomorphs of *Armillaria gallica*, but yet to be shown experimentally (Yafetto et al., 2009). The thalli of several lichens have been shown to undergo intercalary growth along with apical growth to achieve faster growth during thalli expansion (Hestmark, 1997; Sanders, 2001).

1.3.4 Cellular processes associated with intercalary growth

Thus far, a comprehensive mechanism to explain the underlying cellular processes supporting intercalary growth has not yet been proposed. It is plausible to assume that cellular processes involved in apical growth also play a similar role in intercalary growth. Research thus far provides evidence to suggest that cellular processes such as exocytosis and cell wall synthesis occur in sub-apical compartments under standard growth conditions (Read, 2011). The exact involvement of these cellular processes during intercalary growth in vegetative hyphae is yet to be elucidated. However, studies conducted on *C. cinereus* stipe elongation provide an insight into cellular activities that may be occurring during intercalary growth in vegetative hyphae of *E. festucae* and other fungi.

1.3.4.1 Cell wall synthesis

One of the basic and critical requirements of hyphal intercalary growth is the ability of cell walls to adjust and expand during compartment elongation. During intercalary growth, the cell walls need to be flexible for expansion and also undergo nascent cell wall synthesis or incorporation of cell wall constituents. Stipe elongation in mushrooms provides a good analogy to understand the possible activities of the cell wall during intercalary growth. Stipes in mushrooms can elongate 80 mm within 12 hrs (Stephenson et al., 1984; Kües, 2000). In *Coprinus* species during stipe elongation, the sub-apical

hyphal compartments expand rapidly and expanding cell walls are reinforced by deposition of new chitin microfibrils uniformly over the cell wall surfaces (Gooday, 1973; Kamada et al., 1991). Further proof of new cell wall synthesis was provided by the increase in chitin and glucan synthase activity in the regions of stipe elongation (Gooday, 1973; Gooday et al., 1975). In contrary to the randomly-arranged chitin microfibrils of vegetative non-expanding cells (Kamada et al., 1993), chitin microfibrils in stipe compartments are arranged as helices and positioned parallel and transverse to the axis of the elongating stipe cells with cross links between chitin and glucans to provide elasticity for cell expansion and sufficient rigidity to withstand the high turgor pressure (Kamada et al., 1977b; Kamada et al., 1991; Kamada et al., 1993). In *A. bisporus*, autoradiography studies revealed non-polar deposition of new cell wall material in expanding intercalary compartments (Craig et al., 1977). Use of polyxin D, which is a specific chitin synthase inhibitor, and N-acetyl-D-[1-3H] glucosamine, which is a precursor of chitin, has confirmed the importance of chitin synthesis during stipe elongation in *C. cinereus* (Gooday et al., 1976).

Cell walls formed during stipe formation may be accompanied by loosening of the cell wall and resealing between chitin and glucans. As hyphal growth continues, older cell walls become rigid with cross linking between chitin and β (1 \rightarrow 3)-glucan and hydrogen bonding between chitin microfibrils (Vermeulen et al., 1984; Sietsma et al., 2006). Further, as the older cell walls mature, secondary cell wall growth can occur, thickening the cell wall, or additional cell wall layers are added outside the previous cell wall (Klis et al., 2007; Read, 2011). As a result of these changes, the sub apical cell wall can become very rigid and may require loosening before undergoing intercalary extension. Increased activity of cell wall autolytic enzymes during stipe elongation in *Coprinus* species has been also demonstrated (Kamada et al., 1982; Kamada et al., 1985).

A new form of adaptation in cell wall synthesis during intercalary growth has been shown for *Ramalina menziesii* which is a lichen fungus. It is believed that this fungus is capable of intercalary expansion during lichen growth. According to studies conducted using TEM it has been shown that the expanding compartments lay down a new cell wall beneath the old cell wall during expansion and the old cell wall disintegrates and detaches forming a thick matrix around the hypha (Sanders et al., 1995). It is reasonable to assume that some of these processes might be involved in intercalary growth in *E. festucae* in developing leaves due to the mechanical strain applied by rapidly elongating host cells. During this process it is necessary to loosen the cell walls allowing stretching and then to reseal the matrix during or after elongation.

1.3.4.2 Exocytosis

Exocytosis is an essential process that occurs at the tip of an actively growing hypha to provide the necessary enzymes and material for growth. Numerous vesicles continuously fuse with the apical plasma membrane releasing cell wall synthesising enzymes, cell wall constituents, proteins and lipids to facilitate the synthesis of new membrane and cell walls (Wösten et al., 1991; Harris et al., 2005; Steinberg, 2007). In addition to tip-centred exocytosis; there is evidence to support exocytosis away from the hyphal tips in many filamentous fungi (Read, 2011).

A localization study conducted on three soluble *N*-ethylmaleimide-sensitive factor attachment protein receptors (SNARE) proteins SNCI, SSOI and SSO2 of the filamentous fungus *Trichoderma reesei* revealed that some of the protein complexes can be seen in sub apical compartments (Valkonen et al., 2007). SNARE proteins are important in mediating vesicle fusion with cell membranes during exocytosis. In *Aspergillus oryzae*, it has been revealed that secretory vesicles containing EGFP-fused

AoSnc1 always localizes to the plasma membranes in sub apical septal regions (Hayakawa et al., 2011).

Secretion of enzymes necessary for cell wall and membrane extension at the hyphal tip is well established (Wösten et al., 1991; Momany, 2002; Steinberg, 2007). Similarly, recent studies provide strong evidence to support exocytosis of secretory enzyme from sub apical compartments. A study conducted using *A. oryzae* demonstrated that the secretory enzyme α amylase (AmyB) fused with EGFP (AmyB–EGFP) accumulates at the Spitzenkörper in hyphal tips, and also between the plasma membrane and the cell wall of sub-apical septa (Hayakawa et al., 2011). The same study showed that the plasma membrane transporters, AoUapC (purine uptake) and AoGap1 (amino acid permease) of *A. oryzae* accumulate at the septa and lateral plasma membranes and not at the apex. Together these studies suggest that proteins associated with vesicle fusion localise to cell membranes in sub-apical compartments implying that exocytosis may also occur behind the apex.

1.3.4.3 Role of the Spitzenkörper away from hyphal apex

An appropriate mechanism to assist in understanding the role of the Spitzenkörper behind the hyphal apex is the formation of lateral branches behind the hyphal tip in filamentous fungi. Lateral branching can occur just behind the septa or at a random points in sub apical compartments (Harris, 2008). In general, similar to tip growth, *de novo* establishment of the morphogenetic machinery/Spitzenkörper and plasticisation/loosening of the cell wall at the branching site can be considered as two crucial processes associated with branch formation. In *N. crassa*, Spitzenkörper establishment, deformation of the cell wall at the branch initiation site (Riquelme et al., 2004) and the association of microtubules with the Spitzenkörper at the branch initiation

site has been observed (Mouriño-Pérez et al., 2006). Given that mature sub-apical cell walls are rigid, and may have to be loosened to facilitate the emergence of lateral branches, the vesicle composition of the Spitzenkörper in lateral branches may be different from that of the apical Spitzenkörper, possibly with vesicles containing glycosidases to increase cell wall plasticity (Read, 2011). Thus it is possible that vesicles involved in softening the cell wall during intercalary hyphal expansion may contain different compositions of cell wall degrading enzymes.

1.3.5 Signalling mechanisms that may have a role in intercalary growth

Previous molecular studies have demonstrated that disruption of certain genes and their associated pathways disturb the finely-synchronised symbiotic relationship between *E. festucae* and its host, indicating a possible role for some of these factors in intercalary growth, reviewed by (Eaton et al., 2011; Scott et al., 2012). One such factor is reactive oxygen species (ROS). In *E. festucae*, during host colonization, disruption of NoxA (one of the NADPH oxidases responsible for ROS production in fungi) resulted in disruption of the usual synchronised growth *in planta* with hyper-branched hyphae and very high hyphal biomass. This resulted in stunted plants and eventual death of plants (Tanaka et al., 2006; Eaton et al., 2011). In addition disruption of genes such as *noxR*, *racA*, *bemA* (encoding regulators and activators of NoxA) and *proA* (a zinc finger transcription factor) in *E. festucae* resulted in severe breakdown of the synchronised restricted symbiotic growth usually seen *in planta*, similar to the *noxA* disruption (Takemoto et al., 2006; Tanaka et al., 2008; Takemoto et al., 2011; Tanaka et al., 2013) phenotype.

In addition to the *in planta* phenotypes, disruption of these genes resulted in defective hyphal cell fusion in axenic culture (Kayano et al., 2013; Tanaka et al., 2013). Together

these observations (disruption in mutualistic growth and defective hyphal cell fusion) indicate a possible requirement for hyphal cell fusion to maintain the synchronised hyphal growth *in planta* by *E. festucae* (Becker et al., 2014). Further, deletion of the stress-activated mitogen activated protein kinase gene, *sakA*, in *E. festucae* also resulted in loss of controlled, synchronized growth with the host (Eaton et al., 2010). In general, all these factors seem to be important in regulating *E. festucae* growth in the host expansion zone of the developing leaf. Whether these pathways contribute to intercalary growth processes directly or indirectly is not clear at this stage.

1.4 Sensing and signalling mechanical stress in *E. festucae* hyphae

One mechanism, by which hyphae may respond to changes in host development, and initiate intercalary growth, is through membrane-bound sensors that can detect perturbations in hyphal membranes. According to this hypothesis, membrane-located mechano-sensors detect mechanical stretch exerted on hyphae attached to elongating host cells (Fig 1.2). In addition, upon sensing mechanical stress a signalling cascade is activated to initiate cell wall synthesis and the cell cycle resulting in septation and intercalary growth. As part of a broad effort to identify possible mechano-sensors and associated cellular processes involved in intercalary growth, I decided to focus on two putative mechano-sensors, and their signalling pathways, with potential to sensing and initiate intercalary growth. The first was the stretch-activated calcium ion channel MidA, along with Ca^{2+} as a potential signalling molecule, and cell wall integrity sensor WscA.

1.5 Calcium transporters and maintenance of calcium homeostasis in fungi

Calcium ions act as universal secondary messengers in all eukaryotes and regulate a wide range of cellular processes. In yeast and filamentous fungi, Ca^{2+} is involved in cell cycle regulation, morphogenesis, sporulation, spore germination, pathogenesis, circadian rhythms and polarized hyphal extension (Jackson et al., 1993; Torralba et al., 2001; Silverman-Gavrila et al., 2002). When exposed to stress conditions, Ca^{2+} ions play a major role in signalling and modulating a number of downstream effectors involved in gene expression and cytoskeleton rearrangement (Cyert, 2003; Rispaill et al., 2009).

Calcium homeostasis in the cytoplasm of fungi is dependent on an equilibrium between storage, release of calcium from intracellular calcium stores and influx of external calcium into the cell (de Castro et al., 2014). Typically the cytoplasmic calcium concentration in fungi is maintained at low levels, for example in *S. cerevisiae* the free cytoplasmic Ca^{2+} concentration at resting state is 50-100 nM and excessive levels can become toxic (Harren et al., 2013; de Castro et al., 2014). Excess Ca^{2+} in the cytoplasm is stored in intracellular compartments such as the vacuole, Golgi apparatus, mitochondria and the endoplasmic reticulum (Harren et al., 2013; de Castro et al., 2014), or alternatively expelled from cells across the plasma membrane (Miller et al., 1990; Bowman et al., 2011). Intracellular calcium stores are replenished by uptake of calcium from the external environment (Putney Jr, 1990; Hong et al., 2010). In response to stresses or other stimuli, calcium signalling is triggered by transient increases in cytoplasmic Ca^{2+} concentration that are 10 to 100 fold over the basal level, caused by Ca^{2+} release from sequestering organelles or transport across the plasma membrane (Nelson et al., 2004). Immediately thereafter, excess Ca^{2+} is exported from the

cytoplasm across the plasma membrane or sequestered into the vacuole (Cornelius et al., 1987; Miller et al., 1990; Cunningham et al., 1994a). Calcium homeostasis in fungi is therefore usually maintained through the activity of calcium channels, pumps and antiporters located in the plasma membrane, vacuole, endoplasmic reticulum and Golgi apparatus (Lew et al., 2008; Bowman et al., 2011; Bowman et al., 2012; Harren et al., 2013; de Castro et al., 2014). Coordination and regulation between these channels, pumps and antiporters are crucial for eliciting the appropriate calcium signal under internal and external stresses and subsequent maintenance of general calcium homeostasis (Harren et al., 2013). Calcium transporters in *S. cerevisiae* have been very well characterised and recent sequencing of genomes of many filamentous fungi have enabled the identification and characterization of similar systems in other fungi (Zelter et al., 2004; Benčina et al., 2009).

1.5.1 Calcium transporters in the vacuole, Golgi apparatus and endoplasmic reticulum

In fungi, the vacuole is a major store for excess Ca^{2+} (Fig 1.3) (Eilam et al., 1985; Dunn et al., 1994). In *S. cerevisiae*, Pmc1 which is a high affinity plasma membrane Ca^{2+} ATPase (PMCA-type Ca^{2+} ATPase pump) (Cunningham et al., 1994b), and Vcx1 which is a low affinity $\text{Ca}^{2+}/\text{H}^{+}$ exchanger (Cunningham et al., 1996), are involved in transporting calcium from the cytoplasm into the vacuole (Bowman et al., 2012). Yvc1, a vacuole channel protein with homology to transient receptor potential (TRP) channels, is involved in releasing calcium from the vacuole (Palmer et al., 2001; Denis et al., 2002). Pmc1 uses ATP directly for pump activity (Cunningham et al., 1994b) and Vcx1 uses the energy generated through the V-ATPase-mediated proton gradient (Cunningham et al., 1996). In the Golgi body and other related compartments such as

the ER, Pmr1, a secretory pathway Ca^{2+} -ATPase (SPCA) is another crucial calcium pump discovered in *S. cerevisiae* and found to be involved in Ca^{2+} and manganese sequestration (Fig 1.3)(Rudolph et al., 1989; Antebi et al., 1992).

Filamentous fungi have a range of calcium transport proteins additional to those described in *S. cerevisiae* (Fig 1.3) (Bowman et al., 2011). For example, in *N. crassa*, a sarco/endoplasmic reticulum Ca^{2+} -ATPase (SERCA), Nca-1, and two PMCA-type Ca^{2+} -ATPases, Nca-2 and Nca-3, play a crucial role in maintenance of general calcium homeostasis (Bowman et al., 2011). Nca-1 localises to the ER and nuclear envelope, and Nca-2 and Nca-3 co-localise to the vacuoles close to the hyphal tip, and the plasma membrane away from the tip (Bowman et al., 2009). Plasma membrane-located Nca-2 and 3 are involved in pumping excess calcium across the plasma membrane (Bowman et al., 2011). Overall, although *S. cerevisiae* and filamentous fungi share common features in the calcium homeostasis mechanism, the presence of Nca1, 2 and 3 in *N. crassa* also suggest that there are significant differences between the two groups (Fig 1.3).

1.5.2 Calcium uptake systems in the plasma membrane

Studies to date have identified two major calcium uptake systems operating in fungi, a high affinity calcium system (HACS) and a low affinity calcium system (LACS), which operate in response to low or high calcium availability respectively (Lew et al., 2008; Cavinder et al., 2012; Wang et al., 2012). The HACS is a protein complex consisting of the stretch-activated non-selective calcium ion channel/regulatory protein Mid1 (Iida et al., 1994), and the L-type voltage-gated calcium channel Cch1 (Fig 1.3) (Fischer et al., 1997; Paidhungat et al., 1997). Deletion studies of *mid1* and *cch1* in *S. cerevisiae*, and certain filamentous fungi, have demonstrated a common phenotype of impaired growth

under low calcium concentration signifying their role in HACS (Liu et al., 2006; Cavinder et al., 2011; Harren et al., 2013). The calcium channel Fig1, a pheromone-inducible plasma membrane protein, is the major component of the LACS which is responsible for calcium uptake when availability is high (Muller et al., 2003; Cavinder et al., 2012). In addition, in *C. albicans* and *S. cerevisiae*, PMP22 Claudin superfamily member Ecm7 has been shown to be part of the HACS and LACS and involved in hyphal development and oxidative stress responses (Martin et al., 2011; Ding et al., 2013).

The three membrane proteins Mid1, Cch1 of HACS and Fig1 of LACS act as the main calcium influx transporters in the calcium/calcineurin signalling pathway which regulates many responses under stimulatory and stress conditions (Fig 1.3) (Rispaill et al., 2009). This pathway was initially characterized in *S. cerevisiae*, and later, orthologues for most of the proteins in this pathway were found in other fungi (Iida et al., 1994; Rispaill et al., 2009). A comparative analysis conducted by Rispaill et al., 2009 across 10 different fungi from a range of genera (*S. cerevisiae*, *Ashbya gossypii*, *N. crassa*, *Schizosaccharomyces pombe*, *Fusarium graminearum*, *Magnaporthe grisea*, *Ustilago maydis*, *Aspergillus fumigatus*, *C. albicans*, and *Rhizopus oryzae*) has revealed that most of the components in the pathway are conserved (Rispaill et al., 2009). The study revealed that at least one orthologue of each of the proteins in the pathway could be identified in the genomes studied, and for some proteins multiple gene copies could be detected. This underpins the importance of the calcium/calcineurin pathway for growth and development of fungi generally.

This study is focused on investigating the involvement of Mid1 in intercalary growth as a mechanosensor and in the general maintenance of calcium homeostasis in *E. festucae*.

Recent studies in yeast and certain filamentous fungi have indicated that Mid1 forms a complex with Cch1 and acts as one unit during influx of calcium (discussed in detail later). Thus, henceforth, the characteristics of Mid1 in fungi are reviewed along with Cch1 with more emphasis on Mid1.

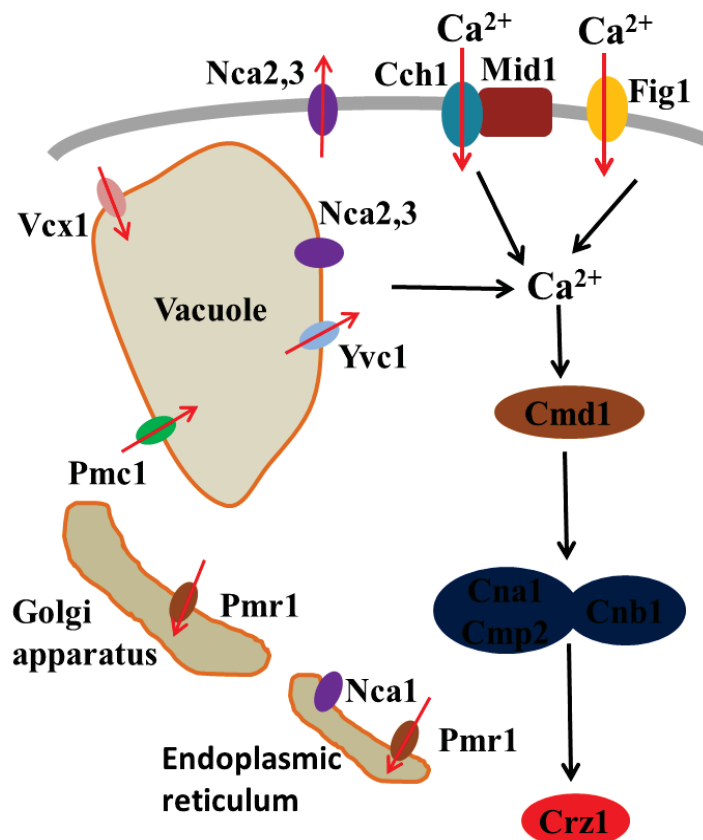


Figure 1.3: Diagram showing the involvement of fungal calcium transporters in the maintenance of calcium homeostasis and calcium signalling. Red arrows indicate the direction of Ca²⁺ movement. Calcium entering the cytoplasm binds to calmodulin (Cmd1) that activates Calcineurin (a complex of Cna1, Cmp2 and Cnb1). Activated calcineurin dephosphorylates Crz1 (a zinc finger transcription factor) resulting in its translocation to the nucleus. Crz1 regulate genes involved in cell wall synthesis and/or in maintenance of calcium homeostasis.

1.5.2.1 Structural characteristics of Mid1 and Cch1 proteins

Mid1 is a stretch-activated channel protein that responds to cell membrane deformation due to environmental stress/stimuli (Garrill et al., 1993; Iida et al., 1994; Kanzaki et al., 1999; Brand et al., 2007). Cch1 however is a voltage gated channel sensitive to membrane potential (Paidhungat et al., 1997; Zelter et al., 2004). In *S. cerevisiae*, Cch1 localizes to the plasma membrane (Locke et al., 2000). Orthologues of Cch1 within different fungi share conserved functional domains. The Cch1 protein consists of an acidic motif with glutamate residues which provide ionic selectivity, and four domains each containing 6 transmembrane helices. These helices assemble to form the aqueous pore of the channel (Zelter et al., 2004; Harren et al., 2013). The structure of the Mid1 protein was first solved in *S. cerevisiae*. It is a 548 amino acid protein with an estimated molecular mass of 61,506 Da (Iida et al., 1994). Structural analysis of *S. cerevisiae* Mid1 revealed important structural and functional domains which appear to be conserved in other fungal Mid1 proteins. It has four hydrophobic transmembrane domains, 16 N-glycosylation sites, and 10 conserved cysteine residues at the C terminus. Of the 10 cysteine residues, four are essential for its function, three are intermediate, and three are dispensable. The cysteine-rich region in the C-terminus is highly conserved and may be involved in protein-protein interactions along with the EF-hand domain (Iida et al., 1994; Maruoka et al., 2002; Zelter et al., 2004; Ozeki-Miyawaki et al., 2005). Mid1 proteins identified in other filamentous fungi have significant structural homology with *S. cerevisiae* Mid1. The *C. purpurea* Mid1, which has 628 amino acids, is 40.6% identical to *S. cerevisiae* Mid1, 48.8% to *N. crassa* and 41.9% to *C. albicans* across the open reading frame with all the key structural features represented (Bormann et al., 2009).

In *S. cerevisiae*, the Mid1 protein is a membrane protein embedded into the lipid bilayer of the plasma membrane via a glycosylphosphatidylinositol (GPI) anchor and has also been shown to localize to the ER membrane (Yoshimura et al., 2004; Pei et al., 2012). The 16 N-glycosylation sites are glycosylated in the ER and the protein is then transported to the plasma membrane by Sec12 (Ozeki-Miyawaki et al., 2005). EGFP-labelled Mid1 protein in *S. cerevisiae* accumulates in the plasma-membrane when exposed to pheromone- α factor (Ozeki-Miyawaki et al., 2005). Similarly, localization studies showed that the Mid1-Cch1 complex in *Cryptococcus neoformans* localises to the plasma-membrane (Hong et al., 2010).

1.5.2.2 Functions of the Mid1 and Cch1 complex

A review of relevant studies conducted to date in *S. cerevisiae* and filamentous fungi has identified three broad roles for Mid1 and Cch1: uptake of calcium under low exogenous calcium conditions, response to ER stress or depleted intracellular calcium levels and response to environmental stresses/stimuli via transient influxes of calcium (Viladevall et al., 2004; Hong et al., 2010; Harren et al., 2013). Mid1 and Cch1 are crucial for calcium uptake under low external concentrations and this is very evident by the inability of *mid1* and *cch1* single or double mutants to survive in low calcium environments created using calcium chelator BAPTA (1,2-Bis(2-Aminophenoxy)ethane-N,N,N',N'-tetra acetic acid) or EGTA (Ethylene glycol-bis (2-aminoethylether)-N,N,N',N'-tetraacetic acid) (Cavinder et al., 2011; Harren et al., 2013).

The other main function of Mid1 and Cch1 is to replenish intracellular calcium stores in the ER. An ER stress response in *S. cerevisiae* is created when calcium levels in ER stores become depleted, and is relieved through influx of calcium via the activity of

Mid1 and Cch1 (Bonilla et al., 2003). In *S. cerevisiae* under ER calcium stress, activation of Cch1–Mid1 occurs via the Mpk1 pathway (Bonilla et al., 2003). Patch clamping of *C. neoformans* protoplasts revealed that the Cch1-Mid1 channel complex is mainly responsible for influx of calcium when intracellular calcium is depleted using BAPTA-AM (1,2-Bis(2-aminophenoxy)ethane-N,N,N',N'-tetraacetic acid tetrakis (acetoxymethyl ester) (Hong et al., 2013).

The third function of Mid1 and Cch1 is to respond to internal or external stresses or stimuli. For an example, in *S. cerevisiae* both Mid1 and Cch1 are involved in influx of Ca^{2+} when exposed to pheromones (Iida et al., 1994; Fischer et al., 1997). In *S. cerevisiae*, *mid1* deletion mutants lose viability upon exposure to the mating pheromone, α factor; they die after differentiating into cells with mating projections/shmoos. These mutants can be rescued by incubating cells in high concentrations of CaCl_2 but not with other salts or cell wall stabilizing sorbitol (Iida et al., 1994). In addition, the importance of Mid1 and Cch1 in thigmotropism (responses to surface ridges), sensitivity to fungicides (Watts et al., 1998; Brand et al., 2009), oxidative stress (Yu et al., 2012) and cell wall perturbation agents is evident in other fungi (Bormann et al., 2009; Cavinder et al., 2011). One of the crucial properties of Mid1 relevant to this study is its assumed ability to act as a mechano-sensor. Mechano-sensitive ion channels are capable of detecting and responding to mechanical stimuli that cause structural changes or deformation to the cell membrane (Kloda et al., 2008; Kumamoto, 2008). It has been shown that Mid1 can import Ca^{2+} ions under mechanical stress imposed on the plasma membrane in a number of organisms such as *Saprolegnia ferax* (Garrill et al., 1993) and *C. albicans* (Watts et al., 1998). Also, it is possible that the Mid1 response to pheromones in *S. cerevisiae* is a mechanical stress response, as exposure to pheromone triggers morphological changes in the cell membrane (Iida et al., 1994).

1.5.2.3 Other proteins in the calcium/calcineurin pathway

Fig1, a component of the LACS, is an alternative calcium ion channel in the calcium/calcineurin pathway (Muller et al., 2003). Fig1 is a member of the PMP22 Claudin superfamily (Fig 1.3). Accordingly, in the calcium/calcineurin signalling pathway, transient calcium changes in the cytosol caused by influx of calcium via Mid1, Cch1 or Fig1 is sensed by the calcium sensor protein calmodulin (CaM) (Fig 1.3). Cytosolic Ca^{2+} binds to the EF-hand motifs of CaM and activates calcineurin (Chin et al., 2000). Calcineurin is a Ca^{2+} and calmodulin-dependent serine/threonine specific phosphatase composed of two subunits (A&B) encoded by genes *cmp2*, *cnal* (the catalytic A subunit) and *cnb1* (regulatory B subunit) (Rispaill et al., 2009). Calcineurin acts as the main regulatory protein of the calcium/calcineurin pathway by dephosphorylating several transcription factors such as Crz1 (a zinc finger transcription factor). Activated calcineurin dephosphorylates Crz1 resulting in its translocation to the nucleus (Matheos et al., 1997). Nuclear-localized Crz1 is responsible for the transcriptional regulation of a number of genes involved in cell wall synthesis and/or in maintenance of calcium homeostasis (Yoshimoto et al., 2002; Cyert, 2003; Viladevall et al., 2004). When cytosolic Ca^{2+} concentration is high calcineurin can inhibit Cch1 and Mid1 activity via a negative feedback loop (Muller et al., 2001). Further, there is evidence to support cross talk between the calcium/calcineurin pathway and the cell wall integrity MAP kinase pathway (CWI) as the Mpk1 protein of the CWI MAP kinase pathway is capable of activating the Mid1 and Cch1 under ER stress (Bonilla et al., 2003).

1.6 Cell wall integrity MAP kinase pathway

The cell wall integrity MAP kinase pathway (CWI) was first discovered in *S. cerevisiae* as a response mechanism to factors that alter the integrity of the cell wall (Verna et al., 1997). Cell wall integrity can be challenged as a result of normal growth and differentiation, or through environmental stresses. The rigid structure of the cell wall of *S. cerevisiae* requires alteration to accommodate changes during growth (budding) and also pheromone-induced morphogenesis (mating projection formation). On the other hand various environmental stresses that can challenge the integrity of the cell wall need to be sensed and responded to accordingly (Levin et al., 1993; Cid et al., 1995; Kamada et al., 1995; Fuchs et al., 2009; Levin, 2011). The cell wall integrity MAP kinase signalling pathway acts as the machinery that senses and monitors these changes or stresses to the cell wall, and activates necessary responsive mechanisms to remodel or repair the cell wall. Hence CWI MAP kinase pathway is important in regulating and maintaining cell shape and synthesis of the cell wall. The signalling pathway is a MAPK signalling cascade composed of sensing proteins and a PKC1-MPK1 signalling cascade (Levin, 2005).

1.6.1 Role of the cell wall integrity MAP kinase pathway

A number of phenotypes relating to this pathway were initially discovered in *S. cerevisiae* via gene mutation studies. Null mutations in genes of this pathway resulted in the inability to acquire thermotolerance when treated with mild heat (37°C); mutants die when exposed to higher temperatures that normal cells are able to survive (temperatures of up to 55°C) (Kamada et al., 1995; Verna et al., 1997; Ketela et al., 1999). Additionally, mutations in the pathway made the cells susceptible to hyper osmotic shock due to inability to activate the PKC1-MPK1 signalling pathway

(Davenport et al., 1995; García-Rodríguez et al., 2005). When *S. cerevisiae* is exposed to the mating hormone pheromone, cells normally undergo morphogenesis by producing mating projections, but when CWI mutants are exposed, this results in cell lysis (Buehrer et al., 1997; Verna et al., 1997).

Stresses that cause changes to the cell wall in *S. cerevisiae* are detected by a family of cell membrane sensors Wsc1, Wsc2, Wsc3, Mid2 and Mtl2 (Verna et al., 1997; Philip et al., 2001). Investigations revealed that Wsc1 and Mid2 perform a more prominent function than the others (Philip et al., 2001; Straede et al., 2007). The Wsc1 and Mid2 sensors activate GTPase Rho1 through the guanine nucleotide exchange factors (GEFs) Rom1 and Rom2 (Fig 1.4) (Ozaki et al., 1996; Philip et al., 2001). Rho1 acts as the crucial mediator in the CWI MAP kinase pathway, as it activates protein kinase C (PKC1) (Nonaka et al., 1995), which then activates a mitogen activated protein kinase (MAPK) signalling cascade (Nonaka et al., 1995; Levin, 2005). The MAPK cascade (Fig 1.4) consists of MAPKKK Bck1 (Lee et al., 1992), the MAPKKs Mkk1 and Mkk2 (Irie et al., 1993) and the MAPK Mpk1 (Lee et al., 1993). MPK1 ultimately activates a number of regulatory factors, cytoskeletal proteins, protein kinases and other enzymes required to activate necessary cell wall responses (Qi et al., 2005). Some of the transcription factors regulated by this cascade include Rlm1, Swi4 and Swi6 (Watanabe et al., 1995; Fuchs et al., 2009; Levin, 2011). Research carried out on *S. cerevisiae* has revealed that regulation of nearly 25 genes is controlled by MPK1 via the transcription factor Rlm1. Approximately 20 genes are up-regulated and about 5 are down regulated. Many of these up-regulated genes are involved in cell wall synthesis (Jung et al., 2002).

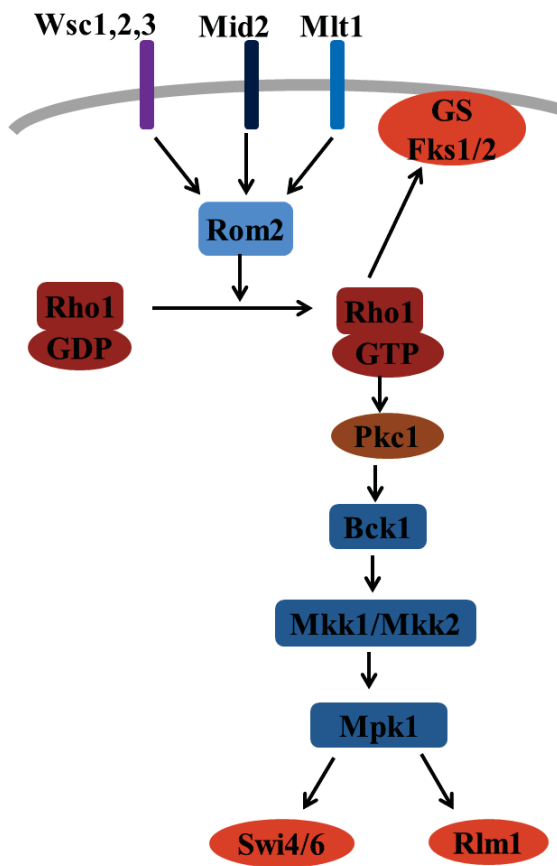


Figure 1.4: Diagram showing the main components and signal transduction in the Cell Wall Integrity (CWI) MAP kinase pathway of *S. cerevisiae*. Cell membrane sensors Wsc1, Wsc2, Wsc3, Mid2 and Mtl2 activate GTPase Rho1. Rho1 activates MAPK cascade (Bck1, Mkk1/2 and Mpk1) via Pkc1 or regulates 1,3- β -glucan synthase (GS) complex. MAPK cascade regulates transcription factors such as Rlm1 (MADS-box protein), Swi4/6 (DNA binding SBF). Diagram compiled using data from Levin, 2005.

1.6.2 The CWI MAP kinase pathway is highly conserved

An analysis of available genome sequences of wide range of fungi by Rispaill et al, 2009 revealed that most of the components associated with the cell wall integrity MAP kinase pathway found in *S. cerevisiae* are conserved in other fungi as well. Characterization of each of these components will reveal whether they perform the same function in filamentous fungi. According to this analysis Wsc1, Wsc2 and Wsc3 proteins are found in most ascomycetes that have been analysed. Other proteins in the pathway (Fig 1.4), Rom1, Rom2, Rho1, Pkc1, Swi4, Swi6, Rlm1 and components of the MAPK cascade were found in all the fungal species studied in this analysis. Multiple orthologues were detected for certain pathway components in some of the fungi (Rispaill et al., 2009). This implies that the cell wall integrity MAP kinase pathway is highly conserved in fungi and that it is involved in regular growth and development. However certain

components in the CWI MAP kinase pathway, particularly upstream components like the sensors Wsc1, Wsc2, Wsc3 and Mid2 have not as yet been functionally characterised in most fungi with the exception of *S. cerevisiae* (Verna et al., 1997), *A. fumigatus* (Dichtl et al., 2012) and *N. crassa* (Maddi et al., 2012).

1.6.3 Structure of Wsc and Mid2 proteins

Wsc1, Wsc2, Wsc3 and Mid2 are integrin-like O-glycosylated proteins that reside in the plasma membrane (Verna et al., 1997; Levin, 2005). An important feature of all these proteins is that they have a high degree of conservation among them and share similar functional and structural domains (Verna et al., 1997; Dichtl et al., 2012; Lengeler et al., 2013). All Wsc1 proteins consist of a cytoplasmic domain at the C terminal followed by a single transmembrane domain. Thereafter, there is a serine/threonine rich highly mannosylated extracellular domain, a cysteine rich motif and a hydrophobic signal peptide at the N terminal. The cysteine motif is extracellular (termed the WSC domain) and is the most conserved domain in the Wsc protein family, but the exact function is not known (Verna et al., 1997; Lodder et al., 1999; Straede et al., 2007). The C terminal cytoplasmic domain is highly charged and interacts with Rom2 to activate Rho1 (Philip et al., 2001; Vay et al., 2004). The serine/threonine domain is variable in length among the three Wsc proteins and it is O-mannosylated by a family of O-mannosyl transferases (Pmt) (Gentzsch et al., 1996; Lommel et al., 2004). Mannosylation of the domain results in extension and stiffening of the protein, thus helping it to act as a probe and sense the changes occurring in the cell wall (Dupres et al., 2009). The importance of glycosylation of Wsc1 proteins is reflected by deletion studies of Pmt proteins. Deletion of Pmt family proteins in various combinations has resulted in phenotypes similar to CWI mutants in *S. cerevisiae*. The cells become non-

viable when exposed to high temperatures and cell wall perturbing agents like Calcofluor white in the absence of an osmotic stabilizer (Gentzsch et al., 1996; Lommel et al., 2004). Studies on *pmt* mutants of *A. nidulans* have also shown susceptibility to cell wall perturbing agents (Kriangkripiat et al., 2009).

The Mid2 proteins in *S. cerevisiae* and *A. fumigatus* are similar to Wsc1 proteins in structure (except the wsc domain is absent) and function, and are also glycosylated by Pmt proteins (Ketela et al., 1999; Rajavel et al., 1999; Lommel et al., 2004; Dichtl et al., 2012). Similar to Wsc1, Mid2 activates Rho1 through Rom2 in the CWI MAP kinase pathway in response to perturbation in the cell wall and the signal is relayed to the downstream signalling cascade by Rho1 (Fig 1.4) (Ketela et al., 1999). Studies conducted with GFP-labelled Wsc1 proteins in *S. cerevisiae* have shown that the proteins localize at the plasma membrane (Verna et al., 1997). Localization studies conducted in *A. fumigatus* demonstrate that constitutively-expressed GFP fusions with Wsc1-3 and Mid1 localise to the plasma membrane (Dichtl et al., 2012). Furthermore atomic force microscopy studies conducted on *S. cerevisiae* have shown that Wsc1 proteins can resist high mechanical stress and sense cell surface stress by acting as a nanospring. The same study emphasized the importance of glycosylation by Pmt proteins to maintain its nanospring property which enables it to act as a sensing probe (Dupres et al., 2009)

1.6.4 Function of Wsc and Mid2 proteins

Functional characterization of the sensors in the CWI MAP kinase pathway has revealed mostly overlapping functions. However there are a few functions that seem to be unique for Wsc1 and Mid2 proteins and in most of the situations Wsc1 and Mid2 have a more prominent role as sensors. Thermotolerance studies using *S. cerevisiae* mutants has

revealed that *wsc1* mutants lyse when exposed to high temperatures (37°C), but mutants of *wsc2* or *wsc3* are able to survive at this temperature. However double mutants of *wsc3* or *wsc2* with *wsc1* exacerbate the lysis effect (Verna et al., 1997). The cell lysis defect can be rescued by over-expression of PKC1 or in the presence of sorbitol at a concentration of 1M, which can act as an osmotic stabiliser (Verna et al., 1997).

A study in *A. fumigatus* showed that *wsc1* deletion slightly altered radial growth rate and conidiation, and a double deletion of *wsc1* with *wsc3* exacerbated the phenotype. However *wsc1* deletion alone in *A. gossypii* and *N. crassa* resulted in a severe growth defect (Maddi et al., 2012; Lengeler et al., 2013) while single deletions of *wsc2*, *wsc3* or *mid2* had no effect on radial growth rate or conidiation. In addition, investigations have revealed that Mid2 is essential for resistance against cell wall perturbing agents such as congo red and Calcofluor white, and tolerance to high temperature, while *wsc1* is redundant in *A. fumigatus* (Dichtl et al., 2012). In contrast, *wsc1* deletion in *N. crassa* has confirmed its role in tolerance to cell wall perturbing agents Caspofungin and Calcofluor white (Maddi et al., 2012).

Extensive studies on the cell wall integrity MAP kinase pathway of *S. cerevisiae* have been able to functionally characterize many of the components involved. Since most of these proteins are conserved in other filamentous fungi, it is likely that it performs similar or related functions involved in protecting cell wall integrity in most species. Taking into consideration the extensive research carried out on the structure of Wsc1 and Mid2 proteins of *S. cerevisiae* and other filamentous fungi, it is clear that Wsc proteins sense the changes in the cell wall by acting as a probe or nanospring. Moreover studies on proteins downstream of the CWI MAP kinase pathway have proved their direct involvement in processes related to cell wall synthesis and cytoskeletal

organization. This implies that Wsc proteins could act as sensors to detect mechanical stress in the cell wall of filamentous fungi; however this is yet to be proven.

1.7 Hypotheses, aims and objectives

Two hypotheses were tested in this study:

1. Intercalary growth in *Epichloë festucae* would occur in response to mechanical stress caused by elongation of host cells to which hyphae are attached.
2. Mechanical stress is sensed via the mechanosensitive membrane proteins MidA and/or WscA which stimulate intercalary growth.

Aims and objectives

The above hypotheses were tested by undertaking the following aims and objectives.

- **Aim 1-** Identification and characterization of WscA and MidA of *E. festucae* and investigation of their role in intercalary growth. The following objectives were addressed under this aim.
 - a. To identify *E. festucae* orthologues of the *wsc1* and *mid1* genes of *S. cerevisiae*.
 - b. To determine the functional characteristics of WscA and MidA in axenic culture.
 - c. To investigate the role of MidA and WscA in host colonization and intercalary growth.
- **Aim 2-** Determining the distribution of calcium and the role of calcium signalling in *E. festucae* hyphal growth. The following objectives were addressed under this aim.
 - a. To optimise a technique to observe calcium distribution and signalling in growing *E. festucae* hyphae.
 - b. To determine calcium distribution and signalling during hyphal apical growth in axenic culture under various conditions.

- c. To determine the impact of deleting MidA (a stretch-activated calcium channel) on calcium distribution and signalling during hyphal apical growth and under mechanical stress.
- **Aim 3** – Investigating the ability of mechanical stretching to trigger intercalary growth in *E. festucae* hyphae under *in vitro* conditions. The following objectives were addressed under this aim.
 - a. To optimise a technique to mechanically stretch fungal hyphae under *in vitro* conditions.
 - b. To determine the pattern of compartmentalization (nuclear division and septation) in sub-apical compartments of *E. festucae* hyphae in axenic culture under un-stretched conditions.
 - c. To determine the effect of mechanical stretching on *E. festucae* hyphae.
 - d. To determine whether mechanical stretching triggers intercalary growth in *E. festucae* hyphae under *in vitro* conditions.

2. Materials and Methods

2.1 Biological material/ strains

Wild type *E. festucae* strain F11 was provided by AgResearch, Palmerston North New Zealand. All transformed strains in this study were created from this strain and a list of modified strains is provided in Table 2.1. All fungal strains were maintained on 2.4% Potato Dextrose Agar (PDA, Difco™, LePont De Claix, France) at 22°C.

For long term storage of cultures, a portion (approximately 50 mg of mycelia from the edge of colony) of an 8 day old colony growing on PDA medium was excised, homogenized with 1 mL of Potato Dextrose Broth (PDB, Difco™, LePont De Claix, France) and 500 µL of the homogenized culture was mixed with 500 µL of 60% (v/v) glycerol (99.5% AnalaR® grade, BDH, VWR International, Australia) and stored at -80°C.

Unless specified otherwise, *Escherichia coli* One Shot® TOP10 or *E. coli* Subcloning Efficiency™ DH5α™ (Invitrogen™, USA) cultures were used to amplify and maintain plasmids. For short term storage, *E. coli* strains were streaked onto Luria-Bertani Agar (LBA, Duchefa-biochemie, Haarlem, Nederland) plates and stored at 4°C after overnight incubation at 37°C. For long term storage, *E. coli* cultures were grown on LB at 37°C and 500 µL of the culture was mixed with 500 µL of 50% (v/v) glycerol and stored at -80°C. *E. coli* strains holding different plasmids created during this study, or obtained via collaborations, are listed in the Table 2.1.

Endophyte-free seeds of *Lolium perenne* L. accession A11104 were provided by AgResearch, Palmerston North, New Zealand, and stored at 4°C until required.

Table 2.1: Organisms and Plasmids used in this study.

Name	Genotype/Characteristics	Source/Reference
Plants		
<i>Lolium perenne</i> L.	Accession A11104	AgResearch
<i>E.festuca</i>		
F11	Wild type	AgResearch
Ef Δ wscA-5	F11/ Δ wscA::Pgpda-hph-TtrpC, Hyg ^R	This study
Ef Δ wscA-21	F11/ Δ wscA::Pgpda-hph-TtrpC, Hyg ^R	This study
Ef Δ wscA-36	F11/ Δ wscA::Pgpda-hph-TtrpC, Hyg ^R	This study
EfEct-8	F11::Pgpda-hph-TtrpC, Hyg ^R	This study
Ef Δ wscAcomp-2	Δ wscA/wscA::PtrpC-nptII-TtrpC, Hyg ^R , Gen ^R	This study
Ef Δ wscAcomp-18	Δ wscA/wscA::PtrpC-nptII-TtrpC, Hyg ^R , Gen ^R	This study
Ef Δ wscAcomp-24	Δ wscA/wscA::PtrpC-nptII-TtrpC, Hyg ^R , Gen ^R	This study
EfwscATEFEGFP-08	F11::Ptef-wscA-egfp-TtrpC::PtrpC-hph-TtrpC, Hyg ^R	This study
EfwscATEFEGFP-11	F11::Ptef-wscA-egfp-TtrpC::PtrpC-hph-TtrpC, Hyg ^R	This study
EfwscATEFEGFP-26	F11::Ptef-wscA-egfp-TtrpC::PtrpC-hph-TtrpC, Hyg ^R	This study
EfwscAEGFP-5	F11::PwscA-wscA-egfp-TtrpC::PtrpC-hph-TtrpC, Hyg ^R	This study
EfwscAEGFP-6	F11::PwscA-wscA-egfp-TtrpC::PtrpC-hph-TtrpC, Hyg ^R	This study
EfwscAEGFP-13	F11::PwscA-wscA-egfp-TtrpC::PtrpC-hph-TtrpC, Hyg ^R	This study
Ef Δ wscAwscATEFEGFP-24	Δ wscA::Ptef-wscA-egfp-TtrpC::PtrpC-nptII-TtrpC, Hyg ^R , Gen ^R	This study
Ef Δ wscAwscATEFEGFP-26	Δ wscA::Ptef-wscA-egfp-TtrpC::PtrpC-nptII-TtrpC, Hyg ^R , Gen ^R	This study
Ef Δ wscAwscATEFEGFP-32	Δ wscA::Ptef-wscA-egfp-TtrpC::PtrpC-nptII-TtrpC, Hyg ^R , Gen ^R	This study
Ef Δ wscAwscAEGFP-2	Δ wscA::PwscA-wscA-egfp-TtrpC::PtrpC-nptII-TtrpC, Hyg ^R , Gen ^R	This study
Ef Δ wscAwscAEGFP-15	Δ wscA::PwscA-wscA-egfp-TtrpC::PtrpC-nptII-TtrpC, Hyg ^R , Gen ^R	This study
Ef Δ wscAwscAEGFP-19	Δ wscA::PwscA-wscA-egfp-TtrpC::PtrpC-nptII-TtrpC, Hyg ^R , Gen ^R	This study
Ef Δ wscAEGFP-8	Δ wscA::Ptef-egfp-TtrpC::PtrpC-nptII-TtrpC, Hyg ^R , Gen ^R	This study
Ef Δ wscAEGFP-14	Δ wscA::Ptef-egfp-TtrpC::PtrpC-nptII-TtrpC, Hyg ^R , Gen ^R	This study
Ef Δ wscAEGFP-17	Δ wscA::Ptef-egfp-TtrpC::PtrpC-nptII-TtrpC, Hyg ^R , Gen ^R	This study
Ef Δ midA-20	F11/ Δ midA::Pgpda-hph-TtrpC, Hyg ^R	This study
Ef Δ midA-36	F11/ Δ midA::Pgpda-hph-TtrpC, Hyg ^R	This study
Ef Δ midA-43	F11/ Δ midA::Pgpda-hph-TtrpC, Hyg ^R	This study

EfEct-7	F11:: <i>PgpdA-hph-TtrpC</i> , Hyg ^R	This study
Ef Δ midAcomp-10	Δ midA/midA:: <i>PtrpC-nptII-TtrpC</i> , Hyg ^R , Gen ^R	This study
Ef Δ midAcomp-20	Δ midA/midA:: <i>PtrpC-nptII-TtrpC</i> , Hyg ^R , Gen ^R	This study
Ef Δ midAcomp-32	Δ midA/midA:: <i>PtrpC-nptII-TtrpC</i> , Hyg ^R , Gen ^R	This study
EfEGFP-7	F11:: <i>Ptef-egfp-TtrpC::PtrpC-nptII-TtrpC</i> , Hyg ^R , Gen ^R	This study
EfEGFP-11	F11:: <i>Ptef-egfp-TtrpC::PtrpC-nptII-TtrpC</i> , Hyg ^R , Gen ^R	This study
EfEGFP-12	F11:: <i>Ptef-egfp-TtrpC::PtrpC-nptII-TtrpC</i> , Hyg ^R , Gen ^R	This study
Ef Δ midAEGFP-2	Δ midA:: <i>Ptef-egfp-TtrpC::PtrpC-nptII-TtrpC</i> , Hyg ^R , Gen ^R	This study
Ef Δ midAEGFP-4	Δ midA:: <i>Ptef-egfp-TtrpC::PtrpC-nptII-TtrpC</i> , Hyg ^R , Gen ^R	This study
Ef Δ midAEGFP-11	Δ midA:: <i>Ptef-egfp-TtrpC::PtrpC-nptII-TtrpC</i> , Hyg ^R , Gen ^R	This study
EfGCaMP5 -4	F11:: <i>GCaMP5::PtrpC-hph-TtrpC</i> , Hyg ^R	This study
EfGCaMP5 -9	F11:: <i>GCaMP5::PtrpC-hph-TtrpC</i> , Hyg ^R	This study
EfGCaMP5-24	F11:: <i>GCaMP5::PtrpC-hph-TtrpC</i> , Hyg ^R	This study
Ef Δ midAGCaMP5-11	Δ midA:: <i>GCaMP5::PtrpC-nptII-TtrpC</i> , Gen ^R	This study
Ef Δ midAGCaMP5-16	Δ midA:: <i>GCaMP5::PtrpC-nptII-TtrpC</i> , Gen ^R	This study
Ef Δ midAGCaMP5-24	Δ midA:: <i>GCaMP5::PtrpC-nptII-TtrpC</i> , Gen ^R	This study
Ef Δ midAcompGCaMP5-17	Δ midA/midA:: <i>PtrpC-nptII-TtrpC::GCaMP5</i> , Hyg ^R , Gen ^R	This study
Ef Δ midAcompGCaMP5-23	Δ midA/midA:: <i>PtrpC-nptII-TtrpC::GCaMP5</i> , Hyg ^R , Gen ^R	This study
Ef Δ midAcompGCaMP5-11	Δ midA/midA:: <i>PtrpC-nptII-TtrpC::GCaMP5</i> , Hyg ^R , Gen ^R	This study
EfH2A-1	F11:: <i>PgpdA-hh2a-TtrpC::PtrpC-hph-TtrpC</i> , Hyg ^R	This study
EfH2A-7	F11:: <i>PgpdA-hh2a-TtrpC::PtrpC-hph-TtrpC</i> , Hyg ^R	This study
EfH2A-9	F11:: <i>PgpdA-hh2a-TtrpC::PtrpC-hph-TtrpC</i> , Hyg ^R	This study
Plasmids		
pPN1688	<i>PtrpC-hph-TtrpC</i> , Amp ^R , Hyg ^R	(Young et al. 2005)
pDONR-SML	Donor vector containing attP sites to clone attB flanked PCR products	Invitrogen™
pDONR-SMR	Donor vector containing attP sites to clone attB flanked PCR products, Kan ^R , Chlo ^R	Invitrogen™
pSAM1	Entry clone with 5' flank of <i>midA</i> and 5' region of <i>hph</i> , Kan ^R	This study
pSAM2	Entry clone with 3' flank of <i>midA</i> and 3' region of <i>hph</i> , Kan ^R	This study
pSAM3	Entry clone with 5' flank of <i>midA</i> and 5' region of <i>hph</i> , Kan ^R	This study
pSAM4	Entry clone with 3' flank of <i>midA</i> and 3' region of <i>hph</i> , Kan ^R	This study

pII99	<i>PtpC-nptII-TtrpC</i> , Amp ^R /Gen ^R	(Namiki et al. 2001)
pSAM5	pII99 with <i>midA</i> complementation fragment, <i>midA::PtpC-nptII-TtrpC</i> , Amp ^R /Gen ^R	This study
pSAM6	pII99 with <i>wscA</i> complementation fragment, <i>wscA::PtpC-nptII-TtrpC</i> , Amp ^R /Gen ^R	This study
pDONR/Zeo-1	Donor vector containing <i>attP</i> sites to clone <i>attB</i> flanked PCR products, Zeo ^R , Chlo ^R	Invitrogen™
pSAM7	Entry clone harbouring <i>PwscA:wscA</i> , Kan ^R	This study
pFPLGh	Destination vector with <i>attR</i> sites, <i>egfp:Ttrpc</i> , Kan ^R , Hyg ^R	(Gong et al. 2015), via Mark Farman lab
pSAM8	Expression vector with <i>PwscA:wscA:egfp</i> , Kan ^R , Hyg ^R	This study
pDONR221	Donor vector containing <i>attP</i> sites to clone <i>attB</i> flanked PCR products, Kan ^R	Invitrogen™
pSAM9	Entry vector harbouring <i>wscA</i> with <i>attL</i> sites, Kan ^R	This study
pDONR-TEF	Entry vector harbouring <i>tef2</i> promoter with <i>attR</i> sites, Kan ^R	AgResearch
pDONR-EGFP	Entry vector harbouring <i>egfp:Ttrpc</i> with <i>attR</i> and <i>attL</i> sites, Kan ^R	AgResearch
pDESTR3-R4	Destination vector with <i>attR</i> sites, Amp ^R	Invitrogen™
pSAM10	Expression vector with <i>Ptef:wscA:egfp</i> , Amp ^R	This study
pYH2A	<i>Pgpd:hh2A:eyfp:Ttrpc</i> , Hyg ^R	(Rech et al. 2007), via Prof. Kelly Craven lab
pTEFEGFP	<i>Ptef:egfp</i> , Amp ^R	(Vanden et al. 1997)
pAM13-9-GCaMP5	<i>Pgpd:GCaMP5-G</i> , Amp ^R , harbouring the Ca ²⁺ sensor GCaMP5	From Prof. Nick Read's lab

2.2 Media preparation

Unless specified otherwise all media were prepared using deionized water obtained using Milli-Q Integral Water Purification System (Merck Millipore, Darmstadt, Germany) and sterilized for 20 min at 120°C (Systec DX-65, Microbiology International, Maryland, USA).

2.2.1 Luria Bertani (LB) medium

LB liquid medium was prepared by dissolving 25 g of LB high salt (Duchefa-biochemie) in 1 L of water. For solid medium 15 g of agar (Difco™ Bacto® Agar, LePont De Claix, France) was added per 1 L of liquid medium.

2.2.2 Potato Dextrose (PD) medium

The PD liquid medium was prepared by dissolving 24 g of PD (Difco™) in 1 L of water, pH 6.5. For a solid medium, 39 g of PDA (Difco™) was added per 1 L of water.

2.2.3 Regeneration medium (RG)

The regeneration medium (RG) was comprised of 24 g of PD (Difco™) and 273.8 g of sucrose [0.8 M] (VWR International, England) dissolved in 1 L of water. The pH was adjusted to 6.5 with NaOH (2 M) or HCl (2 M). For an 0.8 % (w/v) RG medium, 8 g of agar (Difco™ Bacto® Agar, LePont De Claix, France) was added to 1 L of media prior to autoclaving, and for an 1.5% (w/v) of RG medium 15 g was added.

2.2.4 Water agar

Water agar was comprised of 4% (w/v) agar (25 g/L).

2.2.5 Antibiotic selection

When antibiotic selection was necessary, the medium was supplemented with the relevant antibiotics according to Table 2.2. For solid media, the temperature of the liquefied media was brought down to 50°C before adding the antibiotic, and the plates poured immediately.

Table 2.2: Antibiotic concentrations used for transformant selection.

Medium	Antibiotic	Selection	Concentration ($\mu\text{g}/\text{mL}$)
LB and LBA	Ampicillin (Gibco [®] , USA)	<i>E.coli</i> transformants	100
	Kanamycin (Gibco [®])	<i>E.coli</i> transformants	50
	Zeocin [™] (Gibco [®])	<i>E.coli</i> transformants	50
RG, PDA and PDB	HygromycinB (Gibco [®])	<i>E. festucae</i> transformants	100
	Geneticin [®] (Gibco [®])		200

2.3 Growth conditions

2.3.1 *Escherichia coli*

E. coli were grown at 37°C overnight on LB solid media (25 mL/plate), or in LB broth (5 mL) with 200 rpm shaking. For antibiotic selection ampicillin, kanamycin or zeocin[™] was used. See Table 2.2 for concentrations.

2.3.2 *Epichloë festucae*

Unless specified otherwise *E. festucae* strains were grown under continuous light on PDA at 22°C for 8 days or in PDB with 150 rpm shaking for 4 to 5 days. Subcultures were prepared by excising 2 mm² agar plugs from the leading edge of an 8 day old culture and inoculating fresh plates as required. When selection against antibiotic resistance was required, PDA was infused with geneticin or hygromycin (Table 2.2) and incubated as described above.

2.3.3 *Lolium perenne* L.

2.3.3.1 Surface sterilization of seeds

L. perenne L. seeds (Accession A11104) were immersed in 50% (v/v) sulphuric acid (BDH ARISTAR® PLUS, VWR International, England) for 15 min and washed thoroughly with water three times. The seeds were immersed in 10% (v/v) Janola (commercial disinfectant, NaOCl~5%) solution for 15 min and washed again thoroughly with sterile water three times under aseptic conditions. Washed seeds were dried on sterile Whatman paper for 3 h inside a laminar hood and stored under sterile conditions at room temperature (RT).

2.3.3.2 Seedling inoculation and plant growth conditions

Surface sterilised seeds were placed on 4% (w/v) water agar under aseptic conditions in two rows of 8 seeds per petri plate, with all seeds oriented in the same direction. Plates were placed upright (seed rachilla pointed down) and incubated at 22°C for 7 days under dark conditions (covered with aluminium foil). After one week the seedlings were inoculated *in situ* with the appropriate endophyte strain by making an incision into the shoot apical meristem (SAM) and inserting a trace amount of fungal hyphae into the wound site. After inoculation the plates were again placed upright and further incubated for one week at 22°C in the dark. Thereafter, the seedlings were incubated for one more week at 22°C under lights and transferred to plastic pots filled with standard potting mix for acclimatization in a glasshouse. After 6 weeks the plants were tested for the presence of the endophyte using a tissue print immunoassay (Section 2.10.1), and infected plants were transferred into pots (7.5 X 10 cm) with standard potting mix and grown under ambient conditions in a PC2 plant containment glasshouse.

To analyse endophyte colonization and its effect on plant phenotype, a randomised block design of eight treatments, each with three plant replicates was used, and seedlings were inoculated with each strain and acclimatized as described above. The randomised design was followed from the seedling stage in axenic culture to mature plants grown under glass house conditions. As a further control, seedlings taken through the inoculation process and subsequent plant growth, but not inoculated with endophytes, were also analysed.

2.4 DNA isolation and storage

2.4.1 Plasmid DNA isolation

E. coli bacterial broth cultures were grown overnight as described in Section 2.3.1. Depending on the quantity of plasmid DNA required, 1.5-3 mL of bacterial culture was used per cycle of extraction. Plasmid DNA extraction was performed through an alkaline lysis method using the Geneaid High-speed Plasmid Mini Kit (Geneaid Biotech Ltd, New Taipei City, Taiwan) according to the manufacturer's guidelines. Pre-heated elution buffer (50°C) was used to elute plasmid DNA from purification columns.

2.4.2 Isolation of high molecular weight genomic DNA from *E. festucae*

Fungal hyphae from the edge of an 8 day old colony was excised and homogenized in 1 mL of PDB using a bead basher (FastPrep[®]-24 homogenizer, MP Biomedicals, USA) for 10 seconds at 4 m/s. Approximately 300 µL of the homogenate was spread onto cellophane membranes placed onto PDA and grown for 4 to 5 days at 22°C. Thereafter, approximately 75 mg (wet weight) of the mycelial film on the cellophane membranes was homogenized into a fine powder with liquid N₂ using a mortar and pestle. The homogenate was then added to a sterile 1.5 mL tube (Eppendorf) and mixed with lysis buffer provided with the ZR Fungal/Bacterial DNA extraction kit (Zymo Research

Corporation, CA, USA). When higher DNA yields were necessary, the lysate was left at RT for 30 min with occasional mixing. Subsequent steps were performed using the ZR Fungal/Bacterial DNA extraction kit according to manufacturer's instructions.

2.4.3 Rapid isolation of genomic DNA from *E. festucae*

When small quantities with low molecular weight fungal genomic DNA was sufficient for analysis, rapid DNA extraction was performed using fungal mycelia taken directly from 8 day old colonies cultured on PDA plates. Hyphae (100 mg) from the edge of the colony was scraped off the plate, avoiding solid growth media as much as possible, and transferred to a ZR BashingBead™ lysis tube provided with the ZR Fungal/Bacterial DNA extraction kit (Zymo Research). Lysis solution (750 µL) was added and the mixture homogenized using a bead basher for 40 sec at 4 m/s. Thereafter, genomic DNA was extracted from the homogenate using the ZR Fungal/Bacterial DNA extraction kit according to the manufacturer's instructions.

2.4.4 DNA Storage

Genomic and plasmid DNA was stored at 4°C for short term storage (to be used within 24 h) or at -20°C for long term storage.

2.5 DNA manipulation

2.5.1 DNA quantification

The genomic or plasmid DNA concentration and purity was determined using a NanoDrop 2000 UV-Vis spectrophotometer according to the manufacturer's guidelines. Where greater accuracy was necessary, DNA concentration and purity was re-confirmed using the Invitrogen Qubit™ fluorometer (CA, USA). The quantification procedure was

performed at RT using 2-4 μL of the DNA sample using the appropriate Invitrogen Quant-iT™ assay kit and tubes according to the manufacturer's instructions.

2.5.2 DNA concentration

Where the rapid concentration of genomic or plasmid DNA from low volumes was required, the Thermo Scientific™ Savant™ SpeedVac™ (USA) system was used to remove excess water/solvent. Alternatively ethanol precipitation was used to concentrate larger volumes of genomic or plasmid DNA samples. To the DNA sample, 3 M NaOAc (pH 5) was added to a final concentration of 0.3 M, mixed thoroughly, and the DNA precipitated by the addition of 2.5 volumes of 95% (v/v) ethanol. After thorough mixing, the DNA was collected by centrifugation (10000 x g) at room temperature. The supernatant was discarded and the pellet washed with 1 mL of 70% (v/v) ethanol and re-centrifuged at RT at 10000 x g for 5 min. The supernatant discarded and the pellet was lightly dried in a Thermo Scientific™ Savant™ SpeedVac™ to remove residual ethanol. The pellet was re-dissolved in sterile water by incubation at 65°C for 20 min.

2.5.3 Agarose gel electrophoresis

Unless specified otherwise, 1% (w/v) agarose (UltraPure™, Invitrogen™) gels in Tris-acetate-EDTA buffer (TAE, refer to Appendix 1 for composition) were used for DNA electrophoresis. Ethidium bromide (UltraPure™, Invitrogen™) was added to the boiled and cooled agarose solution ($\sim 60^{\circ}\text{C}$) to achieve a final concentration of 1 $\mu\text{g}/\text{mL}$. DNA samples were mixed with a bromophenol blue, xylene cyanol-based loading dye (Appendix 1) and electrophoresed against a 1Kb plus DNA ladder (Invitrogen™) for 60 to 75 min between 80 to 100 volts in TAE buffer using a Bio-Rad gel electrophoresis apparatus (CA, USA) according to manufacturer's instructions. DNA was visualised

using a UV transilluminator gel documentation system (Gel Doc™, Bio-Rad, CA, USA).

2.5.4 DNA recovery from agarose gels

Gel electrophoresis was performed as described in Section 2.5.3 and the DNA visualised (using the preparative setting to avoid DNA shearing) using a Bio-Rad UV transilluminator 2000 (CA, USA). The agarose containing the DNA was excised using a scalpel blade, transferred to a 1.5 mL Eppendorf tube, and weighed. DNA extraction from the agar block was performed using the PureLink® Quick Gel Extraction Kit (Invitrogen™) according to manufacturer's instructions. After extraction the DNA was quantified and gel electrophoresis performed on a sub-sample to ascertain the integrity of the recovered product.

2.5.5 DNA sequencing

DNA sequencing was performed using the BigDye® Terminator v3.1 Cycle Sequencing Kit (Applied Biosystems, MA, USA). The cycle sequencing reactions were performed according to manufacturer's instructions in 10 µL of reaction volumes (Appendix 2). A template quantity of 20-50 ng (depending on the template size) for PCR products and 200-300 ng/reaction for plasmid DNA was used per reaction. Each DNA fragment was sequenced in both directions using forward and reverse primers for greater accuracy.

Cycle sequencing was performed over 25 cycles (Applied Biosystems, 2720 thermal cycler) according to manufacturer's instructions (PCR conditions Appendix 2) for BigDye® Terminator v3.1, and the DNA products purified using ethanol/EDTA precipitation according to manufacturer's instructions. The sequencing products were resuspended in 10 µL of Hi-Di™ Formamide (Applied Biosystems) diluted 5:1 with

25 mM EDTA pH 8.0 and heated at 95°C for 2 min. Capillary separation and detection was carried out in an ABI13730 genetic analyser (Applied Biosystems) or a 3130X genetic analyser (Applied Biosystems). Data analysis and sequence assembly were performed using Vector NTI® (Invitrogen™) software.

2.5.6 Restriction endonuclease digestion

Unless otherwise specified, restriction endonuclease (RE) digestion was performed at 37°C (Unitek HB-130 heat block) with 10 units of RE per 1 µg of DNA. Ten microliter reactions were used for DNA quantities ≤ 0.5 µg with an incubation time of 1 h, and 50 µL reactions with an incubation time of 3 h was used for DNA quantities ≥ 0.5 µg. The optimum reaction buffer was selected according to manufacturer's specifications and the most compatible buffer for both enzymes was selected when performing double digestions in one reaction. Reactions were terminated by heat inactivation according to manufacturer's specifications.

2.5.7 PCR amplification

2.5.7.1 Standard PCR

Platinum® Taq DNA Polymerase (Invitrogen™) was used for all standard PCR reactions in this study. A typical 50 µL reaction contained 5 µL of 10X PCR buffer (minus Mg²⁺), 0.6 µL of dNTP (25 mM), 1.5 µL of MgCl₂ (50 mM), 0.75 µL each of forward and reverse primers (10 µM), 10-20 ng of genomic DNA or 50 ng of plasmid DNA, 0.4 µL Platinum® Taq DNA polymerase (10 U/µL) and deionised water up to 50 µL. Cycle conditions were, 1 cycle at 94°C for 5 min, 30-35 cycles of 94°C for 30 sec, 53-58°C for 30 sec, 72°C for 1 min/1 Kb and final holding temperature of 4°C. Positive and negative controls were used with each set of PCR reactions.

2.5.7.2 High fidelity PCR

Platinum[®] Pfx DNA polymerase (Invitrogen[™]) with proof reading and 3' to 5' exonuclease activity was used for all high fidelity PCR reactions when greater accuracy in replication was crucial. A typical 50 μ L reaction contained 5 μ L of 10X Pfx amplification buffer (minus Mg²⁺), 0.6 μ L of dNTP (25 mM), 1.0 μ L of MgSO₄ (50 mM), 0.75 μ L each of forward and reverse primers (10 μ M), 10-20 ng of genomic DNA or 50 ng of plasmid DNA, 0.4 μ L Platinum[®] Pfx DNA polymerase (2.5 U/ μ L) and deionised water up to 50 μ L. Cycle conditions were, 1 cycle at 94°C for 5 min, 30-35 cycles of 94°C for 15 sec , 53-58°C for 30 sec , 68°C for 1 min/1 Kb and final holding temperature of 4°C. Positive and negative controls were used with each set of PCR reactions.

Table 2.3: Primers used in this study.

Name	Sequence (5'-3')	Used for
smid-1	GGGGACAAGTTTGTACAAAAA GCAGGCTTAAGGCTAGATAGAA TCGGCAGGAC	3' flank of <i>midA</i> deletion vector
smid-2	GGGGACCACTTTGTACAAGAAA GCTGGGTACGGTGGAGAATGCC AATGAG	3' flank of <i>midA</i> deletion vector
M13-F	GTAAAACGACGGCCAG	Sequencing pDONR vectors
M13-R	GAAACAGCTATGACCAT	Sequencing pDONR vectors
smid-3	GCAACCACCCACCAACACC	Sequencing 3' flank of <i>midA</i> deletion vector and synthesising southern blot - probe D
smid-4	GGTGTGGTGGGTGGTTGC	Sequencing 3' flank of <i>midA</i> deletion vector and screening <i>midA</i> complemented strains
smid-5	CCAACCTCAAGACGACCTTCC	Sequencing 3' flank of <i>midA</i> deletion vector
smid-6	GGAAGGTCGTCTTGAGGTTGG	Sequencing 3' flank of <i>midA</i> deletion vector and synthesising southern blot - probe D
smid-7	CCACCCACCAGCATCTTCC	Sequencing 3' flank of <i>midA</i> deletion vector
smid-8	GGAAGATGCTGGTGGGTGG	Sequencing 3' flank of <i>midA</i> deletion vector
smid-9	CTGCCATCTGCATCAAAGAG	Sequencing 3' flank of <i>midA</i> deletion vector
smid-10	CTCTTTGATGCAGATGGGCAG	Sequencing 3' flank of <i>midA</i> deletion vector
smid-11	CGTCTCTGTGCCCTCATTGG	Sequencing 3' flank of <i>midA</i> deletion vector

smid-12	CCAATGAGGGACACAGAGACG	Sequencing 3' flank of <i>midA</i> deletion vector
smid-13	GGGGACCACTTTGTACAAGAAA GCTGGGTAGTCGGGGCTTATGTG ATGGTC	5' flank of <i>midA</i> deletion vector
smid-14	GGGGACAAGTTTGTACAAAAAA GCAGGCTTAGGCAAGCTGCTAT GTCAATTTC	5' flank of <i>midA</i> deletion vector
smid-15	GTCAAAGCGTCCGTCAATGG	Sequencing 5' flank of <i>midA</i> deletion vector and complementation vector
smid-16	CCATTGACGGACGCTTTGAC	Sequencing 5' flank of <i>midA</i> deletion vector and complementation vector
smid-17	GAGCAATTCGGGACCACATTG	Sequencing 5' flank of <i>midA</i> deletion vector and complementation vector
smid-18	CAATGTGGTCCCGAATTGCTC	Sequencing 5' flank of <i>midA</i> deletion vector, complementation vector and screening <i>midA</i> complemented strains
smid-19	GGTGACAAGTTGAACTGATGC C	Sequencing 5' flank of <i>midA</i> deletion vector
smid-20	GGCATCAGTTTCAACTGTACC	Sequencing 5' flank of <i>midA</i> deletion vector
smid-21	TTAGACTAACCTAGGGTTAGCAC CATGTGACGGAAGTG	<i>midA</i> complementation vector
smid-22	ATACAGTAACTCGAGCGAGGTG AGCAACATGGTGG	<i>midA</i> complementation vector
smid-23	CCTCCTCACGTCCTCCACC	Sequencing <i>midA</i> complementation vector
smid-24	GGTGGAGGACGTGAGGAAGG	Sequencing <i>midA</i> complementation vector
smid-25	GGAAGGTGCAGTGAGGGTGAG	Sequencing <i>midA</i> complementation vector
smid-26	CTCACCTCACTGCACCTTCC	Sequencing <i>midA</i> complementation vector
smid-27	GGTGTCTCGTTCAGCCTGC	Sequencing <i>midA</i> complementation vector
smid-28	GCAGGCTGAACGAGGACACC	Sequencing <i>midA</i> complementation vector
smid-29	CCTAGATGGTTCAGCTTCAGC	Sequencing <i>midA</i> complementation vector
smid-30	GCTGAAGCGTGAACCATCTAGG	Sequencing <i>midA</i> complementation vector
smid-31	CAGGACCAGCGATGGGAATC	Sequencing <i>midA</i> complementation vector
smid-32	GATTCCCATCGCTGGTCCTG	Sequencing <i>midA</i> complementation vector
smid-33	GTAGGAGGGCGTGGATATGTCC	Screening gene replacement strains
smid-34	TTCTACACAGCCATCGGTCCAG	Screening gene replacement strains
smid-35	CCTGCCTCAACCTCTGCTGG	Screening <i>midA</i> replacement strains
smid-36	CACACGGCATTTCGTTTCATCC	Screening <i>midA</i> replacement strains
smid-37	GATTCCCATCGCTGGTCCTG	Screening <i>midA</i> replacement strains
smid-38	GCCTTGTCGAAGCTGATGAGC	Screening <i>midA</i> replacement strains
smid-39	TGCCATATTTCTGCTCTCCC	Southern blot - probe D
smid-40	TTCGGTTTCAGGCAGGTCTTG	Southern blot - probe D
swsc-1	GGGGACAAGTTTGTACAAAAAA GCAGGCTTACACACCCATCTCG GAAATACCC	3' flank of <i>wscA</i> deletion vector
swsc-2	GGGGACCACTTTGTACAAGAAA GCTGGGTAATAAAGAAGCGGGC AAATCGTC	3' flank of <i>wscA</i> deletion vector

swsc-3	CTCTCTCCCTCTTGACTCGGC	Sequencing 3' flank of <i>wscA</i> deletion vector, <i>wscA</i> complementation vector and synthesising southern blot - probe A
swsc-4	GCCGAGTCAAGAGGGAGAGAG	Sequencing 3' flank of <i>wscA</i> deletion vector and <i>wscA</i> complementation vector
swsc-5	GTGACCTTGGGCGATACTCTC	Sequencing 3' flank of <i>wscA</i> deletion vector and <i>wscA</i> complementation vector
swsc-6	GAGAGTATCGCCCAAGGTCAC	Sequencing 3' flank of <i>wscA</i> deletion vector, <i>wscA</i> complementation vector, screening <i>wscA</i> complemented strains and synthesising southern blot - probe A
swsc-7	GCATGATTAAGCCAAGAGCG	Sequencing 3' flank of <i>wscA</i> deletion vector
swsc-8	CGTCTTGGCTTAATCATGC	Sequencing 3' flank of <i>wscA</i> deletion vector
swsc-9	GGGGACAAGTTTGTACAAAAA GCAGGCTTAACGCAGCCAGTTT GAGAAACAG	5' flank of <i>wscA</i> deletion vector
swsc-10	GGGGACCACTTTGTACAAGAAA GCTGGGTAGTGGTGGTCAAATC GAGTACGG	5' flank of <i>wscA</i> deletion vector
swsc-11	CTCAAGATCGCTGCGTGTG	Sequencing 5' flank of <i>wscA</i> deletion vector, <i>wscA</i> complementation vector and <i>wscA:egfp</i> expression vector
swsc-12	CAACACGCAGCGATCTTGAG	Sequencing 5' flank of <i>wscA</i> deletion vector, <i>wscA</i> complementation vector, <i>wscA:egfp</i> expression vector and screening <i>wscA</i> complemented strains
swsc-13	CACCAAGCACACCACACAGC	Sequencing 5' flank of <i>wscA</i> deletion vector and <i>wscA</i> complementation vector
swsc-14	GCTGTGTGGTGTGCTTGGTG	Sequencing 5' flank of <i>wscA</i> deletion vector
swsc-15	GATTCACGATTCACGCAAGG	Sequencing 5' flank of <i>wscA</i> deletion vector
swsc-16	CCTTGCGTGAATCGTGAATC	Sequencing 5' flank of <i>wscA</i> deletion vector
swsc-17	CCAGGTTCTTCTTCCATGC	Sequencing 5' flank of <i>wscA</i> deletion vector
swsc-18	GCATGGAAGAAGGAACCTGG	Sequencing 5' flank of <i>wscA</i> deletion vector
swsc-19	CGTTGACTTGCCAGATGAC	Sequencing 5' flank of <i>wscA</i> deletion vector
swsc-20	GTCATCTGGGCAAGTCAACG	Sequencing 5' flank of <i>wscA</i> deletion vector
swsc-21	TTAGACTATTCTAGATGTGGTGT GCTTGGTGGTGTG	<i>wscA</i> complementation vector
swsc-22	TAACATAAGAAGCTTGAGAGTA TCGCCAAGGTCACC	<i>wscA</i> complementation vector
swsc-22	CAAACAACCCGCCCTTCAG	Sequencing <i>midA</i> complementation vector and <i>wscA:egfp</i> and pTEF: <i>wscA:egfp</i> expression vector
swsc-23	CTGAAGGGCGGGTTGTTG	Sequencing <i>midA</i> complementation vector and <i>wscA:egfp</i> and pTEF: <i>wscA:egfp</i> expression vector

swsc-24	CCACAGCAACAACAACAACG	Sequencing <i>midA</i> complementation vector and <i>wscA:egfp</i> and pTEF: <i>wscA:egfp</i> expression vector
swsc-25	CGTTGTTGTTGTTGCTGTGG	Sequencing <i>midA</i> complementation vector and <i>wscA:egfp</i> and pTEF: <i>wscA:egfp</i> expression vector
swsc-26	CAGTGTCGCCATCATTGTC	Sequencing <i>midA</i> complementation vector and <i>wscA:egfp</i> and pTEF: <i>wscA:egfp</i> expression vector
swsc-28	GACAATGATGGCGGACACTG	Sequencing <i>midA</i> complementation vector and <i>wscA:egfp</i> and pTEF: <i>wscA:egfp</i> expression vector
swsc-27	GTAGGAGGGCGTGGATATGTCC	Screening gene replacement strains
swsc-29	AGCGTGCCTTGAGAATGATACG	Screening <i>wscA</i> replacement strains
swsc-30	GCCTCTCCCGACTATCCTCAG	Screening <i>wscA</i> replacement strains
swsc-31	CCTGATAACGCCTTGAATGCC	Screening <i>wscA</i> replacement strains
swsc-32	TGAGCTGTGTCGAGCCATG	Screening <i>wscA</i> replacement strains
swsc-33	CAAGGTCGTTGCGTCAGTCC	Southern blot - probe B
swsc-34	GCAAAGTGCCGATAAACATAAC G	Southern blot - probe B
swsc-35	AAAAAGCAGGCTTATGCGATGC TATGGATTAGTTGGC	<i>wscA:egfp</i> expression vector
swsc-36	AGAAAGCTGGGTACGCATTGGT GACCTGCAGAAG	<i>wscA:egfp</i> expression vector
swsc-37	GGGACAAGTTTGTACAAAAAA GCAGGCTNN	<i>wscA:egfp</i> expression vector
swsc-38	GGGACCACTTTGTACAAGAAA GCTGGGTN	<i>wscA:egfp</i> expression vector
swsc-39	GGGACAAGTTTGTACAAAAAA GCAGGCTTAATGAGATTATCAA CAATCGCATTGG	pTEF: <i>wscA:egfp</i> expression vector
swsc-40	GGGACCACTTTGTACAAGAAA GCTGGGTACGCATTGGTGACCTG CAGAAG	pTEF: <i>wscA:egfp</i> expression vector

2.5.8 Ligation

The ligation of inserts into vectors was performed using T4 DNA ligase (Roche Applied Sciences). Two different RE sites were used for each insert and vector to achieve directional ligation. A typical 30 μ L ligation reaction comprised the vector and insert in a 2:1 molar ratio, 10X ligation buffer (3 μ L), 2 μ L of T4 DNA ligase (1 U/ μ L) and

deionised water. The reaction was incubated at 16°C overnight and 4 µL was used for *E. coli* transformation (see Section 2.6.1).

2.6 Transformation

2.6.1 *E. coli* transformation

One Shot[®] TOP10 chemically competent cells (Invitrogen[™]) or Subcloning Efficiency[™] DH5 α [™] (Invitrogen[™]) were used for plasmid transformation and propagation in this study. One Shot[®] *ccdB* Survival[™] 2 T1^R Chemically Competent Cells were used to transform and propagate unmodified Gateway[®] destination and donor vectors plasmids containing the lethal *ccdB* gene used for negative selection in Gateway recombination. Cells were subjected to heat shock transformation according manufacturer's instructions with pUC19 (Invitrogen[™]) used as the positive control. Transformed cells were spread onto pre-warmed LBA supplemented with the appropriate antibiotic and incubated overnight. Resistant colonies were streaked for single cells on the same medium and single colonies were transferred to LB liquid culture prior to plasmid extraction as described above (Section 2.4.1).

2.6.2 *E. festucae* protoplast preparation

E. festucae protoplast preparation was carried out based on the method described by Young et al., (Young et al., 1998). The *E. festucae* strain was cultured on cellophane membranes as described in Section 2.4.2. After 4-5 days of growth, fresh mycelia were scraped off the cellophane membrane and macerated in 1 mL of PDB using a high speed cell disrupter at 4 m/s for 30 seconds (FastPrep[®]-24 homogenizer, MP Biomedicals, CA, USA). A further 500 µL of PDB was added to the macerate, mixed, and 200 µL was used to inoculate each 250 mL flask containing 50 mL of PDB (8 flasks). The cultures were incubated at 100 rpm on an orbital shaker at 22°C for 4 days. Mycelia

from all 8 flasks were harvested by filtration through 2 layers of 3M Whatman filter papers in a Buchner funnel, and washed with 1 L of sterile water followed by a few millilitres of OM buffer (Appendix 1). Thereafter, mycelia were scraped off the filter paper and added to a flask containing 15 mg/mL of lysis enzyme (Sigma, MO, USA, Lysing Enzymes from *Trichoderma harzianum*, L1412) in 30 mL of OM buffer for digestion. The flasks were incubated for 4-5 hours at 30°C at 100 rpm on an orbital shaker. The resulting protoplasts were harvested by filtration through 2 layers of Miracloth (Calbiochem[®], EMD MILLIPORE, MA, USA) into 15 mL falcon tubes (about 5 mL each). The filtrates containing the protoplasts were overlaid carefully with 2 mL of ST buffer (Appendix 1) and centrifuged at 1008 x g for 15 min. Protoplasts at the interface between the ST buffer and lysis enzyme solution were harvested (using a cut pipette tip) and placed into fresh 15 mL Falcon tubes. Thereafter 10 mL of STC buffer (Appendix 1) was added and the protoplasts collected by centrifugation at 1575 x g for 5 min. The pellet was washed twice with 5 mL of STC buffer, centrifuged at 1575 x g and the washed pellet resuspended in 500 µL of STC buffer. The protoplast concentration was calculated using a haemocytometer and the protoplasts diluted to achieve a final concentration of approximately 1.25×10^8 protoplasts/mL. For long term storage, 80 µL of protoplast suspension was mixed with 20 µL of 40% (w/v) PEG 4000 and stored at -80°C.

2.6.3 Transformation of *E. festucae* protoplasts

The method used for transformation was adapted from two previous methods used for transformation of *Fulvia fulva* (Oliver et al., 1987) and *Neurospora crassa* (Vollmer et al., 1986). Freshly prepared protoplasts (80 µL of 1.25×10^8 protoplast/mL) were used to transform *E. festucae* with the linearised (RE digested) gene deletion or expression

vectors described below. For gene deletions, the entire coding region of the gene was replaced with an expression cassette harbouring the *hph* gene (for hygromycin B resistance).

To the protoplast solution 20 μL of 40% (w/v) PEG 4000 was added followed by 2 μL of 50 mM spermidine (Sigma) and 5 μL of 5 mg/mL in STC heparin. After mixing gently, approximately 5 μg of plasmid DNA from each vector was added and mixed gently. The vectors were linearized by restriction digestion and gel purified in advance to achieve higher transformation rates. Thereafter the protoplasts were incubated on ice for 30 min. A further 900 μL of 40% (w/v) PEG 4000 solution was added and incubated at room temperature for 20 min. The transformed protoplasts were plated on 1.5% regeneration media (Section 2.2.3) by overlaying 200 μL of transformed protoplast solution mixed with 4 mL of molten 0.8% regeneration media (Section 2.2.3) at 50°C. The plates were incubated at 22°C overnight. After the overnight incubation, plates were overlaid with 4 mL of 0.8% regeneration media at 50°C containing the appropriate antibiotic for positive selection (Table 2.2). The overlaid plates were incubated at 22°C for 15-20 days. At the end of the incubation period, colonies with antibiotic resistance were selected for nuclear purification by three rounds of sub-culturing to obtain homogeneous colonies (Section 2.8). Plasmid pPN1688 (Young et al., 2005), which contains a hygromycin resistance gene, was used as the positive control, and water was used for the negative control. To determine the viability of the protoplasts, concentrations ranging from 10^2 to 10^4 protoplast/ mL in STC buffer were prepared and 100 μL of each dilution was mixed with 4 mL of 0.8% molten regeneration media and poured on to 1% regeneration media plates. Protoplast viability was calculated by counting the number of live colonies from each dilution.

2.7 Plasmid Construction

2.7.1 Overview of the Gateway cloning system

The MultiSite Gateway[®] Three-Fragment Vector Construction Kit (Invitrogen[™]) was used to create the deletion, EGFP expression vectors used in this study. Gateway cloning is based on recombination between phage and *E. coli* DNA via specific recombination sequences denoted as *att* sites (Landy, 1989; Hartley et al., 2000). Recombination occurs between different compatible *att* sites enabling the efficient transfer of DNA between plasmids. In the Gateway cloning system, PCR fragments created with primers flanked with *attB* sites are recombined into donor vectors containing compatible *attP* sites to create entry clones with the desired DNA inserts via a BP reaction catalysed by BP Clonase[™]. Thereafter the three entry vectors are recombined with a destination vector in a single LR reaction catalysed by LR Clonase[™] enzyme mix to create an expression vector containing the three elements within the *att* sites of the entry clones, in the desired order, and in frame if required.

BP recombination reactions were performed by adding equimolar concentrations (10 fmole) of purified *attB*-flanked PCR product and the pDONR[™] vector (50 fmoles each), 2 μ L of BP Clonase[™] II enzyme and TE buffer pH 8.0 (Appendix 1) in 10 μ L reactions, and incubated overnight at 25°C on a heat block according to the manufacturer's instructions. The reaction was terminated by using 1 μ L of Proteinase K, and 3-4 μ L of the reaction mix was used to transform *E. coli* (One Shot[®] TOP10 or DH5 α [™]) list strain used) as described in Section 2.6.1.

LR recombination reactions were performed by combining equimolar concentrations of each entry clone (10 fmole), and 20 fmoles of destination vector (pDEST[™] R4-R3 vector II), 2 μ L of LR Clonase[™] II plus enzyme and TE buffer (pH 8.0, Appendix 1) in

a 10 μ L reaction mix, and incubated at 25°C overnight according to manufacturer's instructions. The reaction was terminated by adding 1 μ L of Proteinase K and incubating for 10 min at 37°C, and 4 μ L was used for *E. coli* (One Shot[®] TOP10 or DH5 α [™]) transformation.

2.7.2 Construction of *E. festucae* gene replacement vectors

2.7.2.1 Overview

Replacement vectors pSAM1, pSAM2, pSAM3 and pSAM4 (Section 2.7.2.2 and 2.7.2.3) were constructed using the split marker strategy (Fairhead et al., 1996), based on homologous recombination using MultiSite Gateway[®] technology (Invitrogen), to generate vectors able to replace the entire coding region of the target gene. Primers specific to the 5' and 3' flanking regions of the *E. festucae* target gene were designed, and PCR amplified using high fidelity Platinum[®] Pfx DNA polymerase (Invitrogen[™]). PCR conditions were as described in Section 2.5.7.2. The purified PCR products (Section 2.5.4) were cloned into donor vectors pDONR-SML and pDONR-SMR (Invitrogen[™], Appendix 3, Fig 8.1) via a BP recombination (Section 2.7.1) and transformed into Invitrogen One Shot[®] TOP10 cells (Section 2.6.1). Plasmid extraction and restriction digestions (Section 2.4.1 and 2.5.6) were performed followed by sequencing (Section 2.5.5) to confirm the correct clone. Replacement vectors were linearised with NotI RE digestion before *E. festucae* protoplast transformation.

2.7.2.2 Construction of *midA* replacement vectors

The *midA* left and right replacement vectors (pSAM1 and pSAM2) were constructed according to the procedure described above (Section 2.7.2.1). Primer pairs smid-13/smid-14 and smid-1/smid-2 (Table 2.3) were used to amplify the 5' flank (1.5 kb) and 3' flank (2.5 kb) respectively. The left flank was recombined into pDONR-SML to

generate plasmid pSAM1 (Appendix 3, Figure 8.2) and the right flank was recombined to pDONR-SMR to generate plasmid pSAM2 (Appendix 3, Figure 8.2). Plasmid pSAM1 was RE digested with Sal1 (Appendix 3, Figure 8.2) and sequenced with primers M13-F, M13-R, smid-15, smid-16, smid-17, smid-18, smid-19 and smid-20 (Table 2.3). Plasmid pSAM2 was digested with Pst1 and Xba1 (Appendix 3, Figure 8.2) and sequenced with primers M13-F, M13-R, smid-3, smid-4, smid-5, smid-6, smid-7, smid-8, smid-9, smid-10, smid-11 and smid-12 (Table 2.3).

2.7.2.3 Construction of *wscA* replacement vectors

The *wscA* replacement vectors (pSAM3 and pSAM4) were constructed according to the procedure described in Section 2.7.2.1. Primer pairs swsc-9/swsc-10 and swsc-1/swsc-2 (Table 2.3) were used to amplify the 5' flank (1.5 kb) and 3' flank (2.5 kb) respectively. The left flank was cloned to pDONR-SML to generate plasmid pSAM3 (Appendix 3, Figure 8.3) and the right flank was cloned to pDONR-SMR to generate plasmid pSAM4 (Appendix 3, Figure 8.3). Plasmid pSAM3 was RE digested with Pst1 and Xho1 (Appendix 3, Figure 8.3) and sequenced with primers M13-F, M13-R, swsc-11, swsc-12, swsc-13, swsc-14, swsc-15, swsc-16, swsc-17, swsc-18, swsc-19 and swsc-20 (Table 2.3). Plasmid pSAM3 was digested with Pst1 and Xba1 (Appendix 3, Figure 8.3) and sequenced with primers M13-F, M13-R, swsc-3, swsc-4, swsc-5, swsc-6, swsc-7 and swsc-8 (Table 2.3).

2.7.3 *E. festucae* complementation vector construction to complement $\Delta midA$ and $\Delta wscA$

2.7.3.1 Overview

To generate the complementation vectors a fragment that spans upstream and downstream of the target gene coding region was generated by high fidelity PCR

(Section 2.5.7.2) using forward and reverse primers with restriction sites for AvrII and XhoI respectively. The PCR product was purified via gel purification and quantified (Sections 2.5.4 and 2.5.1). The purified product was double digested with AvrII and XhoI (Section 2.5.6) to generate the insert and gel purified and quantified again. The insert was ligated to the restriction digested (with XbaI and XhoI) and purified vector pII99 (Appendix 3, Figure 8.4) (Namiki et al., 2001). Thereafter the clones were transformed into Invitrogen DH5 α TM *E. coli* (Section 2.5.1). Plasmid extraction, restriction digestions and sequencing (Sections 2.5.6 and 2.5.5) were performed to confirm the vectors were constructed as planned.

2.7.3.2 Construction of *midA* complementation vector

To construct the *midA* complementation vector (according to Section 2.7.3.1), a 3716 bp DNA fragment that spans the region 989 bp upstream and 722 bp downstream of the *midA* coding region was amplified using primer pair smid-21/smid-22 (Table 2.3) and ligated into vector pII99 to generate the complementation vector pSAM5 (Appendix 3, Figure 8.5). Plasmid pSAM5 was RE digested with EcoRI and HindIII (Appendix 3, Figure 8.5) and sequenced with primers smid15, smid16, smid17, smid18, smid23, smid24, smid25, smid26, smid27, smid28, smid29, smid30, smid31 and smid32 (Table 2.3).

2.7.3.3 Construction of *wscA* complementation vector

To generate the *wscA* complementation construct (according to Section 2.7.3.1), a 2622 bp fragment that spans the region 837 bp upstream and 879 bp downstream of the *wscA* coding region was generated using primer pair swsc-21/swsc-22 (Table 2.3) and ligated into vector pII99 to generate the complementation vector pSAM6 (Appendix 3, Figure 8.6). Plasmid pSAM6 was RE digested with EcoRI and XbaI (Appendix 3,

Figure 8.6) and sequenced with primers swsc-22, swsc-23, swsc-24, swsc-25, swsc-26, swsc-27, swsc-3, swsc-4, swsc-5 and swsc-6 (Table 2.3).

2.7.4 *E. festucae* expression vector construction

MultiSite Gateway[®] technology (Invitrogen, Section 2.7.1), was used to generate expression vectors with either the native promoter (Section 2.7.4.1) of the target gene or a constitutive promoter (Section 2.7.4.2).

2.7.4.1 Construction of the *wscA:egfp* expression vector with the native promoter

Expression constructs with the native promoter were created by in-frame fusion of EGFP to the C terminal of the gene of interest with its native promoter. A fragment harbouring the entire coding region of the target gene (excluding the stop codon) and 989 bp upstream of the coding was generated by high fidelity PCR (Section 2.5.7.2) using primer pair swsc-35/swsc-36 (Table 2.3) with half *attB* site adaptors. The PCR product was gel purified (Section 2.5.4) and high fidelity PCR amplified using full *attB* adaptors (primer pair swsc-37/swsc-38, Table 2.3) as primers to generate the full *attB* PCR product. The resulting PCR product was gel purified again and cloned into vector pDONR-Zeo (Invitrogen[™], Appendix 3, Figure 8.7) via BP recombination (Section 2.7.1) to generate the vector pSAM7 (Appendix 3, Figure 8.8). The clones were transformed into Invitrogen One Shot[®] TOP10 cells (Section 2.6.1), plasmid extracted (Section 2.4.1) and digested with REs EcoRI and NcoI (Section, Appendix 3, Figure 8.8) to confirm the correct clone. The pSAM7 vector was then recombined into the destination vector pFPLGh (Appendix 3, Figure 8.9, contains the EGFP coding region and hygromycin resistant gene) (Gong et al., 2015) via LR recombination (Section 2.7.1) to generate the expression clone pSAM8 (Appendix 3, Figure 8.10). The clones were transformed into Invitrogen One Shot[®] TOP10 cells followed by plasmid

extraction, restriction digestion with EcoRI and sequencing with primers M13-F, M13-R, swsc-11, swsc-12, swsc-22, swsc-23, swsc-24, swsc-25, swsc-26 and swsc-27 (Table 2.3).

2.7.4.2 Construction of *Ptef:wscA:egfp* expression vector

To generate *Ptef:wscA:egfp* construct, the open reading frame (ORF) of the *wscA* gene (without the stop codon) was PCR amplified with a high fidelity polymerase (Section 2.5.7.2) using the primer pair swsc-39/swsc-40 flanked with *attB1* and *attB2* sites (Table 2.3). The PCR product was gel purified and recombined into pDONRTM 221 (Appendix 3, Figure 8.11) using BP Clonase II (Section 2.7.1) to create the entry clone pSAM9 (Appendix 3, Figure 8.12). The entry clone was confirmed by RE digestion with EcoRI and EcorV (Appendix 3, Figure 8.12) and sequenced using primers M13-F, M13-R, swsc-22, swsc-23, swsc-24, swsc-25, swsc-26 and swsc-27 (Table 2.3). The 5' and 3' Gateway Multisite entry clones were available in the laboratory from a previous study (unpublished). The 5' entry clone, pDONR-TEF (Appendix 3, Figure 8.13) contained the *tef2* promoter from *Aureobasidium pullulans* (Vanden et al., 1997) and the 3' entry clone, pDONR-EGFP (Appendix 3, Figure 8.14) contained the EGFP open reading frame (including stop codon) in donor vectors pDONRTM P4-P1R (InvitrogenTM) and pDONRTM P2R-P3 (InvitrogenTM) respectively. The three entry clones were recombined into destination vector pDEST R3-R4 (InvitrogenTM) using LR Clonase plus (Section 2.7.1) to create expression vector pSAM10 (Appendix 3, Figure 8.15). The expression clones were transformed into Invitrogen One Shot[®] TOP10 cells, followed by plasmid extraction, restriction digestion with HindIII and ApaLI (Appendix 3, Figure 8.15) to confirm the correct clone.

2.8 Purification of *E. festucae* F11 transformants

The apex of an individual hypha from each colony was sub-cultured serially 3 times on PDA containing the relevant antibiotic to obtain genetically homogenous colonies. When *E. festucae* protoplasts were transformed with fluorescent fusion proteins, putative transformants were analysed by epifluorescence microscopy using an Olympus BX50 microscope, and independent purified transformants expressing the fusion proteins at the appropriate level were selected at each round of sub culturing.

2.9 Southern blotting

To screen gene replacement strains, *E. festucae* wild type, four putative mutants (already confirmed by PCR) and an ectopic strain were subjected to Southern blot analysis. Approximately 3.5 µg of genomic DNA from each strain was digested overnight with the relevant RE enzymes in 50 µL reactions (see Appendix 2 for reaction conditions). In independent reactions, EcoRI and PstI were used to characterise *midA* replacement strains, and for *wscA* replacement strains RE enzymes HindIII and EcoRI were used. Agarose gel electrophoresis (Section 2.5.3) was conducted subsequent to digestion, using approximately 100 ng of digested DNA from each reaction to ascertain complete digestion. Thereafter digested genomic DNA of each strain was separated on a 0.8% agarose gel in TAE buffer overnight (16 h) at 40 volts. After obtaining the necessary gel photographs along with the DNA ladder, separated DNA was transferred onto a nylon membrane using the Invitrogen iBlot[®] Dry Blotting System apparatus according to manufacturer's instructions. The nylon membrane was infused with a solution containing NaCl (1.5 M) and NaOH (0.5 M) for 10 min to denature the DNA which was then cross-linked to the nylon membrane using the Statagene UV stratalinker 1800.

Two probes were designed for each gene replacement analysis. For *wscA* gene replacement analysis, probe A was generated using primer pair swsc-3/swsc-6 (Table 2.3) and probe B using primer pair swsc-33/ swsc-34 (Table 2.3). Similarly for *midA* gene replacement analysis, probe C was generated using primer pair smid-3/ smid-6 (Table 2.3) and probe D using primer pair smid-39/smid-40 (Table 2.3). The probes were synthesized and tested using a PCR DIG Probe Synthesis Kit (Roche) according to the protocol provided. Each probe was incubated independently with the hybridisation membranes. Pre-hybridization was carried out using DIG Easy Hyb solution (Roche) at 42°C for 1 h. This was followed by hybridization using Roche DIG Easy Hyb solution containing the relevant DIG-labelled denatured probe (2 µL of PCR-labelled probe per 1 mL of hybridization buffer) at 42°C overnight. Pre-hybridization and hybridizations were carried out in a Thermo Hybaid Maxi14 hybridization chamber. Low stringency washing was carried out using 2x SSC, 0.1% (w/v) SDS (Appendix 1) followed by high stringency washing with 0.5x SSC, 0.1% SDS (Appendix 1) at 68°C for 30 min. Hybridised probe was detected using the chemiluminescent substrate for alkaline phosphatase, CDP-Star (Roche) according to the manufacturer's instructions. The membrane was then exposed to X-ray film for between 2 and 20 min until optimal resolution had been achieved. The sizes of the luminescent DNA fragments were estimated using the 1 Kb+ DNA ladder (Invitrogen™) from the same gel.

2.10 Endophyte colonization in plants

2.10.1 Endophyte detection in plants by tissue print immunoassay

Plants were assayed for the presence of endophyte when inoculated seedlings were approximately 7 weeks old (6 weeks post inoculation). Three tillers from each plant were tested for endophyte by tissue print immuno-assay using an *Epichloë*-specific

polyclonal anti-serum method (Hahn et al., 2003). Tillers were transversely excised 5 mm from the crown of the plant, dead tissues were removed, and the cut end blotted directly onto nitrocellulose membrane (NCM, 0.45 mm). Known endophyte positive and negative tillers were used as positive and negative controls whenever possible. NCMs were immersed in a solution of non-fat milk powder blocking solution for 2 h at RT while shaking. Blocking solution (BS) was decanted and the membranes washed twice with BS, and immersed again in 25 mL of BS containing 1:1000 diluted primary antibody (specific to *Epichloë* endophytes). The membranes were incubated at room temperature for 15 min with shaking, followed by incubation at 4°C overnight. The primary antibody solution was decanted and the membranes washed twice with BS before immersion in 25 mL of BS solution containing the secondary antibody (1:4000 dilution, goat anti-rabbit IgG-AP, Santa Cruz Biotechnology, USA). The membranes were incubated at room temperature for 15 min followed by a further incubation at 4°C for 5 h. The membrane was twice rinsed with BS and then immersed in the chromogen with shaking for 15 min until development was complete. Further development was halted by rinsing the membrane in reverse osmosis (RO) water.

2.10.2 Endophyte detection in plants via aniline blue staining

Epidermal peels were taken from the abaxial surface of a mature leaf sheath and immersed in a drop of aniline blue (0.05% [w/v] aniline blue in lactic acid/glycerol/water 1:2:1) on a glass slide, a cover slip was placed on top and the slide was heated for few seconds by holding it over a small flame to remove air bubbles and facilitate stain penetration. The stained tissue samples were observed using a light microscope (Olympus BX50, Section 2.12.2).

2.11 Staining techniques

2.11.1 Calcofluor White staining

Fungal hyphae were stained with Calcofluor White (Sigma), which binds chitin, a component of the fungal cell wall (Elorza et al., 1983), to visualise cell walls and septa using fluorescence microscopy. To stain hyphae, a square block of the culture was immersed in a solution of Calcofluor White (25 μ M) for 2 min. Thereafter the block was rinsed with water and mounted on a slide for microscopy. For time lapse live imaging of cell wall and septa formation, the block of agar with hyphae was mounted and retained on a diluted solution of Calcofluor White (4 μ M) prepared with half strength PDB. Low concentrations of CW minimise the effect of CW on cell wall fidelity (Hickey et al., 2005).

2.11.2 FM4-64 staining

FMTM 4-64 (Invitrogen, Molecular Probes[®]) fluoresces intensely upon binding to the outer layer of the plasma membrane and thus acts as a vital stain to visualise plasma membranes. Fungal hyphae were stained with FMTM 4-64 by immersing a square block of agar with hyphae (or on silicon membrane) in a solution of FMTM 4-64 (2 μ g/mL in water) on ice for 2 min and immediately mounting on a cover slip for confocal microscopy (Section 2.12.3). Microscopy was performed within 20 min before the stain permeated the cells via endocytosis.

2.12 Microscopy

2.12.1 Obtaining leaf and tiller tissue samples for microscopy

Longitudinal sections (4 mm x 10 mm) of whole leaf tissue from different parts of the grass tiller were obtained by dissecting the tiller under a dissecting microscope. To

obtain transverse sections and longitudinal sections across the meristematic region, tillers were embedded in melted 4% (w/v) agarose. The embedded tillers were dissected manually in the appropriate orientation using a blade to obtain transverse or longitudinal sections across the shoot meristematic zone manually using a blade. All sections were mounted in water for confocal microscopy analysis.

2.12.2 Light, DIC and fluorescence microscopy

Light, differential interference contrast (DIC) and fluorescence microscopy was conducted using an Olympus BX50 epifluorescence light microscope (Olympus UPlan F1 10X, 20X objectives and Olympus UPlanFL N 40X objective) and images were taken using a fitted Olympus Colourview III soft imaging system digital camera. DIC images were taken using an Olympus-HGLGP5 DIC filter. The images were analysed and processed further using Olympus AnalysisB software.

2.12.3 Confocal laser scanning microscopy

Confocal microscopy was conducted using an Olympus Fluoview FV10i-LIV self-contained confocal laser scanning microscope. Two dimensional, Z-stack and time lapse images were taken using 10X (numerical aperture 0.4, equivalent to UPLSAPO 10X) or 60X (numerical aperture 1.2, equivalent to UPLSAPO 60X) phase contrast objectives. The microscope was operated according to manufacturer's instructions and the laser output, photomultiplier sensitivity, numerical aperture, scanning speed and image resolution were adjusted accordingly. When comparisons between images were necessary these parameters were kept constant between images. Images were analysed and processed using Olympus confocal software FV10-ASWRS. For visualising EGFP and YFP emission was detected at 490-540 nm (excitation 473 nm), Calcofluor White at 420-460 nm (excitation 405 nm) and FM™ 4-64 at 570-670 nm (excitation 473 nm). To

visualise EGFP labelled endophyte hyphae within plant tissues an image resolution of 1024*1025 pixels, numerical aperture of 2.5, laser transmissivity of 40% and laser sensitivity of 54.5% were used for all imaging. To image EGFP tagged wscA localization, an image resolution of 1024*1024 pixels, numerical aperture 2.5, laser transmissivity of 45% and laser strength of 40% were used.

2.12.3.1 Calcium imaging using confocal laser scanning microscopy

To investigate Ca^{2+} distribution in *E. festucae* (expressing GCaMP5 Ca^{2+} sensor) growing in culture, strains were cultured on PDA for 8 days at 22°C. For confocal laser scanning microscopy, a square block of medium (1 cm²) from the edge of the culture was inverted onto half-strength PDB (500 µL) on a cover glass (24X60, thickness-0.13 to 0.17mm). Time lapse imaging was performed using the 60X water-based objective with excitation and emission wavelengths of 473 and 490-540 nm respectively. For all imaging, the numerical aperture was maintained at 2.5, laser strength at 45%, sensitivity at 54.5%, resolution at 512 x 512 and scanning speed at 2 sec 274 ms per frame. Parameters were set to minimise photobleaching. A low resolution had to be maintained to perform high speed scanning to capture rapid changes in fluorescence. Images were acquired simultaneously from two channels, EGFP and phase contrast. Fluorescence intensity with time graphs was obtained using the Olympus confocal software FV10-ASWRS after background subtraction.

2.12.3.2 Visualising nuclear tagged hyphae using confocal laser scanning microscopy

Agar blocks (1 cm²) containing nuclear tagged hyphae (transformed with pYH2a) from the edge of 8 day old colonies were cut and inverted onto half-strength PDB (500 µL) on a cover glass (24X60, thickness-0.13 to 0.17mm) for observation. When necessary,

hyphae were stained with Calcoflour White as described in Section 2.11.1, to visualise cell walls and septa.

2.12.3.3 Hyphal apical growth rate determination using confocal microscopy

Blocks of PDA obtained from the edge of the colony were mounted in half-strength standard PDB and phase contrast time lapse imaging was conducted for 5 min with an imaging speed of 2.274 sec per image. Using time lapse phase contrast images, the distance travelled by the tip of an individual hypha within 5 min was recorded (using Olympus confocal FV10-ASWRS image processing software), and apical growth rate was calculated by dividing the distance travelled by the time.

2.13 Radial colony growth rate determination

The radial growth rates of strains were determined on standard PDA (Potato Dextrose Agar) media. The effect of altered conditions on growth rate was determined by adding supplements to the standard PDA medium. Supplements were added and mixed thoroughly before or after sterilization (media was cooled down to 50°C) depending on the stability of the compound used. Twenty millilitres of media per Petri plate was used for all analyses. To determine colony growth rate, 1 mm² plugs from the edge of 8 day old colonies of four test strains were cultured on each plate according to a randomized block design plate assay. The cultures were incubated at 22°C under 16 h light. The diameter of the colony was measured after 4 days and subsequently in 5 day intervals until the colonies reached the edge of the Petri plate. The diameter of each colony was measured at four equidistant points. The growth rate for each time interval was determined by subtracting the previous diameter and dividing by the number of days. A randomized block design was used with 3 biological replicates for each deletion strain, with 5 clonal replicates each, and the results were analysed via ANOVA using Minitab

statistical software. For determination of colony morphology, 8 day old colonies of each strain were photographed using an Olympus SZX12 dissecting microscope fitted with an Olympus DP20 digital camera.

2.14 Statistics

The statistical significant difference ($P < 0.05$) between two or more groups was analysed using the student's t-test or analysis of variance (ANOVA) using Minitab 16 statistical analysis software. When necessary, P values for pair wise comparisons were derived using Tukey's HSD post-hoc test. Pearson's linear correlation coefficient was calculated to test whether there is a statistically significant correlation between two variables.

2.15 Bioinformatics

Sequences of *mid1* and *wsc1* genes of *S. cerevisiae* were obtained from SGD (Saccharomyces Genome Database, <http://www.yeastgenome.org/>). Sequences of *mid1* and *wsc1* orthologues in other fungi were obtained through a database search using the Entrez cross database search tool of NCBI (<http://www.ncbi.nlm.nih.gov/sites/gquery>). The putative orthologous *midA* and *wscA* genes of *E. festucae* were identified through tBLASTn (Basic Local Alignment Search Tool) analyses against the *E. festucae* genome (<http://www.endophyte.uky.edu/>, *E. festucae* F11, 2011-03 assembly, version 2) (Schardl et al., 2013). Gene predictions and annotation models for putative *midA* and *wscA* genes of *E. festucae* performed using the Maker and FGeneSH were obtained through the Gbrowse interface provided in <http://www.endophyte.uky.edu/>, *E. festucae* F11, 2011-03 assembly, version 2.

Multiple sequence alignment was performed using amino acid sequences of known Mid1 and Wsc1 proteins using ClustalW (<http://www.ebi.ac.uk/Tools/msa/clustalw2/>) with default settings (Larkin et al., 2007). The conceptual structural and functional

domains of MidA and WscA were identified via bioinformatics tools such as SignalP (<http://www.cbs.dtu.dk/services/SignalP/>-to predict signal peptides) (Petersen et al., 2011), TMHMM (<http://www.cbs.dtu.dk/services/TMHMM/> - to predict transmembrane helices) (Sonnhammer et al., 1998; Krogh et al., 2001), TMPred (<http://www.ch.embnet.org/software/TMPRED> - to predict helices) (Hofman, 1993), NetNGlyc (<http://www.cbs.dtu.dk/services/NetNGlyc> - to predict N-glycosylation sites), WoLF PSORT (<http://wolfpsort.org/>- to predict localization) (Horton et al., 2007) and InterProScan (<http://www.ebi.ac.uk/Tools/pfa/iprscan/> - to predict conserved functional domains) (Zdobnov et al., 2001).

Chapter 3: Characterisation of *E. festucae* WscA and its role in intercalary growth

3.1 Identification of the *S. cerevisiae* *wscA* gene orthologue in *E. festucae*

At the start of this project, only the Wsc1 (also known as SLG1) and Wsc1 proteins of *S. cerevisiae* and *A. fumigatus* respectively had been identified and characterised, along with the other Wsc proteins in *S. cerevisiae*, Wsc2, Wsc3 (in the CWI MAP kinase pathway) and Wsc4 (an ER membrane protein), which are structurally similar to Wsc1 (Verna et al., 1997; Dichtl et al., 2012). The putative *wscA* orthologue was retrieved from *E. festucae* by interrogating the Fl1 (also known as E894) genome sequence database located at University of Kentucky, USA (<http://www.endophyte.uky.edu/>, *E. festucae* FL1, 2011-03 assembly, version 2) (Schardl et al., 2013) using the tBLASTn algorithm (Altschul et al., 1990; Altschul et al., 1997). Query sequences included protein sequences of Wsc1 from *S. cerevisiae* (NP_014650.1 or SGD ID: S000005534) and Wsc1 of *A. fumigatus* (XP_751464). A total of three putative *wscA* sequences were recovered from the *E. festucae* genome. The Maker and FGeneSH gene prediction protein sequences for the Wsc proteins were retrieved from the genome database for further analysis.

Reciprocal tBLASTn analysis of the putative *E. festucae* Wsc proteins against the *S. cerevisiae* (<http://www.yeastgenome.org>) and *A. fumigatus* (<http://www.aspergillusgenome.org>) genomes revealed that one of the putative Wsc protein sequences aligned better with Wsc1 of *S. cerevisiae* and Wsc1 of *A. fumigatus*. This protein was selected as the most likely candidate to be the *E. festucae* orthologue of *S. cerevisiae* Wsc1 and was named WscA (Maker gene prediction contig_1037-snap-gene-0.47 or FGeneSH prediction A.4.345) according to the recommended gene nomenclature for *E. festucae* (Schardl et al., 2012). However the identity (21%) and E-values ($3e-06$) indicated low similarity between the Wsc1 and WscA of *S. cerevisiae* and *E. festucae* respectively. Therefore the domain architecture of the putative WscA of

E. festucae was further analysed to investigate the presence of functionally important domains and conserved regions.

The conceptual *E. festucae* WscA protein contains 306 amino acids (Appendix 4). Structural domain analysis using appropriate bioinformatics tools (Section 2.15) revealed the presence of functionally important domains and conserved regions in common with the yeast protein. *E. festucae* putative WscA protein consisted of the WSC domain (carbohydrate binding domain) that contains eight conserved cysteine residues (Pfam protein families database ID: PF01822 and InterProScan ID: IPR002889). A similar WSC domain with eight conserved cysteine residues is found in Wsc1 of *S. cerevisiae* (Fig 3.1). Further, the protein contained a signal peptide of 19 amino acids at the N-terminus and a transmembrane domain of 23 amino acids that embeds the protein (a single pass through the membrane) into cell membranes. The N-terminus extra-cellular domain consists of 212 amino acids and the highly conserved C-terminus intracellular region has 71 amino acids. In addition a serine/threonine rich region in the N-terminus, similar to the yeast Wsc1 (Fig 3.1) is also present.

As BLAST results indicated, the *wscA* gene identified in the *E. festucae* genome shared very low homology with *wsc1* of *S. cerevisiae*. Nevertheless the candidate selected represented the most likely orthologue, given the available data at the time of analysis. The other two putative *E. festucae* Wsc proteins identified aligned better with Wsc2 (CWI MAP kinase pathway) and Wsc4 (ER membrane protein) of *S. cerevisiae*, these proteins were not characterised further in this study.

```

E.festucae      ---MRLSTIAFGAIMAATGVHAQT-----PKPKQPALQIPVDGISTSSGCYGSYGNMT 50
N.crassa       -MKSISVLVTAFAANCAIATAHQPLGSLFVRDDPPWPTIEKPAFLQNTYHGCYNDSGTLK 59
A.fumigatus    -----MKPFTARSAFTASVLLLT-----TNLPAVFAAEMVSQGCFSDSTPLV 42
S.cerevisiae   MRPNKTSLLLALLSILSQAN-----AYEYVNCFSSLPSPDF 35
               . . : : : . . . * : . . .

E.festucae      MHKP-ISADKMS-----TAACNNACKADG-FWLAAMHGG-QCLCGYALPPPK 94
N.crassa       LFTTRMNTQQMMNFGNGLEKDLGVSSGLCFQWCKDNK-TTVAAMSQDQCWCGTEYPPES 118
A.fumigatus    DQGP--YTYQSN-----GYCQQLCMKTSNNLVFALTKGSNCLCGNQLPAKS 86
S.cerevisiae   SKADSYNWQSS-----HCNSECSAKG-ASYFALYNHSECYCGDTNPSPGS 79
               . * . * * : * : * * * * . .

E.festucae      DLVEDESECNQPCFAYPPEACGGIDSYSIYNVGIQLQINRYEPSSSSTTGGSKTSAASPTP 154
N.crassa       AQTDIQNCDITCSGYNLEYCGGADTWSVYNLGVPKVAN-SKPKVSSTSAAPSTAAAKTS 177
A.fumigatus    AKTADSDCNVKCAGWPDVMCGGQNTFSVYLTGLSSNVAYYHDDDASTANANSSSTSTTN 146
S.cerevisiae   ESTS-SSCNTYCFGYSSEMCGGEDAYSVYQLDSDTNSNSISSSDSSTESTSASSTTSST 138
               . . . * : * . : * * * : : * : * . . . * * . . : : : : :

E.festucae      TDTSSSTNTGGNNNNNHSNNNNNHSNNNNGGGGGTTVTQTS----- 195
N.crassa       SISSAVSEP-----TVTTTES----- 193
A.fumigatus    GGSTVTTGSQQ-----VVTQGEQTVVVTAPAGNG----- 176
S.cerevisiae   TSSTTSTTSSTTSSTTSSMASSSTVQNSPESTQAAASISTSQSSSTVTSESSLSDTLAT 198
               : : . . . . : . .

E.festucae      -----VPTET---PKPEKS 206
N.crassa       -----ILPDD---SKKGKS 204
A.fumigatus    -----VGATNGLNEEKNKD 190
S.cerevisiae   SSTSSQSDATSIIYSTTFHTEGGSTIFVTNTITASAQNSGSATGTAGSDSTSGSKTHKK 258
               . . . . : * .

E.festucae      GPNVAGIAAGVVVGVFAAAAAIAGVFFYVRRKRNSEIEE-----EHRRNAAV 253
N.crassa       --NTAGIVAGTVVAVVVVLSAVGGVFLMRRRKRKEIED-----EHRRNAAV 249
A.fumigatus    GPNTAAIAAGVVVGVFCSLVGAGFLWRFRKRTNVRP-----QYSNNAGA 237
S.cerevisiae   KANVGAIVGGVVGVAIALCILLIVRHINMKREQDRMEKEYQEAIKPVEYPKLYA 318
               * . . . * . . * . * . : : * . . . . : : : .

E.festucae      NAFISGSKPSSSHGSISMTDSRLD--PVMAHRRMSDGSIADNEDYSRR-ILRVTNA---- 306
N.crassa       NAFVG--KPPSTSDGMSMADARLD--PVLVQRRLSDGSIADNQDYSRR-ILRVTNA---- 300
A.fumigatus    TEHFG--KPMSQD--SMSDSRFDG-DFMAQRRQSNGSIDDDQDFSRR-ILQVRLFSSAL 290
S.cerevisiae   SSFSSNHGPSSSGSFEEHTKGQTDINPFDDSRRISNGTFINGGPGGKNNVLTVVNPDEAD 378
               . . . * * . . : : * . * * * : : . . : : * *

E.festucae      ---
N.crassa       ---
A.fumigatus    GIS 293
S.cerevisiae   ---

```

Figure 3.1: Multiple sequence alignment between Wsc1 of *S. cerevisiae* (NP_014650.1) and orthologues of *E. festucae*, *N. crassa* (XP_011395260) and *A. fumigatus* (XP_751464). Highlighted grey - signal peptide. Underlined – WSC domain (Pfam ID: PF01822, carbohydrate binding domain). Red letters - conserved cysteine residues, Green letters – Serine/threonine rich region. Blue letters - transmembrane domain. Multiple sequence alignment was performed using ClustalW2 from <http://www.ebi.ac.uk>.

3.2 Targeted deletion of the *wscA* gene in *E. festucae*

In order to determine the functional role of WscA in sensing mechanical stress and stimulating hyphal growth, the *wscA* gene in *E. festucae* F11 was deleted by targeted gene replacement using the split marker strategy based on homologous recombination (Fairhead et al., 1996). Through gene replacement the entire coding region of *wscA* was replaced with an expression cassette harbouring the gene *hph*. Linearised whole replacement vectors, pSAM3 & pSAM4 (Appendix 3, Fig 8.3) were generated (Section 2.7.2 and 2.7.2.3) and *E. festucae* F11 protoplasts were transformed (Section 2.6.3) to achieve a targeted gene replacement. Plasmid pPN1688 which contains the hygromycin-resistant gene *hph* was used as the positive transformation control and water was used for the negative control. Protoplast transformation resulted in around 70 hygromycin-resistant colonies per 4×10^6 protoplasts. There was no growth observed in the negative control, while the positive control resulted in around 50 resistant colonies per 4×10^6 protoplasts. The viability of the protoplasts was 11% (calculated using the number of colonies formed against the number of protoplasts cultured on hygromycin-free negative control regeneration plates). After sub culturing from hyphal tips three times to generate homogenous lines (Section 2.8), DNA was isolated from resistant colonies and PCR-screened to confirm replacement of *wscA*. Primers were designed to target the *wscA* flanking regions (primer pair swsc-30/swsc-31) and regions beyond the 3' flanking region (primer pair swsc-27/swsc-32) on either side to check whether the deletion cassette had integrated at the correct locus to replace the WT copy of the gene (Fig 3.2). PCR screening revealed that targeted replacement of *wscA* was successful in nearly 30% of the total transformed colonies screened (Fig 3.2). Accordingly, strains $\Delta wscA$ -5, 21, 26 and 36 were selected for Southern blotting for further confirmation.

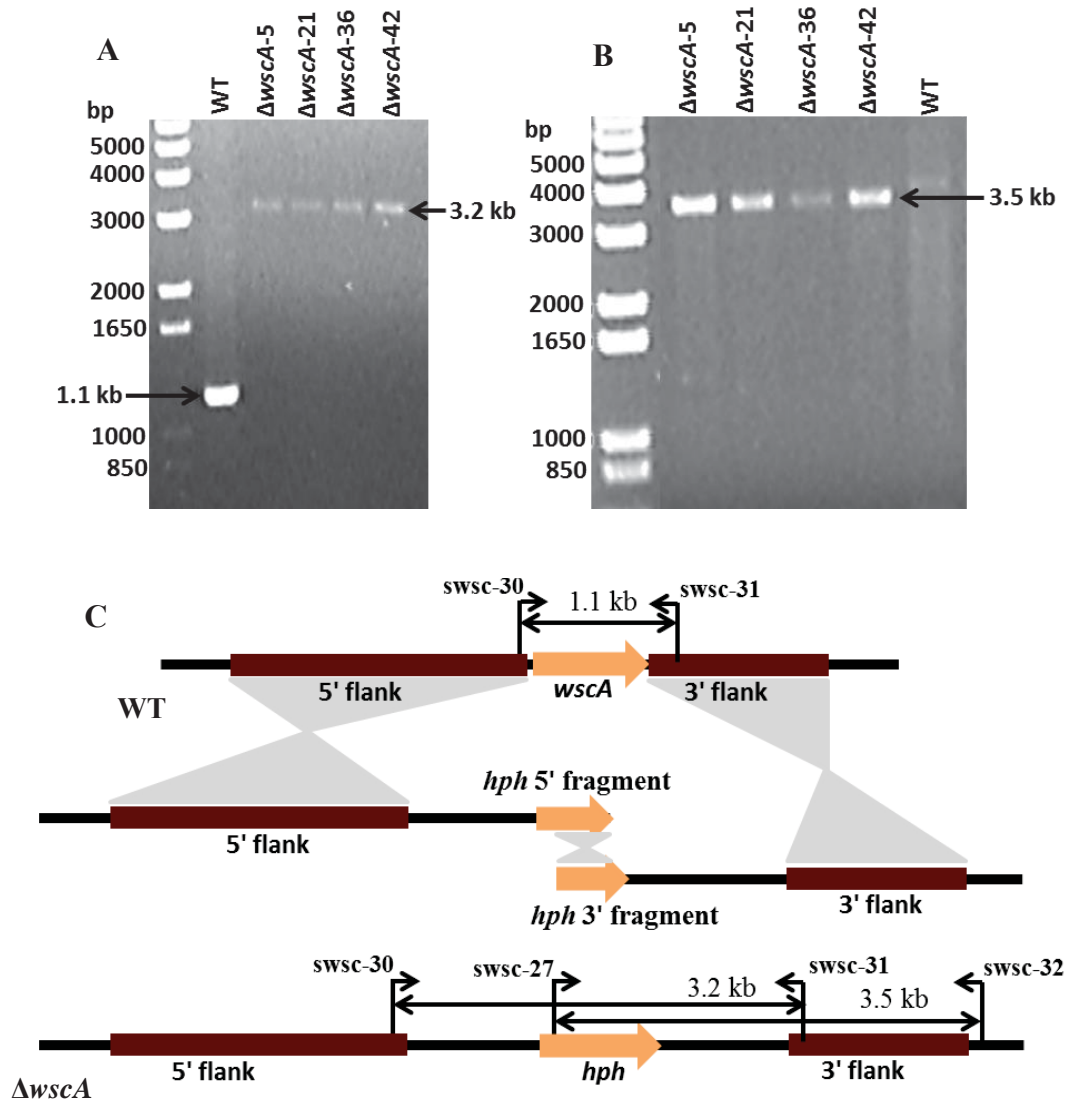


Figure 3.2: PCR screening to identify *E. festucae* *wscA* gene replacement mutants. **A** - In a targeted replacement of *wscA* the primer pair swsc-30 & swsc-31 is expected to yield a PCR product of 3.2 kb, and in WT and ectopic insertions a product size of 1.1 kb is expected. **B** -The putative mutants were further analysed via primer pair swsc-27 & swsc-32: expected band sizes were 3.5 kb for the mutant and no product was expected for the WT and ectopic colonies. **C** -Schematic diagram (not drawn to scale) showing the replacement of *wscA* with the *hph* gene (hygromycin resistant) by the 5' and 3' flanking fragments through 3 homologous recombination events (shown as grey shaded areas).

Southern blotting (Section 2.9) was carried out to confirm the targeted deletion of *wscA*, and to ensure that the strains had a single integration event with no ectopic insertions.

Four PCR-confirmed putative *wscA* replacement strains ($\Delta wscA$ -5, 21, 36 and 42) were selected along with strain Ect 8 containing a putative ectopic integration. As shown in Fig 3.3, probes (A and B) were designed to detect deletion of the *wscA* coding region and to confirm the absence of any ectopic or tandem integration. According to the Southern hybridisation results obtained from both EcoRI and HindIII digested genomic DNA it was clear that *wscA* replacement mutant strains 5 and 36 contained a single integration event at the desired locus. Strains $\Delta wscA$ -21 and 42, when digested with HindIII, both appeared to have the desired integration event at the *wscA* locus plus an additional hybridising band. Because the size of the additional HindIII bands were similar in both strains, and because no additional ectopic fragment was seen with an EcoRI digest of $\Delta wscA$ -21 (Fig 3.3), the additional HindIII bands were taken to represent a partially digested fragment common to both strains. Based on this, strain $\Delta wscA$ -21 was also selected for further analysis (along with strains $\Delta wscA$ -21 and 42). Consequently, strains $\Delta wscA$ -5, 21 and 36 were selected as the three biological replicate deletion strains for all analyses.

As the phenotype of the *wscA* mutants were different to the wild type in axenic culture (shown in Sections 3.3.1 and 3.3.3 along with the complemented strains), the mutant phenotypes were complemented by ectopic integration of a single copy of the *wscA* gene into the $\Delta wscA$ -5 strain using the PEG-mediated protoplast transformation procedure (Section 2.6.3) with complementation vector pSAM6 (Geneticin[®] resistant, Sections 2.7.3.3). To confirm the integration of the *wscA* gene, transformants were PCR-screened using primers swsc-12 and swsc-6 (Table 2.3) that amplify a region of the *wscA* coding region. Based on PCR results, three independent transformants (Comp-2, 18 and 24) were selected for all studies.

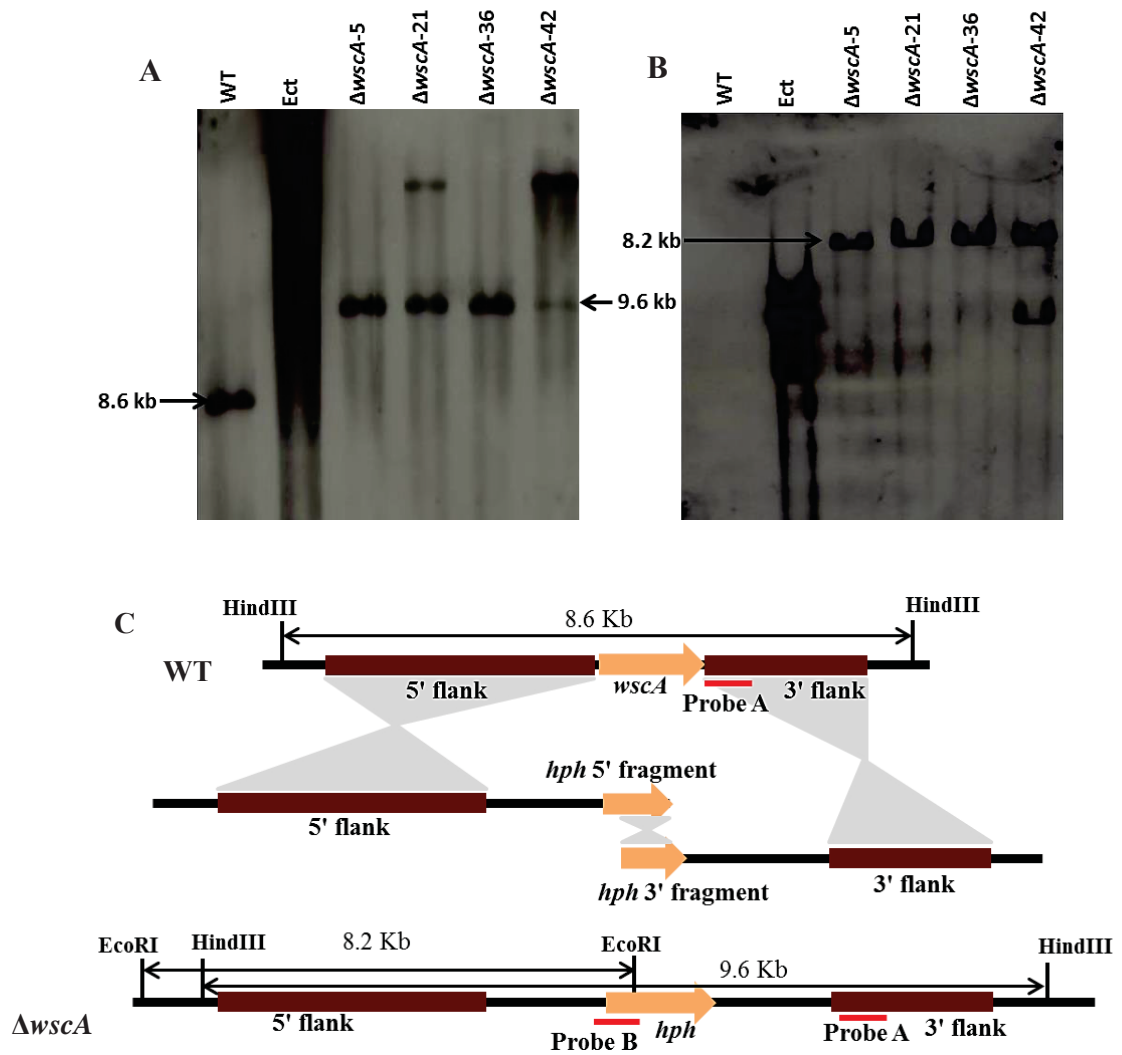


Figure 3.3: Southern blot analysis to confirm the *wscA* replacement locus in putative *wscA* replacement mutants. **A-** Genomic DNA digested with HindIII and hybridized with probe A. The expected fragment size for the *wscA* replacement mutants is 9.6 kb, with 8.6 kb expected for the WT locus. **B-** Genomic DNA digested with EcoRI and hybridized with probe B. The expected fragment size for the *wscA* replacement mutants is 8.2 kb, no bands will be obtained for wild type strains, and bands of various sizes are expected for ectopic integrations, dependent on where in the genome they integrated. **C-** Schematic diagram (not drawn to scale) showing the replacement of *wscA* with the *hph* gene (for hygromycin resistance) through a homologous recombination event. The sites of restriction enzymes used and the probe annealing positions are shown.

3.3 Functional characterisation of the *E. festucae wscA* gene during growth in culture

3.3.1 Deletion of *wscA* in *E. festucae* affects radial growth and morphology in axenic culture

The effect of *wscA* deletion on radial growth rate, colony morphology and hyphal morphology was determined by growing mycelial plugs on a PDA medium (Section 2.2.2). The cultures were inoculated in a random block design and incubated at 22°C under continuous light for 8 days. The radial growth rate was measured and the values presented are the mean and standard deviation derived from 5 replicates. ANOVA was performed using Minitab software. Images of colony morphology were obtained using an Olympus SZX, and DIC and fluorescent images of hyphal morphology were taken using an Olympus BX50 (Section 2.12.2).

The *E. festucae wscA* mutants, in comparison to the wild type, showed a significantly ($p < 0.05$) reduced vegetative radial colony growth rate (Fig 3.4). The radial colony growth rates of mutants were approximately 40% lower than that of the WT. The colony radial growth rates of the complemented strains (Comp-2 and 18) and the ectopic strain were not significantly different to the WT (Fig 3.4). To better understand the reasons for reduced colony radial growth, the apical growth rates of individual hyphae of the WT, $\Delta wscA$ and complemented strains growing on PDA were analysed using a confocal laser scanning microscope as described in Section 2.12.3.3. The data revealed that the apical growth rate of the $\Delta wscA$ mutants was 0.79 ± 0.11 $\mu\text{m}/\text{min}$ (mean \pm SD of 12 individual hyphae), significantly ($p < 0.05$) lower than the apical growth rate of the WT hyphae (1.29 ± 0.10 $\mu\text{m}/\text{min}$ (mean \pm SD of 12 individual hyphae)). The complemented strains showed a growth rate of 1.23 ± 0.07 $\mu\text{m}/\text{min}$ (mean \pm SD of 12 individual hypha) not significantly ($p < 0.05$) different from the WT confirming that disruption of *wscA* was the cause of the reduction in apical growth rate observed. Other than the reduced apical

growth rate, no other aberrations in $\Delta wscA$ growth were observed (except for occasional ruptured hyphal tips) within the time period analysed.

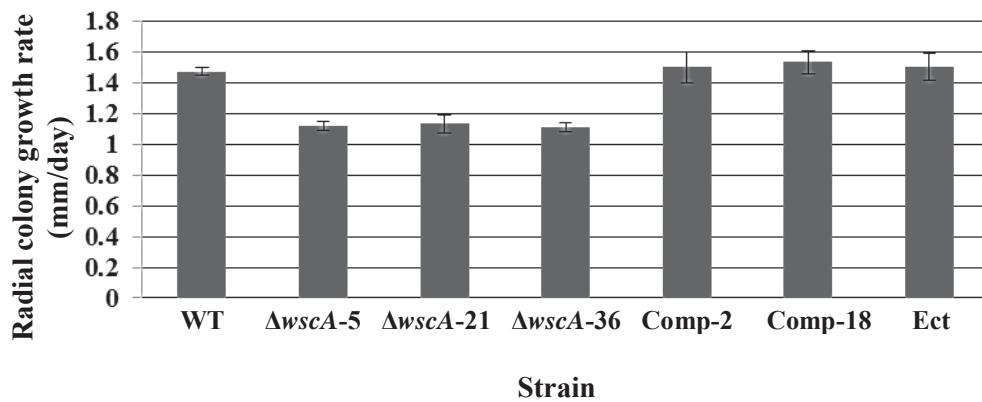


Figure 3.4: Comparison of *E. festucae* WT and $\Delta wscA$ radial growth rates in culture on the PDA medium. All three $\Delta wscA$ mutants showed significantly ($p < 0.05$, using ANOVA) reduced growth rates compared to the WT, and the complemented strains had a radial colony growth rate similar to the WT. WT- *E. festucae* WT strain; $\Delta wscA$ -5, $\Delta wscA$ -21 and $\Delta wscA$ -36 - independent *wscA* deletion mutants; Comp-2 and Comp-18 - independent *wscA* strains complemented with the full length *wscA* gene with its native promoter and termination region ectopically restored; Ect - strain with an ectopic *hph* (hygromycin B phosphotransferase) gene integration.

In addition to the reduced colony size, the colony morphology of all three *wscA* mutants was different to the wild type, with a marked reduction in aerial growth of hyphae, and darker colony centres that appeared to be undergoing senescence (Fig 3.5-A). Colony morphology of the complemented strains and the ectopic strain appeared similar to the WT, including the presence of aerial hyphae. Cross sections through mutant colonies revealed no differences in the ability of mutant mycelia to penetrate the agar medium (1.5%) in comparison to the WT (Fig 3.5-B). Visual microscopic observations of mycelia growing at the edge of the colony revealed that $\Delta wscA$ mutants were hyper-branched in comparison with the WT, and that the frequency of branching in

complemented strains was similar to the WT (Fig 3.5-C), demonstrating that the WscA protein is involved in restricting hyphal branching in *E. festucae* during growth in culture.

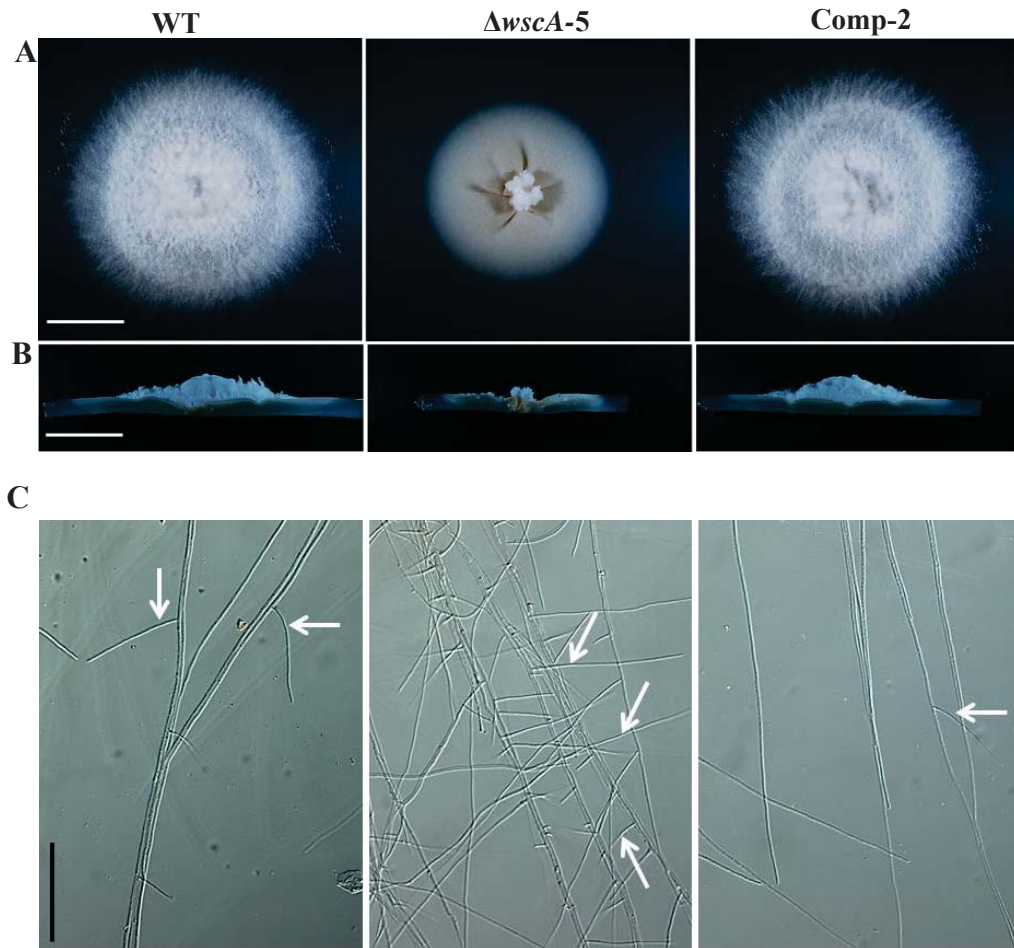


Figure 3.5: Aberrant colony morphology in *E. festucae* $\Delta wscA$ mutants. **A-** Comparison of the colony morphology of *E. festucae* $\Delta wscA$ with the wild-type & complemented strain cultured on PDA. **B** – Cross sections of the colonies comparing aerial hyphae production. **C-** DIC images of WT, $\Delta wscA-5$ and a complemented strain (Comp-2) showing the branching pattern (white arrows) at the edges of the colony margin. Frequent branching was observed in $\Delta wscA$ hyphae. White scale bar = 2 mm, black scale bar = 200 μ m

When hyphae on PDA blocks, stained with CW (25 μ M in half strength standard PDB), were observed by fluorescence microscopy (Section 2.11.1), WT hyphae stained uniformly except for regions very close to the hyphal tip, where one or two CW patches

(2-4 μm in length and 3.5 ± 0.20 μm in diameter) could be seen immediately behind the tip (Fig 3.6-A). In sub-apical compartments and beyond, the cell walls were evenly stained and hyphae had a uniform diameter of 3.25 ± 0.20 μm (mean \pm SD, $n=10$) over the approximately 500 μm measured (Fig 3.6-A). However, in comparison, hyphae of *wscA* mutants, when stained with CW, contained recurring cell wall aberrations with globular swollen patches of CW accumulations (3-6 μm in length) along the cell walls (Fig 3.6-A). The distance between two CW stained patches in mutant hyphae was on average between 5-8 μm and were prevalent close to the apex (first 2-3 compartments) and appeared to diminish as the hypha aged. Due to the occurrence of swollen aberrations, the diameter of mutant hyphae was variable, with diameters of 3.4 ± 0.6 μm and 3.0 ± 0.5 across swollen and septal regions respectively. Consequently, DIC images revealed an uneven and coarse cell wall surface in mutant hyphae compared to the even and smooth surface observed in the WT (Fig 3.6-B). Complementation of the *wscA* deletion with the full length *wscA* gene restored the phenotype back to the WT with no cell wall aberrations observed, indicating that this cell wall phenotype was due to deletion of the *wscA* gene. Apart from the cell wall aberrations, a slight increase in hyphal tip damage was observed in $\Delta wscA$ versus WT hyphae which further suggested cell wall defects had occurred. Overall, these observations showed that *wscA* deletion has a profound effect on apical growth and maintenance of cell wall integrity in *E. festucae*.

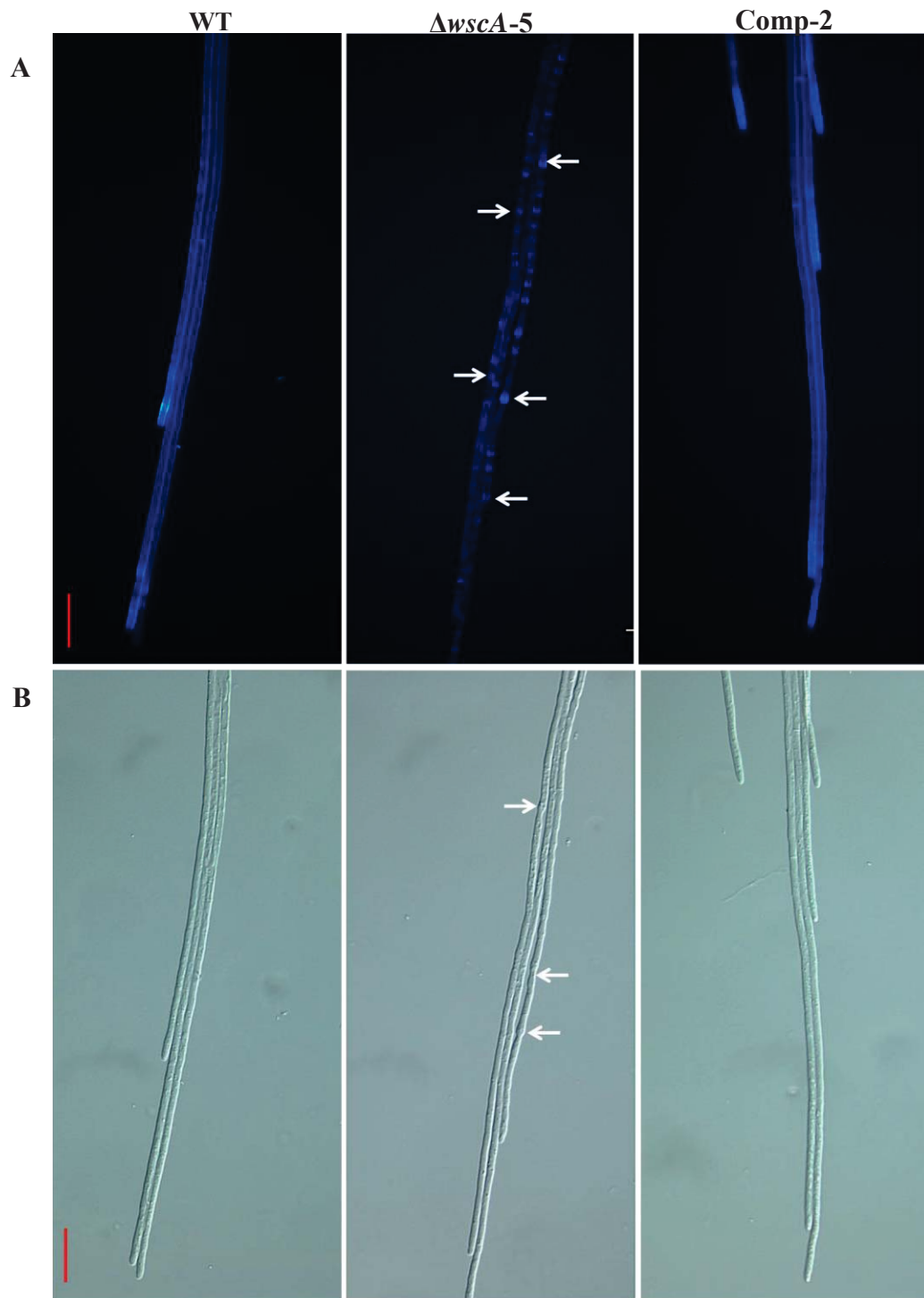
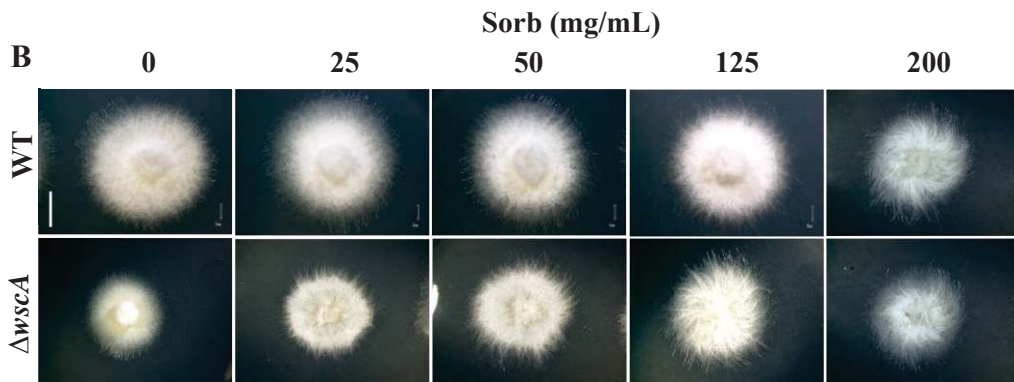
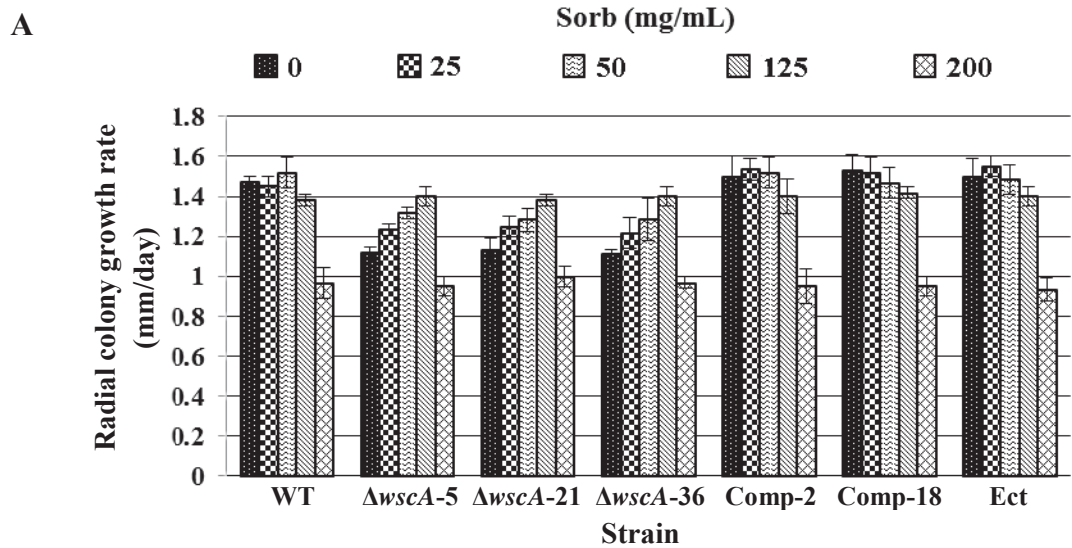


Figure 3.6: Cell wall aberrations in *E. festucae* $\Delta wscA$ mutants. Comparison of cell wall morphology in $\Delta wscA$ with the WT and a *wscA*-complemented strain growing on PDA. **A-** Hyphae stained with CW (25 μ M). **B** - DIC images of hyphae. Mutant hyphae contained noticeable cell wall aberrations (white arrows). Scale bar = 20 μ m

3.3.2 Osmotic stabilization can rescue *E. festucae* $\Delta wscA$ phenotypes on the PDA culture medium

Cell wall aberrations observed in $\Delta wscA$ mutants suggested a weakened cell wall in these hyphae, consistent with the putative role of this protein as a cell wall integrity sensor. Previous studies showed that use of an osmotic stabilizer can suppress some defects of cell walls (Levin, 2011). Therefore in order to test the hypothesis that *wscA* disruption results in a weakened cell wall, mutants were cultured on PDA media infused with sorbitol to act as an osmotic stabilizer. The impacts of sorbitol on radial growth rate, colony morphology and hyphal morphology in WT and $\Delta wscA$ deletion mutants and complemented strains were determined as described in Section 2.13 and 3.4.1. Sorbitol concentrations of 25 and 50 mg/mL partially restored the radial colony growth rate, colony morphology and hyphal morphology of $\Delta wscA$ mutants to WT levels (Fig 3.7-A and B). However, radial colony growth rates (Fig 3.7-A and B) and cell wall aberrations in $\Delta wscA$ hyphae reverted to the WT phenotype when cultured on PDA supplemented with 125 mg/mL of sorbitol (Fig 3.7-C). Similarly, colony morphology and the presence of aerial hyphae also reverted to the WT at 125 mg/mL of sorbitol. At 200 mg/mL of sorbitol, both WT and $\Delta wscA$ strains showed impaired growth due to the high osmolarity of the substrate (Fig 3.7-A and B). An additional observation made during the study was that 125 mg/mL of sorbitol also abolished the characteristic band of CW staining usually seen immediately behind the tips in WT hyphae growing on PDA (Fig 3.7-C). This indicates that this region is inherently sensitive to osmotic stress, probably because the nascent cell wall has not yet fully hardened. The complemented and ectopic strains behaved similarly to the WT in all sorbitol concentrations used in this study. Overall, these observations indicated that osmotic stabilizers can rescue $\Delta wscA$ phenotypes observed when growing on PDA culture, and further supports the

microscopy evidence that the colony and hyphal growth defects of *wscA* mutants are due to a substantial weakening of the cell wall. Together these data point towards a role for *E. festucae wscA* in hyphal growth in culture, primarily in the regulation of cell wall synthesis.



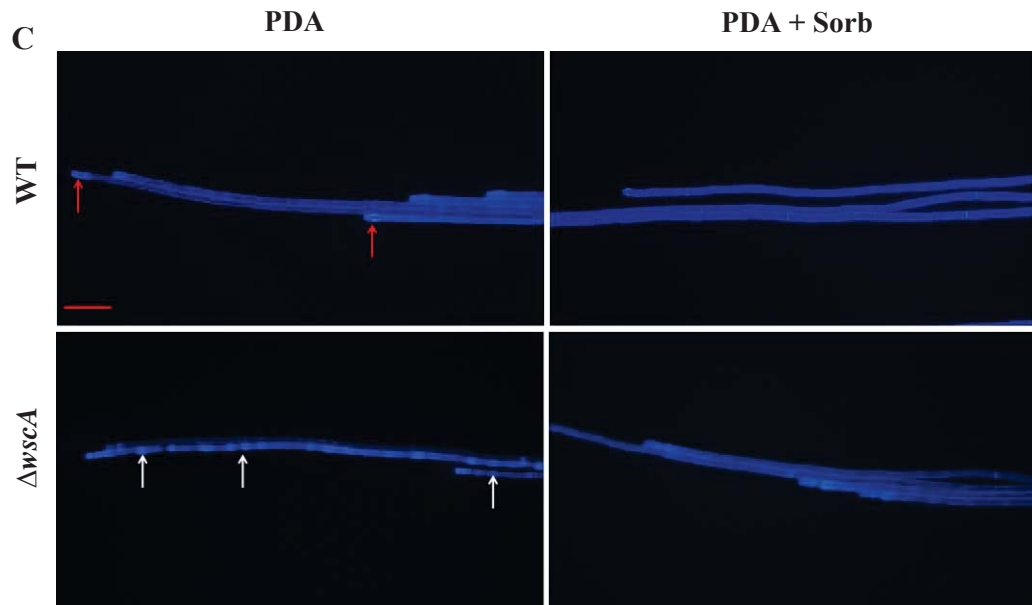


Figure 3.7: Effect of sorbitol concentration on the growth rate, colony morphology and hyphal morphology of *E. festucae* WT and $\Delta wscA$ mutants.

A- Comparison of colony radial growth rates on PDA media supplemented with increasing sorbitol concentration (25, 50, 125 and 200 mg/mL).

B- Colony morphologies of WT and $\Delta wscA$ on PDA infused with different sorbitol concentrations (0, 25, 50, 125 and 200 mg/mL). Colony morphology of $\Delta wscA$ looks most similar to that of WT at 125 mg/mL sorbitol in PDA. White scale bar = 3 mm.

C- Hyphal morphology of WT and $\Delta wscA$ on PDA and PDA+ sorbitol (125 mg/mL). Hyphae are stained with CW (25 μ M). Cell wall aberrations seen in $\Delta wscA$ (white arrows) on PDA are absent on PDA+ sorbitol (125 mg/mL). The CW- stained band present at the tip of WT hyphae (red arrows) are absent when grown on PDA+ sorbitol (125 mg/mL). Scale bar = 20 μ m.

3.3.3 *E. festucae* $\Delta wscA$ mutants are sensitive to cell wall perturbing agents

The cell wall integrity MAP kinase pathway that includes WscA as an integrity sensor has been shown previously in *S. cerevisiae* and the filamentous fungus *A. fumigatus* to be important in maintaining cell wall integrity under stress conditions caused by cell wall perturbing agents such as CW (Dichtl et al., 2012). CW acts as a cell wall perturbing agent by binding to chitin and disrupting cell wall synthesis. To further characterise the integrity of the cell wall in *E. festucae* after deletion of *wscA*, the effect of cell wall perturbing agents were tested by growing *E. festucae* WT and $\Delta wscA$ on PDA infused with CW at concentrations of 0.1, 0.25 and 0.5 mg/mL. The radial colony growth rates of both the WT and $\Delta wscA$ strains were significantly reduced ($p < 0.05$) by exposure to 0.25 and 0.5 mg/mL CW in PDA, by a similar percentage for WT and $\Delta wscA$, compared to their respective growth rates on PDA alone. Further, since sorbitol was able to rescue growth and cell wall defects in $\Delta wscA$ mutants when grown on standard PDA (Section 3.3.2), the effect of cell wall perturbing agents were also tested in the presence of 125 mg/mL of sorbitol. In the presence of 125 mg/mL sorbitol, both WT and $\Delta wscA$ were more resistant to the effect of CW, and colony growth rates increased twofold compared to rates in the absence of sorbitol (Fig 3.8-A). However, the effect of CW in the presence of 125 mg/mL of sorbitol was more pronounced in $\Delta wscA$ strains compared to the WT under the same conditions (Fig 3.8-A and B). The greater impact of sorbitol in mitigating the impacts of CW on the $\Delta wscA$ strains provides a further line of evidence that the cell walls of the mutants are compromised. A distinctive feature of all the colonies (WT and $\Delta wscA$) in the presence of CW was the formation of aggregated hyphal strands and the apparent clockwise rotation of all these strands (Fig 3.8-B). The reason for this was not investigated in this study.

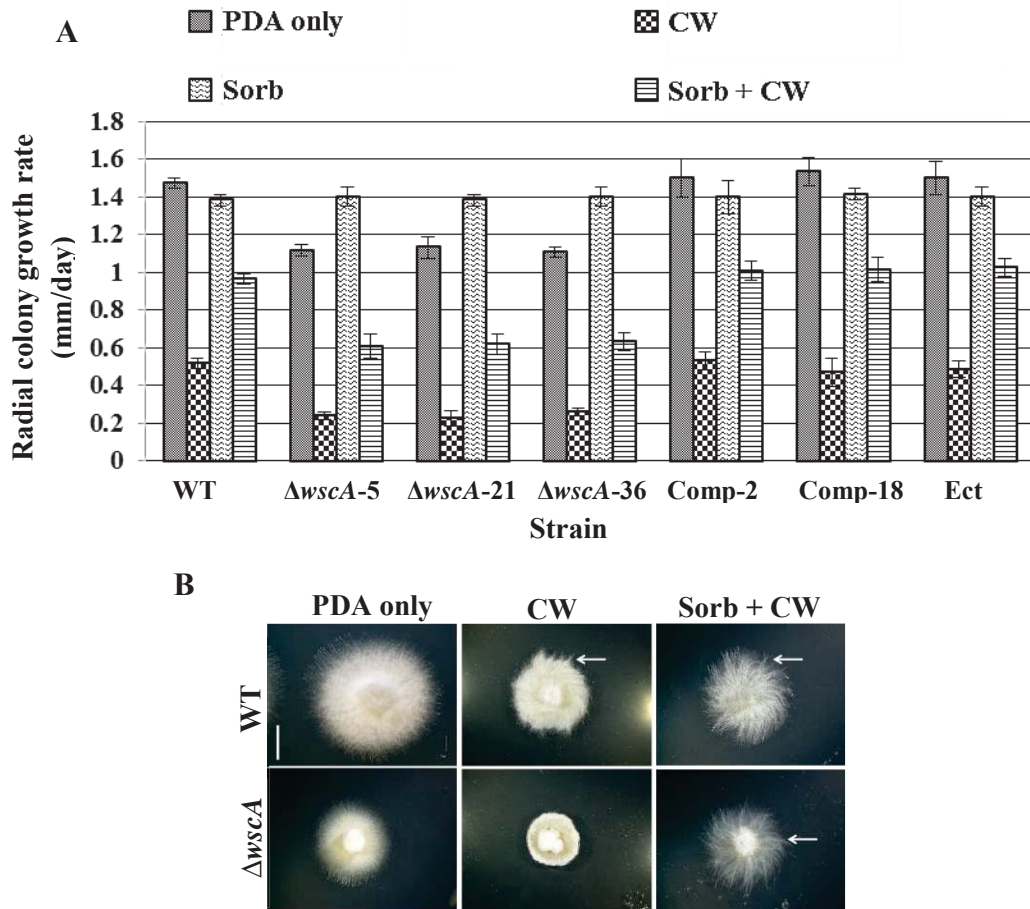


Figure 3.8: Sorbitol mitigation of defects in radial growth rate and colony morphology caused by Calcofluor White in *E. festucae* WT and $\Delta wscA$.

A- Comparison of radial growth rates on PDA supplemented with CW (0.5 mg/mL) with and without sorbitol (125 mg/mL).

B- Colony morphology of WT and $\Delta wscA$ on PDA and PDA infused with CW (0.5 mg/mL) in the back ground of sorbitol (125 mg/mL, osmotic stabiliser). Effect of CW was reduced in the presence of sorbitol. Clock wise-oriented hyphal strands in the presence of CW (white arrows).

Scale bar = 3 mm.

3.4 WscA localization in *E. festucae* hyphae

Due to the structural features of the *E. festucae* WscA protein (Section 1.6.3), it has potential to be a mechano-sensing protein, and therefore to play a possible role in intercalary growth. In *A. fumigatus*, using C terminal-fused fluorescent proteins, Wsc1 was shown to localise to the plasma membrane and the septa (Dichtl et al., 2012). Taking these features into consideration, it was decided to investigate the distribution of WscA in *E. festucae* growing in culture (in standard growth conditions), and *in planta* where intercalary growth is taking place. To investigate WscA localisation, the *wscA* gene was fused with EGFP at the 3' end and expressed under its native promoter or the TEF (Transcription Elongation Factor) constitutive promoter (Section 2.7.2.4). Expression vectors pSAM8 (with the native promoter, Appendix 3, Fig 8.10) and pSAM10 (with the constitutive promoter, Appendix 3, Fig 8.15) were transformed into *E. festucae* WT protoplasts as described (Section 2.6.3), nuclear purified by three rounds of sub-culturing (Section 2.8), and three independent transformants selected for localization studies. Comparison of colony growth rates, colony morphology and hyphal morphology of the selected strains with the WT indicated that the ectopic integrations had not affected these traits. Further, to test whether EGFP fusion to the C-terminal of WscA had any effect on its functionality (and therefore localisation), *E. festucae* $\Delta wscA$ protoplasts (strain $\Delta wscA-5$) were transformed with the same expression vectors (pSAM8 and pSAM10). Three independent strains were selected from each transformation event and their growth rates and morphologies compared with those of the WT as described above. If the fusion protein WscA-EGFP was fully functional, a partial or complete complementation of the *wscA* mutant phenotype was expected. Imaging was performed using a confocal laser scanning microscope (Section 2.12.3).

When $\Delta wscA$ was complemented with either of the *wscA:egfp* constructs (expressed under the native or TEF promoter), a partial complementation was observed in terms of colony growth rate, hyphal and colony morphology in all three independent transformants observed. The average radial colony growth rate of all three $\Delta wscA$ complemented strains (with *wscA:egfp* constructs, expressed under the native or TEF promoter) was higher (1.34 ± 0.01 mm/day) than that of the $\Delta wscA$ mutant (0.94 ± 0.09 mm/day) and lower than the WT ($1.61 \pm .09$ mm/day). This observation suggested a partial complementation of $\Delta wscA$ indicating that the Wsc1-EGFP fusion protein is functional, albeit with a partial impairment.

EGFP-tagged WscA, expressed under its native promoter, mostly localised into vacuoles and small vesicles (Fig 3.9). However, closer to the hyphal tip, and in irregular sub-apical positions, a faint florescence was seen on the hyphal periphery suggesting localisation to the plasma membrane in polar and sub apical regions. In contrast, WscA-EGFP expressed under the TEF constitutive promoter showed distinct localization to the septal regions and hyphal periphery at both at the hyphal tip and sub-apical regions (Fig 3.9). The fused protein also showed pronounced accumulation into vacuoles and small vesicles as before, indicating possible misfolding of the protein and/or mislocalization. In order to further confirm WscA-EGFP localization, hyphae were stained with CW to visualise the hyphal cell walls and septa. CW-stained cell walls and septa overlapped with WscA-EGFP distribution, further supporting WscA localization at plasma membranes (Fig 3.9). Expression of EGFP-fused WscA in both the WT and $\Delta wscA$ strains exhibited similar distribution patterns.

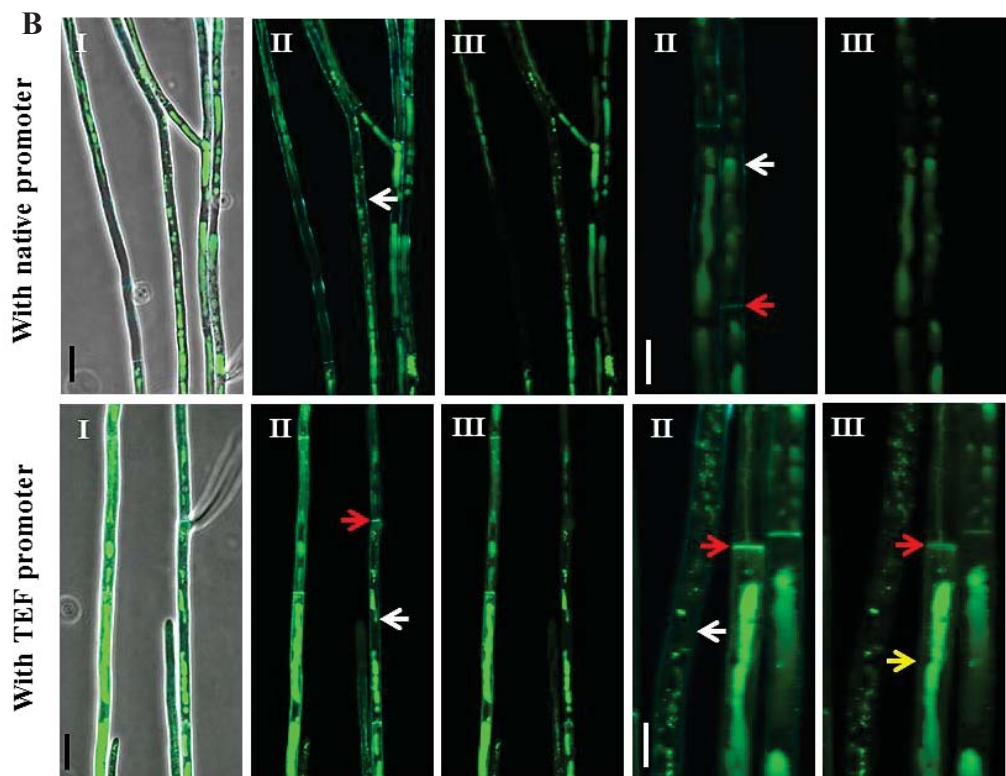
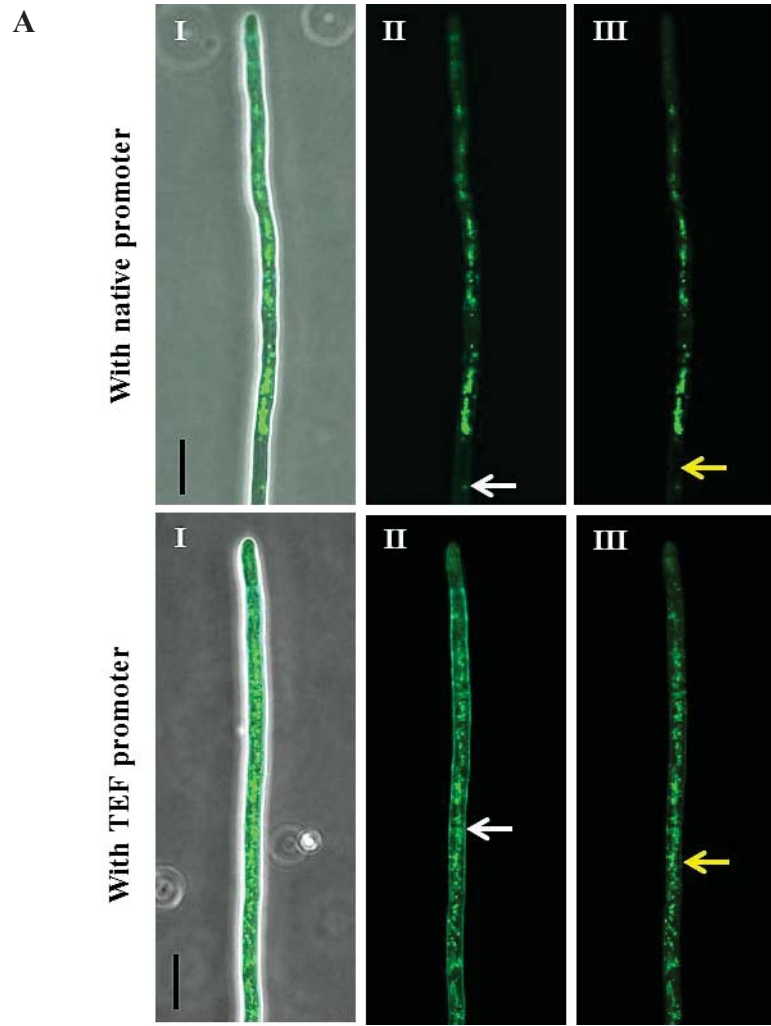


Figure 3.9: Subcellular localization of WscA fused to EGFP expressing in *E. festucae* WT hyphae . **I**-Phase contrast images with overlapping EGFP and CW fluorescence. **II**-Overlaid EGFP and CW fluorescent images. **III** – Images showing only EGFP fluorescence.

A- WscA distribution close to the hyphal tip. WscA localization to the cell periphery is observed when the fusion protein is expressed under the constitutive TEF promoter (Strain *EfwscATEFEGFP-08*). **B-** WscA distribution in sub-apical compartments. WscA localises to the cell periphery and septa when expressed under the constitutive TEF promoter. No distinct localization of EGFP-fused WscA is discernable when the the fusion protein is expressed under its native promoter (Strain *EfwscAEGFP-5*). White arrows – CW stained hyphal cell walls, Red arrows – hyphal septa, Yellow arrow – WscA-EGFP localization to the cell periphery. Black scale bar = 10 μm , White scale bar = 5 μm .

Epichloë fungi utilise different growth strategies to infect grass tissues at different stages of host development. Hyphae that are colonising meristematic cells grow at the tip, while those in the leaf elongation zone grow by intercalary extension. To investigate whether WscA localization alters in hyphae during colonisation of different host tissues (particularly in the meristematic, elongation and mature regions of a tiller), both WT and $\Delta wscA$ strains expressing WscA-EGFP (under native or constitutive promoters) were infected into perennial ryegrass seedlings. Tissue samples from 8 week old endophyte-infected plants were examined using confocal laser scanning microscopy as described above. Whole leaf tissues were used (1 cm X 2-3 mm) to minimise disturbance to the endophyte, and imaging was conducted immediately after tissue harvesting. Irrespective of the host tissue type or the strain of endophyte analysed, no distinct WscA localization patterns could be observed in endophyte hyphae within host tissues. In all hyphae observed within the different tissues, WscA-EGFP appeared to localize into vacuoles, and no septal or plasma membrane localization could be seen

(Fig 3.10). It was therefore not possible to use these strains to investigate whether WscA expression or localization altered during key stages of endophyte and host development, such as the stage where host cell expansion begins and endophyte hyphae switch from tip growth to intercalary growth.

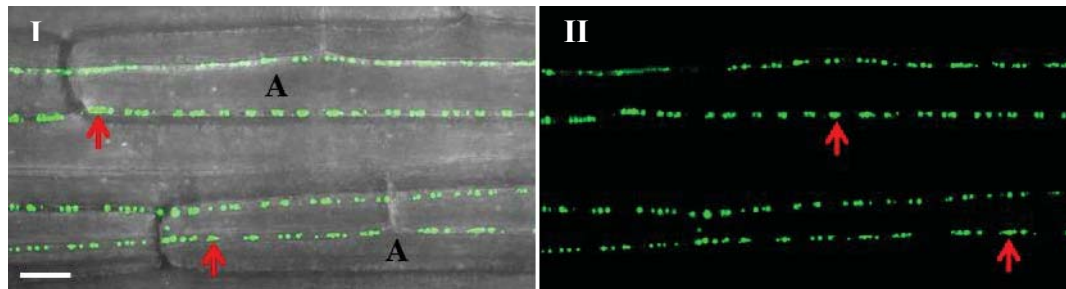


Figure 3.10: Perennial ryegrass leaf sheath showing sub-cellular localization of WscA-EGFP (expressed under the constitutive TEF promoter) in *E. festucae* WT hyphae (Strain EfwscATEFEGFP-08) growing *in planta*. WscA-EGFP is concentrated into vacuoles and vesicles and localization of WscA to cell membranes or septa is not observed. **I**-Phase contrast image overlaid on EGFP fluorescence image. **II**- Image showing only EGFP fluorescence. **A**- host cells, Red arrows – WscA-EGFP distribution within hyphae. Scale bar = 20 μ m.

3.5 Impact of *wscA* deletion on colonization of plants by *E. festucae*

3.5.1 Deletion of *wscA* does not influence *E. festucae* colonization of its host (*L. perenne*)

E. festucae, as described previously, colonises the *L. perenne* shoot apical meristem through apical growth, and then switches to a predominantly intercalary growth mechanism when colonizing the elongation zone of the developing leaf. Thereafter, further colonization of leaf tissues ceases as the leaf matures and stops growth. This unique colonization pattern, synchronised with the host development, is hypothesised to be triggered by mechanical stress imposed on hyphae by rapidly elongating host cells in the leaf elongation zone. Given the potential for *E. festucae* WscA to be a mechanosensor, it was decided to test whether deletion of *wscA* had any impact on the

ability of *E. festucae* to colonise the host, particularly the expansion zone. *E. festucae* WT, three independent $\Delta wscA$ deletion mutants, three independent $\Delta wscA$ complemented strains and a strain with an ectopic *hph* integration (through ectopic insertion of the original *wscA* deletion vector) were used (Section 2.3.3.2). All inoculated plants survived the first eight week period after inoculation. Plants were tested for the presence of endophyte both by tissue print immunoassay (Section 2.10.1) and microscopy using aniline blue-stained epidermal peels (Section 2.10.2). Three tillers were tested from each plant. A plant was considered endophyte positive if one or more tillers tested positive for endophyte. The percentage of infection was calculated by dividing the total number of infected plants by the total inoculated for each strain.

Results from tissue print immunoassay and microscopy revealed that *wscA* deletion had no impact on infection and colonization of perennial ryegrass by *E. festucae*, as all strains tested showed an infection rate of above 90%. Epidermal peels from the leaf sheaths of infected plants, stained with aniline blue and observed under bright field microscopy, did not show a visible difference in hyphal density between the WT and $\Delta wscA$ infected plants. However, aniline blue-stained epidermal peels do not provide a comprehensive representation of the colonization pattern of endophytes within the plant. To better understand impacts on colonization, the WT and one $\Delta wscA$ strain ($\Delta wscA$ -5) were labelled with EGFP (by co-transforming protoplasts with the constitutively-expressed vector pTEFEGFP and pII99 to confer resistance against geneticin) (Vanden et al., 1997). Three independent WT and $\Delta wscA$ isolates labelled with EGFP were selected and the colony growth rates, plant infection rates and hyphal and colony morphologies were compared with those of unlabelled WT and $\Delta wscA$. The labelled strains were similar to their unlabelled counterparts indicating that ectopic integration of TEF-EGFP had not affected these traits. EGFP-labelled strains were inoculated into

seedlings and endophyte positive plants were identified via tissue print immunoassay. To determine endophyte colonization within the meristematic tissues of a tiller and emerging leaves, longitudinal sections (LS) were made (5 mm) within 1 cm from the base of the tiller (including the SAM and leaf primordia). Further transverse sections (TS) of the same tiller (0.5 cm from the base of the tiller) were also taken (Section 2.12.1). Confocal imaging was performed and a Z stack of 20-30 images through 40 - 60 μm of tissue was captured to maximise the visualisation of endophyte hyphae within the tissue sections (Section 2.12.3).

In WT infected tillers, endophyte hyphae were seen colonising the SAM and the stem tissues below the SAM (Fig 3.11). Low numbers of hyphae were observed at the very tip of the SAM, and highest colonization densities were observed in stem tissues below the SAM region and in the base of the leaves. Endophyte hyphal colonization in these regions seemed random, disorganized and branched. Disorganized hyphae were also observed in the base of each developing leaf; however when entering the elongation zone of the developing leaves, hyphal morphology changed to long parallel hyphae, which were seldom branched. A similar distribution of hyphae was also observed in *E. festucae* $\Delta wscA$ infected tillers with no apparent difference in distribution or morphology when compared with WT hyphae. Disorganised $\Delta wscA$ hyphae in the leaf base, similar to the WT, entered the elongation zone of the developing leaf and formed long parallel hyphae, indicating that $\Delta wscA$ mutants are able to undergo intercalary growth (Fig 3.11). Transverse sections obtained from the same tiller (from tillers used to obtain LS through the SAM) demonstrated that endophyte hyphae of both WT and $\Delta wscA$ are distributed similarly throughout their respective leaves. Generally the youngest leaf (in the middle of the tiller) and the oldest leaf (at the outside) appeared to have a lower density of hyphae compared to the leaves of intermediate age (Fig 3.11).

When longitudinal sections of the leaf sheath were observed, both WT and $\Delta wscA$ had similarly dense, elongated, continuous and parallel arranged hyphae, evenly distributed within the whole leaf. These observations indicated uniform entry of both WT and $\Delta wscA$ hyphae into the elongation zone of the developing leaf and intercalary growth thereafter to form long continuous strands of endophyte hyphae.

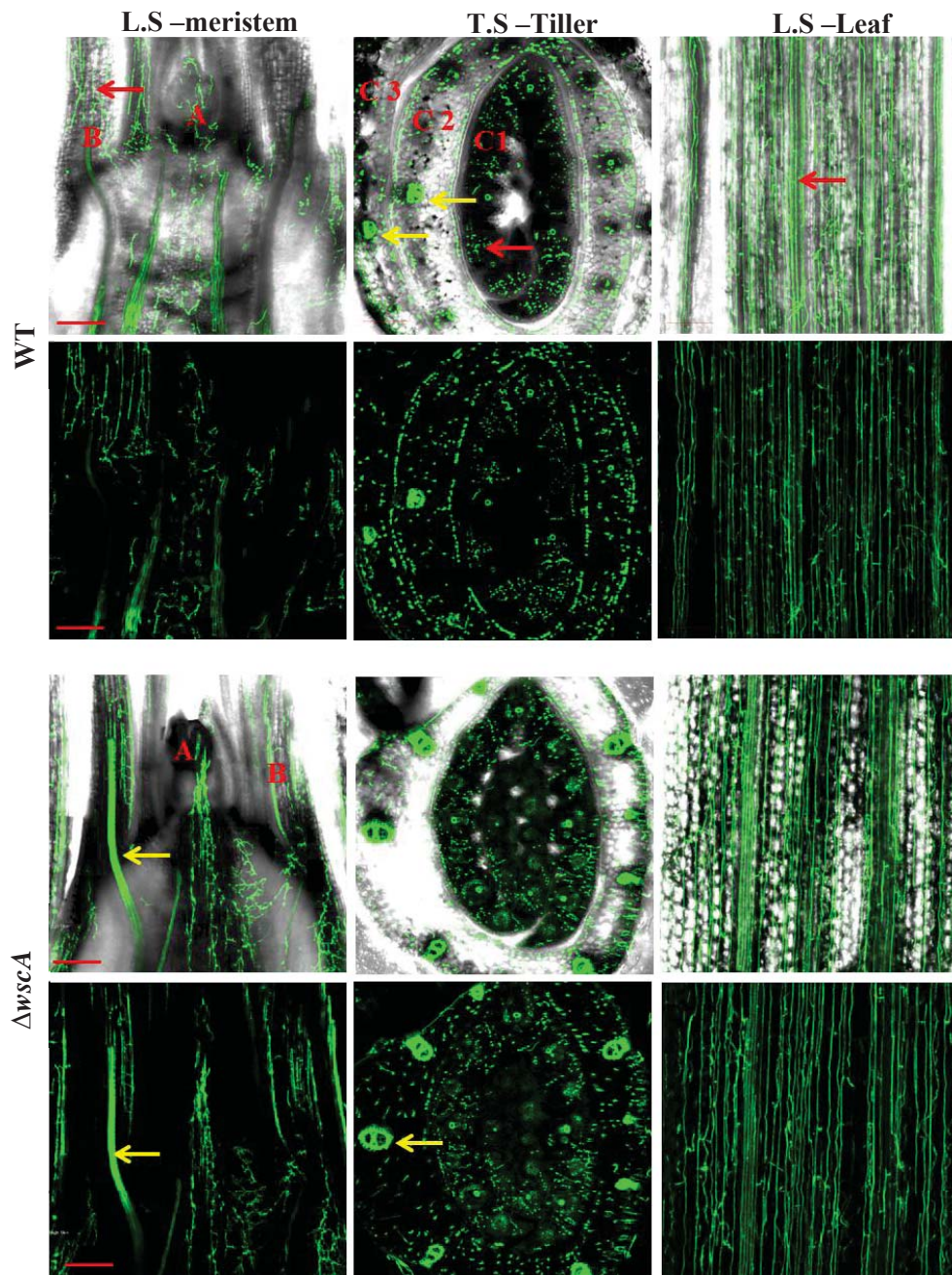


Figure 3.11: Comparison of hyphal colonization in *L. perenne* tillers infected with *E. festucae* WT and *wscA* deletion mutants expressing EGFP. Longitudinal sections (LS) of meristem and leaf and transverse sections (TS) were obtained from the same grass tiller. Fluorescent and phase contrast images are compressed Z stack confocal images. Green strands and spots represent endophyte hyphae (red arrow) in LS and TS respectively. Yellow arrows show auto fluorescing vascular bundles A-Shoot Apical Meristem, B- developing leaves, C1, 2 & 3 are concentrically arranged leaves in a grass tiller, from youngest to oldest respectively. Deletion of *wscA* did not result in any apparent defects in colonization. Scale bar = 200 μ m.

3.5.2 Deletion of *wscA* has no impact on the phenotype of the host

The eight week old plants used to investigate infection rate and colonization (section above) were also used to determine the impact of $\Delta wscA$ deletion on the host plant phenotype. The plants were assessed for visual appearance, number of tillers, tiller height and leaf morphology. Colonization by $\Delta wscA$ mutants did not have a visible impact on the host, however, due to the variations observed between plants infected with the same strain; further investigations were conducted to confirm this conclusion.

3.6 Discussion

This study was undertaken with the primary objective of identifying putative mechanosensors that are hypothesised to be involved in sensing mechanical stretch and stimulating intercalary growth in *E. festucae* endophyte hyphae during host leaf colonization (Christensen et al., 2008). Wsc1 of *S. cerevisiae*, and its orthologues identified recently in a few other filamentous fungi, is a crucial sensory membrane protein in the cell wall integrity (CWI) MAP-kinase pathway (Verna et al., 1997; Futagami et al., 2011; Dichtl et al., 2012; Maddi et al., 2012). Primarily responsible for sensing alterations in cell wall structure, shape and composition due to internal and external stresses, Wsc1 activates the CWI MAP kinase signalling pathway that subsequently coordinates cell wall biosynthesis for remodelling and maintenance of the cell wall (Klis et al., 2006; Rodicio et al., 2010; Levin, 2011).

We hypothesised that mechanical stress imposed on *E. festucae* hyphae by rapidly elongating host cells in the expansion zone of a developing leaf is sensed by mechanical stress sensors located on the endophyte membrane (the endophyte is attached to elongating host cells) that subsequently trigger intercalary growth. The ability of Wsc1 of *S. cerevisiae* to act as a nano-spring (Dupres et al., 2009) and its importance in

resistance against cell wall perturbing agents that interfere with the synthesis and structure of the cell wall (Dichtl et al., 2012; Maddi et al., 2012) were further evidence to support its role as a mechnosensor. Accordingly, *E. festucae* WscA was investigated for its potential role as a mechanosensor that stimulates intercalary growth in response to cell wall stress.

Characterization of the *S. cerevisiae* CWI MAP kinase pathway membrane sensors Wsc1, Wsc2, Wsc3, and Mid2 and their orthologues in filamentous fungi indicate that, although there is some functional redundancy among the sensors, in most cases Wsc1 and Mid2 play the leading roles in sensing cell wall stresses in fungi (Verna et al., 1997; Futagami et al., 2011; Dichtl et al., 2012). Therefore, as the initial step in characterising these CWI sensors in *E. festucae*, and their possible involvement in intercalary growth, I decided to conduct a gene replacement study on WscA in *E. festucae*. Further, the signalling components of the CWI MAP kinase pathway upstream of protein kinase C have been characterised in only a few filamentous fungi before (Dichtl et al., 2012), making this study important in providing new insights into CWI signalling in fungi in general.

E. festucae WscA shares very low identity with Wsc1 of *S. cerevisiae*. Nevertheless, the domain structure was mostly consistent with Wsc1 of *S. cerevisiae* and its characterised orthologues in *A. fumigatus* and *N. crassa* (Fig 3.1) (Verna et al., 1997; Straede et al., 2007; Dichtl et al., 2012; Maddi et al., 2012). Consistent with Wsc1 of *S. cerevisiae*, the N- terminal extracellular domain of WscA of *E. festucae* had a serine/threonine rich region that could be sites for O- and N-glycosylation (Lommel et al., 2004; Futagami et al., 2011). The length of the serine/threonine region in WcsA is short compared to that of the *S. cerevisiae* Wsc1, but similar in length to the characterised orthologous Wsc1 of

filamentous fungi (Fig 3.1). Glycosylation of the extracellular domain (catalysed by O-mannosyltransferases) is crucial for WscA function which gives it the rod-like structure required to sense cell wall stress (Lommel et al., 2004; Dupres et al., 2009; Kriangkripipat et al., 2009). The eight conserve cysteine residues important for clustering proteins/sensors and mediating non-covalent binding with cell wall glucans (Heinisch et al., 2010) were also found in WscA of *E. festucae*. Multiple sequence alignment of WscA with the orthologues from other fungi showed that the extracellular domain is less conserved among fungi than other domains, highlighting potential differences in their sensory functions (Fig 3.1) (Maddi et al., 2012). In contrast, the intracellular WscA C-terminus shares a high level of homology with orthologues, suggesting the common function of activating GTPase Rho1 through the GDP-GTP exchange factor, Rom2 (Philip et al., 2001; Maddi et al., 2012) is also conserved in the *E. festucae* gene. However since *E. festucae* WscA shared very low identity with Wsc1 of *S. cerevisiae*, complementation of the *S. cerevisiae* *wsc1* deletion mutant with *wscA* would also be required to verify this gene as the yeast orthologue.

During the analysis to find orthologues for Wsc1 of *S. cerevisiae* in *E. festucae*, two further proteins that shared a similar domain structure to WscA were recovered from the genome sequence which aligned independently with Wsc2 (CWI MAP kinase pathway) and Wsc4 (ER membrane protein) of *S. cerevisiae*. Previous investigations have shown that only two *wsc* family genes exist in the CWI MAP kinase pathway in the other filamentous ascomycetes that have been studied so far (Futagami et al., 2011; Dichtl et al., 2012). Consistent with these fungi, and with the bioinformatic analyses in this project, it is likely that *E. festucae* harbours only two Wsc family genes in the CWI MAP kinase pathway as well. Therefore, the other Wsc protein of *E. festucae* which

aligned most closely with Wsc2 of *S. cerevisiae* may be the orthologue of *S. cerevisiae* Wsc2.

The most notable features of the *E. festucae* $\Delta wscA$ strains, in comparison with the WT, was their significantly reduced radial colony growth rate (Fig 3.4), lack of aerial hyphae (Fig 3.5) and pronounced cell wall aberrations (swollen CW patches along the hypha) (Fig 3.6) observed when grown on a standard PDA medium. Similar and contrasting phenotypes in Δwsc have been reported in other fungi. In *A. fumigatus*, *wscA* deletion resulted only in a slight reduction in radial colony growth rate with a slightly less dense colony fringe (Dichtl et al., 2012), while in *A. nidulans* (Futagami et al., 2011), *Ashbya gossypii* (Lengeler et al., 2013) and *N. crassa* (Maddi et al., 2012) a significant reduction in growth rate was observed (with reduced aerial hyphae in *N. crassa*). Contrary to the $\Delta wscA$ culture phenotypes observed in *E. festucae*, deletion of downstream components of the CWI MAP kinase pathway, *mkkA* and *mpkA* in *E. festucae* resulted in normal colony growth and morphology with a branching pattern similar to that of the WT (Becker et al., 2014). However, TEM studies on hyphae of these mutants showed structural changes in the cell wall with the absence of the outer cell wall layer. Due to the unmasking of chitin in the cell walls, an increase in cell wall fluorescence has been observed in *mkkA* and *mpkA* mutant hyphae *in planta* when stained with Alexafluor 488 WGA (Becker et al., 2014). This observation resembles the in culture phenotype observed in $\Delta wscA$ hyphae when stained with CW. In addition, $\Delta mkkA$ and $\Delta mpkA$ of *E. festucae* are defective in hyphal cell-cell fusion and form intra-hyphal hyphae which are considered to be a consequence of cell wall weakening and damage (Becker et al., 2014). These phenotypes have not yet been investigated in the *wscA* mutants created in this study.

Osmotic stabilization of *E. festucae* $\Delta wscA$ hyphae with the higher (e.g 125 mg/mL) concentrations of sorbitol used in this study rescued the aberrant cell wall phenotype and restored the colony growth rate to the WT level (Fig 3.7). Similarly, in *S. cerevisiae* the cell lysis defects in CWI MAP kinase pathway mutants was also rescued by supplementation of media with 1M sorbitol (Cid et al., 1995). A more detailed study on the *A. nidulans* *wscA* disruption mutants demonstrated comparable results, with reduced colony growth rates and swollen structures on aerial and submerged hyphae when grown on YG (yeast extract and glucose) medium which were fully rescued by growth on a hyper-osmotic medium supplemented with 0.6 M KCl (Futagami et al., 2011).

The reduced colony and hyphal growth rates, cell wall aberrations, and the ability of osmotic stabilisers to rescue these phenotypes, suggests an alteration in cell wall structure and composition caused by *wscA* deletion in *E. festucae*. The underlying causes of observed defects in colony morphology have not been reported in detail for the *wsc1* deletion mutants of *A. fumigatus* and *N. crassa*. However, in *A. gossypii*, *wsc1* deletion resulted in frequent hyphal tip lysis and polarity disruption resulting in dichotomous tip branches which was believed to be the primary reason for the colony growth defects observed (Lengeler et al., 2013). In comparison, *wscA* deletion in *E. festucae* resulted in a slight increase in hyphal tip lysis but no tip branching. Nevertheless, the apical growth rate of individual hyphae of *E. festucae* $\Delta wscA$ mutants was significantly reduced suggesting that impaired apical growth might be the primary reason for reduced colony growth and lack of aerial hyphae. Given that apical growth rates have not been reported for individual hyphae in other fungi with similar gene deletions, a detailed comparison of hyphal growth rates between relevant fungi was not possible.

To understand the defects in cell wall and hyphal growth in $\Delta wscA$, it is important to understand the link between the CWI MAP kinase pathway and cell wall synthesis. In the CWI MAP kinase pathway of *S. cerevisiae*, Rho1 is a membrane-localized Ras-related GTP-binding protein activated by CWI sensors including Wsc1 (Nonaka et al., 1995). Rho1 activation leads to three processes involved in protecting cell wall integrity. Firstly, by activating protein kinase C 1 (PKC1) (Nonaka et al., 1995) Rho1 stimulates synthesis of cell wall biosynthetic enzymes such as 1, 3- β -glucan synthase via induction of transcription factors such as Rlm1 and Swi4/Swi6 (Jung et al., 1999; Zu et al., 2001; Jung et al., 2002). Secondly, acting as a regulatory subunit of the 1, 3- β -glucan synthase (GS) complex, Rho1 directly activates 1, 3- β -glucan synthase (Drgonová et al., 1996; Qadota et al., 1996) and thirdly, Rho1 reorganizes the actin cytoskeleton during growth via the Bni1 protein (Fujiwara et al., 1998). Performing a similar role in other yeasts and filamentous fungi such as in *C. albicans*, *A. fumigatus* and *A. nidulans*, Rho1 is essential for cell viability, radial growth, branching, and cell wall synthesis (Smith et al., 2002; Guest et al., 2004; Dichtl et al., 2012). Moreover, a study on *A. nidulans* indicated that *wscA* deletion also alters the expression of α -1,3-glucan synthase genes (decreasing the transcription of *agsA* and increasing transcription of *agsB*) while increasing the amount of α -glucan and alkali soluble β -1,3/1,6-glucan in the cell wall when cultured on a YG medium (considered to be hypo-osmotic). In contrast, when cultured on YG containing 0.6 M KCl, the transcription of cell wall synthesis genes and cell wall composition of $\Delta wscA$ was similar to the WT. The chitin content of the cell wall did not change in the $\Delta wscA$ compared to the WT under either condition (Futagami et al., 2011). This indicated that under hypo-osmotic conditions WscA in *A. nidulans* could be playing a crucial role in regulating cell wall synthesis, but

under hyper-osmotic conditions it is dispensable and another signalling pathway may take over, possibly the HOG pathway.

Considering the high conservation in CWI MAP kinase pathways among filamentous fungi, it is possible that the Rho1 orthologue in *E. festucae* performs a similar central role, and deletion of *wscA* may affect cell wall synthesis causing changes in structure and composition of the cell wall as demonstrated in other fungi. Hence, defective cell wall synthesis in $\Delta wscA$ of *E. festucae* is a likely cause of reduced hyphal growth and cell wall aberrations observed in culture, although this remains to be tested. One possible explanation for the absence of certain in culture phenotypes (reduced growth and cell wall aberrations) in the *mkkA* and *mpkA* mutants (presumed to be down stream of $\Delta wscA$ in the CWI MAP kinase pathway) could be the existence of an alternate signalling cascade in *E. festucae* that bypasses the MAPK cascade, possibly through RhoA as mentioned before. One other possible candidate is the HOG MAP kinase pathway as suggested for *A. nidulans* (Futagami et al., 2011). However, the ability of osmotic stabilisers to reverse the $\Delta wscA$ mutant phenotypes (reduced growth and cell wall aberrations) may also be due to the supportive effects of osmo-protectants on weakened cell surfaces. In standard PDA the damaged cell wall can be seen as CW accumulation in swollen patches, presumably as a result of internal turgor pressure pushing on a weakened cell wall and greater stain penetration. Osmotic stabilization of *E. festucae* $\Delta wscA$ hyphae allowed hyphae with weakened cell walls to grow and to appear morphologically similar to the WT. Similarly, in WT hyphae growing on PDA, CW mostly stains the wall at the nascent tip, where the cell wall is under stretch (due to turgor pressure) and has not yet solidified. As the cell wall hardens away from the tip CW penetration becomes less efficient.

In the presence of damaging concentrations of the cell wall perturbing agent CW, both the *E. festucae* $\Delta wscA$ and WT strains showed sensitivity, however when exposed to CW in the background of a osmotic stabiliser (sorbitol) the sensitivity of $\Delta wscA$ was higher than the WT suggesting a role for WscA in resistance against cell wall perturbation in *E. festucae* (Fig 3.8). Similar to *E. festucae*, Wsc1 is important in resistance against cell wall perturbing agents in *S. cerevisiae* and *N. crassa* but not in *A. fumigatus* and *A. nidulans* (Reinoso-Martín et al., 2003; Levin, 2005; Futagami et al., 2011; Maddi et al., 2012). In *A. fumigatus* MidA (instead of WscA) is specifically required for resistance against cell wall perturbing agents (Dichtl et al., 2012). These observations again reveal the variation shown in the sensory roles of Wsc1 in different fungi. Further, the *mkkA* and *mpkA* mutants of *E. festucae* did not show any increased sensitivity to cell wall perturbing agents above the WT (Becker et al., 2014), again suggesting an alternative to the PKC pathway downstream of WscA. Previous studies have shown an increase in chitin content in the cell walls of various *Candida* species when exposed to cell wall perturbing agents and WscA of *E. festucae* may have a similar role (Walker et al., 2013). This remains to be determined.

Attempts to investigate the distribution of WscA in *E. festucae* indicated that C terminal-tagged EGFP, expressed under its native promoter, did not show any distinct localization, while the constitutively-expressed (TEF promoter) WscA tagged with EGFP showed clear localization to the fungal surface (Fig 3.9). The WscA localization pattern (when expressed under a constitutive promoter) clearly overlapped with the CW-stained cell walls and septa (Fig 3.9), indicating that WscA in *E. festucae* could be localising to the plasma membrane. A study in *A. fumigatus* showed a similar localization pattern for WscA, where a clear localization to the cell periphery was observed only when expressed under a constitutive promoter (Dichtl et al., 2012).

Failure of *wscA-egfp* constructs expressed under native or constitutive promoter to fully complement the $\Delta wscA$ in terms of colony radial growth rate and hyphal morphology revealed that the EGFP fusion to the C terminal of the WscA protein may have compromised its functionality.

The main objective of *wscA* deletion in *E. festucae* was to investigate its role in intercalary growth in plants. Investigations on the ability of $\Delta wscA$ to colonize the host (*L. perenne*) revealed that the mutants are able to grow within all host plant tissues in a similar manner to the WT without any major impairment, despite the significant growth defects shown in culture (Fig 3.11). Hyphal densities in different plant tissues were similar to the WT and no other apparent abnormalities were observed. In the elongation zone of developing plant leaves where the endophyte switches from tip growth to intercalary growth, mutant hyphae were elongated, arranged in parallel and seemed to be synchronised with host cell elongation (the WT phenotype). In a situation where intercalary growth only is impaired, the mutants would be expected to either fail to enter the elongation zone of the developing leaf (as intercalary growth is a prerequisite for growth in the elongation zone) or hyphae could be present, but heavily fractured as the host cells would be expected to pull the attached endophyte hyphae apart. No such observations were made suggesting that $\Delta wscA$ can undergo intercalary growth (Fig 3.11). However, it will be useful to further investigate the mechanosensing role of WscA of *E. festucae* and its possible involvement in intercalary growth under *in vitro* conditions, thus eliminating other potential influences in the complex plant environment. During this study, a successful method was developed to apply mechanical stress by stretching fungal hyphae under *in vitro* conditions (Section 5.3) and this system should be used to test further the ability of WT and $\Delta wscA$ to sense mechanical stress and undergo intercalary growth.

The ability of *wscA* mutants to colonize leaf tissue in a similar manner to WT, despite the severe growth defect shown in culture, could be due to osmotic stabilization provided by the apoplastic fluids which usually contain high concentrations of sugars, amino acids and other solutes (Lohaus et al., 2001). Studies conducted before on $\Delta wscA$ (discussed above) indicate that mutant growth defects (reduced colony growth rate and aberrant cell walls) can be restored in culture using osmotic stabilisers such as sorbitol. Further studies are required to determine whether the apoplastic fluid of perennial ryegrass is able to support apparently normal hyphal growth of *wscA* mutants in plants. Contrary to the normal colonization demonstrated by the *WscA* mutants, a study on *mkkA* and *mpkA* mutants (downstream of the CWI MAP kinase pathway) of *E. festucae* has revealed the importance of these genes in maintaining synchronised mutualistic growth within *L. perenne* (Becker et al., 2014). Deletion of these genes resulted in reduced infection rates, decreased seedling and plant survival rates, stunting of plants, an increase in hyphal density within intercellular spaces, and colonization of vascular bundles, indicating the loss of a synchronised symbiotic relationship with the host. None of these phenotypes were evident in the $\Delta wscA$ mutant of *E. festucae*. This could be due to overlapping functions in CWI sensors. Loss of *WscA* may be complemented by other potential CWI sensors such as *Wsc2*. A preliminary analysis of the genome has indicated the presence of *WscB* (orthologue of *Wsc2* of *S. cerevisiae*) as well as a *Mid2*-like protein (orthologue of *Mid2* of *S. cerevisiae*) in *E. festucae*. It is therefore possible that other CWI sensors may complement the loss of *wscA*. However, such complementation of *WscA* loss is not observed in culture where *wscA* mutants show severe defects in apical growth and maintenance of cell wall integrity. These complex phenotypes imply that the CWI sensor in *E. festucae* not only shows differential

sensitivity to various stimuli but also may use different signalling cascades to transduce signals for different stimuli.

In summary, based on the observations made so far, the WscA of *E. festucae* is a membrane protein consisting of a serine/threonine rich region N-terminus (possibly glycosylated), plus conserved cysteine residues (for possible clustering) and a C-terminus that is possibly intracellular for signal transduction. It has a role in hyphal apical growth, maintenance of cell wall integrity (cell wall synthesis) and resistance against cell wall perturbing agents in culture, but is not essential for host colonization or growth in the host expansion zone. The sensory role of WscA appears to differ among fungi, possibly reflecting the high degree of variation shown in the extracellular N terminal (Maddi et al., 2012). Further, considerable redundancy among the CWI sensors in *E. festucae* could be expected as shown in other filamentous fungi. The ability of the mutants to colonise plants in a similar manner to the WT may be due to the ability of other CWI sensors to complement the loss of WscA. In most filamentous fungi such as *N. crassa*, *A.gossypii* and *A. fumigatus* the phenotypes of mutants defective in Wsc sensors of the CWI MAP kinase pathway most often overlapped with the phenotypes (reduced radial growth, defective conidiation, sensitivity to cell wall perturbing agents) of mutants defective in downstream components of the CWI MAP kinase (Park et al., 2008; Valiante et al., 2009; Dirr et al., 2010; Maddi et al., 2012; Lengeler et al., 2013). In *E. festucae*, no such resemblance between the phenotypes of *wscA* and the *mkkA* and *mpkA* mutants in the CWI MAP kinase components was observed. Thus, in *E. festucae*, signals emanating from WscA may be transduced through an alternative pathway to the MAPK cascade. The ability of $\Delta wscA$ to colonise developing host leaf tissues indicated that it is not individually essential for intercalary growth in the host environment.

Chapter 4: Characterisation of *E. festucae* MidA and its role in intercalary growth

4.1 Identification of the *S. cerevisiae mid1* orthologue in *E. festucae*

The putative *midA* orthologue (Maker gene prediction contig_726-gene-0.103 or FGeneSH prediction A.11.1486) was retrieved from *E. festucae* by interrogating the F11 (also known as E894) genome sequence database located at University of Kentucky, USA (<http://www.endophyte.uky.edu/>, *E. festucae* FL1, 2011-03 assembly, version 2) (Schardl et al., 2013) using the tBLASTn algorithm (Altschul et al., 1990; Altschul et al., 1997). Mid1 from *S. cerevisiae* (AKB00818.1 or SGD ID- S000005235) and Mid1 proteins of *Claviceps purpurea* (CAU66903.1), *Gibberella zeae* (ESU13681) and *N. crassa* (EAA31782.3) were used as query sequences. This putative orthologue for *mid1* of *S. cerevisiae* in *E. festucae* was named *midA* according to the recommended gene nomenclature for *E. festucae* (Schardl et al., 2012). The putative MidA amino acid sequence of *E. festucae* was very similar to those from filamentous fungi such as *C. purpurea* (66% identity, E value-0.0) and *G. zeae* (46% identity, E value – e-141). However, it was comparatively distantly related to *S. cerevisiae mid1*, with an E value of 2e-32 and 31% identity. The *mid1* genes of *C. purpurea* and *G. zeae* have been functionally characterized (Bormann et al., 2009; Cavinder et al., 2011) providing some supporting evidence that the putative orthologue identified in the *E. festucae* F11 genome is the orthologue of the *mid1* gene in *S. cerevisiae*.

Reciprocal tBLASTn analysis of the *E. festucae* putative MidA protein against the *S. cerevisiae* (<http://www.yeastgenome.org>) and *N. crassa* (<http://www.broadinstitute.org/annotation/genome/neurospora>) genomes produced Mid1 as the top hit, and reciprocal tBLASTn against the NCBI data base (<http://www.ncbi.nlm.nih.gov/>) returned Mid1 of *C. purpurea* as the top hit. Further evidence to support the function of the *E. festucae mid1* gene was obtained by analysing the domain structure of the predicted protein.

The conceptual *E. festucae* MidA protein contains 638 amino acids (see Appendix 4 for sequence). According to available details, both *C. purpurea* (653 amino acids) and *S. cerevisiae* (548 amino acids) Mid1 proteins contain a signal peptide and N-glycosylation sites towards the N-terminus. The C-terminus consists of a cysteine rich region with ten conserved cysteine residues (Iida et al., 1994; Ozeki-Miyawaki et al., 2005; Bormann et al., 2009). Similarly MidA of *A. fumigatus* (642 amino acids) contains an N-terminal signal peptide and 13 deduced N-glycosylation sites. MidA of *S. cerevisiae* and *C. purpurea* contain 4 transmembrane domains while in *A. fumigatus* 4 or 6 transmembrane domains have been reported (Iida et al., 1994; de Castro et al., 2014). Structural domain analysis of *E. festucae* MidA using bioinformatics tools (Section 2.15) revealed the presence of functionally important domains and conserved regions in common with Mid1 of yeast and other filamentous fungi.

Analysis using InterProScan revealed that the putative *E. festucae* MidA protein belongs to the stretch-activated cation channel Mid1 (IPR024338) family. A signal peptide is present (35 amino acids) at the N-terminus and a cysteine-rich region is present close to the C-terminus with 10 conserved cysteine residues including the four residues which are essential for its function (Fig 4.1). According to the N-glycosylation site prediction tool NetNGlyc, MidA of *E. festucae* has 9 sites (with 3 more potential sites) while a similar analysis in *N. crassa*, *C. purpurea* and *G. zeae* showed 9, 9 and 8 sites respectively (Fig 4.1). Analysis of protein sequences for transmembrane domains using the prediction tool TMpred returned two domains (Fig 4.1), whereas analysis with TMHMM revealed only one transmembrane helix from Q⁷ to V²⁹ overlapping with the predicted signal peptide sequence. According to TMpred analysis *N. crassa*, *G. zeae* and *C. purpurea* have 2, 2 and 3 transmembrane domains respectively. A previous study has shown that most Mid1 proteins are GPI-anchored

(Glycosylphosphatidylinositol) (Pei et al., 2012). An investigation using the GPI-anchor prediction tool revealed the presence of possible GPI anchor sites in *E. festucae* MidA and the Mid1 proteins of *C. purpurea*, *G. zeae* and *N. crassa* (Fig 4.1) but not in *S. cerevisiae*.

```

N. crassa      MHLGPHLHRFFAASFIALSLLVFNITLFLSLDCALAAELEDAPPILLDDVDSLDLVSQGS
G. zeae       MIPNASISRLPISRKTYILTLVLSLFLCAFGNAHASELLHD-SIF---DAETHERSDAS
E. festucae   MQLSPLQSRLVASLAATFCLLVLSLLLVKGAVAHEFLHE-SFL-TSSTRPDLASFEED
C. purpurea   MQLSPLQSRLAASLAATVCLFLLYLLLLLAPQGAVFELPLD-SLSRSSSSWTDLASIEGN
*   ..   * : * :   . : *   * * * :   . :   .   . :   . .

N. crassa      VSDLGSPLDQMYEPEFAAFDRSIIGRDQVRDTNALINNEAFQLNVRQGDTE-RFVFKLSQ
G. zeae       -----NLIYEPDFGAFDRSILGRAP-AEQSLLTNNGPDSRKLSPGATV-CYVVDKKT
E. festucae   GHSPDSQ-ISSYEPILNFLGRSILGRA--GDTIPLENDKPLAFNIQPGGAPICYI IKKGS
C. purpurea   -DDLGSHTPFYEPILNFLGRSILGRA--GDTIPLGDEAPLAFNLQPGNAPICYI IKKGS
* * * :   . : * * * * * :   * : : .   . : * :   . : . .

N. crassa      LSERELEVVQLELRDEEHTWEDIDEDEDEDEAEDEKDENNDLSGKGLDRDSVDLNLAS
G. zeae       LFGKD-----KRDDDGHEPRNAEDDPGHQNF-----
E. festucae   L-GNS-----TSQGKQVPRQTDDDNNERTG-----
C. purpurea   L-GNS-----TDPASRKRDDDDDDDDDPDDT-----
*   ..   .   .   .   .   .   .   .   .   .   .   .   .   .   .   .   .

N. crassa      AKQKLGKRQGARRLFLSANTCLQPAFNATKTTQP-----PPQLTLYVSTSTDNVPEP
G. zeae       --RRAE-----SKTVYISVNTCSRPTMKSKDKDNNPET-----APQLSLYTSMS--KIK
E. festucae   --QEVK-----NATIYISANTCLQPIVQSGGKRSKP-----PQLILFLSNGT--EAG
C. purpurea   --ADASVYEGMNTTYISANTCLQPKIRPKGNDTDKSNKSGPKPPQLIMFLSNGTDKDVG
* * * * * : : * * * * * :   . .   * * * : : * * * :

N. crassa      GPGADSNSQVS-----MVFNEGAIMYN-FTTTTDVYVGVHAPNVAEIFDKPYNIKIAI
G. zeae       CPDSSNYNKTN--SDLKRIPFDEGAAMVT-VNATDAIYISVAAPNITKKHDGWEYQIAI
E. festucae   CPQVTSNPKGHLARGFTSHTFEEGAVRVS-ANATSDIYIGLYAPNITDSFEGSYDYQVAA
C. purpurea   CPRITNSTSGEVTQGFTAHNFEGAVTVSLINATTDVYIGIYAPNIEDDYEGVYNYQVAA
*   .   .   .   .   .   .   .   .   .   .   .   .   .   .   .   .

N. crassa      STDGYYYSYN--VDDADLIWVDSDSQGALLITHNLTDSNDEKEQQRIMN-TPPYVMFAQ
G. zeae       SFDEYYHNYDS-QNGTARLLLMDTDSTSALLVTSNLTE--DSSETQQIMKRPPYQLFVG
E. festucae   SSTEYFHQYQSNETEGAKLLWMSDSTAALLITRNLTT--EASEARRIWSEDPPYQLVS
C. purpurea   SSTDYFHDYQSNAEDGAELLWMSDSTAALLMTRNLTD--DASETREVSEDPPYQLVS
*   * : : * :   * * : : * * * * * : * * * :   . * . :   . * * * : :

N. crassa      DKSNPSINGVRYSFCGLEQNAQIATTKDG--KYSNMVQTGMTKRGQGNFPKQQFFFSGLK
G. zeae       DEKLRSIDGLRHSACGLKQSAEIWANSNRTGRHNDLVTGVTTRGPGQLPKQQFLIAGLN
E. festucae   GQDWPMLDGLHHSACGLERNALVGGANKEGTAKNNGMVKTSMTLRGPGGMPKQQFYVGLN
C. purpurea   GQDWPVLDGLRRSACGLENNAPIGSNGHGTAKNNEMVRTSMTLRGPGGLPKQQFYVLGLN
* * * : : * :   * * * * * : :   . .   * * * * * : * * * * * : * * * :

N. crassa      PSTSYLGILAKTNVT--DTGSPNLVGG-----GGHVFKATNFQTKSDHGNCNIVLNLTF
G. zeae       HSSSYLGILVKMEG--NGKRAETTGG-----GGTVYRATSFETSSSS-NCKMVTNLDF
E. festucae   ATTSYSGVLVQPANVTVNSKRQANGGQSLRKPGSVVFQGTTFQTNAAP-NCKVVTDLEF
C. purpurea   ATTSYSGMLVLPANTTVNVKRQDDASGSS-RKRGSIVFEGTTFQTNAAP-NCKVVTDLEF
* * * * * :   .   .   .   .   .   .   .   .   .   .   .   .   .   .

N. crassa      CDQVAYSVPSPNPNFGNASVLAKFYDDYAAEAWGYFKKALAQVACEAPVTQRYSLTRNCSD
G. zeae       CNETQYAVPGNDKKFNNALAKHYDDYARKMYANFEKVMMQMPCETTPESLYSLVRNCDE
E. festucae   CDEIQYAVPGNDGKFNNTELAKVYDKQAKTVYDNFLKVMQQIQCEADRTSKYSLARTCED
C. purpurea   CDEIQYAVPGNDGKFNNTELAKTYDKQAKSIYDNFLKVMQQIQCEADRTSRYSLARTCED
* : :   * * * * * :   * : * * * * * :   * * * : * * * :   . * * * * * :

N. crassa      CEAYKDWLCSVTIPRCEFSNNASYLHPRAMSQPFPDGERLDNATMSLYAENYGDGKVL
G. zeae       CRAAYKRWLCTVTIPRCEDVMGSSRFSVVRNAFQAFPNG-----TLLPDNFRKGL-N
E. festucae   CKRAYKRWLCTVSFPRCEFLDGSSRFSVLRNVNQAFPNG-----TLLPTEIRQELAK
C. purpurea   CKRAYKRWLCTVSLPRCEFLDGSSRFSVVRNVNQAFPNG-----TFLPTDIRQELAK
*   * * * * * : : * * * * * :   . :   *   * * * * * :   . :   .   .

```

```

N. crassa      GKAFFLQSRSSRIDEFIKPGPYKEVLPCDYLCYRLVQSCPSSMGFGCPLPGQKGFNSSYYI
G. zeae       SSANSSRNAWIDETVKPGPYKELLPCQDICYDVVQSCPSAIGFTCPQPGFPSFDVSYGE
E. festucae   VPAQNASRNSFIDETIQPGPYKEIMPCEDICYQVVQSCPAMIKFNCPQPGMYGFNVTYGR
C. purpurea   LPSQNASRNAFIDQTIQPGPYNELMPCEDICYQVVQSCPAAIQFKCPQPGMYGFNMTYGV
              :   *.:   **.:   ::*****:*.:**.:   **.:*****:   :   *. **. **.   .*:.*
N. crassa      KNETNGEVVCNYPCSAHIFSGSSKDAVSVGLTIVVLVLSLLAC---
G. zeae       RNSDTSSITCNYPGEARTKISAARVIRP-GTFMLGVVSLMMWLAV---
E. festucae   RNADNTVVSCNFPGEARTRTSAGHDTIP-NLALLTCIMSVFSILVMAR
C. purpurea   RVANSTVVSCNFPGEARTPTSAGTVTMP-GLALVAWVALFLFGLLVVW
              .   .   :   **.:**.*.   ..   .   .   ::   :   :

```

Figure 4.1: Multiple sequence alignment between *E. festucae*, *C. purpurea* (CAU66903.1), *N. crassa* (EAA31782.3) and *G. zeae* (ESU13681), Mid1 orthologues of of *S. cerevisiae* (AKB00818.1). Underline – Signal peptide. Red letters – Conserved cysteine residues. Highlighted red - Conserved cysteine domains shown to be essential in *S. cerevisiae*. Highlighted green – GPI anchor sites. Highlighted blue – potential N-glycosylation sites. Highlighted grey – Transmembrane domains (according to TMpred). The multiple sequence alignment was performed using ClustalW2 from <http://www.ebi.ac.uk>.

4.2 Targeted deletion of the *midA* gene in *E. festucae*

To determine the functional role of MidA in sensing mechanical stress, stimulating growth, and in general calcium homeostasis, the *midA* gene in *E. festucae* F11 was replaced by targeted gene replacement using the split marker strategy (Section 2.7 & 2.7.2). Protoplast transformation with *midA* replacement vectors pSAM1 and pSAM2 (Appendix 3, Fig 8.2) resulted in 90 hygromycin-resistant colonies per 4.0×10^6 protoplasts. There was no growth observed in the negative controls (water only), while transformation with the positive control plasmid (pPN1688) resulted in 65 resistant colonies per 4.0×10^6 protoplasts. After hyphal tip purification genomic DNA was isolated from individual colonies (Section 2.4.3 & 2.5.7.1) and PCR screened using primer pair smid-36/smid-37 and smid-33/smid-38 (Table 2.3) to identify putative *midA* replacement mutants (Fig 4.2). PCR screening revealed that targeted deletion of *midA* was successful in nearly 36% of the total colonies screened. Based on PCR results, strains $\Delta midA$ -20, 28, 36 and 43 were selected for further confirmation by Southern blotting.

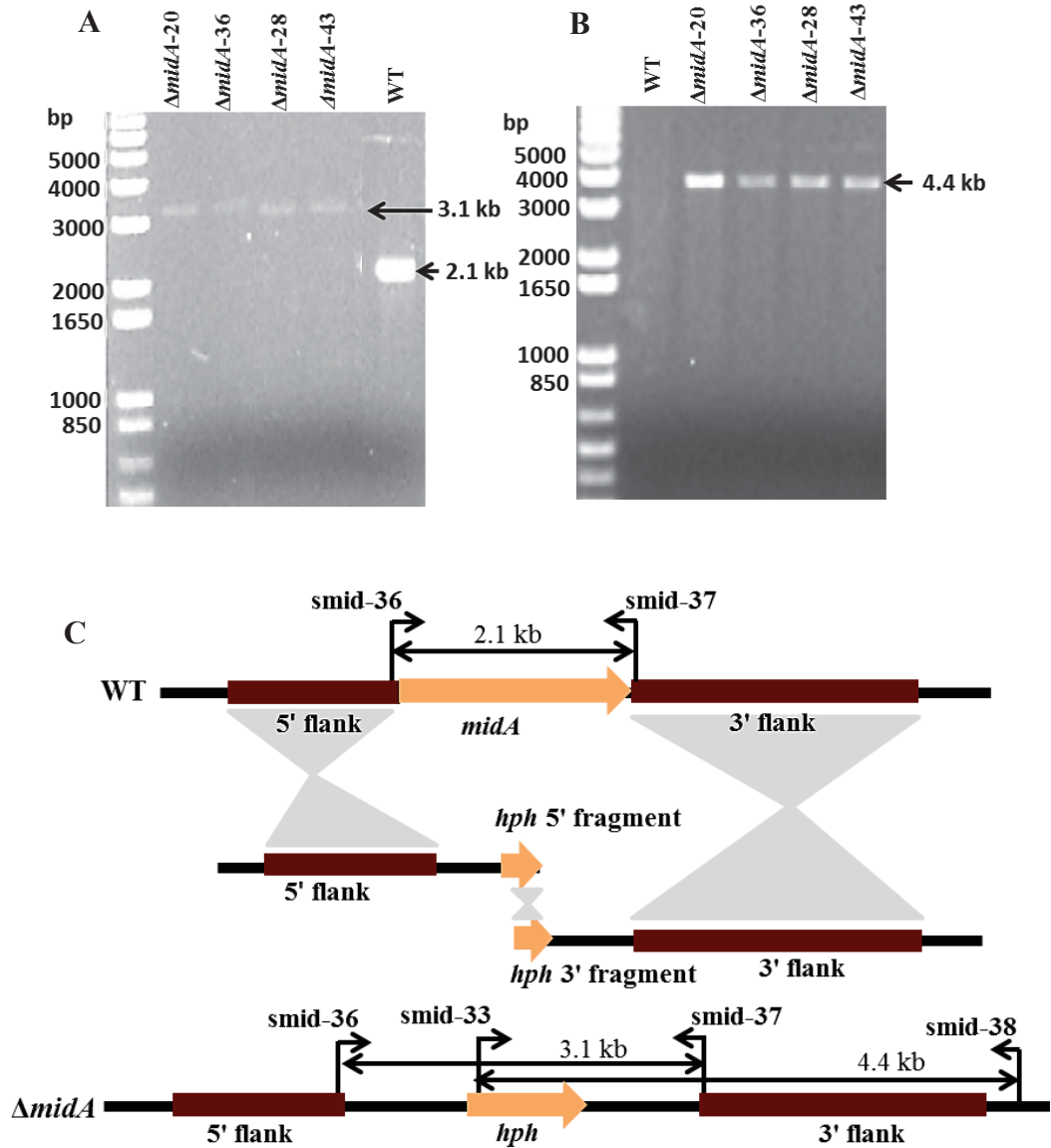


Figure 4.2: PCR screening to identify *E. festucae* *midA* gene replacement mutants. **A**-In a targeted replacement of *midA* the primer pair smid-36 and smid-37 is expected to yield a PCR product of 3.1 kb, and for WT and ectopic insertion a product size of 2.1 kb is expected. **B**-The putative mutants were further analysed via primer pair smid-33 and smid-38. Expected band sizes were 4.4 kb for the mutants and no product for the WT and ectopic colonies. **C**- Schematic diagram (not drawn to scale) showing the replacement of *midA* gene with the *hph* gene (for hygromycin resistance) by the 5' and 3' flanking fragments through 3 homologous recombination events shown as shaded areas.

Similar to the strategy used for confirmation of *wscA* replacement mutants (Section 3.2), Southern blotting was carried out to confirm the targeted replacement of *midA* and absence of ectopic insertions. Four PCR-confirmed putative *midA* deletion strains were selected, along with a strain with an ectopic integration Ect 7. As shown in Fig 4.3 probes C and D were designed to confirm replacement of *midA*. According to the Southern blotting results obtained from both EcoRI and PstI digested genomic DNA it was clear that *midA* mutants 20, 36 and 43 did not have any ectopic integration or tandem integrations in the *midA* locus. It is not clear whether the additional band present in the EcoRI-digested $\Delta midA$ -28 strain is due to an ectopic integration or partial digestion of genomic DNA. Strains $\Delta midA$ -20, 36 and 43 were selected for further analyses on the basis of unambiguous Southern blotting results.

As the phenotype of the *midA* mutants were different to the wild type in axenic culture (shown in Sections 4.3.1), the mutant phenotypes were complemented by ectopic integration of a single copy of the *midA* gene into the $\Delta midA$ -20 strain using the PEG-mediated protoplast transformation procedure (Section 2.6.3) with complementation vector pSAM5 (Geneticin[®] resistant, Sections 2.7.3.2). To confirm the integration of the *midA* gene at the new locus, transformants were PCR screened using primer pair smid-18/smid-4 (Table 2.3). Based on PCR results, three independent transformants were selected as *midA* complemented strains (Comp-10, 20 and 32) for further analyses.

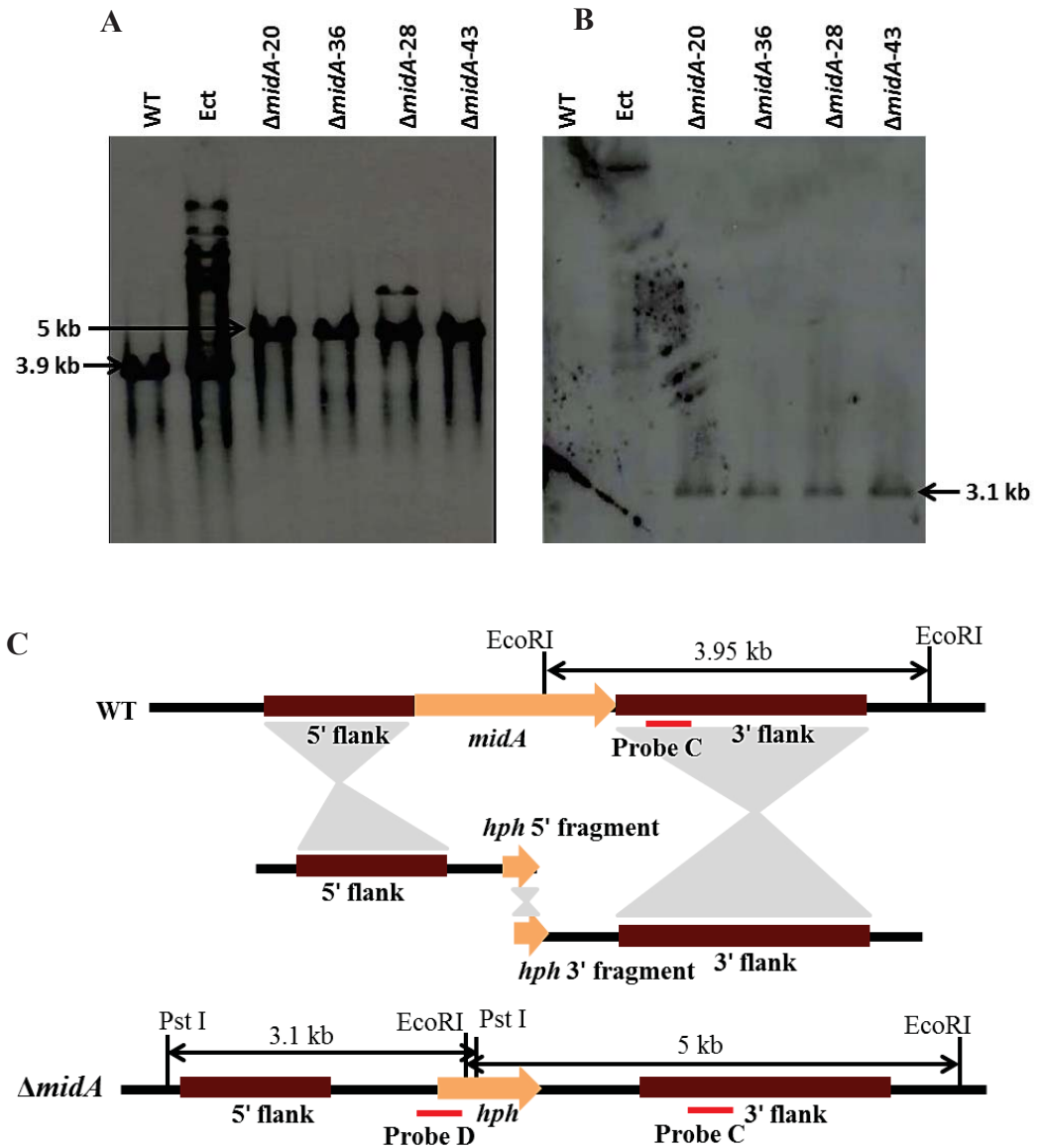


Figure 4.3: Southern blot analysis to confirm *midA* replacement and absence of ectopic integration in putative *E. festucae* *midA* replacement mutants. **A** - Genomic DNA was digested with EcoRI and hybridized with probe C. Expected band sizes for WT and *midA* replacement mutants were 3.9 kb and 5 kb respectively. **B** - Genomic DNA was digested with PstI and hybridized with probe D. Expected band size for the *midA* replacement mutants was 3.1 kb and no bands were expected for the WT. The presence of additional bands of different sizes was indicative of ectopic integration. **C** - Schematic diagram (not drawn to scale) showing the replacement of the *midA* gene with the *hph* gene through homologous recombination events. The sites of restriction enzymes used and the probe annealing positions are shown.

4.3 Functional characterisation of the *E. festucae midA* gene during growth in culture

4.3.1 Deletion of *midA* in *E. festucae* affects radial growth and morphology on PDA

The effect of *midA* deletion on radial growth rate, colony morphology and hyphal morphology was determined by growing mycelial plugs on a PDA medium (Section 2.13). Similar to the $\Delta wscA$ (Section 3.3.1), the *E. festucae midA* mutants also showed a significantly ($p < 0.05$) reduced vegetative radial growth rate (Fig. 4.4-A), a marked reduction in aerial growth and darker colony centres in comparison to the wild type (Fig. 4.4-B). No differences in branching pattern was observed in mutant hyphae within the first 15 compartments and cross sections through *midA* mutant colonies revealed no differences in the ability of mutant mycelia to penetrate the agar medium (1.5%) in comparison to the WT (Fig. 4.4- C). Complementation of the *midA* deletion with the full length *midA* gene restored radial colony growth rate and colony morphology to the level of the WT with no significant ($p < 0.05$) difference.

To better understand reduced colony radial growth shown by $\Delta midA$, the apical growth rates of individual hyphae of the WT, $\Delta midA$ and complemented strains growing on PDA were analysed using an Olympus Fluoview FV10i-LIV confocal laser scanning microscope as described in Section 2.12.3.3. Apical growth rate of the $\Delta midA$ mutants, $1.17 \pm 0.11 \mu\text{m}/\text{min}$ (mean \pm SD of 12 individual hyphae), was not significantly ($p < 0.05$) different to the apical growth rate of the WT hyphae, $1.29 \pm 0.10 \mu\text{m}/\text{min}$ (mean \pm SD of 12 individual hyphae) indicating that the reduced colony radial growth rate shown by $\Delta midA$ was not due to reduction in individual hyphal apical growth rate. Observations revealed that the cell walls at the hyphal tips of $\Delta midA$ mutants appeared weaker than WT as damaged hyphal tips were frequently observed by microscopy when

hyphal plugs were mounted in water or PDB (Fig. 4.5-A & C). Hyphal tip damage in WT and complemented strains was rarely observed under similar conditions. Further, in $\Delta midA$ strains at the hyphal tip, some hyphae appeared to produce a branch immediately behind the apex seemingly in response to tip damage (Fig. 4.5-B). These observations suggested that reduced radial colony growth observed in $\Delta midA$ was largely due to the frequent hyphal tip damage halting apical growth and not due to a reduction in individual hyphal apical growth.

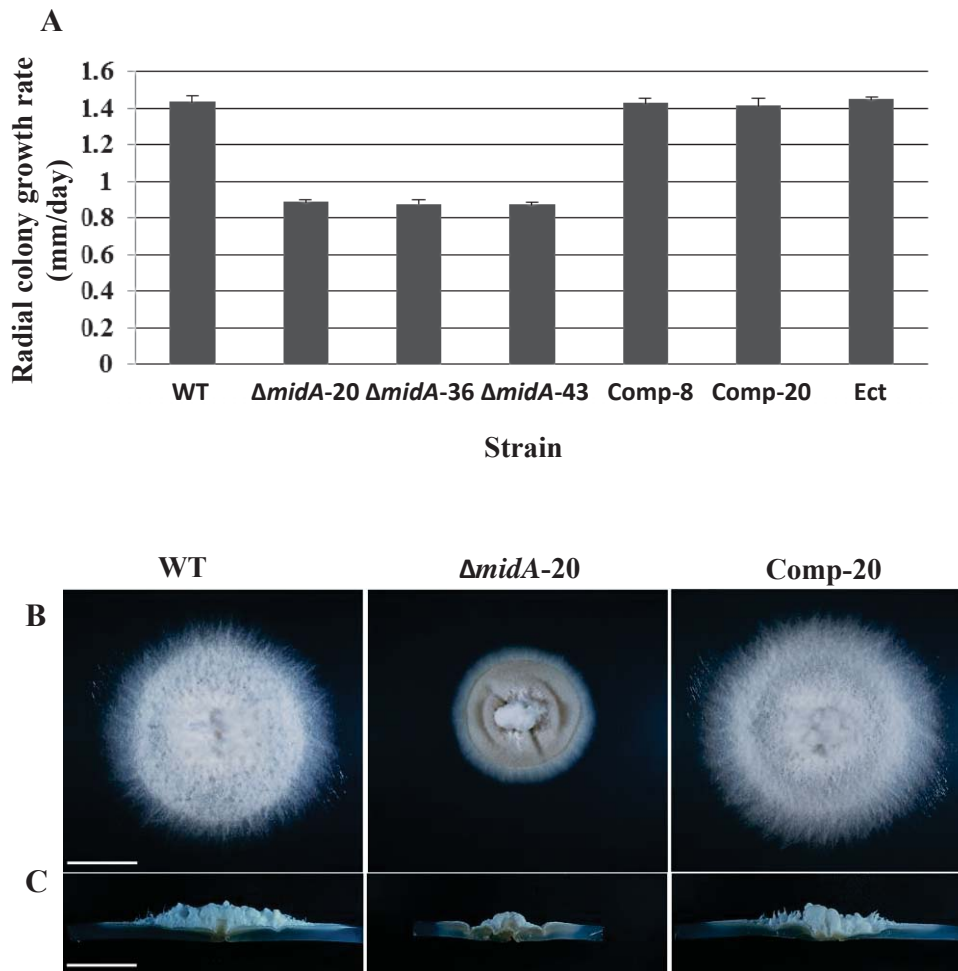


Figure 4.4: A comparison of the colony radial growth rate and colony morphology of *E. festucae* $\Delta midA$ with the wild-type & complemented strains cultured on PDA.

A- Comparison of colony radial growth rates. WT - *E. festucae* wild type; $\Delta midA-20$, $\Delta midA-36$ and $\Delta midA-43$ - independent *midA* deletion mutants; Comp-8 and Comp-20 independent *midA* complemented strains; Ect-7 - ectopic *hph* (hygromycin B phosphotransferase) gene integrated strain.

B- Comparison of the colony morphology. **C** - Cross sections of the colonies comparing aerial hyphae production. White scale bar = 2 mm.

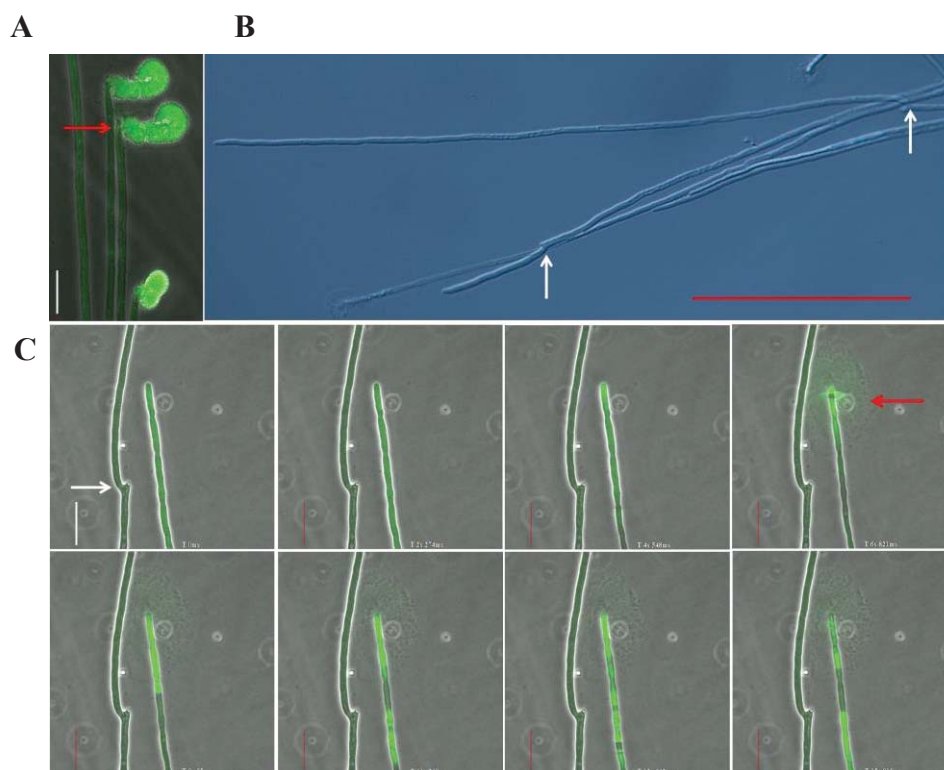


Figure 4.5: Hyphal tip damage in *E. festucae* $\Delta midA$ in culture.

A- GFP-labelled hyphae of $\Delta midA$ damaged at the apex with leaked cell contents (red arrow) at the tip. Hyphae were grown on PDA and mounted in a solution of PDB for microscopy. **B-** DIC image of hyphal tips with tip branching (white arrow). **C-** Frames of time lapse imaging showing tip burst occurring (red arrow) in a $\Delta midA$ hypha expressing GCaMP5 (calcium sensor protein). See supplementary movie in PowerPoint presentation ‘*E. festucae* $\Delta midA$ hyphal tip lysis’ in attached CD. Red scale bar = 100 μm , White scale bars = 20 μm

Interestingly, similar to $\Delta wscA$ hyphae (Section 3.3.1), hyphae of *midA* mutants, when stained with Calcofluor White, contained recurring cell wall aberrations with globular-shaped swollen patches of CW accumulations (4-8 μm in length) along the cell walls (Fig 4.6-A). In comparison WT hyphae stained uniformly with CW (see Section 3.3.1 for more details). The size and distribution of $\Delta midA$ cell wall aberrations seemed to be similar to that observed in $\Delta wscA$. The average distance between two CW stained

patches was between 6-10 μm and the patches were prevalent close to the apex and appeared to diminish as the hypha aged. The average diameter of swollen patches was $3.6 \pm 0.4 \mu\text{m}$. As a result of these swollen patches, *midA* mutant hyphae had uneven and coarse cell walls when observed using DIC microscopy (Fig 4.6-B). Complementation of the *midA* deletion with the full length gene fully restored the cell wall defect (no cell wall aberrations were observed in complemented strains) indicating a crucial role for the putative stretch-activated calcium ion channel *midA* in maintenance of cell wall integrity and general growth in *E. festucae* in axenic culture.

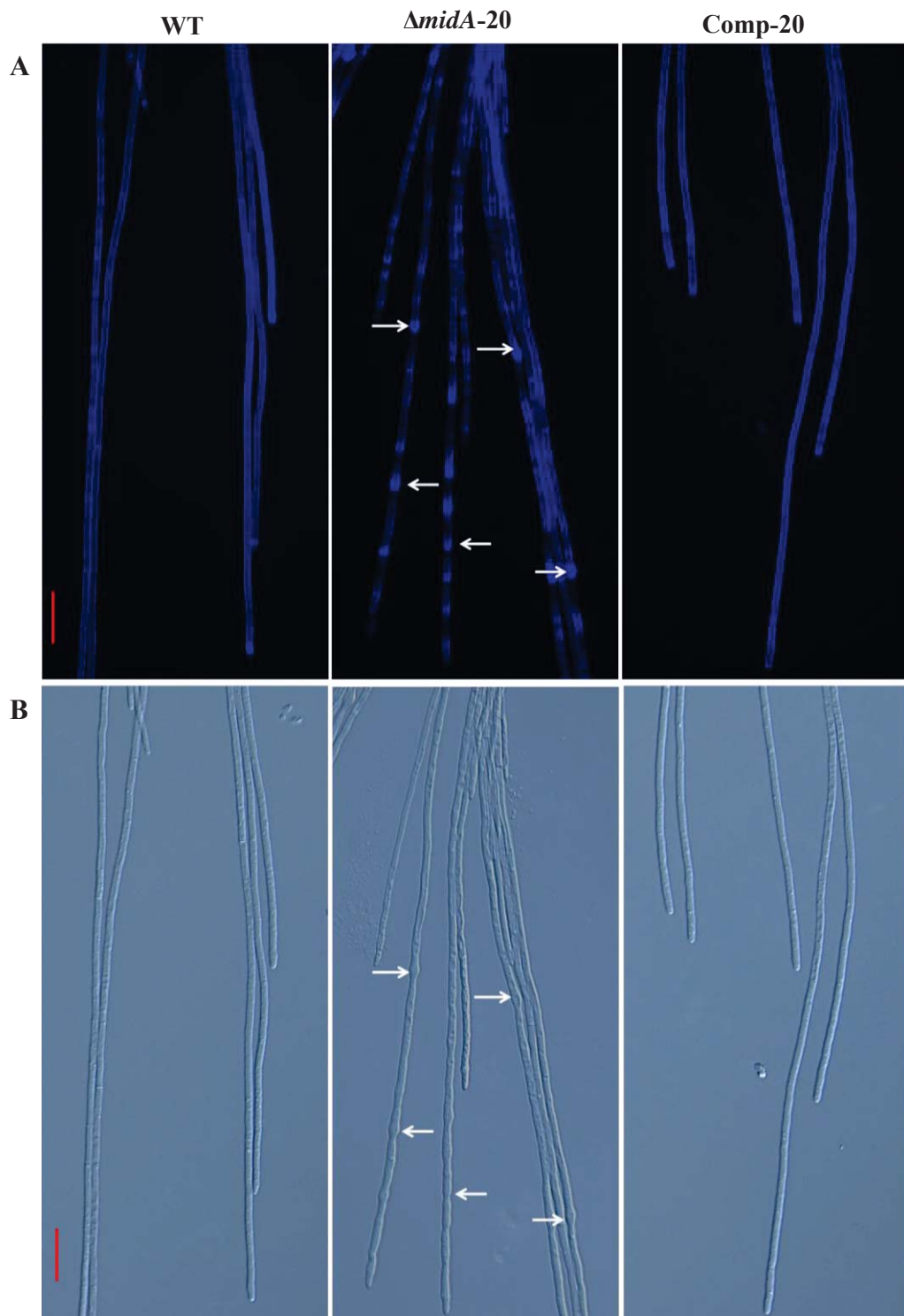


Figure 4.6: Comparison of the hyphal morphology of *E. festucae* $\Delta midA$ ($\Delta midA-20$) mutant with the WT & complemented strain (Comp-20) cultured on PDA. **A-** Fluorescent images of CW stained hyphae. **B** -DIC images of the same hyphae. Mutant hyphae contained noticeable cell wall aberrations (white arrows). Red scale bars = 20 μm

4.3.2 Osmotic stabilization can rescue *E. festucae* $\Delta midA$ phenotypes on the PDA culture medium

Cell wall aberrations and the frequent tip damage observed in $\Delta midA$ suggested a weakened cell wall in these hyphae. As described earlier, previous studies have shown that use of an osmotic stabilizer can suppress the defects of cell walls (Levin, 2011). Further, use of sorbitol (125 mg/mL) in PDA as an osmotic stabilizer restored similar cell wall defects in $\Delta wscA$ hyphae as shown in Section 3.3.2. Therefore, in order to test whether sorbitol had a similar effect on defective $\Delta midA$ hyphae, $\Delta midA$ mutants were cultured along with WT and complemented strains on PDA media infused with sorbitol (Section 2.13). The impacts of sorbitol on radial growth rate, colony morphology and hyphal morphology in WT and *midA* deletion mutants were determined as described in Sections 2.12.2 & 2.13.

Sorbitol was able to restore $\Delta midA$ radial colony growth rate, colony morphology (presence of aerial hyphae) and hyphal morphology (absence of cell wall aberrations) to WT levels on standard PDA with 125 mg/mL of sorbitol (Fig 4.7-A). With 125 mg/mL of sorbitol, $\Delta midA$ colonies had aerial hyphae similar to WT colonies and cell wall aberrations were completely absent in CW stained $\Delta midA$ hyphae (Fig 4.7-B & C). No ruptured hyphal tips were observed at 125 mg/mL. At 200 mg/mL of sorbitol, both WT and *midA* showed impaired growth due to the high osmolarity. Complementated strains and the ectopic strain behaved similar to the WT at all sorbitol concentrations used in this study. Similar to $\Delta wscA$, the ability of osmotic stabilizers to restore cell wall defects and prevent hyphal tip rupture suggested a substantial weakening of the cell wall in $\Delta midA$.

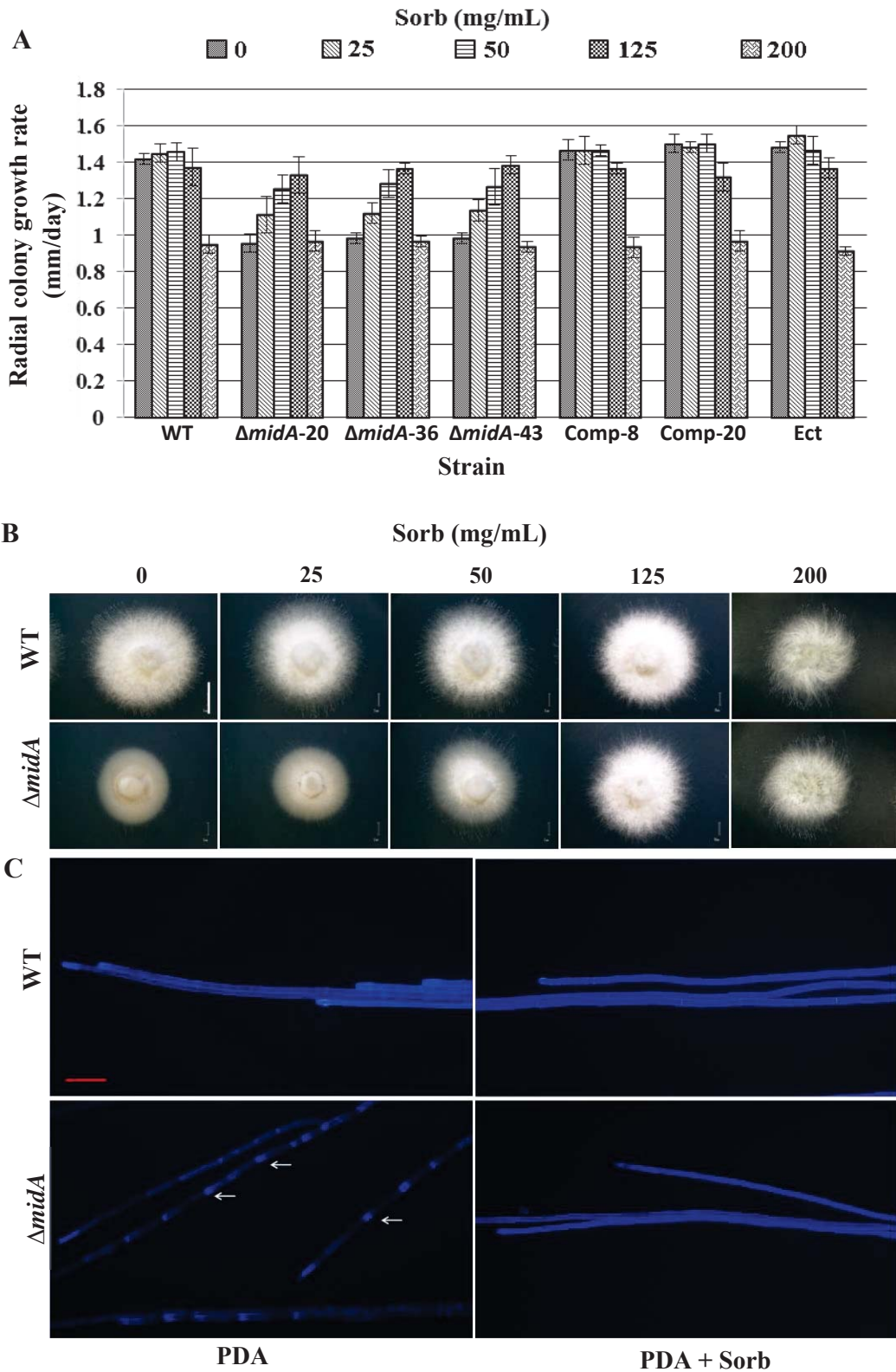


Figure 4.7: Effect of sorbitol concentration on growth rate, colony morphology and hyphal morphology of *E. festucae* WT and $\Delta midA$.

A- Comparison of radial colony growth rates on PDA media supplemented with increasing sorbitol concentration (25, 50, 125 and 200 mg/mL).

B- Colony morphologies of WT and $\Delta midA$ -20 on PDA infused with increasing sorbitol concentration (0, 25, 50, 125 and 200 mg/mL). Colony morphology of $\Delta midA$ looks similar to that of WT at 125 mg/mL of sorbitol in PDA. White scale bar = 2 mm

C- Hyphal morphology of WT and $\Delta midA$ on PDA and PDA+ sorbitol (125 mg/mL). Hyphae are stained with CW. Cell wall aberrations seen in $\Delta midA$ (white arrows) on PDA are absent on PDA+ sorbitol (125 mg/mL). Red scale bar = 20 μ m

4.3.3 Influence of calcium supplementation on the phenotype of *E. festucae* $\Delta midA$ in culture

MidA is part of the high affinity Ca^{2+} uptake system in association with the voltage gated channel Cch1 (Brand et al., 2007). This system is involved in Ca^{2+} uptake under low [Ca^{2+}] environments. In contrast, Fig1 is a low affinity calcium channel capable of calcium import in high Ca^{2+} environments (Section 1.5). I therefore hypothesised that if the $\Delta midA$ phenotypes observed when cultured on PDA were due to impaired intake of Ca^{2+} in a low Ca^{2+} environment, elevating Ca^{2+} levels in the medium, and thereby activating the low affinity system, Fig1, should restore certain $\Delta midA$ phenotypes. On the other hand, low calcium levels in the medium would be expected to affect $\Delta midA$ more severely than the WT as both the high affinity and the low affinity calcium uptake systems should be compromised in $\Delta midA$ affecting its growth further compared to the WT. To test these hypotheses, $\Delta midA$ was cultured on PDA supplemented with different concentrations of $CaCl_2$ or the Ca^{2+} chelator Ethylene Glycol Tetraacetic Acid (EGTA).

The radial growth rate of $\Delta midA$ on PDA supplemented with calcium increased significantly ($p < 0.05$) compared to growth on standard PDA, demonstrating that

calcium at these levels can rescue the growth defect of $\Delta midA$. The WT growth rate was not significantly ($p < 0.05$) affected at these elevated Ca^{2+} levels (Fig 4.8-A & B). Use of NaCl instead of $CaCl_2$ at similar concentration failed to restore the growth defect. The growth rate of both the $\Delta midA$ and WT reduced significantly ($p < 0.05$) in response to 10 mM of EGTA in standard PDA, and the $\Delta midA$ failed to grow completely. In contrast, at 5 mM of EGTA in PDA, there was no significant effect ($p < 0.05$) on the radial growth rate of the WT, while $\Delta midA$ showed a significant growth reduction ($p < 0.05$) (Fig 4.8-A & B).

As demonstrated previously (Section 4.3.2), an osmotic stabilizer can restore the impaired growth rate of $\Delta midA$ on PDA to the WT rate. Therefore to further test the importance of the high affinity calcium uptake system in the background of the osmotic stabiliser, $\Delta midA$ was cultured on PDA supplemented with both 125 mg/mL of sorbitol plus two concentrations of EGTA (5 and 10 mM). Under these conditions, the WT radial growth rate was significantly affected ($p < 0.05$) at 10 mM of EGTA but not at 5 mM in the presence of sorbitol (125 mg/mL). However, $\Delta midA$ growth was significantly affected ($p < 0.05$) at both 10 and 5 mM of EGTA with only very slight growth observed at 10 mM of EGTA (Fig 4.8-C & D). These observations further demonstrated that a low calcium level in the medium has a more profound effect on the growth of $\Delta midA$ than the WT even in the presence of an osmotic stabiliser that can protect the weakened cell walls. Colony morphologies of both WT and $\Delta midA$ were not visibly affected by EGTA except for small colony size due to the reduced growth rate. However, when growing on PDA infused with calcium, a reduction in aerial hyphal growth was observed in both the WT and $\Delta midA$ (Fig. 4.8-B & D).

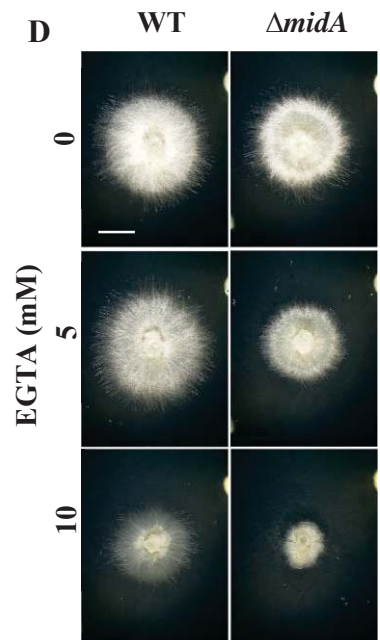
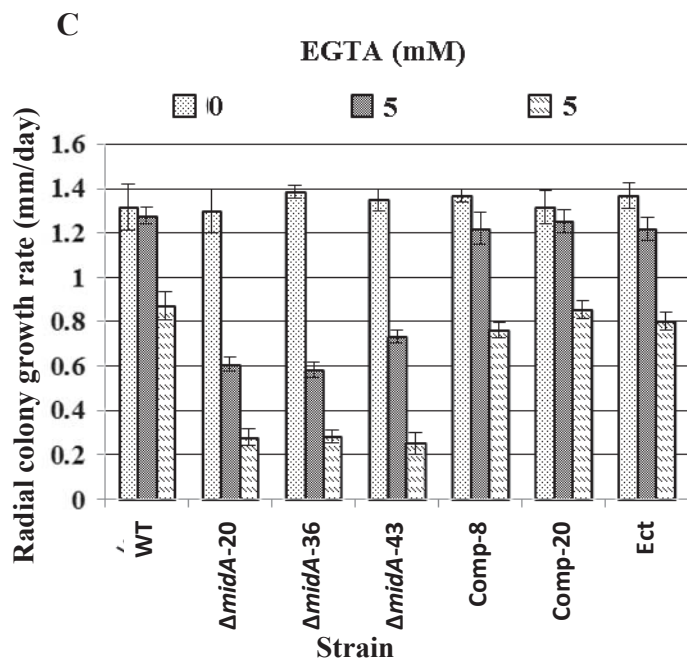
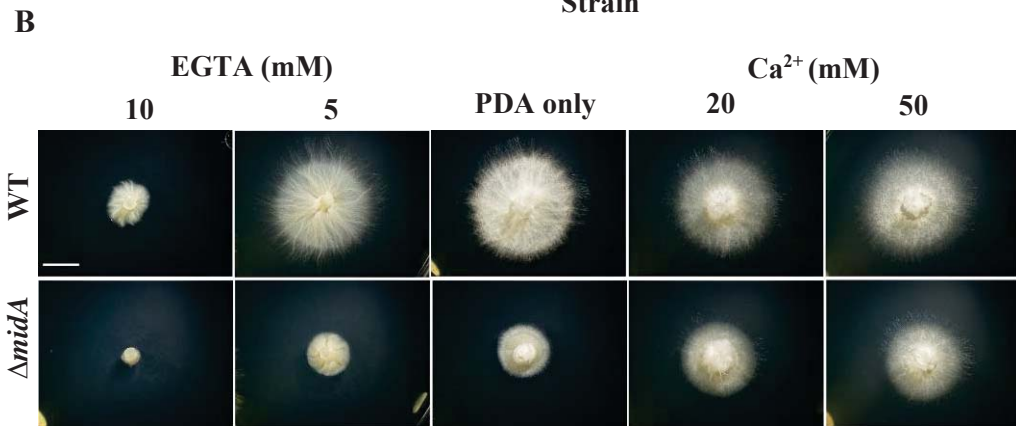
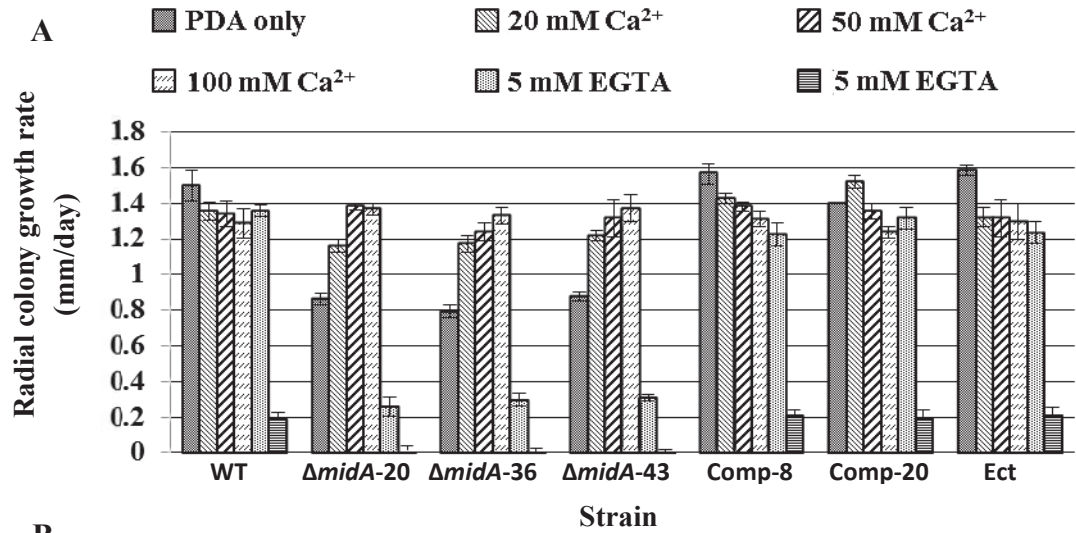


Figure 4.8: Analysis of *E. festucae* WT and $\Delta midA$ radial growth rate and colony morphology on PDA with elevated Ca^{2+} or EGTA.

A & C- Comparison of radial growth rates on PDA media infused with different $[Ca^{2+}]$ and $[EGTA]$ (A), and PDA infused with both sorbitol (125 mg/mL) and different EGTA concentrations (0, 5 and 10 mM) (C).

B- Colony morphologies of WT and $\Delta midA$ on PDA and PDA infused with different Ca^{2+} concentrations (20 and 5 mM) and EGTA concentrations (5 and 10 mM). Colony morphology of $\Delta midA$ on Ca^{2+} (50 mM) is similar to WT.

D- Colony morphology WT and $\Delta midA$ on PDA infused with sorbitol (125 mg/mL) and different EGTA concentrations (0, 5 and 10 mM). Depleted Ca^{2+} has a more severe effect on $\Delta midA$ colonies than on wild type. White scale bar = 2 mm.

Microscopy analysis of hyphal morphology of $\Delta midA$ on PDA infused with Ca^{2+} (50 and 100 mM) revealed that the cell wall aberrations seen when hyphae were growing on PDA alone were no longer visible, and hyphal cell walls looked similar to the WT, demonstrating that a high concentration of extracellular calcium can rescue the cell wall defect of $\Delta midA$ (Fig 4.9-A & B). These data also showed that calcium is essential for cell wall integrity. This observation was further supported by the effect of 10 mM EGTA on WT hyphae which induced similar cell wall aberrations (such as CW stained patches) and tip cell lysis that was usually seen in $\Delta midA$ on PDA alone. The cell wall phenotype was further exacerbated when $\Delta midA$ was grown on PDA containing EGTA (Fig 4.9-E). Hyper-branching of both WT and $\Delta midA$ was also observed, with $\Delta midA$ always showing more severe branching than WT, on 5 or 10 mM of EGTA (Fig 4.9-C & D), again demonstrating the importance of MidA in low calcium environments.

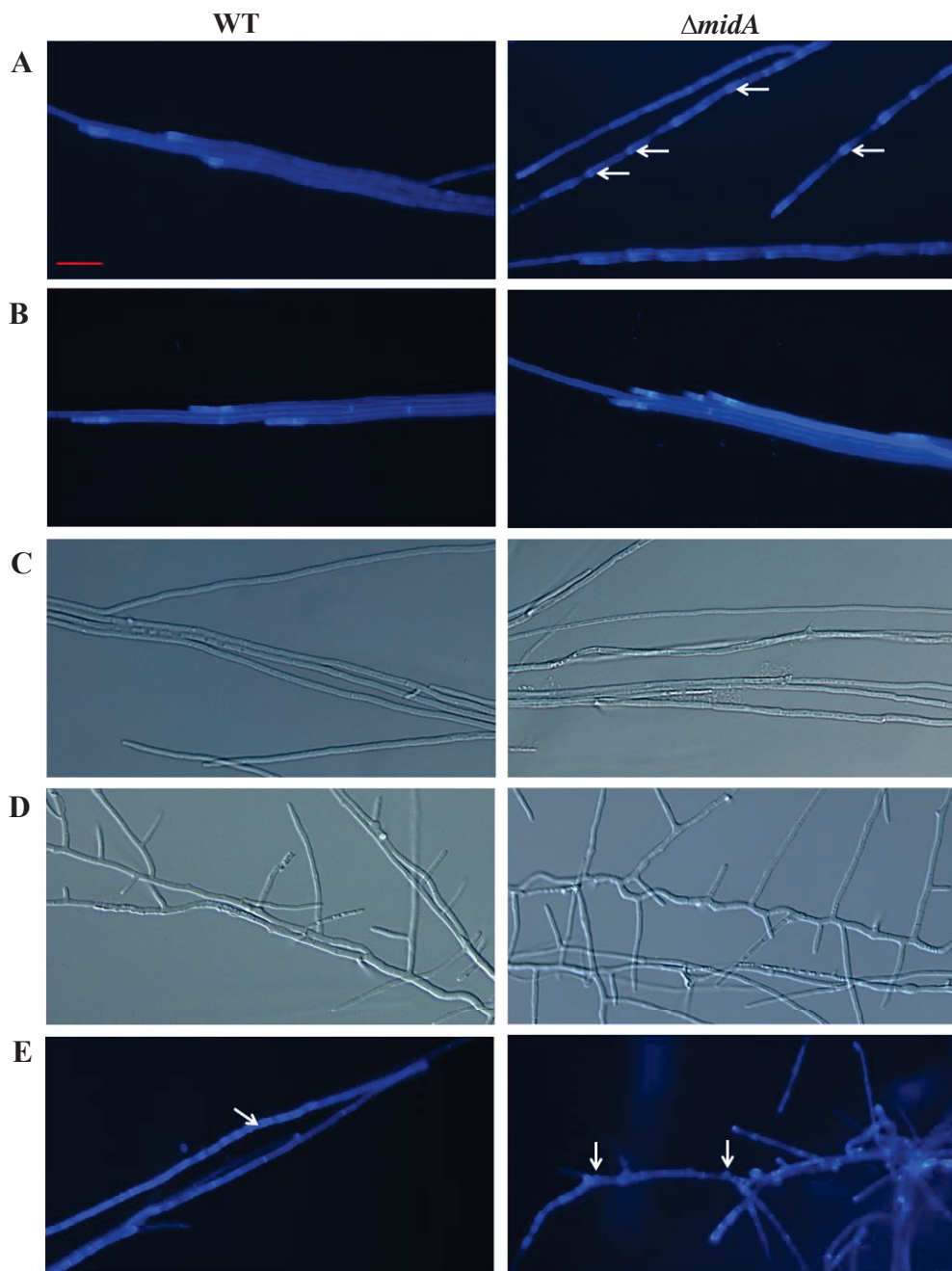


Figure 4.9: Analysis of hyphal morphology of *E. festucae* WT and $\Delta midA$ on PDA supplemented with different $[Ca^{2+}]$ or $[EGTA]$. CW-stained hyphae on PDA (A) and PDA + Ca^{2+} (50 mM) (B). Cell wall aberrations (white arrows) of $\Delta midA$ when growing on PDA alone is absent in PDA + Ca^{2+} (50 mM). DIC images of WT and $\Delta midA$ hyphae on PDA (C) and PDA infused with EGTA (WT in 10 mM and $\Delta midA$ in 5 mM), with some hyper-branching in WT and very intense hyper-branching in $\Delta midA$ (D). WT and $\Delta midA$ hyphae stained with CW showing cell wall aberrations on PDA containing 10 mM and 5 mM of EGTA respectively (E). Red scale bar = 20 μm

4.3.4 *E. festucae* $\Delta midA$ mutants are sensitive to cell wall perturbing agents

Calcofluor White (CW) and Congo red (CR) act as cell wall perturbation agents by binding to chitin and disrupting cell wall synthesis. In *C. purpurea* both CW and CR have a significant effect on the growth rate of $\Delta midA$ mutants (Bormann et al., 2009). To further characterise the integrity of the cell wall in *E. festucae* after deletion of *midA*, the effect of cell wall perturbing agents were tested by growing *E. festucae* WT and $\Delta midA$ on PDA infused with CW and CR at various concentrations. Further, as osmotic stabilizers (sorbitol) and elevated exogenous calcium are able to rescue growth and cell wall defects in $\Delta midA$ when grown on standard PDA (Section 4.3.2 & 4.3.3), the effect of cell wall perturbing agents were also tested in the presence of 125 mg/mL sorbitol or Ca^{2+} (50 mM).

The radial growth rate of WT and $\Delta midA$ strains was significantly reduced ($p < 0.05$) by exposure to 0.25 and 0.5 mg/mL CW and 0.1 and 0.15 mg/mL of CR in PDA (Fig 4.10-A & B). In contrast, in the presence of 125 mg/mL sorbitol the reduction in growth rate in $\Delta midA$ at 0.25 and 0.5 mg/mL CW concentrations was significantly greater ($p < 0.05$) than the reduction observed in WT under similar conditions (Fig 4.10-A & C). This demonstrated that CW has a more profound effect on growth of the $\Delta midA$ mutant than on WT in the presence of an osmotic stabiliser.

Radial growth rates of $\Delta midA$ and WT were also measured on CR-infused PDA with 50 mM Ca^{2+} . Elevated Ca^{2+} lessened the effect of CR on the radial growth rate of both WT and $\Delta midA$. In PDA + CR (0.15 mg/mL) both WT and $\Delta midA$ showed significantly increased ($p < 0.05$) growth rates in the presence of Ca^{2+} (50 mM) when compared to CR in PDA without Ca^{2+} (Fig 4.10-B & C). This demonstrated that calcium increased the resistance of both WT and $\Delta midA$ to the cell wall perturbing agent CR. The effect of

CW in the presence of Ca^{2+} could not be assessed as CW reacts with CaCl_2 and precipitated in the medium. A visible reaction or precipitate was not observed between CR and Ca^{2+} . Considering colony morphology, a notable feature of all the colonies (WT and $\Delta midA$) in the presence of CW and CR was the formation of aggregated hyphal strands and the apparent clockwise rotation of all these strands (Fig 4.10-C). Colonies on PDA infused with CR demonstrated a similar clockwise rotation of hyphal strands but not as intense as on CW.

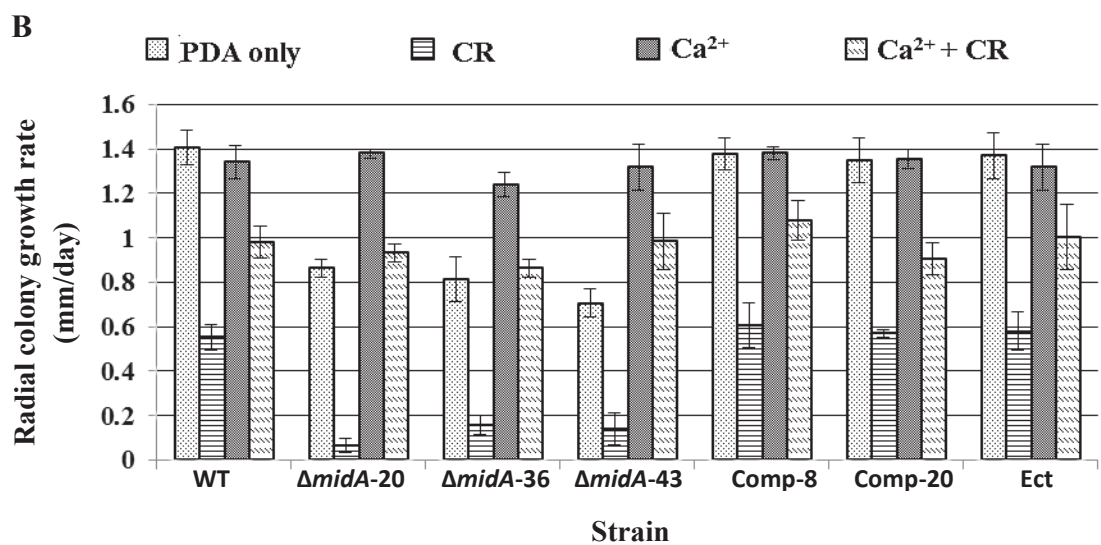
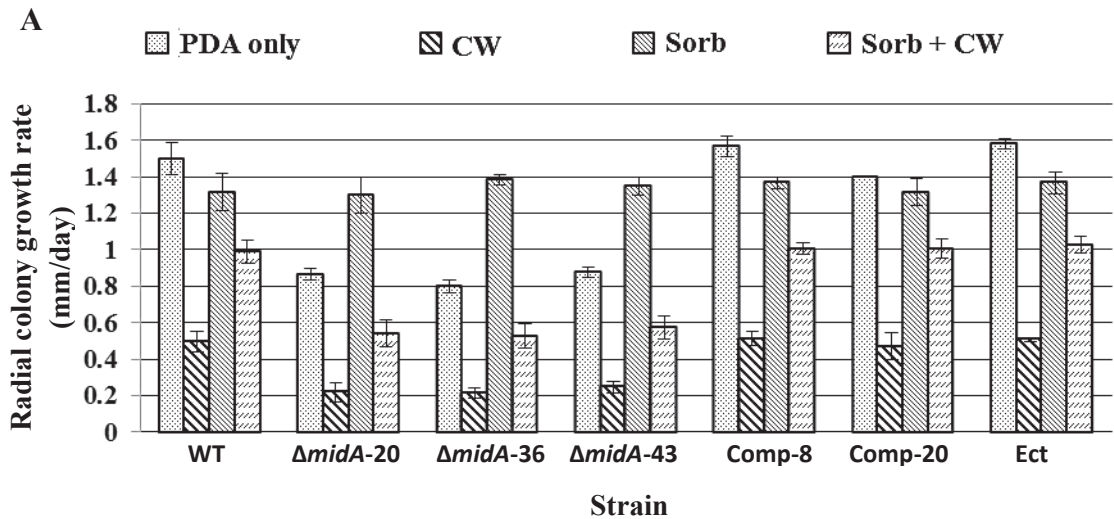




Figure 4.10: Analysis of radial growth rate and colony morphology of *E. festucae* WT and $\Delta midA$ on PDA in the presence of cell wall perturbing agents CW and CR.

A&B- Comparison of radial growth rates on CW (0.5 mg/mL) infused PDA and PDA with sorbitol (125 mg/mL) (A); on CR (0.15 mg/mL) infused PDA and PDA with Ca²⁺ (50 mM) (B).

C- Colony morphology of WT and $\Delta midA$ on PDA and PDA infused with CW (0.5 mg/mL) or CR (0.15 mg/mL) in the background of sorbitol (125 mg/mL, osmotic stabiliser) or Ca²⁺ (50 mM). The detrimental effects of CW and CR were reduced in the presence of sorbitol or Ca²⁺. Clock wise turned hyphal strands in CW (white arrows).

4.4 Deletion of *midA* in *E. festucae* restricts hyphal entry into the host intercalary growth zone

4.4.1 $\Delta midA$ host colonization

Similar to $\Delta wscA$ host colonization studies presented earlier (Section 3.5), the ability of *midA* replacement mutants to infect and colonize host plants (*L. perenne*) was investigated with the objective of testing whether *midA* has a role in hyphal intercalary growth shown by *E. festucae*. Mid1 of *S. cerevisiae* and its homologues in other filamentous fungi have been characterised as stretch-activated calcium channels that function in association with Cch1 (Section 1.5.2). Hence, given my hypothesis that mechanical stretching exerted by the elongating host cells on the attached hyphae triggers intercalary growth, MidA appeared to be a very good candidate to test as a potential sensor of mechanical stretch exerted on hyphal membranes. If MidA has a pivotal role in intercalary growth, $\Delta midA$ would be expected to be defective in host colonization during the transition from apical growth in the host meristematic region to intercalary growth in the elongation zone immediately above.

To determine the ability of *midA* deletion mutants to infect and colonize host plants (*L. perenne*), seedlings were inoculated as described in Section 2.3.3. Seedlings were inoculated with the WT strain, a strain with an ectopic integration of the *midA* deletion vector, three independent strains with the $\Delta midA$ and two strains with the $\Delta midA$ complemented with the *midA* gene. The ability of these strains to infect and colonize *L. perenne* was analysed in a similar way to the $\Delta wscA$ colonization studies described in Section 3.5.

All inoculated plants survived the first 8 week period after inoculation. Tissue print immunoassay and microscopic observation of aniline-blue stained epidermal peels were

used to identify endophyte positive plants. When $\Delta midA$ inoculated plant tillers were tested for the presence of endophyte in epidermal peels (stained with aniline blue) using bright field microscopy, a difference in the density of hyphae between endophyte positive plants and within tillers of the same endophyte positive plant was observed. Leaf sheath tissues inoculated with *midA* mutants were sparsely colonised, if at all, and hyphal distribution was usually confined to one or two regions of the sheath. The variation within $\Delta midA$ infected plants ranged from complete absence of endophyte hyphae in leaves to highly dense regions similar to the WT. Conversely in plants infected with WT, the ectopic strain or the complemented strains, epidermal peels showed a uniform distribution of relatively densely colonising hyphae within all endophyte positive tillers. This indicated that *midA* mutants are defective in their ability to colonise host tissues uniformly and in the usual density and suggests that calcium influx is required for optimal hyphal colonisation of host plants.

Although $\Delta midA$ showed variation in the ability to colonise host plants compared to WT as mentioned above, it was difficult to calculate a specific inoculation rate for $\Delta midA$. Since there is an infection defect in $\Delta midA$ with respect to colonisation of the expansion zone, the hyphae are not uniformly distributed and can be easily missed during microscopic analysis. Hence for a more accurate calculation of $\Delta midA$ inoculation rate, the meristematic regions of all tillers needed to be checked for the presence of hyphae which is time consuming.

As aniline blue-stained epidermal peels did not provide a comprehensive representation of the colonization pattern, both the WT and $\Delta midA$ -20 strains were transformed with plasmid pTEFEGFP to create strains capable of constitutive expression of EGFP (Section 3.5). Three independent EGFP-expressing strains of both $\Delta midA$ -20 and the

WT were selected for further analysis. Selection of strains, inoculation of seedlings, obtaining tissues for microscopy and confocal microscopy to analyse colonization patterns were performed as described previously (Section 3.5).

In WT infected tillers, hyphae demonstrated the typical colonization pattern (Fig 4.11) with randomly distributed hyphae in the meristematic regions and long parallel arranged hyphae in the expansion zone of the leaf (see Section 3.5 for further details). In comparison, in $\Delta midA$ infected tillers, endophyte hyphal colonization similar to the WT was observed, with a similar density and organisation in the tissues surrounding the shoot apex and the base of the developing leaf (Fig 4.11 & 4.12). This indicated that the *midA* mutants had the ability to colonize the SAM in a similar manner to WT hyphae. However, when transverse sections were obtained from the same tiller, a clear difference in the colonization pattern between WT and $\Delta midA$ was visible. In transverse sections, leaves infected with WT hyphae were evenly distributed indicating a uniform entry of hyphae near the shoot apex into the primordia of developing leaves. Generally the youngest (the leaf in the middle of the tiller) and the oldest leaf (at the outside) appeared to have a lower density of hyphae compared to the leaves of intermediate age (Fig 4.11). In comparison, transverse sections of leaves infected with $\Delta midA$ showed variation in hyphal density and distribution while the total number of hyphae was always lower than WT infected leaves (Fig 4.11 & 4.12). Hyphae were confined to certain regions of the leaves but no preference for specific tissue types within the leaf was observed. A comparison of hyphal colonisation in transverse and longitudinal sections of the same tiller confirmed that $\Delta midA$ hyphal colonization in the region of the shoot apex, and immediately below the expansion zone of the developing leaves, was similar to that of WT, with the exception that hyphae were often unable to enter the expansion zone of the leaves where intercalary growth takes place (Fig 4.12).

When longitudinal sections of leaf tissues were observed, *ΔmidA* had hyphae segregating to certain regions of the leaf coinciding with the hyphae distribution seen in TS of the same tiller. However most of the hyphae were elongated and parallel arranged similar to the WT and seemed continuous within the tissues observed indicating that some hyphae were able to undergo intercalary growth. To better understand the continuity of hyphae throughout the length of the leaf sheath, transverse sections were taken at 1.5 cm intervals along the length of a single tiller covering 3 cm of the pseudostem starting from the base (close to the SAM). As it was not possible to track individual hyphae over this distance, arrangement of hyphal patches/regions was observed for their consistency relative to other sections of the same tiller. Visual observations indicated that the distribution of hyphae was consistent between transverse sections indicating that the *ΔmidA* hyphae are continuous within the leaves and that, if the hyphae are able to get into the host expansion zone, they are able to grow by intercalary growth (Fig 4.13).

Colonization by *ΔmidA* complemented strains analysed via aniline blue staining confirmed the colonization pattern is similar to that of the WT in the longitudinal section of leaf peels and transverse section of tillers. Together these observations suggested that *ΔmidA* hyphae are able to colonise the SAM similar to the WT but may encounter a hurdle in getting in to the elongation zone of developing leaves. Hyphae that manage to enter the elongation zone of the leaf are capable of undergoing growth similar to the WT.

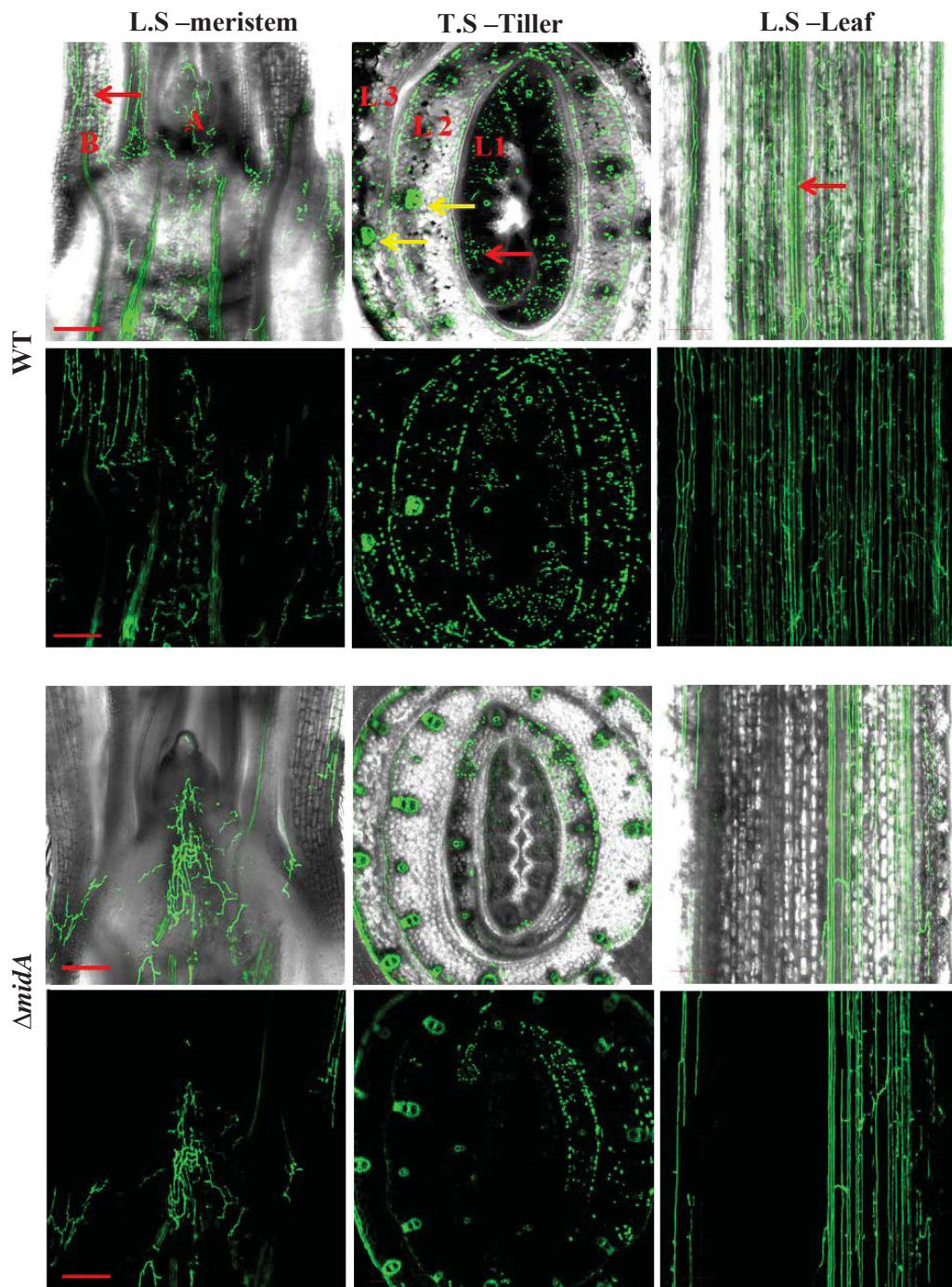


Figure 4.11: Comparison of hyphal colonization in *L. perenne* tillers infected with WT and *midA* deletion mutants expressing EGFP. Sections of meristem, tiller and leaf were obtained from the same grass tiller. Florescence and phase contrast images are compressed z stack confocal images. Green strands and spots represent endophyte hyphae (red arrow). Yellow arrows show auto fluorescing vascular bundles **A**-Shoot apical meristem, **B**- Developing leaves, **L 1-3** -Concentricly arranged leaves in grass tiller. Scale bars-200 μ m.

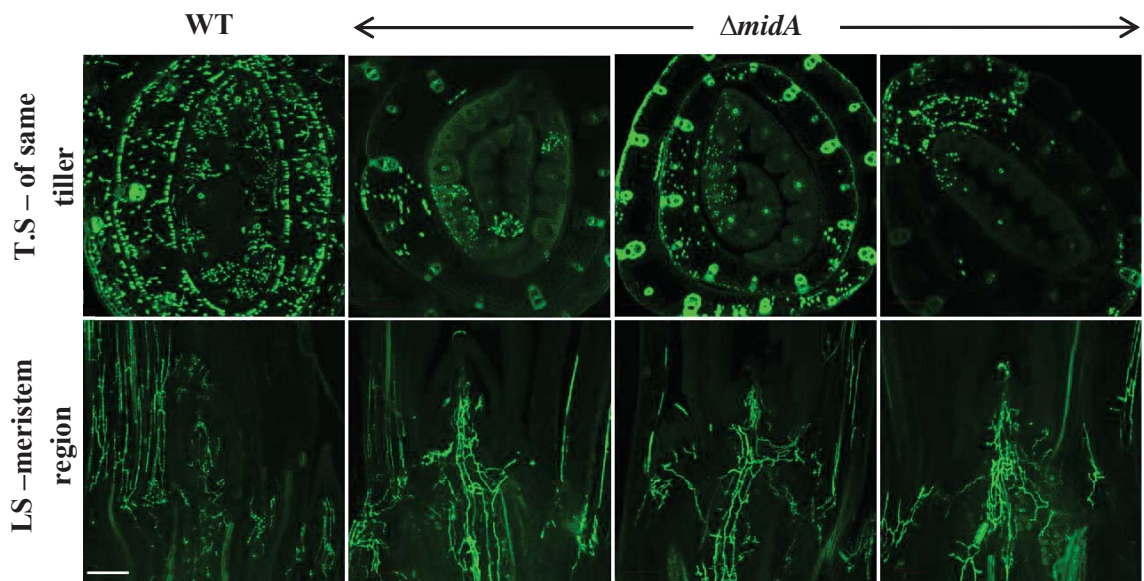


Figure 4.12: Comparison of hyphal colonization in the meristem and the developing leaves by WT and $\Delta midA$ expressing EGFP. Transverse and corresponding meristem sections were obtained from the same tiller. Magnification bar = 200 μm .

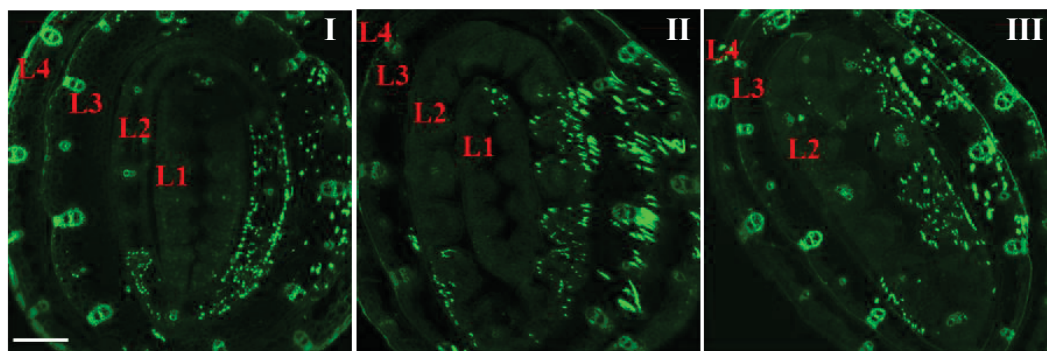


Figure 4.13: Transverse section from a pseudostem of a single tiller infected with $\Delta midA$ showing distribution of hyphae along the length of the leaves. Three sections were taken every 1.5 cm starting from base of the tiller. I – TS closest to the base, L1-4 - Concentricly arranged leaves in grass tiller. Magnification bar=200 μm .

4.4.2 Deletion of *midA* has no impact on the phenotype of the host

To determine whether *midA* deleted strains have any effect on host plants, the same plants used for the colonization studies above were assessed for overall visual appearance, number of tillers, plus tiller height and leaf morphology. The plants infected with $\Delta midA$ resembled the WT plants, and no apparent differences were observed in any of the variables tested (Fig 4.14). Minor variations observed within plants infected with the same strain were inconsistent and therefore did not warrant further analysis.



Figure 4.14: The effect of $\Delta midA$ colonisation on morphology of *L. perenne* host plants. A representative sample of plants 8 weeks after inoculation with WT, three independent *midA* mutants and *midA* complemented strain are shown.

4.5 Calcium distribution in *E. festucae* hyphae and the role of MidA in calcium uptake

Calcium plays a major role as an intracellular signalling molecule (second messenger) in translating external stimuli into various cellular responses. However, in filamentous fungi, not much is understood about calcium due to the limitations in techniques to measure calcium in living hyphae. In animal cells, Genetically Encoded Calcium Indicators (GECI) which have the advantage of providing a non-invasive long-lasting imaging method (Akerboom et al., 2012) have been used extensively. One such GECI is the single wavelength sensor GCaMP (Nakai et al., 2001), for which a series of improvements have been made, and several versions produced (Tian et al., 2009). The latest of the series is a single wavelength sensor GCaMP5 (Akerboom et al., 2012). It is composed of a circular permuted green fluorescent protein (cpGFP), calmodulin (CaM) and the M13 peptide which is a Ca^{2+} /CaM binding moiety. In the presence of Ca^{2+} , CaM binds to four Ca^{2+} molecules and interacts with the M13 peptide. This brings about the conformational change required in the cpGFP for excitation and emission to occur. This sensor has fast kinetics, and good sensitivity and photostability.

The GCaMP vector series, including one of the latest, GCaMP5, have been optimised and used in animal cells, in particular in neurons, to investigate Ca^{2+} signalling. To date no reports have been published on the use of the GCaMP sensors in fungi. However, considerable success has been achieved with them in *A. fumigatus* and *N. crassa* at the University of Manchester, U.K., with two papers on their use in these species are 'in preparation' (Prof Nick Read, pers. comm). Taking this into consideration, an attempt was made to investigate the possibility of using the GCaMP5 calcium sensor in *E. festucae*. The initial objective was to determine whether the GCaMP5 sensor would function in WT *E. festucae* hyphae. Subsequently, investigations were conducted to

understand the spatial and temporal Ca^{2+} signatures in *E. festucae* during both apical and intercalary growth. The GCaMP5 sensor was also used to assess the effect of *midA* deletion on Ca^{2+} distribution in *E. festucae*.

To determine calcium distribution within *E. festucae* WT hyphae, protoplasts were co-transformed with vectors pAM13-9-GCaMP5 (harbours the genetically-encoded calcium sensor GCaMP5) and pPN1688 (to confer hygromycin resistance) (Section 2.6.3), transformants selected using hygromycin resistance, nuclear purified by sub-culturing (Section 2.8) and tested for expression of GCaMP5 using confocal laser scanning microscopy. Then growth rate, colony and hyphal morphology and plant colonization characteristics were compared with a WT strain to check that the ectopic integrations had not altered these traits. Three independent transformed strains were selected for further studies. Imaging was performed as mentioned in Section 2.12.3.1.

4.5.1 Calcium pulses in apical compartments of *E. festucae* during growth in axenic culture

Time lapse live imaging of growing *E. festucae* hyphae expressing GCaMP5, using the conditions described above, revealed high intensity pulsatile fluorescent signals emanating from the hyphal tips (see supplementary movies 4.2-3 in PowerPoint presentation ‘Calcium imaging in *E. festucae*’ in attached CD). These fluorescent pulses were not observed in hyphae of the WT (without GCaMP5) or in those expressing EGFP constitutively (transformed with pTEFEGFP) indicating that the fluorescent pulses are representative of changes in cytoplasmic calcium concentration ($[\text{Ca}^{2+}]_c$) in the hyphal apex. This observation demonstrated that the GCaMP5 calcium sensor is functional within *E. festucae* and can be used to investigate Ca^{2+} dynamics within actively growing hyphae. The pulsatile fluorescent signals at the hyphal tip correlated

with Ca^{2+} dynamics observed in other fungi during Ca^{2+} signalling studies conducted using techniques such as Cameleon vectors and aequorin (Nelson et al., 2004; Kim et al., 2012).

A qualitative comparison of the nature of Ca^{2+} pulses at the hyphal tip within three independent WT strains that expressed GCaMP5 (using five actively growing hyphae from each colony) showed that the temporal and spatial dynamics of the pulses are unique to each hypha. A fluorescent intensity peak was counted as a pulse when it was above the basal fluorescent level. The fluorescence intensity away from the tip (70 μm) in the same hypha was taken as the basal fluorescence. Graphs showing fluorescence intensity variation (Ca^{2+} concentration) over time at the tip (at a region 5 μm away from the hyphal apical end) was plotted using Olympus confocal software FV10-ASWRS for each hyphal tip (Fig 4.15-A & B). The plots demonstrated that pulses of Ca^{2+} at the hyphal tip occurred in all *E. festucae* WT hyphae observed, except for a few where no pulses were present at the time of observation (3/15 hyphae observed). The plots revealed that the spatial and temporal dynamics of Ca^{2+} pulses were unique to an individual hypha in terms of the amplitude (fluorescence intensity), distribution area and the frequency (Fig 4.15-A). The dynamics of Ca^{2+} pulses also differed over time within the same hypha. The fluorescence intensity graphs of hyphal tips (5 hyphal tips from each independently-transformed *E. festucae* strain) with the GCaMP5 sensor for a period of 5 min revealed that on average a high amplitude Ca^{2+} pulse occurs every 45-60 sec with many low amplitude pulses (10-15 sec between pulses) in-between (Fig 4.15-A). See supplementary movies 4.4-7 in PowerPoint presentation 'Calcium imaging in *E. festucae*' (attached CD) for examples of unique pulsatile patterns of individual hyphae.

When the growth rates of these hyphae were compared with the frequency of the fluorescent pulses it revealed no apparent relationship. Growth rates of individual hyphae were calculated in $\mu\text{m}/\text{min}$ using the same time lapse images used to capture Ca^{2+} pulses. All hyphae observed ($n=15$) had a constant tip growth rate of 1.26 ± 0.09 $\mu\text{m}/\text{min}$ (mean \pm SD, $N=15$), while exhibiting variable Ca^{2+} pulsatile characteristics. No statistical analysis on Ca^{2+} intensity was attempted due to high variation in pulses between hyphae, and uncertainty over the correlation between calcium levels and fluorescence intensity.

Previous studies have reported a tip high gradient of Ca^{2+} in growing hyphae and its importance in hyphal apical growth (Jackson et al., 1993). Analysis in *E. festucae* hyphae revealed high fluorescence intensity that appeared to originate close to the apex and rapidly spread away from the tip indicating a high gradient of Ca^{2+} in tips of actively growing hyphae (Fig 4.16-A and see supplementary movie 4.3 in PowerPoint presentation 'Calcium imaging in *E. festucae*'). Therefore to better understand the nature of the Ca^{2+} gradient present in *E. festucae* hyphae, Ca^{2+} pulses of 15 actively growing hyphae were analysed at the peak Ca^{2+} concentration (maximum intensity peak/peak profile) within the observed period of 5 min as mentioned in (Kim et al., 2012) . Of the hyphae selected, a longitudinal line starting from the hyphal tip was drawn dividing the centre of the hypha and, along the line, the change in fluorescence intensity was plotted (line profiles) over distance for each hyphal tip using Olympus confocal software FV10-ASWRS. When the Ca^{2+} concentration at the tip was at its peak, the gradient extended up to 20 - 30 μm from the tip until it reached a basal level from there onwards (Fig 4.16-B).

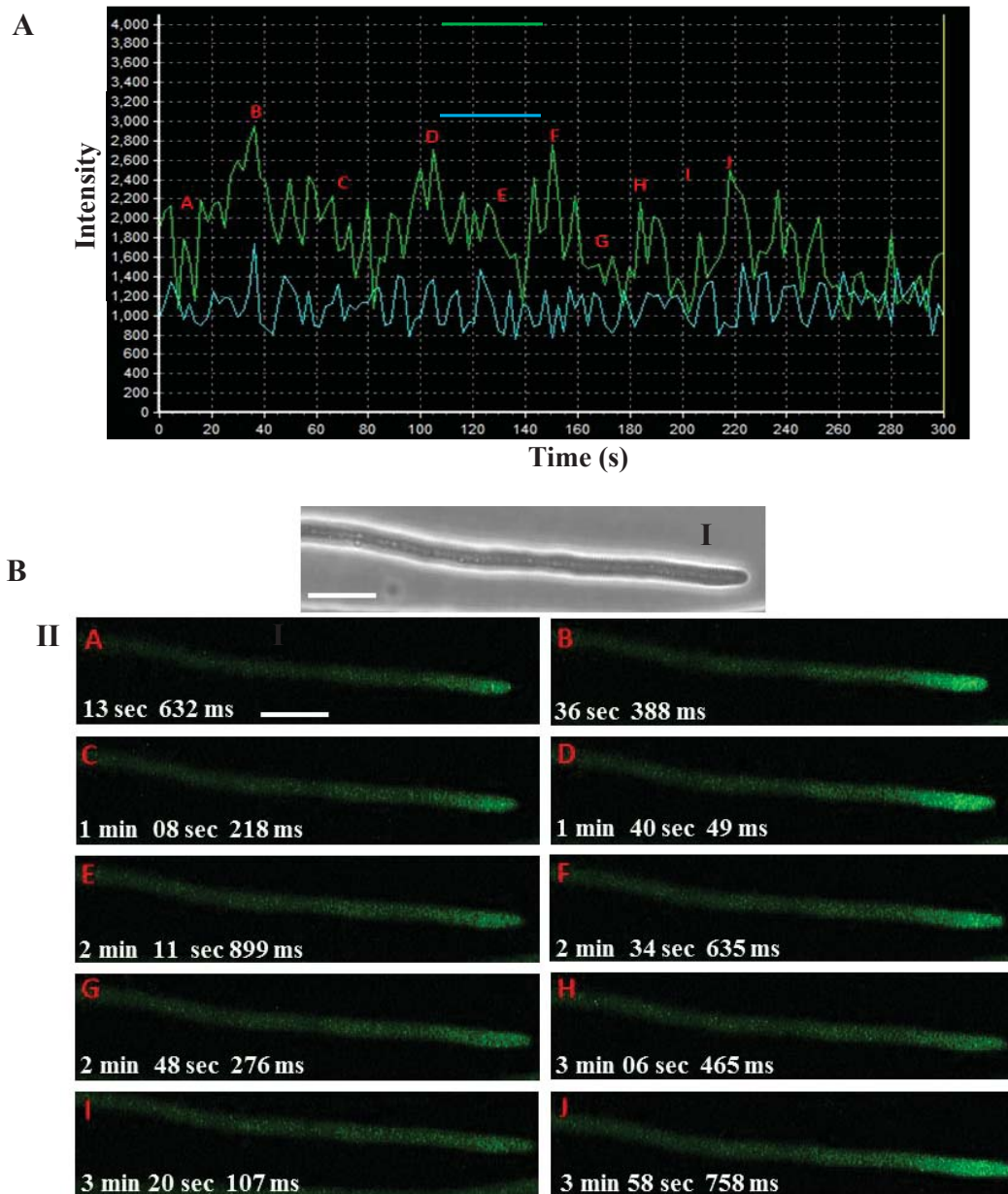


Figure 4.15: Temporal Ca^{2+} dynamics in *E. festucae* WT hyphal tips expressing calcium sensor GCaMP5. **A** – A representative graph showing fluctuation in fluorescence intensity with time at the tip (green line) compared to basal fluorescence (70 μm away from hyphal tip, blue line) in a WT hypha. In comparison to the basal static fluorescence, fluorescence intensity at the WT hyphal tip showed recurring irregular high amplitude pulses indicating the pulsatile nature of Ca^{2+} at the hyphal tip. **B-II** - Corresponding fluorescent images of the hyphal tip at the exact time points indicated in the graph (red letters) showing the pulsatile nature of fluorescence intensity. **B-I** - Phase contrast image of the same hypha. Scale bar = 10 μm .

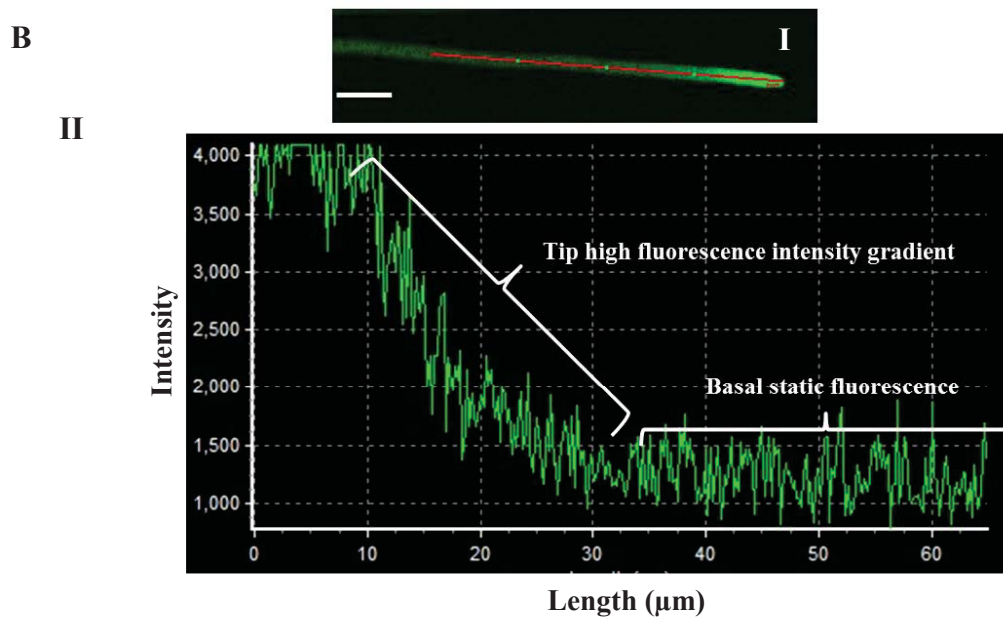
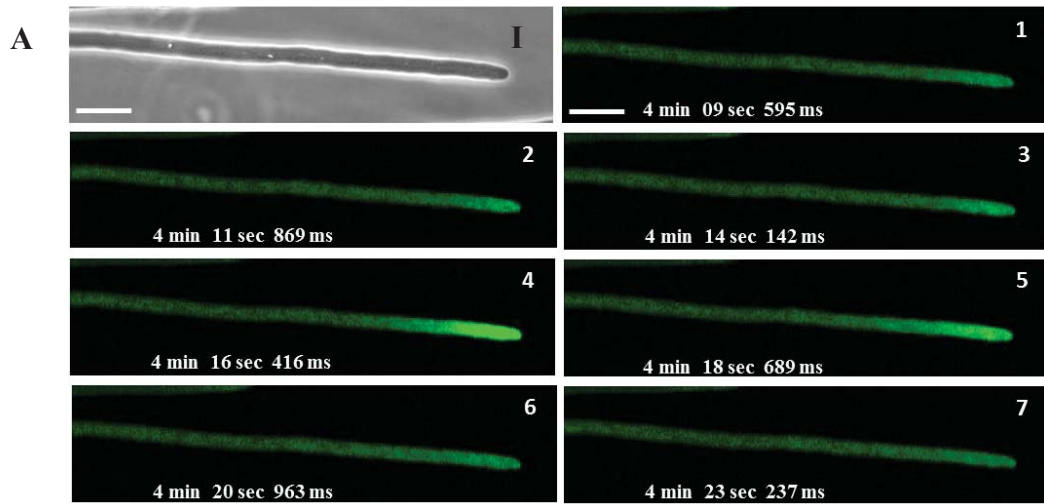


Figure 4.16: Analysis of spatial distribution of Ca^{2+} at the *E. festucae* WT hyphal tip expressing the GCaMP5 calcium sensor. **A** -Series of time lapse images (1-7 represent the time sequence of images) showing the origin and distribution of a single Ca^{2+} pulse at the tip of a representative WT hypha. The Ca^{2+} pulse is highest at the tip and reduces progressively to background levels approximately 30 μm from the tip. **A-I** – Phase contrast image. **B-I** - Line transecting the centre of the hypha. **B-II**- A representative intensity line profile at the hyphal tip of WT hypha (expressing GCaMP5) transecting the centre of the hypha.

4.5.2 Deletion of *midA* in *E. festucae* effects dynamics of Ca²⁺ pulses

The importance of MidA in maintenance of overall hyphal calcium homeostasis has been reported before in other fungi (Bormann et al., 2009; Cavinder et al., 2011). To investigate the effect of *midA* deletion on Ca²⁺ dynamics in *E. festucae*, protoplasts from strain $\Delta midA$ -20 were co-transformed with vector pAM13-9-GCaMP5 (harbouring calcium sensor GCaMP5) and pII99 (to confer Geneticin resistance), tips were purified and selected for further studies on the basis of fluorescence intensity using confocal laser scanning microscopy (Section 4.5). The growth rates, and colony and hyphal morphologies of GCaMP5-expressing transformants were compared with $\Delta midA$ -20 to confirm that the ectopic integration had no effect on these traits. The nature of Ca²⁺ pulses in three independent $\Delta midA:GCaMP5$ strains were analysed as described above using the same laser scanning confocal microscopy parameters.

Time lapse imaging revealed that Ca²⁺ pulses could not be observed in most $\Delta midA$ mutant hyphae tested (70%, n = 15) for the standard 5 min period. This indicates that, similarly to other fungi, MidA is required to generate the frequent (Ca²⁺ pulse occurs every 45-60 sec with many low amplitude pulses) calcium pulses observed at the hyphal tip (see supplementary movie 4.8-9 in PowerPoint presentation 'Calcium imaging in *E. festucae* $\Delta midA$ ' - attached CD). The small proportion of hyphae that did exhibit Ca²⁺ pulses within the 5 min time lapse period, showed either a single pulse or an array of 2-3 pulses in quick succession. Therefore, compared to the WT, Ca²⁺ pulses in $\Delta midA$ hyphae seemed to be irregular with a very low number of peak pulses within a given period (Fig 4.17–A & B). However, notably, the growth rate of $\Delta midA$ hyphae (calculated as described in Section 4.5.1) of 1.18 ± 0.11 $\mu\text{m}/\text{min}$ (mean \pm SD, N=15) did not differ significantly ($p < 0.005$) from that of the WT despite the apparent difference observed in Ca²⁺ pulses in $\Delta midA$ hyphal tips. In general WT and $\Delta midA$

hyphae grew at a constant and similar rate regardless of the pattern of Ca^{2+} pulses. See supplementary movies 4.10-14 in PowerPoint presentation ‘Calcium imaging in *E. festucae* $\Delta midA$ ’ (attached CD) for examples of unique pulsatile patterns of individual hyphae.

The spatial distribution of the Ca^{2+} gradient in $\Delta midA$ hyphal tips was analysed in a similar way to that in the WT hyphal tips along a longitudinal line through the apical compartment at a time of maximum Ca^{2+} intensity (Fig 4.18-A & B). In $\Delta midA$, in comparison to WT hyphae, extension of the maximum Ca^{2+} peak gradient was significantly more variable and returned to basal levels within 25-70 μm from the tip, whereas in WT hyphae the range was within 20-30 μm from the tip in all hyphae observed (see supplementary movie 4.9 in PowerPoint presentation ‘Calcium imaging in *E. festucae* $\Delta midA$ ’). To confirm that the observed differences in Ca^{2+} dynamics in $\Delta midA$ compared to the WT were due to absence of MidA functionality, protoplasts from *E. festucae* $\Delta midA$ ($\Delta midA$ -20) were simultaneously transformed with the *midA* complementation vector pSAM5 and pAM13-9-GCaMP5 (harbouring the GCaMP5 calcium sensor). Geneticin-resistant transformants were tip-purified and checked for ability to fluoresce. Colonies were further screened by PCR to confirm the presence of complemented *midA* gene. Thereafter, growth rate, colony and hyphal morphology of the selected complemented strains (with the GCaMP5 sensor) were compared with WT and $\Delta midA$ complemented strains to ascertain that ectopic integration had not affected these traits. In terms of the three main Ca^{2+} dynamics investigated above, frequency of pulses, Ca^{2+} gradient distribution at the tip and growth rate, the $\Delta midA$ complemented strains with GCaMP5 sensor were similar to the WT (Fig 4.19). This demonstrated that the difference observed in Ca^{2+} dynamics at the hyphal tip between the *E. festucae* $\Delta midA$ and WT was due to the absence of MidA. See supplementary movies 4.15-16 in

PowerPoint presentation ‘Calcium imaging in *E. festucae* $\Delta midA$ complemented’ (attached CD) for examples of unique pulsatile patterns of individual hyphae.

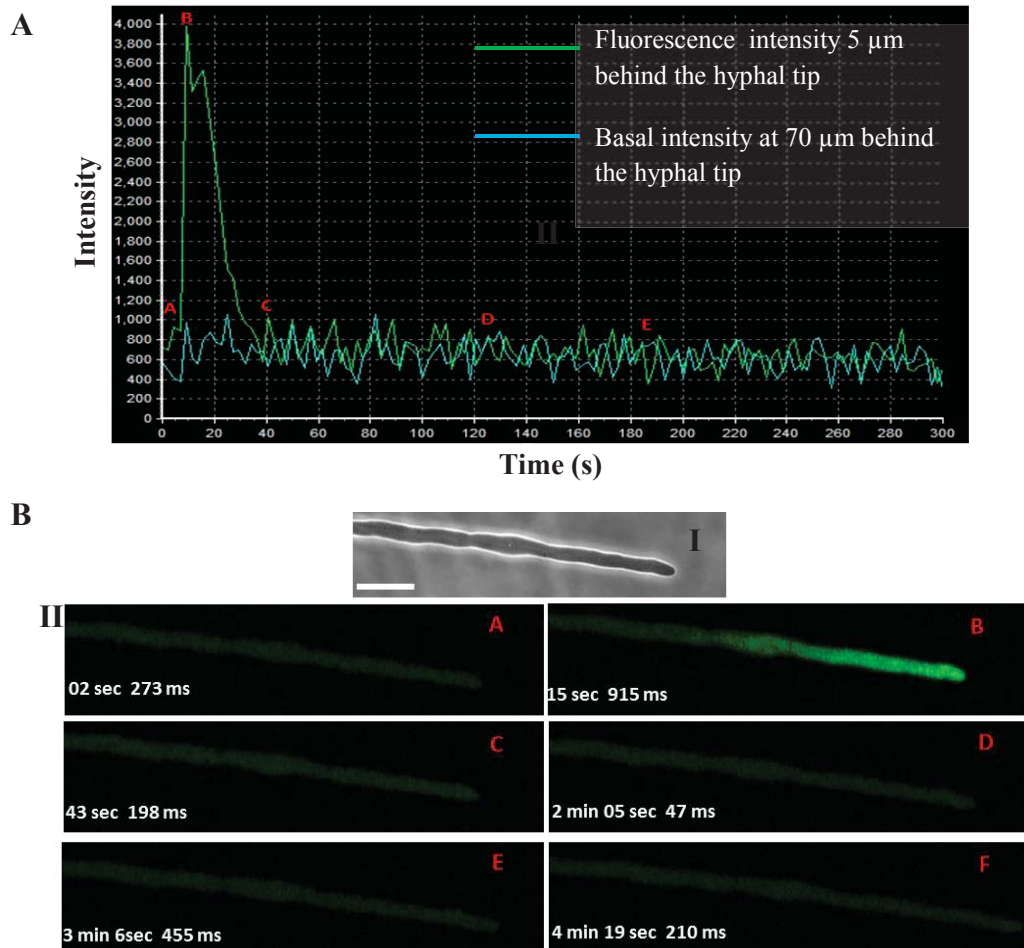


Figure 4.17: Temporal Ca^{2+} dynamics in *E. festucae* $\Delta midA$ hyphal tips expressing calcium sensor GCaMP5. **A** – A representative graph showing fluctuation in fluorescence intensity with time at the hyphal tip (green line) in comparison to basal fluorescence (70 μm behind the hyphal tip, blue line). **B-II** - Corresponding fluorescent images of the hyphal tip at the time points indicated in the graph A (red letters). **B-I** - Phase contrast image. Scale bar = 10 μm .

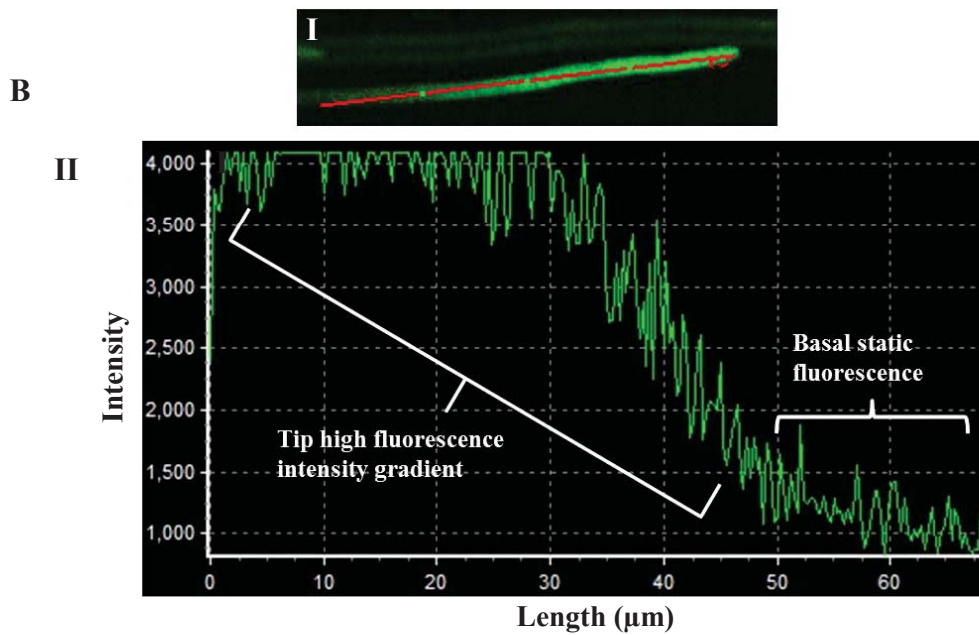
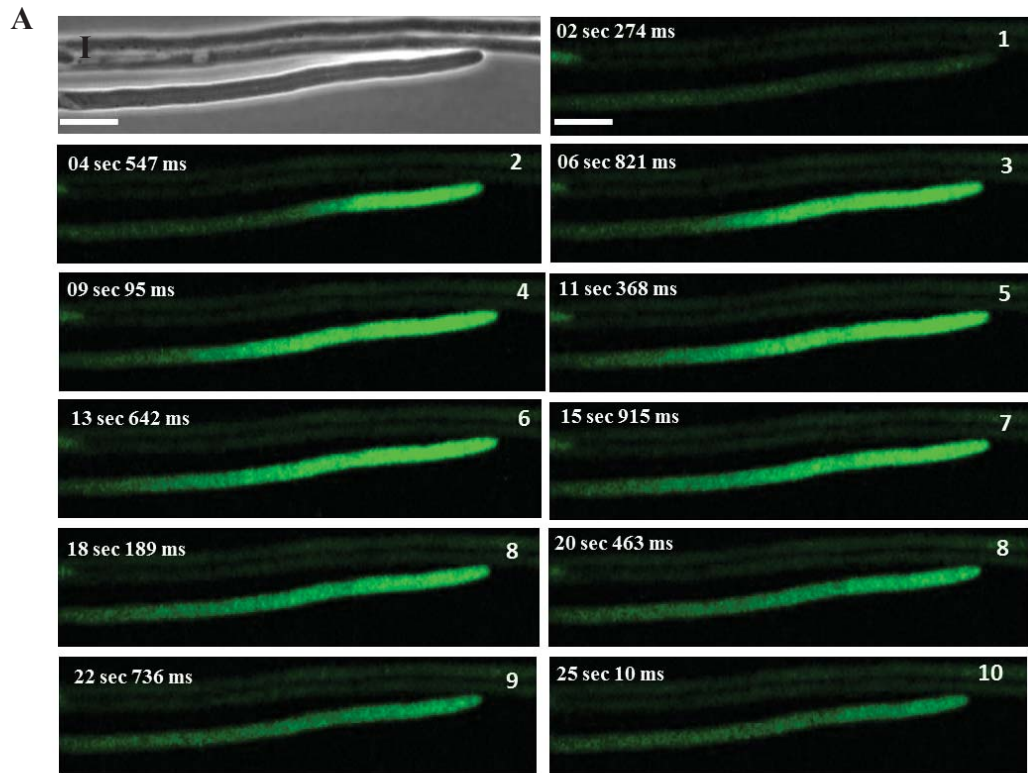


Figure 4.18: Spatial distribution of Ca^{2+} at the hyphal tip of *E. festucae* ΔmidA expressing the GCaMP5 calcium sensor. **A**-Series of time lapse images (1-10 represent the time sequence of images) showing the origin and distribution of a single Ca^{2+} pulse. **A-I**-phase contrast image **B-II** – A representative line intensity profile at the hyphal tip of a ΔmidA hypha. **B-I**– Longitudinal line transecting the hyphal tip. A tip high gradient of Ca^{2+} could be seen that spread to approximately 50 μm from the tip.

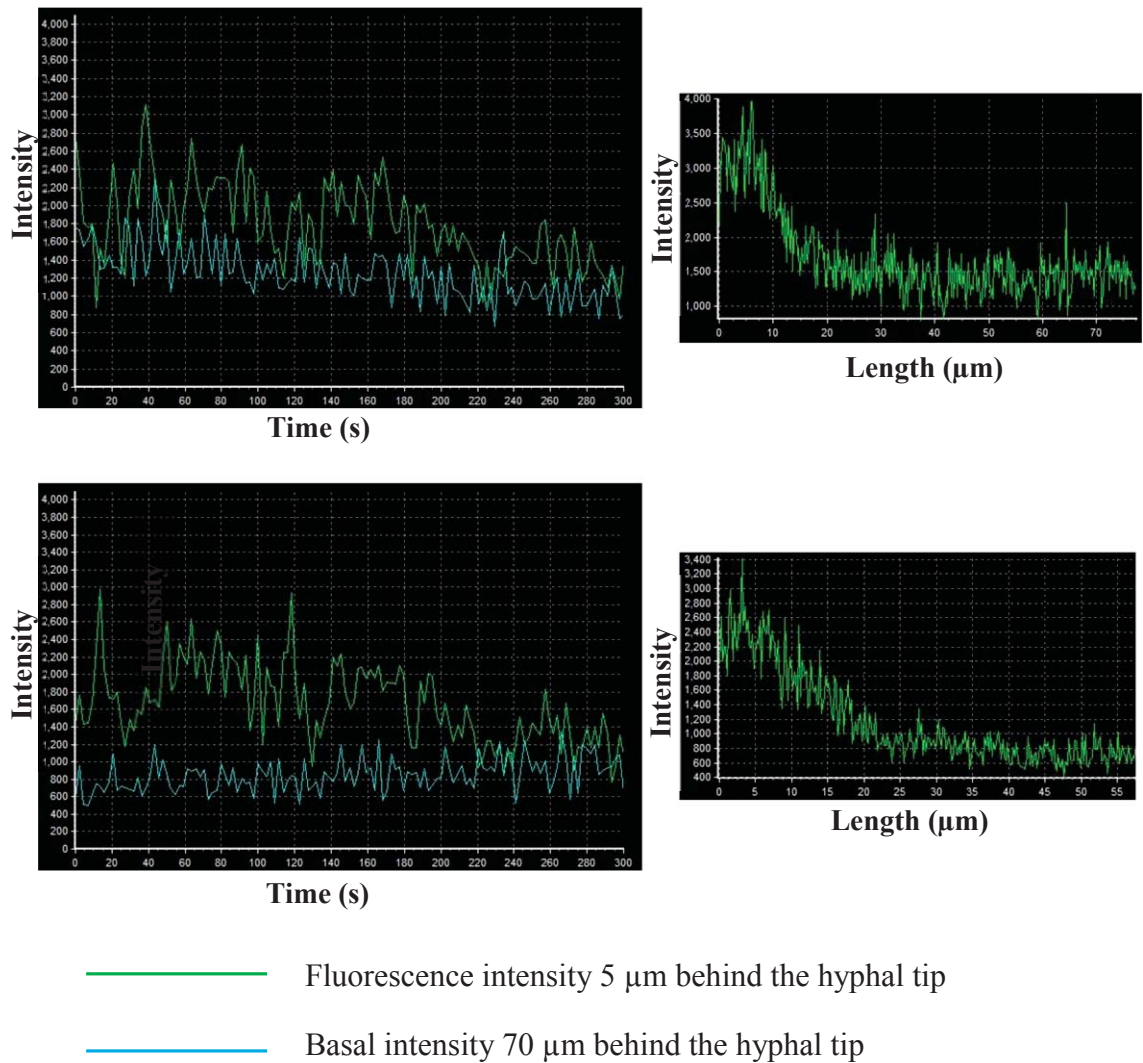


Figure 4.19: Ca^{2+} pulses in *E. festucae* ΔmidA complemented strains expressing calcium sensor GCaMP5. Representative fluorescent intensity graphs and corresponding line intensity profile graphs of two separate hyphal tips from ΔmidA complemented strains. The nature of Ca^{2+} uptake in complemented strains is similar to the dynamics observed in WT hyphal tips.

4.5.3 Ca²⁺ pulses occur in intercalary compartments in *E. festucae* WT and $\Delta midA$ hyphae

Ca²⁺ pulses and the presence of a calcium gradient at the hyphal tip in fungi have been documented previously (Jackson et al., 1993; Kim et al., 2012). An investigation of Ca²⁺ dynamics in intercalary compartments would provide additional insight into the mechanism of intercalary growth occurring in *E. festucae* hyphae. To investigate whether such calcium pulses occur away from the hyphal tip or in intercalary compartments, *E. festucae* WT and $\Delta midA$ hyphae expressing GCaMP5 were grown in axenic culture and mounted in PDB as described above. Time lapse imaging using a confocal laser scanning microscope was performed under the same conditions and parameters as described in Sections 4.5 and 4.5.1. Compared to the pulses observed at hyphal tips, Ca²⁺ pulses in intercalary regions were seldom observed and, without exception, only a single pulse occurred in an intercalary position even when observed for an extended 8 min period. These pulses were seen in two positions, either in intercalary compartments (Fig 4.20-A) or in sub-apical regions of the first compartment (Fig 4.20-B). The pulses originated from a centric position and spread to either side of the hypha evenly (see supplementary movie 4.17 in PowerPoint presentation ‘Calcium imaging in sub-apical regions of *E. festucae* hyphae). The pulses that occurred in the apical compartments were located about 60-80 μm away from the tip (deduced from 6 pulses observed). Pulses in intercalary compartments were always low relative to the tip in fluorescent intensity (visual observation) and seemed to occur in random positions of compartments (5 pulses were observed out of 40 regions observed). The presence of EGTA (10 and 20 mM in PDB) diminished these intercalary Ca²⁺ pulses (from 40 intercalary regions observed) and increasing external calcium (50 and 100 mM) did not result in any apparent increase in the occurrence of intercalary pulses compared to PDB.

However, due to randomness in position of pulses in intercalary regions, capturing these pulses and assessing spatial and temporal nature was difficult. No discernible differences were observed in the Ca^{2+} pulses of intercalary compartments in WT and $\Delta midA$ hyphae

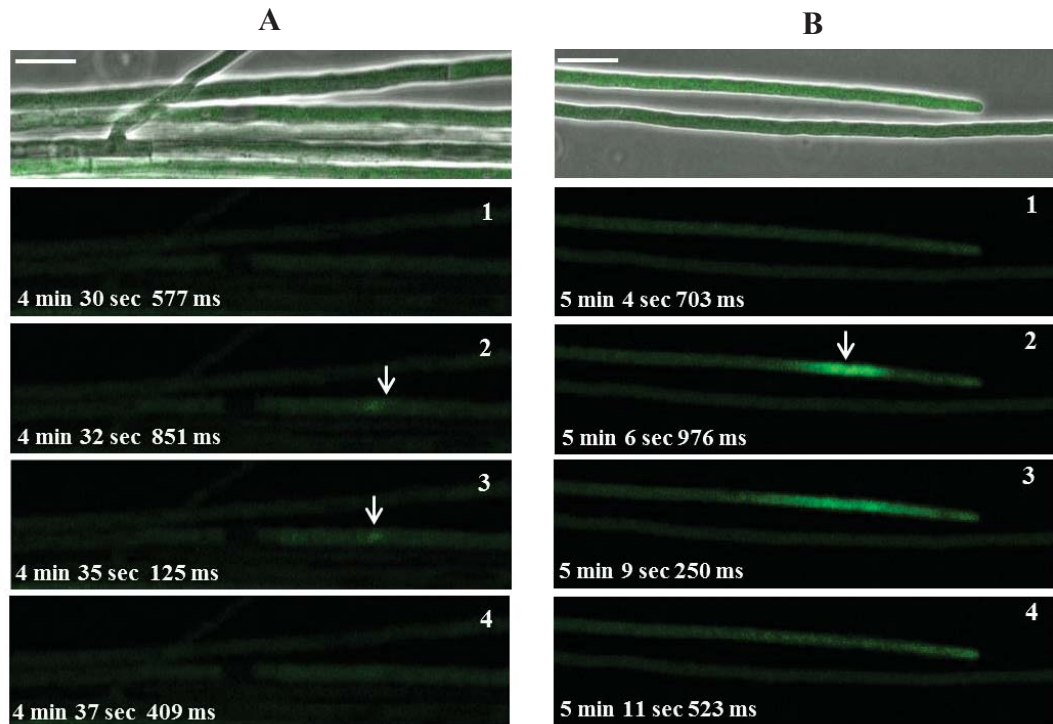


Figure 4.20: Ca^{2+} pulses in an intercalary compartment and in a sub-apical region of *E. festucae* hyphae. Time lapse phase contrast and fluorescent images (time series 1-4) of a Ca^{2+} pulse occurring in a sub-apical compartment (A) and away from the hyphal tip of the apical compartment (B) of a WT hypha expressing GCaMP5. Ca^{2+} pulses in sub-apical compartments are low in intensity compared to the pulses occurring in the apical compartment. Imaging time was extended to 8 min to capture these rare sub-apical Ca^{2+} pulses. The white arrows indicate the origins of Ca^{2+} pulses. Scale bar = 10 μm .

4.5.4 Ca²⁺ pulses in *E. festucae* are due to influx of exogenous Ca²⁺

To determine whether the Ca²⁺ pulses observed in *E. festucae* hyphal tips and intercalary compartments were due to influx of exogenous Ca²⁺ through the membrane, or release of Ca²⁺ from internal storages (vacuoles and Golgi apparatus) or a combination of both, mycelial PDA blocks of hyphae expressing the GCaMP5 sensor were mounted in PDB infused with various concentrations of EGTA (Ca²⁺ chelator). Fluorescence at the hyphal tips were observed as mentioned in Section 4.5 after 5 min of incubation using same confocal laser scanning microscopy parameters. At least 10 hyphae were observed for each treatment. Due to the limitation in the confocal microscope immediate effect of EGTA or Ca²⁺ addition was not possible to observe as there was a time gap between addition of EGTA or Ca²⁺ and imaging.

Time lapse observation of WT hyphal tips revealed that Ca²⁺ pulses could be observed in the presence of 5 and 10 mM of EGTA, but not in 20 and 30 mM of EGTA in PDB within the 5 min period in all hyphae observed (Fig 4.21). Under similar conditions 5 mM EGTA did not show any effect on Ca²⁺ pulses in $\Delta midA$ hyphae as the usual frequency of pulses were observed (4/10 observed showed a pulse). In comparison, under similar conditions, in 10 mM of EGTA, Ca²⁺ pulses were not seen in $\Delta midA$ hyphae within 5 min of observation. Therefore, lower levels of exogenous Ca²⁺ were required to inhibit Ca²⁺ pulses altogether in the *midA* replacement mutants. Additionally, in $\Delta midA$ strains an occasional pulse occurred simultaneously with a massive visible disturbance in the cytoplasm indicating hyphal tip rupture (3/11 observed), the pulse presumably occurred as a result of spilled cytoplasmic contents coming into contact with residual Ca²⁺ in the media (see supplementary movie 4.18-19 in PowerPoint presentation 'Calcium imaging in *E. festucae* hyphae in EGTA). No such hyphal tip rupture was observed in WT hyphae indicating that calcium depletion

rendered the already weak $\Delta midA$ hyphae more susceptible to tip rupture. In contrast, addition of extra Ca^{2+} (50 mM) did not lead to a visible change in the periodicity or intensity of Ca^{2+} pulses in WT or $\Delta midA$ hyphal tips (Fig 4.21). This suggests a strong connection between the MidA and the frequent calcium pulses seen in WT hyphal tips. The interpretations are based on visual observations and no statistical analysis was performed.

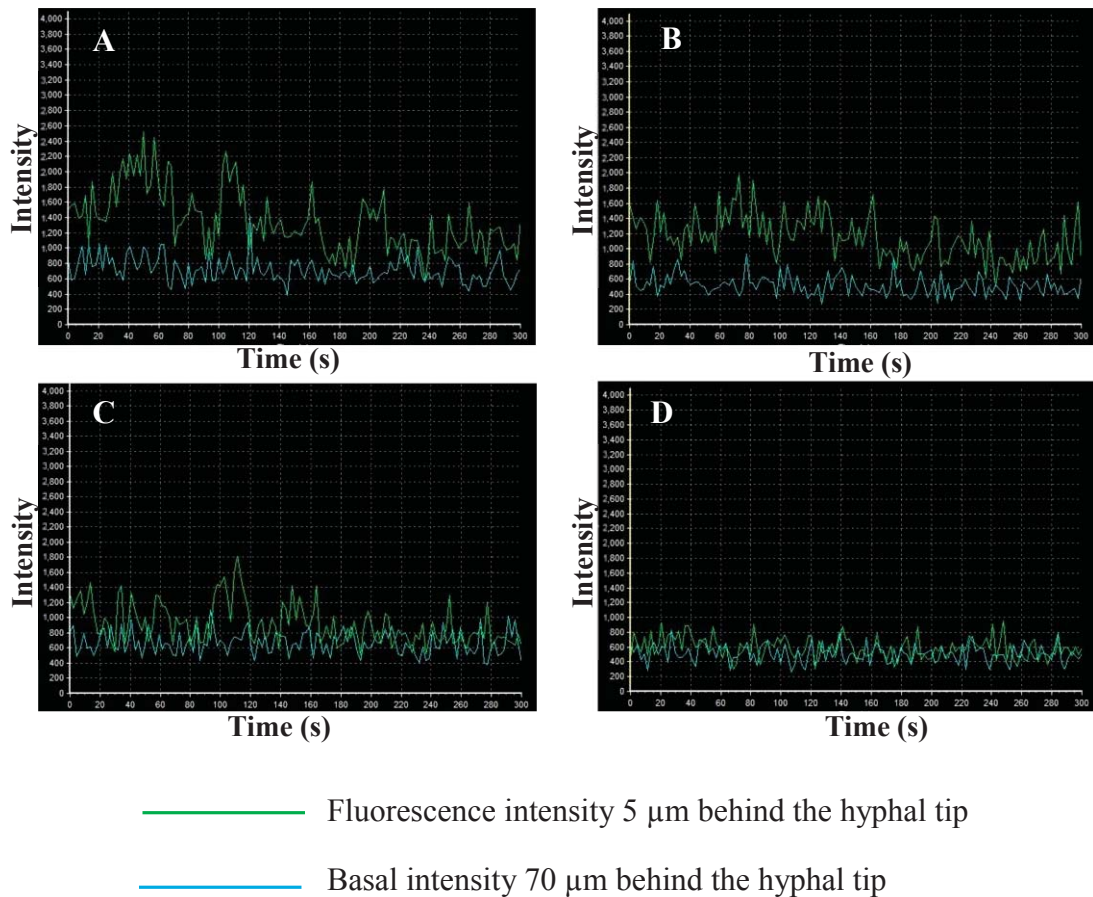


Figure 4.21: Effect of elevated or depleted exogenous calcium on Ca^{2+} pulses in *E. festucae* WT hyphal tips expressing GCaMP5. Representative graphs showing fluorescence intensity change with time in 4 different hyphae when mounted in standard PDB (A), PDB with 50 mM of Ca^{2+} (B) PDB with 10 mM of EGTA (C) and PDB with 20 mM of EGTA (D). Hyphae were incubated for 10 min after mounting before imaging.

4.5.5 Intensely-labelled calcium foci visible at hyphal tips

A closer look at *E. festucae* WT hyphae expressing the GCaMP5 calcium sensor revealed an intensely fluorescent spot (0.4 μm in diameter) located centrally at the very apex of all the hyphal tips observed when mounted in standard PDB (Fig 4.22). The fluorescence intensity of these foci changed with time in cycles of intense spots to barely visible spots in the same hyphal tip (Fig 4.22-A 1-3). When WT hyphae were mounted in PDB containing 5, 10 or 20 mM of EGTA, a faint spot was visible in 5 mM EGTA, however at higher concentrations the spot was no longer visible during the 5 min observation period (Fig 4.22-B). To determine the effect of *midA* deletion on the intensely labelled spot at the tip, ΔmidA hyphae expressing GCaMP5 were mounted in PDB. Out of the 25 hyphal tips observed, the majority (70%) had a spot similar to WT hyphae with varying fluorescent intensities in different hyphae (Fig 4.22-C). Addition of Ca^{2+} to the PDB did not alter the intensity of the spot in the WT or in ΔmidA hyphae in comparison to what was observed in PDB lone. See supplementary movie 4.20 in PowerPoint presentation ‘Calcium foci in *E. festucae* hyphal tips’ (attached CD).

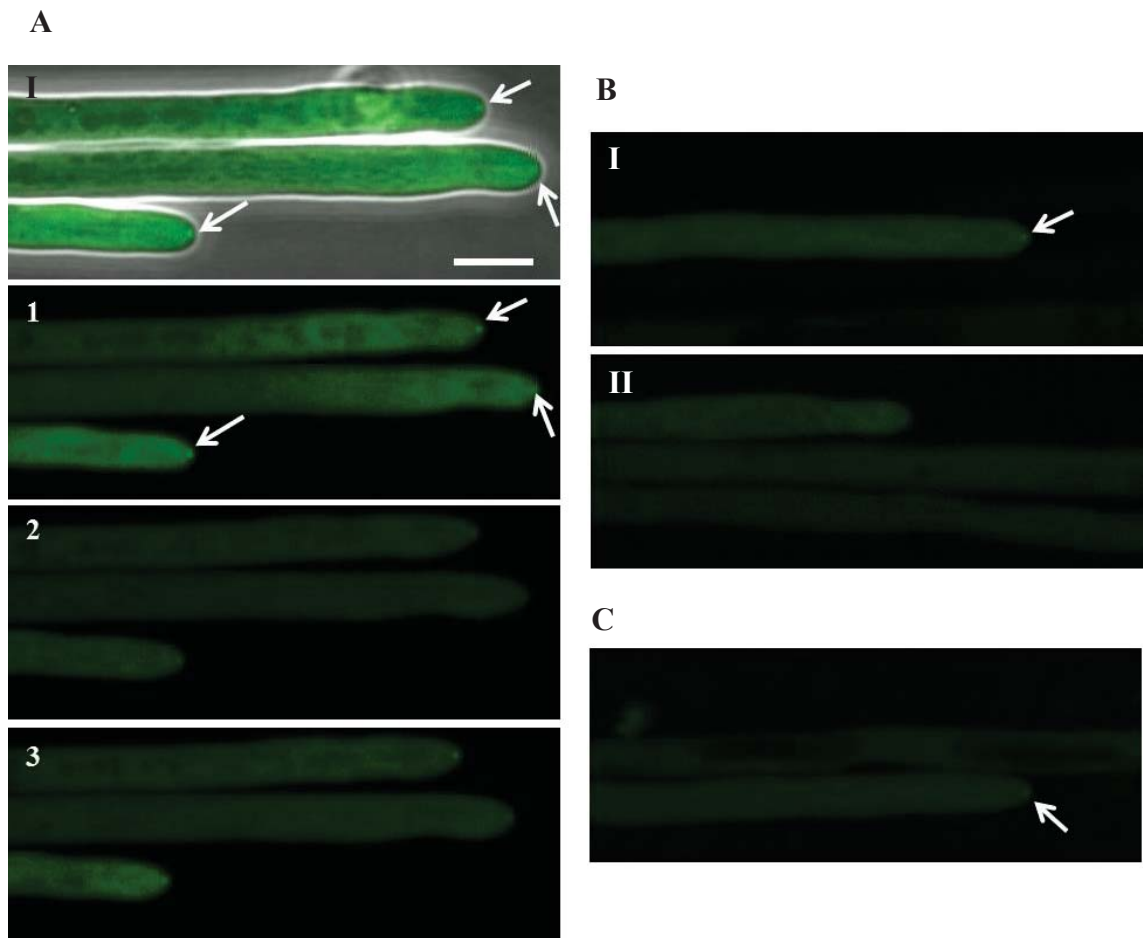


Figure 4.22: Fluorescent foci in *E. festucae* hyphal tips expressing the GCaMP5 calcium sensor. **A-** Phase contrast (**A-I**) and fluorescent images overlaid, showing the intensely-labelled spot (white arrow) present at the hyphal tip of WT hyphae mounted in standard PDB. Images **1-3** represent the fluctuation in intensity of the spot with time. Images were taken under similar conditions and microscopy parameters. **B-** WT hyphae mounted on PDB containing 5 mM EGTA (**B-I**) and 10 mM EGTA (**B-II**). The intensely-labelled spot at the tip is visible in 5 mM EGTA but cannot be seen in 10 mM of EGTA. **C-** Intensely-labelled spot (white arrow) in $\Delta midA$ hyphal tips. Scale bar = 5 μm .

4.6 Discussion

Similar to WscA characterization, the investigation on MidA of *E. festucae* was undertaken as part of a broad attempt to identify the underlying cellular mechanisms of intercalary growth in *E. festucae*. In *S. cerevisiae* Mid1 has been functionally characterised as a stretch-activated calcium-permeable non-selective cation channel activated by cell membrane deformations (Iida et al., 1994; Ozeki-Miyawaki et al., 2005). As we hypothesised that mechanical stretching (potentially causing membrane deformation and stretching) of fungal hyphae trigger intercalary growth, MidA of *E. festucae* (orthologue of Mid1 of *S. cerevisiae*) was considered as a suitable candidate to be tested for its role in intercalary growth. Further, given the crucial role of Ca^{2+} as a signalling molecule, we hypothesized that Ca^{2+} acts as a signalling molecule in triggering intercalary growth. Hence along with MidA analysis, preliminary studies on Ca^{2+} dynamics of *E. festucae* hyphae were initiated during this study.

Recent studies have shown that Mid1 forms a complex with Cch1 and acts as one unit in regulating influx of Ca^{2+} (Brand et al., 2007). Cch1 is a voltage gated channel sensitive to membrane potential (Harren et al., 2013). In this complex, Cch1 is considered to be the channel responsible for Ca^{2+} influx, while Mid1 is believed to be the activator of Cch1 under stimulatory or stress conditions and does not appear to possess any independent channel activity (Hong et al., 2010; Hong et al., 2013). A co-immunoprecipitation study conducted in *S. cerevisiae* indicated that Mid1 interacts with Cch1 (Locke et al., 2000). Likewise, in *A. nidulans* the yeast two hybrid system also confirmed the two proteins interact (Wang et al., 2012). A study in *C. neoformans* has revealed that the C-terminal tail of Mid1 intrudes and modulates channel activity of Cch1 (Hong et al., 2013). In *S. cerevisiae*, Mid1 and Cch1 are not essential for vegetative growth, and deletion of *cch1* and the double deletion of *mid1* and *cch1*,

exhibited similar phenotypes (Fischer et al., 1997; Muller et al., 2001). Studies on mutants of *mid1* and *cch1* conducted using filamentous fungi such as *A. fumigatus* (de Castro et al., 2014), *A. nidulans* (Wang et al., 2012), *B. cinerea* (Harren et al., 2013) and *C. albicans* (Yu et al., 2012) have resulted in common as well as unique phenotypes supporting coordinated as well as unique functions for Mid1 and Cch1. Given the high conservation of the calcium/calcineurin pathway in filamentous fungi, *E. festucae* MidA and CchA may also function together as a complex and possess conserved or independent roles for Mid1 and Cch1 during influx of calcium.

The most visible colony phenotype of $\Delta midA$ was the reduced radial growth rate (by 40% of that of the WT) and lack of aerial hyphae on standard PDA medium (Fig 4.4). In addition, $\Delta midA$ hyphae contained cell wall aberrations and showed frequent tip lysis when mounted in water or PDB (Fig 4.6). Also evident in *E. festucae* $\Delta midA$ hyphae were a phenomenon where the polar directional growth of hyphal tips would stop, and a new branch would initiate and continue to grow (Fig 4.5). All these mutant phenotypes were restored by osmotic stabilization indicating a severe cell wall defect that weakens its integrity (Fig 4.7). These results suggested a crucial role for *E. festucae* MidA in hyphal growth and morphology.

Similar to *E. festucae*, in *C. albicans* (Yu et al., 2012), *A. fumigatus* (de Castro et al., 2014), *B. cinerea* (Harren et al., 2013), *N. crassa* (Lew et al., 2008) and *Magnaporthe oryzae* (Nguyen et al., 2008), *mid1* replacement mutants showed impaired colony growth in axenic culture. Resembling the cell wall aberrations seen in *E. festucae* $\Delta midA$ hyphae, *A. fumigatus* *mid1* mutants showed similar cell wall aberrations in the presence of EGTA (Jiang et al., 2014). Further, *A. nidulans* $\Delta midA$ had defects in cell wall synthesis (Wang et al., 2012) and defects in hyphal maintenance in *C. albicans*

$\Delta mid1$ (Yu et al., 2012). A detailed study on *C. purpurea mid1* showed that the mutants displayed a significant reduction in growth rate while maintaining wild type colony morphology with a normal polar growth and branching pattern in axenic cultures (Bormann et al., 2009). Cell wall perturbing agents such as Congo Red and Calcofluor White caused significant defects in growth in *mid1* mutants including large aggregations of cell wall polysaccharides (Bormann et al., 2009). In *G. zeae* the growth rate of the *mid1* and *cch1* mutants was 50% of the wild type and the colonies showed a cottony morphology (Cavinder et al., 2011). Although all $\Delta mid1$ mutants in filamentous fungi have impaired colony growth and hyphal morphology, the severity of the deletions is variable depending on the species.

Even though the *E. festucae* $\Delta midA$ showed reduction in colony radial growth rate, the individual hyphal apical growth was not significantly ($p < 0.05$) different from that of the WT indicating that even in the absence of MidA hyphal apical growth can continue. Therefore the primary cause for reduced colony growth rate seen in $\Delta midA$ appears to be the frequent tip lysis and polarity disruption seen in individual hyphae which could be due to an alteration in cell wall structure and composition caused by *midA* deletion in *E. festucae*. Impaired cell wall polysaccharide synthesis and defective accumulation at hyphal tip cell wall can cause a severe weakening in nascent cell wall. Results of *mid1* deletion in *C. purpurea* (Bormann et al., 2009) and *ehs1* (orthologue of *mid1*) deletion in *S. pombe* (Carnero et al., 2000) has suggested such alteration in polysaccharide composition in cell walls. Further, for proper cell wall formation during apical growth, adequate transport and deposition of cell wall material is also important (Harris et al., 2004).

MidA activation results in an influx of Ca^{2+} that triggers a signalling cascade through calmodulin and calcineurin that dephosphorylates and activates Crz1 (a zinc finger transcription factor)(Chin et al., 2000). This results in localization of Crz1 to the nucleus and regulation of genes including cell wall-related genes (Yoshimoto et al., 2002; Viladevall et al., 2004). Hence loss of MidA maybe expected to have a direct impact on the integrity of cell walls of growing hyphae, resulting in hyphal lysis. In addition, as was seen during this study, MidA is necessary to create pulsatile Ca^{2+} signatures at the hyphal tip. These Ca^{2+} signatures might have a crucial role in organizing the morphogenetic machinery, cytoskeleton, vesicle transport, vesicle fusion and enzyme activation at the hyphal tip, which when disrupted might cause severe defects in the cell wall (discussed further in the subsequent sections).

The ability of exogenous CaCl_2 (50 mM) but not NaCl at similar concentrations to rescue the $\Delta midA$ phenotypes (colony radial growth rate and cell wall aberrations) in *E. festucae* (Fig 4.8) clearly shows the presence of an alternative calcium uptake system that gets activated (such as Fig1 of low affinity calcium uptake system) under high calcium concentrations. The ability of high exogenous Ca^{2+} to restore *mid1* replacement mutant phenotypes in other filamentous fungi appears to be variable. In *A. fumigatus* (de Castro et al., 2014) and *B. cinerea* (Harren et al., 2013) exogenous calcium was able to rescue the growth rate defect as seen in *E. festucae*, while in *N. crassa* (Lew et al., 2008) and *C. purpurea* (Bormann et al., 2009) external elevated calcium failed to restore defects in vegetative growth. In *G. zae* increasing intracellular Ca^{2+} with ionophores had a slight effect on restoring mutant phenotypes to wild type, and complementing the medium with Ca^{2+} (80 mM) partially restored the growth rate, while supplementation with Mg^{2+} had no effect (Cavinder et al., 2011).

The inability of NaCl in *E. festucae* and Mg²⁺ in *G. zeae* to restore growth defects similar to CaCl₂ confirmed the importance of Ca²⁺ in colony growth. In addition to the ability of exogenous Ca²⁺ to restore the growth defects due to influx of Ca²⁺, the potential osmotic stability provided by very high CaCl₂ concentrations (much higher than in a standard growth medium) similar to high concentrations of sorbitol (50 mM for *E. festucae* and 80 mM for *G. zeae*) cannot be ruled out. Depleted exogenous Ca²⁺ (using EGTA) resulted in defective WT hyphal growth and exacerbated the growth defects of $\Delta midA$ hyphae at a lower EGTA concentration than the WT (Fig 4.8). Even in the presence of an osmotic stabiliser (where $\Delta midA$ growth defects are restored), $\Delta midA$ showed higher sensitivity to EGTA than the WT, showing its important role in Ca²⁺ uptake under low exogenous Ca²⁺ concentrations.

Investigation of the ability of $\Delta midA$ to inoculate and colonise host plants revealed that mutant hyphae were able to colonise the SAM and the stem tissues below the SAM, similar to the WT (Fig 4.11). Nevertheless, transverse sections of tillers infected with $\Delta midA$ showed that hyphal density is lower than in WT infected leaves, and the $\Delta midA$ hyphae were confined to particular regions of leaves (Fig 4.12), suggesting that competency for infection of the intercalary growth zone was determined by an unknown factor in the SAM. Further analysis of longitudinal sections through such $\Delta midA$ infected regions revealed that the hyphae are continuous, elongated and not split into segments (Fig 4.11 and 4.13). When all these results are combined, it appears that $\Delta midA$ can colonise the meristematic regions of a tiller similar to the WT, and to a limited extent, the developing leaves, despite the severe growth defect displayed in axenic culture. The ability of these mutants to grow within the host tissues may be due to localised osmotic stabilization provided by apoplastic fluids which usually contain high concentrations of sugars, amino acids and other solutes (Lohaus et al., 2001).

Interestingly, *wscA* mutants that displayed somewhat similar phenotypes (reduced colony growth rate and aberrant and weak cell walls) in axenic culture were able to colonise the host tissue similar to the WT. This indicates that MidA may have a crucial role in host colonization as well beyond its role in hyphal growth and cell wall synthesis.

The presence of elongated and continuous $\Delta midA$ hyphae in leaf tissues including the elongation zone indicated that some hyphae can undergo intercalary growth within the developing leaf. If $\Delta midA$ hyphae were defective in intercalary growth, the hyphae might be expected to split due to mechanical stretch exerted on fungal compartments by elongating host cells. The $\Delta midA$ appears to be defective (low density and localised hyphae in leaves) at the entry point between apical growth in the meristematic tissues and intercalary growth when the host and endophyte cells start to elongate in the expansion zone. Once the $\Delta midA$ hyphae manage to enter the expansion zone, and transit from apical to intercalary growth, they appear to be able to maintain intercalary growth.

Based on these data I can hypothesise that when host cells start to elongate the attached hyphae are stretched and membrane distortion stimulates the stretch-activated MidA to facilitate influx of Ca^{2+} , which initiates signalling pathways that regulate intercalary growth. In the absence of MidA, influx of Ca^{2+} is attenuated which results in a defect in transition from apical growth to intercalary growth. However since loss of MidA can be complemented with high exogenous Ca^{2+} , in regions of the developing leaf where there is high Ca^{2+} this transition might still occur resulting in patches of $\Delta midA$ hyphae in leaves. Similarly high exogenous Ca^{2+} in leaf tissues may contribute to the intercalary growth of $\Delta midA$ in the expansion zone resulting in elongated hyphae similar to the

WT. As described before there are other mechanisms through which calcium may enter the compartments such as the FigA of the low affinity calcium system. However LACS is activated under high exogenous Ca^{2+} levels and no data is available on Ca^{2+} levels in the grass leaf expansion zone yet to support this postulation. Also, the contribution of the CchA component of the Ca^{2+} channel in *E. festucae* and other Ca^{2+} channels under these conditions is not clear. We cannot rule out the possible presence of another uncharacterised high affinity Ca^{2+} channel or the functioning of CchA independent of MidA (CchA possesses the channel activity in the MidA-CchA complex) under these conditions. The presence of Ca^{2+} pulses in $\Delta midA$ hyphae expressing Ca^{2+} sensor GCaMP5 also supports this notion. The technique developed during this study to apply mechanical stretch (by stretching hyphae similar to the leaf expansion zone, presented in Chapter 5) under *in vitro* conditions will allow the importance of exogenous Ca^{2+} during intercalary growth of $\Delta midA$ to be tested in future.

Although extensive studies have been carried out to understand calcium signalling in plants and animals, not much has been done in fungi until recently due to the lack of suitable techniques to image spatial and temporal dynamics of cytoplasmic Ca^{2+} concentration ($[\text{Ca}^{2+}]_c$) (Kim et al., 2012). Dual wavelength fluorescent dyes such as Indo-1 and Fura-2 have been used before in fungi. However leakage of loaded dye, sequestration in organelles and conversion to membrane impermeable forms make them unreliable to use (Read et al., 1992; Silverman-Gavrila et al., 2003). Subsequently, genetically encoded aequorin has been used successfully to investigate $[\text{Ca}^{2+}]_c$ dynamics in cell populations (Nelson et al., 2004). This technique nevertheless has limitations in the study of $[\text{Ca}^{2+}]_c$ dynamics in individual cells as the signal produced by the fluorescent protein is too weak. In the recent past, a FRET (Forster Resonance Energy Transfer) based Ca^{2+} biosensor Cameleon (used in dual wavelength ratiometric

imaging) has been used successfully (Kim et al., 2012). In addition, currently attempts are being made to use the genetically encoded single wavelength (single fluorescent protein) Ca²⁺ biosensor GCaMP5 that offers better sensitivity and accuracy in fungal systems; our study reports its first successful use in *E. festucae* (please refer to Section 4.5 for more details on GCaMP5).

The temporal and spatial dynamics (amplitude, distribution area and the frequency) of the Ca²⁺ pulses at the hyphal tip were different and unique in each hypha and also changed with time within an individual hyphal tip (Fig 4.15). In general a high amplitude Ca²⁺ pulse occurred every 45-60 sec with many low amplitude pulses in-between (about 10-15 sec apart). Pulses originated in a region within about 10 μm from the tip and extended up to 20-30 μm from the tip until they reached a basal level (Fig 4.16). Hence Ca²⁺ pulses in growing *E. festucae* hyphal tips, corresponding to changes in cytoplasmic Ca²⁺ concentration ([Ca²⁺]_c) appeared to have a unique signature. A similar study conducted using a FRET based Ca²⁺ biosensor, Cameleon, revealed comparable results with similar pulsatile Ca²⁺ signatures in the actively growing hyphal tips of *M. oryzae*, *F. oxysporum* and *F. graminearum*. An average of 28 and 15 sec between pulses in *F. oxysporum* and *F. graminearum* respectively has been observed, with occasional high amplitude pulses (Kim et al., 2012). A high amplitude pulse usually had the highest fluorescence in the region 10 μm from tip and a gradient that spread 20-30 μm from the tip until it reached the basal level (Kim et al., 2012).

Further investigation indicated that these signatory Ca²⁺ pulses in *E. festucae* hyphal tips were due to influx of Ca²⁺ from the external environment, and that MidA plays a crucial role in maintaining these frequent pulses (Fig 4.17 and 4.21). Replacement of *midA* resulted in absence of visible Ca²⁺ pulses in most hyphae, however an occasional

single pulse (or an array of 2-3 pulses in quick succession) that spread up to 25-70 μm from the tip, higher than the WT in terms of distance from tip was detected. This indicates the presence of a further oscillating ion channel independent of the MidA/CchA. Use of Ca^{2+} chelator EGTA in the medium diminished Ca^{2+} pulses in both WT (20 mM) and ΔmidA (10 mM) after 5 min of incubation indicating that the Ca^{2+} originated from the medium and not from internal cellular stores (Fig 4.21). Interestingly increasing exogenous Ca^{2+} did not have any visible effect on the usual Ca^{2+} pulsatile signature of both WT and ΔmidA , again highlighting the role of MidA in producing these pulses. However the confocal microscopy set up limited the ability to observe the immediate effect of EGTA or Ca^{2+} addition. In a study conducted in *Aspergillus niger* and *A. awamori* using aequorin addition of Ca^{2+} (0.05 and 5 mM CaCl_2) to the medium resulted in a transient strong spike in $[\text{Ca}^{2+}]_c$ at the hyphal tip. The amplitude was dose dependent (the higher the Ca^{2+} added the greater the amplitude) and settled after the initial burst (Nelson et al., 2004). Addition of the divalent cation ion chelator BAPTA inhibited the generation of $[\text{Ca}^{2+}]_c$ transients in response to mechanical perturbation and hypo-osmotic shock (Nelson et al., 2004).

The above mentioned observations indicate that influx of external Ca^{2+} through the plasma membrane causes Ca^{2+} pulses at the hyphal tip. The $[\text{Ca}^{2+}]_c$ depends on influx/efflux through the plasma membrane plus sequestration and release of Ca^{2+} from intracellular storages. Maintenance of calcium homeostasis in fungi and the involvement of Ca^{2+} channels/pumps/transporters have been discussed in detail in the introduction Section 1.5. Accordingly, unique pulsatile signatures of $[\text{Ca}^{2+}]_c$ at the hyphal tip could be created through fine coordination of these Ca^{2+} channels/pumps/transporters (Nelson et al., 2004) depending on the stimulus, and MidA

seems to have a crucial role in this. Pulsatile signatures produced might deliver a unique message each time, triggering the appropriate signalling cascade.

Although the above mentioned results give a general depiction of $[Ca^{2+}]_c$ dynamics at the hyphal tip, the results also show that these dynamics are complex and variable. *E. festucae* hyphal tips exhibited variable Ca^{2+} pulsatile characteristics/signatures; nevertheless the apical growth rates were constant in all the WT hyphae observed ($1.26 \pm 0.09 \mu\text{m}/\text{min}$). Another noticeable observation was that, even though pulses were observed frequently in WT hyphae, there were hyphae that did not show Ca^{2+} pulses (at the time of observation) but continued to grow at the same rate. Further, while *midA* replacement mutants did not show frequent Ca^{2+} pulses at the hyphal tip similar to WT, the apical growth rate of individual $\Delta\textit{midA}$ hyphae was not significantly ($p < 0.005$) different to that of the WT.

Previous studies conducted using dual Ca^{2+} indicator dyes has suggested that maintenance of a tip high gradient is necessary for continued hyphal apical growth and the hyphal growth rates depend upon the tip-localized calcium concentration (Jackson et al., 1993; Silverman-Gavrila et al., 2003). In studies conducted in *M. oryzae*, *F. oxysporum* and *F. graminearum* the pulsatile nature of $[Ca^{2+}]_c$ was observed only in old hyphae (48 h post inoculation) (Kim et al., 2012). In germ tubes and young hyphae occasional high $[Ca^{2+}]_c$ transient pulses have been observed (but not frequent oscillation) that also somewhat resembles the pattern seen in *E. festucae* $\Delta\textit{midA}$. Also, on the other hand Silverman-Gavrila and Lew (2003) have reported that what is important for hyphal growth rate is not the steepness of the calcium gradient, but a difference in concentration between the apical and the sub-apical region. Minimum

concentrations of 30 nM have been shown to be sufficient for apical growth to continue (Silverman-Gavrila et al., 2003).

Overall these observations indicate that existence of a continuous oscillation in $[Ca^{2+}]_c$ at the tip, or a continuous steep tip high gradient may not be essential to maintain hyphal apical growth rate. One explanation could be the existence of prolonged intervals between two arrays of Ca^{2+} pulses (a resting phase). During hyphal apical growth, since MidA is stretch-activated, as the hyphal tip grows forward through turgor pressure, the stretching of the membrane at the tip may activate the MidA-CchA complex allowing a sudden influx of Ca^{2+} which gives rise to frequent increases in $[Ca^{2+}]_c$ at the tip. When there is sufficient calcium a negative feedback loop might inhibit MidA activity creating a resting phase until $[Ca^{2+}]_c$ depletes and MidA is re-activated. Hence, even though pulses are absent apical growth can continue. Previous studies have shown that when $[Ca^{2+}]_c$ is high, calcineurin can inhibit Cch1 and Mid1 activity via a negative feedback loop (Muller et al., 2001; Muller et al., 2003). This would also explain why high exogenous Ca^{2+} fails to affect the Ca^{2+} oscillations in the WT. Similarly, in $\Delta midA$, the occasional high intensity Ca^{2+} pulse may be the result of a sudden influx of Ca^{2+} that is sufficient to replenish intracellular Ca^{2+} . The sequestered Ca^{2+} might be enough to maintain a minimum Ca^{2+} concentration difference between the hyphal tip and sub-apical region for apical growth to continue between pulses.

Given that the existence of continuous Ca^{2+} pulses at the tip is not essential for apical growth, a question arises about the exact role of these pulses. The pulses occur at the very tip and studies have shown that the highest Ca^{2+} concentration is within the 10 μm from the tip, which overlaps with the Spitzenkorper. The Spitzenkorper consists of various vesicles, cytoskeletal components and proteins, and acts as a vesicle supply

centre (Harris et al., 2004; Harris et al., 2005); Ca^{2+} is involved in regulating the structure and function of the actin network (Adamíková et al., 2004). Hence, the function of these $[\text{Ca}^{2+}]_c$ signatures, as suggested by Kim et al., (Kim et al., 2012), could be the regulation of the actin network and other Spitzenkorper associated processes in apical growth and cell wall synthesis. Accordingly, weakened cell walls with frequent tip lysis, and branching at the tip seen in $\Delta midA$ could be a result of disturbing the pulsatile Ca^{2+} signature at hyphal tip.

Ca^{2+} pulses in sub-apical regions were observed randomly in sub-apical compartments or in the sub-apical region of the first compartment and appeared to be due to influx of Ca^{2+} , as high concentrations of EGTA eliminated these pulses (Fig 4.20). In *F. oxysporum* and *M. oryzae* Ca^{2+} pulses have been observed in sites of hyphal branching (sporadic large Ca^{2+} transients) and septum formation confirming that Ca^{2+} pulses can occur in sub-apical regions (most probably in growth initiation sites) other than at the hyphal tip (Kim et al., 2012). The presence of sub-apical Ca^{2+} pulses indicates activity of Ca^{2+} channels in sub-apical regions and the potential involvement of these pulses in intercalary growth and mechanical stretch requires further study.

A closer look at the *E. festucae* WT and $\Delta midA$ hyphae expressing GCaMP5 calcium sensor revealed an intensely fluorescent spot (0.4 μm in diameter) located centrally at the very apex of all the hyphal tips observed when mounted on standard PDB (Fig 4.22) which faded with high concentrations of EGTA but did not change with addition of Ca^{2+} . Due to time constraints no further tests were conducted to investigate its association with any cellular structure. However, in the study conducted in *F. graminearum* using Cameleon vectors a similar single large apical spot has been observed at the hyphal tip that was shown to overlap with the Spitzenkorper actin core

(Kim et al., 2012). The presence of a Spitzenkorper in *E. festucae* hyphal tips has not yet been shown. However it would be interesting to know whether the bright spot seen in *E. festucae* has any association with a Spitzenkorper as this would be the first such visualization of the Spitzenkorper in *E. festucae*.

Given the pivotal role Ca^{2+} has in apical growth, it is plausible that Ca^{2+} has a similarly crucial role as a signal molecule in triggering intercalary growth. Our hypothesis that mechanical stretch of endophyte hyphae in the elongation zone of the plant is a likely stimulus for intercalary growth is supported by experiments in axenic culture (presented in Chapter 5, Section 5.4). Hence it is important to understand the Ca^{2+} dynamics of *E. festucae* hyphae under mechanical stress. In studies conducted on other fungi such as in *A. niger* and *A. awamori*, mechanical perturbation resulted in unique transient $[\text{Ca}^{2+}]_c$ increases (Nelson et al., 2004), while in *F. oxysporum* (using Cameleon vectors) cell-cell contact between *M. oryzae* with the host produced signatory large amplitude $[\text{Ca}^{2+}]_c$ transients, not only at the hyphal tips but also in the distal regions (Kim et al., 2012). Preliminary investigations showed that *E. festucae* can produce Ca^{2+} pulses at the tip and sub-apical regions under mechanical perturbation (presented in Chapter 5, Section 5.6.1). In addition, during this study a mechanism to stretch *E. festucae* hyphae under *in vitro* conditions was developed and the technique will be used to study Ca^{2+} dynamics when hyphae are subjected to mechanical stress.

The results obtained from this study to date indicate that MidA of *E. festucae* is required for hyphal apical growth, cell wall integrity (shape and structure), host colonization and maintenance of pulsatile Ca^{2+} signatures at growing hyphal tips. The defect shown by *midA* mutants during host colonization hinted at a possible role for MidA in intercalary growth. During this study an *in vitro* technique was developed to mechanically stretch

fungal hyphae (discussed in next Chapter 5) to investigate the role of mechanical stretch in initiating intercalary growth. This technique will be used in future to test the importance of MidA in intercalary growth as a mechano-sensor and also to further study Ca^{2+} dynamics during mechanical stretching of fungal hyphae.

Chapter 5: Intercalary growth in *E. festucae* hyphae in culture

5.1 Evidence of intercalary growth in sub-apical compartments of *E. festucae* hyphae

5.1.1 Nuclear division and septation occurs in sub-apical compartments of *E. festucae* hyphae

Intercalary growth in developing grass leaves, as well as in fungal fruiting bodies is a process largely involving cell wall expansion, and is generally not accompanied by significant cell division. Previous results however suggest that intercalary growth of *E. festucae* hyphae in plants is accompanied by nuclear division and septation (Christensen et al., 2008). To understand nuclear behaviour in *E. festucae* hyphae, WT protoplasts were transformed with plasmid pYH2A, to label the nuclei, and purified via tip culture (Section 2.6.3 and 2.8). The plasmid pYH2A harbours the histone H2A protein gene fused to a yellow fluorescence protein (YFP) gene. Once expressed, the fused histone protein localises and labels the nuclei, enabling them to be observed by fluorescence microscopy (Rech et al., 2007).

Growth rate, colony and hyphal morphology and colonisation of the host by pYH2A transformants were compared with those of the WT to ascertain that ectopic integrations had not interfered with these traits. Three independent nuclear-labelled strains were cultured on PDA for 8 days under standard conditions (Section 2.3.2) and imaged as mentioned in Section 2.12.3.

The apical and sub-apical compartments of *E. festucae* hyphae were almost entirely uni-nucleate (Fig 5.1). Nevertheless, multi-nucleate sub-apical compartments were observed occasionally in random positions along hyphae revealing that mitosis does occur in sub-apical compartments irrespective of their position in a hypha (Fig 5.2). Due to the very low number of multi-nuclear compartments against the number of uni-nuclear

compartments, no attempt was made to quantify the ratio. The number of nuclei observed in multi-nuclear compartments ranged from 2-3 nuclei with 2 nuclei being the most frequent. Nuclear division in sub-apical compartments seemed to occur before branch initiation (as signs of branching could be seen in some multi-nuclear compartments), or before division of an existing sub-apical compartment where nuclear division was followed by septation as discussed later (Fig 5.2).

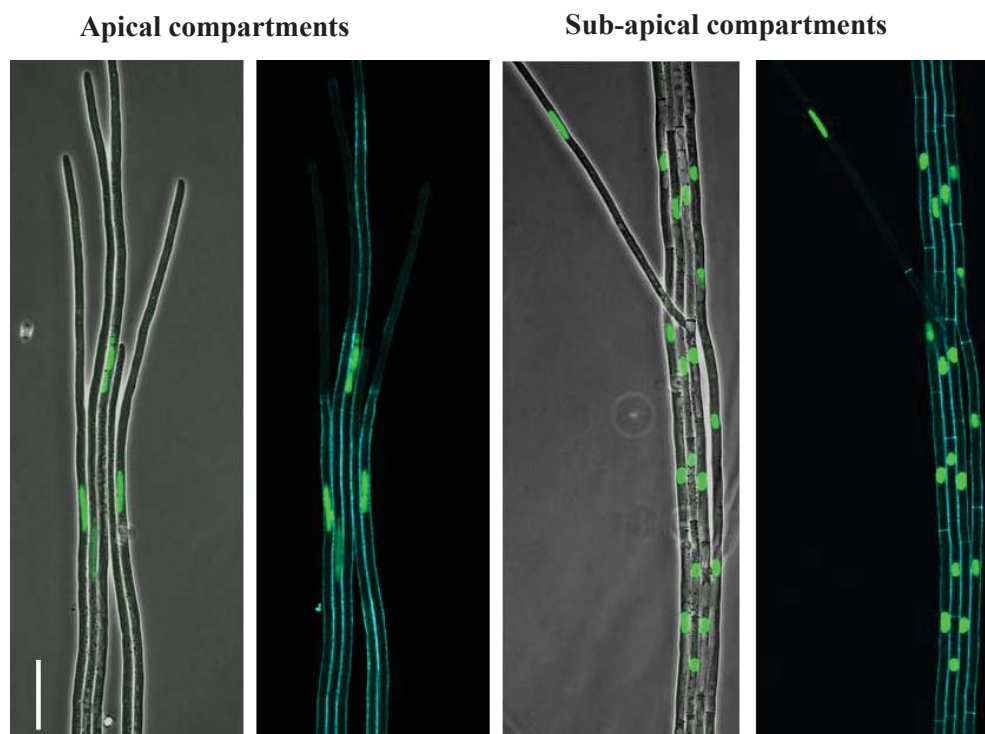


Figure 5.1: Phase contrast and fluorescence images of CW-stained (stains cell walls and septa) and nuclear-labelled apical and sub-apical compartments of *E. festucae* WT hyphae grown on PDA, showing typical nuclear shape, distribution and variation in compartment lengths. Pale blue lines represent cell walls and septa. In general, the hyphae consist of uni-nuclear compartments and the nuclear shape and compartment length differs along hyphae. White scale bar = 20 μm .

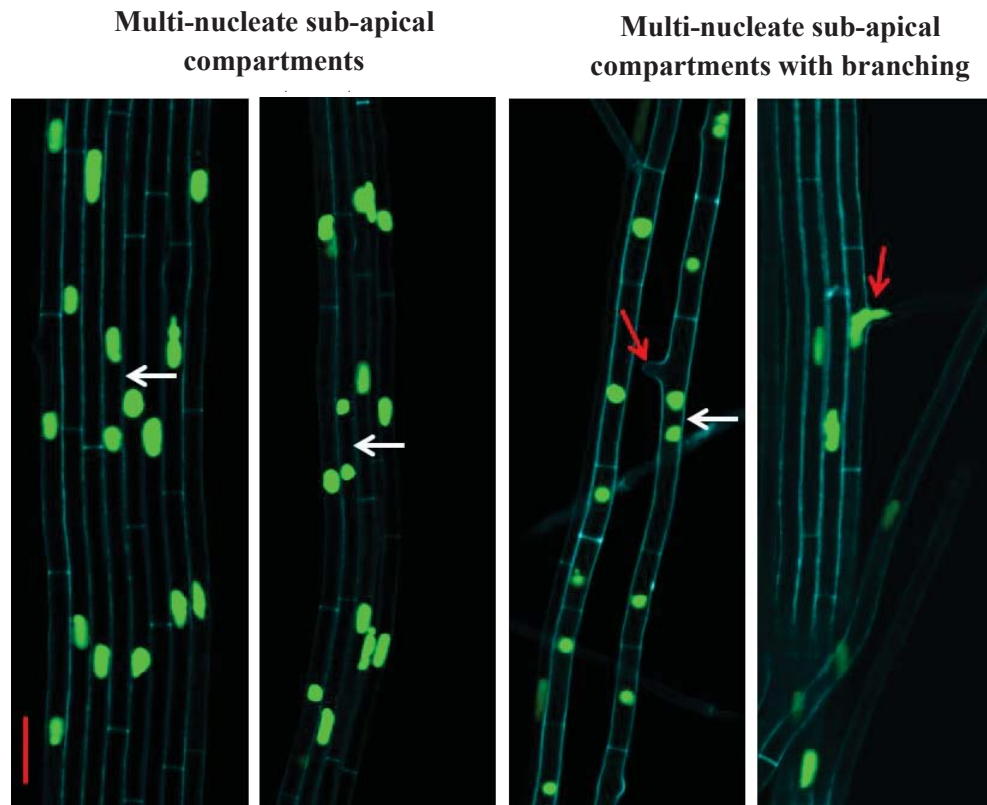


Figure 5.2: Positions of nuclei relative to cell walls and septa in sub-apical compartments of nuclear-tagged *E. festucae* hyphae (transformed with pYH2A) growing on PDA. Multi-nuclear sub-apical compartments (white arrow) were present in hyphae at the time of observation (8th and 11th compartment from the tip in the representative images shown). Some of the multi-nuclear compartments showed signs of branching and nuclear migration (red arrows). Red scale bar = 10 μm .

Nuclei in apical compartments and long intercalary compartments of *E. festucae* hyphae appeared elongated compared to spherical shaped nuclei in small compartments. Hence, an analysis was conducted to determine whether there is a relationship between compartment length and the longitudinal length of the nuclei along the hypha axis. Images of CW-stained (stains cell walls and septa) hyphae were taken from 8 day old cultures of three independent nuclear-labelled WT strains growing on PDA (Section 2.12.3). Five hyphae were imaged from each strain starting from the hyphal tip to the

30th compartment. For each compartment, the nuclear longitudinal length along the hyphal axis and the corresponding compartment length and width were measured. In general, the apical compartment is the longest followed by the second compartment. The compartment lengths further down the hyphae were highly variable (Fig 5.3-A). A typical hypha is a mix of short (35-45 μm) and longer (>50 μm) sub-apical compartments seemingly located in random order, although a trend towards shorter compartments was seen in older regions of a hypha.

To test whether there is a statistically significant correlation between the compartment length and the longitudinal nuclear length, Pearson's linear correlation coefficient was calculated between the natural logarithms of compartment length and nuclear length (as the measures were highly skewed, the coefficient was calculated between the logarithms of the data). The analysis revealed that there is a strong, positive correlation between compartment length and nuclear length which was statistically significant ($r = 0.8634$, $n = 150$, $p < 0.001$, Fig 5.3-B). Given that the apical compartments are continuously elongating and then dividing, elongated nuclei appeared to correlate with compartments undergoing further compartmentalization (examined further in the following section). Therefore, during investigations on intercalary growth, I hypothesised that the presence of elongated nuclei in intercalary compartments is an indirect indication of their readiness for further division/compartmentalization. The width of hyphal compartments was uniform at around $2.87 \pm 0.23 \mu\text{m}$ (mean \pm SD) except in the apical compartments where the hyphae tapered towards the tip.

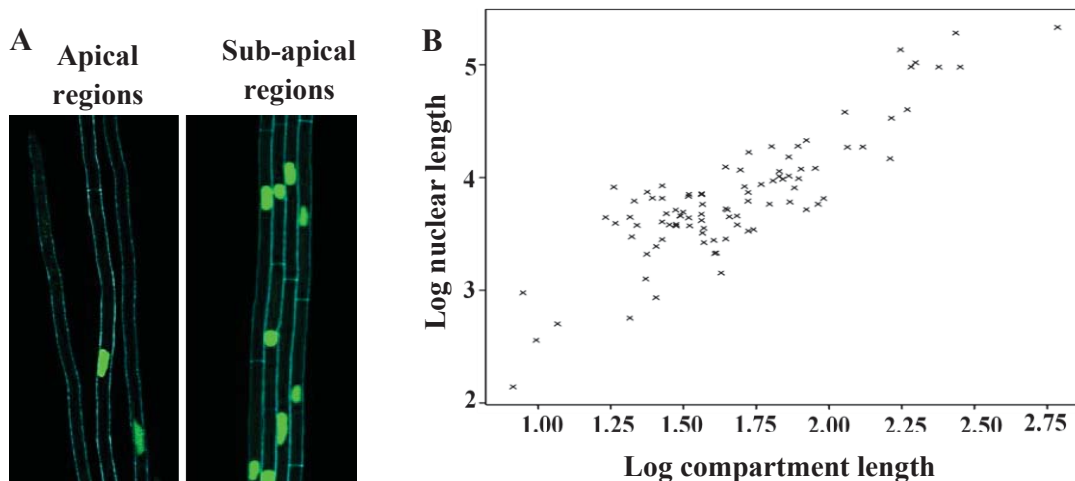


Figure 5.3: Comparison of compartment lengths and longitudinal nuclear lengths along WT *E. festucae* hyphae.

A- Florescence images of CW-stained and nuclear-labelled WT *E. festucae* hyphae showing various nuclear shapes and compartment lengths taken from random positions in apical and sub-apical regions of hyphae. White scale bar = 20 μm .

B- Logarithmic plot showing the regression analysis between compartment length and longitudinal length of the corresponding nuclei.

5.1.2 Sub-apical compartment division occurs according to a compartment length-dependent hierarchy

To further understand the pattern of nuclear division and septation in intercalary compartments of *E. festucae* hyphae growing in culture, nuclear-labelled WT hyphae (Section 5.1.1) were cultured on PDA for 8 days. Images of CW stained (2-4 μM in PDB) compartments, from the apical compartment to the 11th compartment, were obtained in 3 h intervals (T = 0 to 9 h) as described in Sections 2.12.3.2 and 2.11.1. Five hyphae from three independent nuclear-labelled *E. festucae* strains were observed. Compartment lengths were measured and tabulated at each time interval and new septation events recorded (Fig 5.4 & Table 5.1). The pattern of septation/compartment formation in the sub-apical compartments with time (from the 2nd to the 11th

compartment from the tip) was analysed. Observations were made only up to the 11th compartment due to the practical difficulties of following a single hypha through a longer time period as colony growth entangles hyphae.

The apical compartments grew and divided continuously as expected, therefore they were not included in the analysis. The patterns of septation in the sub-apical compartments from the 2nd to the 11th, recorded every three hours from time zero, showed that there was a hierarchy in the order of compartment division, with the longest compartments dividing first, irrespective of their position from the tip (Fig 5.4 & Table 5.1). Sub-apical compartments continued to divide until a minimum length was reached, and no further division was observed over the 9 h period. The minimum length of sub-apical compartments observed ranged from 15-30 μm over this time period. However data gathered were not sufficient to provide a definitive length and compartments as short as 4 μm have been observed in hyphae growing in plants (Christensen et al., 2008). Except in the apical compartment where tip growth continues, the overall length of sub-apical compartments remained constant over the time period observed. In addition, consistent with the results mentioned in the previous section (5.1.1), the short sub-apical compartments (that presumably do not undergo further division) seemed to have globular shaped nuclei whereas longer compartments that underwent further division contained elongated nuclei. In summary, the above observations indicate that sub-apical compartments of *E. festucae* hyphae growing in culture continue to undergo mitosis and septation, forming new compartments in a compartment length-dependent hierarchy, and the presence of elongated nuclei in compartments seemed to be indicative of further division in a compartment.

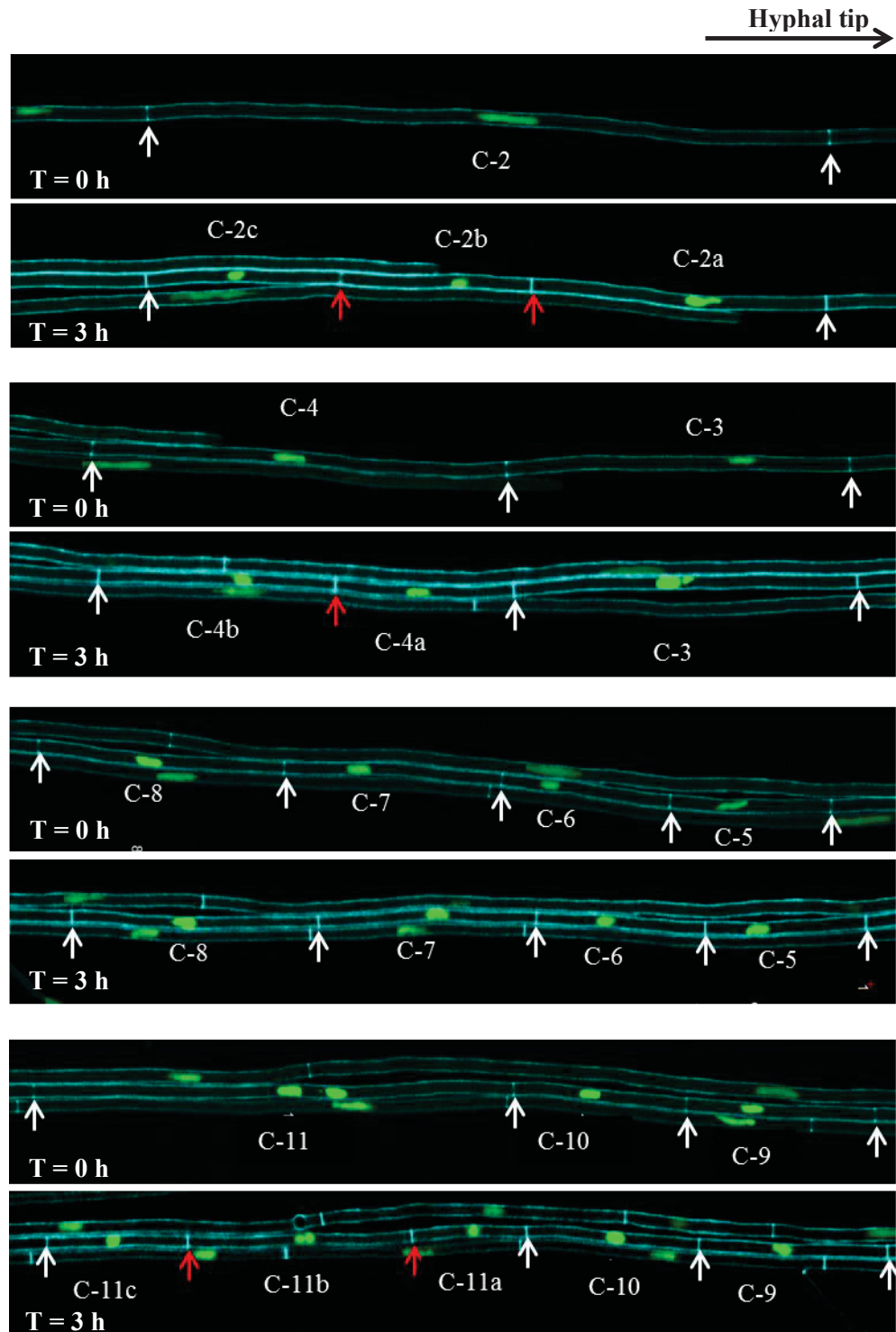


Figure 5.4: Fluorescence images of a nuclear-tagged *E. festucae* WT hyphal segment (stained with CW) showing compartmentalization in sub-apical compartments from the 2nd to 11th compartment along the same hypha within 3 h (T = 0-3 h). C - Compartment position from tip (apical compartment = C-1). White arrow - Positions of the septa at T = 0 h. Red arrows - Positions of new septa formed within the 3 h period. The 2nd, 4th and 11th compartment at T = 0 h has further divided within 3 h but not compartments 3, 5, 6, 7, 8, 9 and 10.

Table 5.1: A representative table showing the division of sub-apical compartments with time (in 3 h intervals) in a hypha from the 2nd to the 11th compartment growing on PDA (measurements are not from same hypha shown in Fig 5.4).

Time	Comp-2 ^b				Comp-3	Comp-4	Comp-5	Comp-6	
T=0 ^a	194.2				43.2	42.4	50.6	71.0	
T=3 h	83.2		110.8		44.2	42.2	51.1	70.9	
T=6 h	33.5	49.7	50.0	60.9	43.7	41.4	50.2	70.4	
T=9 h	33.7	49.8	50.2	59.3	43.9	42.1	50.2	34.2	36.0

Comp-7	Comp-8	Comp-9	Comp-10	Comp-11	
36.2	36.9	49.7	64.3	72.2	
37.0	38.1	48.6	64.1	72.5	
36.9	37.1	48.3	64.0	37.8	35.2
36.9	37.1	48.0	64.2	37.7	35.6

^aCompartment lengths (in μm) at each time point and the subsequent further division of each compartment from the starting point to 9 h later. Vertical lines within the table indicate septa.

^bCompartment position from the hyphal tip (apical compartment = Comp-1).

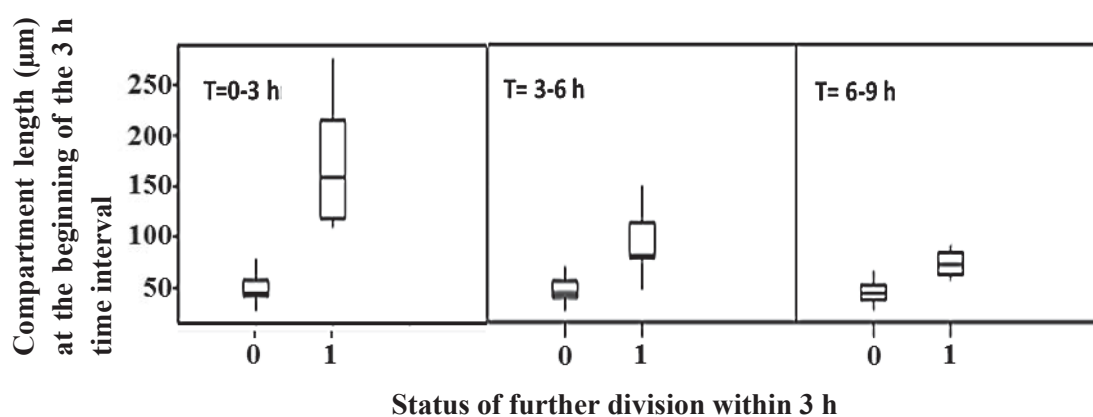


Figure 5.5: Analysis of compartmentalization in sub-apical compartments of nuclear tagged *E. festucae* hyphae. Graph shows compartment lengths at the beginning of the 3 h time interval and the status of further division within the next 3 h. **0** - Compartments with no division within the time period. **1** - Compartments that divided within the time period. The data indicate a length-dependent hierarchy in division of sub-apical compartments.

5.2 Nuclear shape differs in different plant regions

As demonstrated in Section 5.1.1, in-culture analysis of the nuclear shape of hyphae growing on PDA revealed that long sub-apical compartments (that have the potential to undergo further division) appeared to have elongated nuclei, and older short sub-apical compartments (that do not undergo further division) contained globular-shaped nuclei. The same study also established that there is a compartment length-dependent hierarchy in division of sub-apical compartments (Section 5.1.2). There is therefore a correlation between the shape of the nucleus and the probability that the compartment will shortly undergo further division. Extending this correlation to *E. festucae* colonization of developing leaves, we would expect to find more elongated nuclei in the elongation zone of the developing leaf where hyphal intercalary growth is taking place via continuous compartment elongation, mitosis and septation, and more globular-shaped nuclei in hyphae (no longer growing) in mature leaves. To test this hypothesis, leaf tissues colonized by nuclear-tagged (YFP) *E. festucae* hyphae were imaged by Z stack confocal laser scanning microscopy with a depth of between 15-20 μm and 1.5-2 μm per slice, depending on the specimen under observation. Leaf tissues were obtained from the meristematic region where the endophyte grows at the hyphal apex, the young leaf where the endophyte grows via intercalary growth (within 2 cm from the base of the inner most leaf) and the mature leaf sheath where the endophyte has ceased growing (outer-most mature leaf). Using fluorescent images, longitudinal lengths of at least 75 nuclei were measured from each tissue, and analysis of variance was used to compare the nuclear lengths for the three different tissues.

Significant differences between the mean lengths of nuclei in each region were clearly demonstrated ($P < 0.01$), with the highest mean longitudinal nuclear length observed in the young leaf sheath tissue where intercalary growth was occurring (Fig 5.6 and 5.7).

In the meristematic region and the mature leaf tissues, endophyte nuclei were more globular in shape. These observations support in-culture data where elongated nuclei were present in longer and dividing compartments (Section 5.1.1), suggesting that the presence of elongated nuclei in the elongation zone of the developing leaf is further evidence for continuing mitosis and compartmentalization occurring in this region.

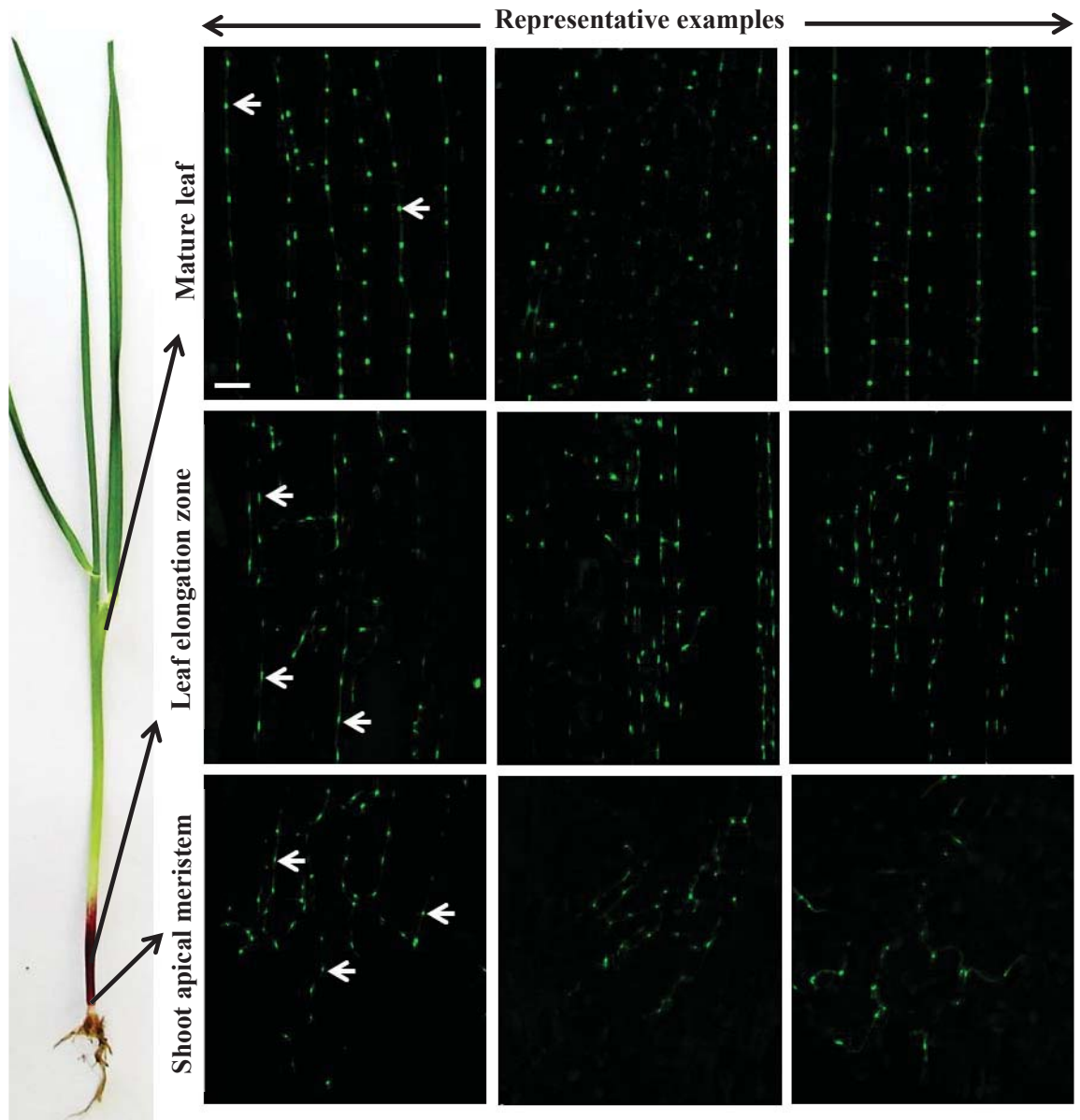


Figure 5.6: *E. festucae* nuclear shape variation in different tissues of a developing leaf. Compressed Z stack confocal images (15-20 μm with 1.5-2 μm thickness per frame) of nuclear-tagged (YFP) hyphae colonizing different leaf tissues of *L. perenne*. Endophyte nuclei in the elongation zone of the developing leaf were more elongated in comparison to the more globular-shaped nuclei in the meristematic tissues and mature leaf tissues. White arrow – Endophyte nuclei. Scale bar = 10 μm .

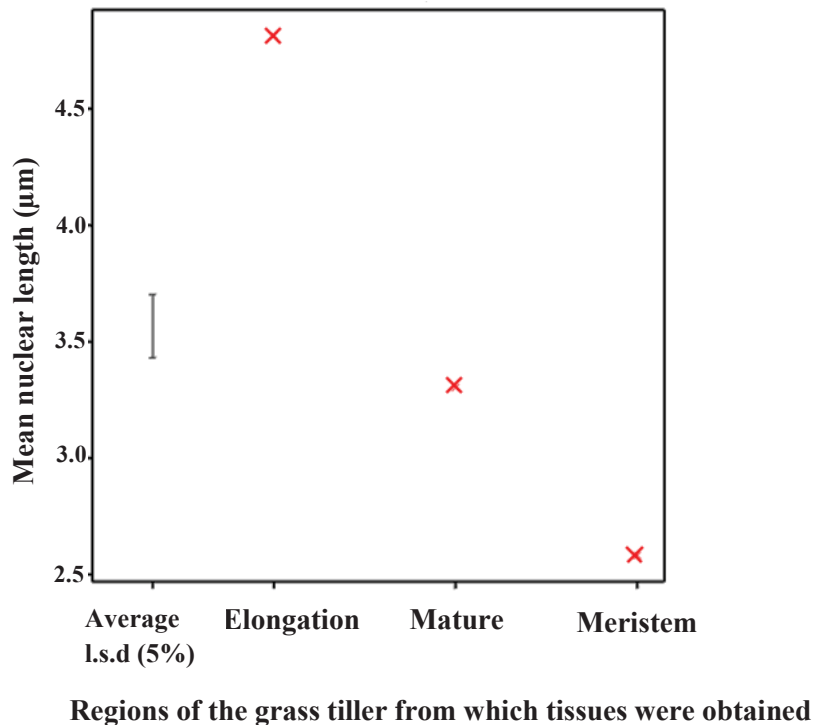


Figure 5.7: Calculation of *E. festucae* longitudinal nuclear lengths in different growth zones (meristematic, elongation and mature) of the developing leaf. Analysis of variance was used to compare the nuclear lengths from the three different regions. Means were calculated from at least 75 nuclei per region. The standard errors of differences of means is 0.1387, l.s.d is the least significant differences of means (at the 5% level). The data demonstrated that nuclear lengths in hyphae in the three regions differs significantly from each other with nuclei in the leaf elongation zone having the highest mean longitudinal length.

5.3 Can mechanical stretching trigger intercalary growth in *E. festucae* hyphae?

Intercalary growth in *E. festucae* hyphae in the elongation zone of the developing leaf has been experimentally shown using microscopic evidence of changes in hyphal length between lateral branches (Christensen et al., 2008). At that time, it was hypothesised that the factor responsible for intercalary growth in the elongation zone of the developing leaf is mechanical stretch applied by rapidly elongating host cells, as endophyte hyphae are attached to the walls of these elongating cells (Section 1.3.1). To test this hypothesis it was necessary to separate the endophyte from the host and apply

mechanical stretching to hyphae under *in vitro* conditions. Such an attempt would isolate endophyte hyphae from other factors that may be influencing intercalary growth within the developing leaf. However, due to the unavailability of literature or an established method for apply mechanical stretch to fungal hyphae, a novel technique had to be designed, optimised and tested for this purpose.

I aimed to achieve a number of objectives through these experiments. The first objective was to optimize a simple and reproducible method to apply mechanical stretch to *E. festucae* hyphae *in vitro*. Secondly, using the optimised technique, I intended to test whether hyphae can tolerate mechanical stretching and, if so, to what extent. The third objective was to observe the changes in hyphae caused by applied mechanical stress in terms of sub-apical compartment length, nuclear division and septation. In general, these latter phenomena are considered as the three vital events of intercalary growth. Thus preliminarily investigations were made to determine the possible underlying mechanism of intercalary growth in *E. festucae* hyphae under mechanical stress.

5.3.1 Optimization of a technique to mechanically stretch fungal hyphae under *in vitro* conditions

5.3.1.1 The strategy

A novel technique was developed to investigate the effect of mechanical stretching on fungal hyphae. The method was based on similar principles used to test the responses of vertebrate heart and muscle cells to mechanical stress. In this novel method, fungal hyphae were grown on a suitable stretchable membrane and then the membrane was stretched by known degrees on an apparatus designed to apply appropriate mechanical stretch/stress on the attached hyphae. The stretching membrane transfers stretching

forces onto attached fungal hyphae. Trials were initially carried out to select a suitable membrane and to optimise a technique to grow hyphae on the membrane.

5.3.1.2 Selection of a suitable membrane

The criteria used to select a suitable membrane included its ability to attach to fungal hyphae firmly during colony growth, ability to stretch evenly, and transparency to allow hyphae to be observed under a microscope. Firm fungal attachment to the membrane was crucial to enable transfer of mechanical stress applied to the membrane, by way of stretching, onto fungal hyphae. Membranes tested included cellophane and silicon membranes (both amino-coated and non-amino-coated). Based on optimization trials (data not shown), an amino-coated silicon membrane (Flexcell^R International Corporation, Burlington, USA) was selected as the most suitable for this purpose. The ability of hyphae to attach and stretch with the membrane was tested as described in Section 5.3.1.4 below. These membranes stretch evenly, the amino coating on the membrane surface facilitated firm attachment of *E. festucae* hyphae, and the membrane was sufficiently thin and transparent to enable hyphae to be viewed clearly (although the membrane was autofluorescent when hyphae were being examined for the position of YFP-labelled nuclei).

5.3.1.3 Selection of a suitable nutrient medium

The second task was to supply nutrients to the growing hyphal colony. As silicon membranes are not permeable to nutrients and water, nutrients had to be directly supplied to the colony from above. Having a liquid growing medium (PDB) or a solid medium (PDA) directly on the growing colony encouraged the hyphae to grow up into the medium rather than onto the amino-coated membrane surface. Therefore, to avoid this, an impenetrable cellophane membrane was placed on the colony and a block of

solid nutrient medium placed on top (Fig 5.8). The block of medium provided nutrients for hyphal growth through the permeable cellophane membrane. Further, this system permitted the growth conditions to be altered by changing the composition of the growth medium (e.g. calcium concentration) at the start of, or during, the experiment. Tests conducted to find a suitable growth medium that promoted optimum *E. festucae* hyphal growth under these altered conditions showed that elevated Ca^{2+} (50 mM) in standard potato dextrose medium gave the best growth (Fig 5.9). Therefore, for initial trials to optimise the system and see the effect of mechanical stress on intercalary growth, it was decided to use this medium of standard potato dextrose with Ca^{2+} (50 mM). Agar (4% w/v) was used to solidify the medium.

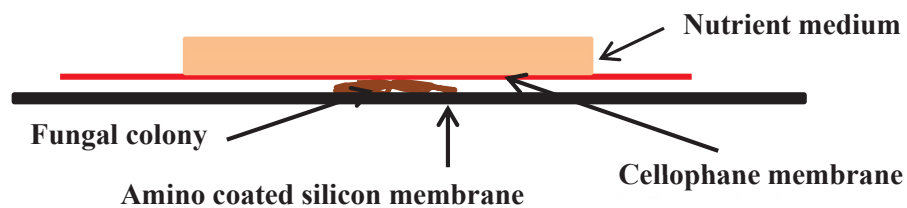


Figure 5.8: Diagrammatic representation showing the arrangement of components used to grow *E. festucae* hyphae on amino-coated silicon membranes. The nutrient medium on top of the hyphal colony provided necessary moisture and nutrients via the permeable cellophane membrane. The cellophane membrane also prevented the hyphae growing into the medium, forcing them to grow in between the two membranes. This facilitated the attachment of hyphae onto the amino coating of the silicon membrane. Not drawn to scale.

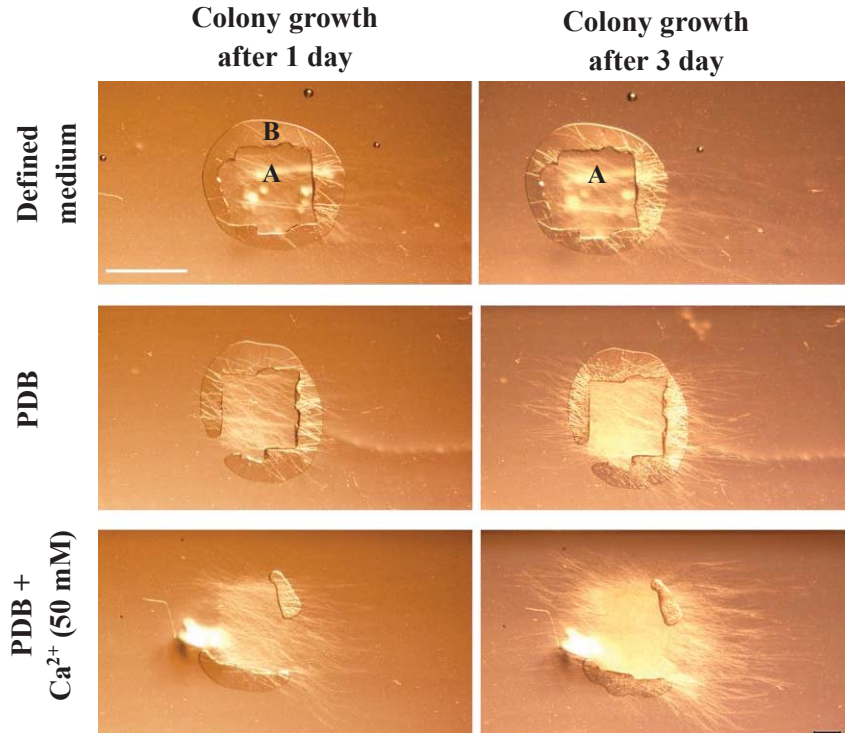


Figure 5.9: Selection of the best medium to grow hyphae on amino-coated silicon membranes under growth conditions shown in Fig 5.8. Silicon membranes inoculated with hyphae (setup as shown in Fig 5.8) were placed in sealed containers and incubated at 22°C under continuous light. Images were obtained using an Olympus SZ100 dissecting microscope. Although all three media tested facilitated hyphal growth under these conditions, standard PDB with elevated Ca²⁺ (solidified with 4% (w/v) agar) resulted in robust growth. Therefore this medium was used for initial trials to optimise a technique to stretch fungal hyphae. A – Thin plug of agar in-between the silicon and cellophane membranes acting as the inoculum, B- Trapped air in-between the silicon and cellophane membranes. Scale bar = 2 mm

5.3.1.4 Stretching hyphae

To stretch the hyphae, 5 mm wide and 4.5 cm (4 cm after being clamped) long strips of amino-coated silicon membranes were cut from a 3-1/2" x 5-1/4" sheet (Flexcell, Burlington, USA, Silicone Membrane Amino Coated, 020" Thick) and attached using clamps (indicated as A and B in Fig 5.10-A) onto the stretching frame tailor made for

this purpose. The attached membrane was slightly stretched and tightened using screws (C and D in Fig 5.10-A) to form an even surface. To grow hyphae on the membrane, a thin plug of mycelia (1 mm²) was placed in the middle of the membrane and, on top, a block of growth medium (5 mm wide and 2.5 cm long) was placed above, separated by a cellophane membrane as shown in Fig 5.10-B. These steps were conducted under aseptic conditions. To prevent contamination occurring during the experiment, the plug of agar was infused with an antibiotic (hygromycin or geneticin) as appropriate for the fungal strain (EfH2A-9) being used. The whole assembly was placed in a sealed plastic container and incubated at 22°C for three days under continuous light. After three days of incubation, a few well-separated hyphae were selected for observation under stretching using bright field and fluorescence microscopy (Fig 5.10-C). Fungal strains expressing the nuclear tag YH2A (Section 5.1.1) were used for easy identification of nuclei and individual compartments (Fig 5. 10-D).

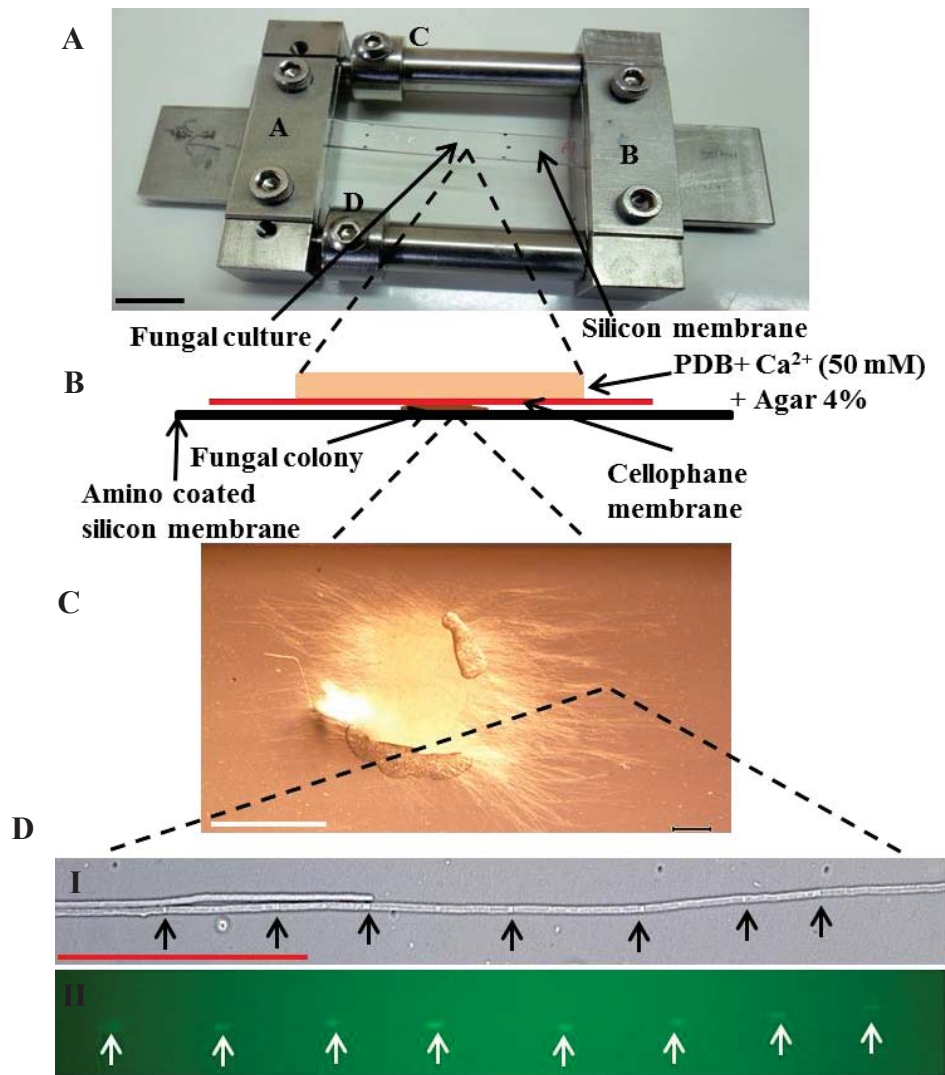


Figure 5.10: The apparatus used to stretch *E. festucae* hyphae under *in vitro* conditions.

A- Stretch frame with an amino-coated membrane attached by the clamps (A and B), and a fungal colony growing in the middle of the membrane. Black scale bar = 1 cm

B- A diagrammatic representation showing the cross section of the arrangement used to grow fungal hyphae on the silicon membrane and provide nutrients. Not drawn to scale.

C- A microscopic image of hyphae growing between the silicon and cellophane membranes for 3 days, while attached to the silicon membrane. White scale bar = 2 mm.

D- Bright field and fluorescent microscopic images of hyphae expressing a nuclear tag YH2A, on silicon membrane showing septa (black arrows) and corresponding nuclei (white arrows) in each compartment. Red scale bar = 100 μm

To stretch hyphae, the above assembly (stretch frame with a 3 day old fungal culture on the silicon membrane) was fixed to a stretcher as shown in Fig 5.11-A (the stretcher used for this purpose was originally designed by engineers at AgResearch Ltd, New Zealand to stretch wool fibres under a microscope). The stretch frame was clamped to the two arms of the stretcher (E and F) and the two screws, C and D, were loosened to allow free movement of the bars of the stretch frame, allowing the attached membrane to stretch proportionately. By turning the bolt G of the stretcher steadily, clock wise or anti clockwise, the arms of the stretcher can be moved inwards or outwards, simultaneously moving the arms of the attached stretch frame, thereby stretching the membrane and the attached hyphae (Fig 5.11-B). Before applying stretch this way, the cellophane membrane needed to be lifted briefly (~6-8 sec) to prevent it dragging on the silicon membrane and preventing it from stretching evenly. The calibrator connected to the arms (H) of the stretcher was used to measure the amount of stretch applied to the membrane in terms of the distance the arms moved. After applying the required degree of stretch by moving the stretcher arms, the screws C and D of the stretch frame were tightened (to maintain the applied stretch) and the stretch frame removed from the stretcher (Fig 5.11-B). The dislodged stretch frame was either used for microscopy or transferred back to the sealed box for further incubation while maintaining the applied stretch. It was possible to repeat this several times a day for 3-4 days depending on the experimental requirements.

To observe and investigate the resulting responses in hyphae; images of fungal hyphae were obtained at appropriate stages using an Olympus BX50 microscope. The stretch frame was inverted onto the microscope stage with the PDA free side of the membrane (PDA block remained *in situ* to prevent drying) facing the objective lens (Fig 5.11-C). The hyphae were then examined by microscopy through the silicon film.

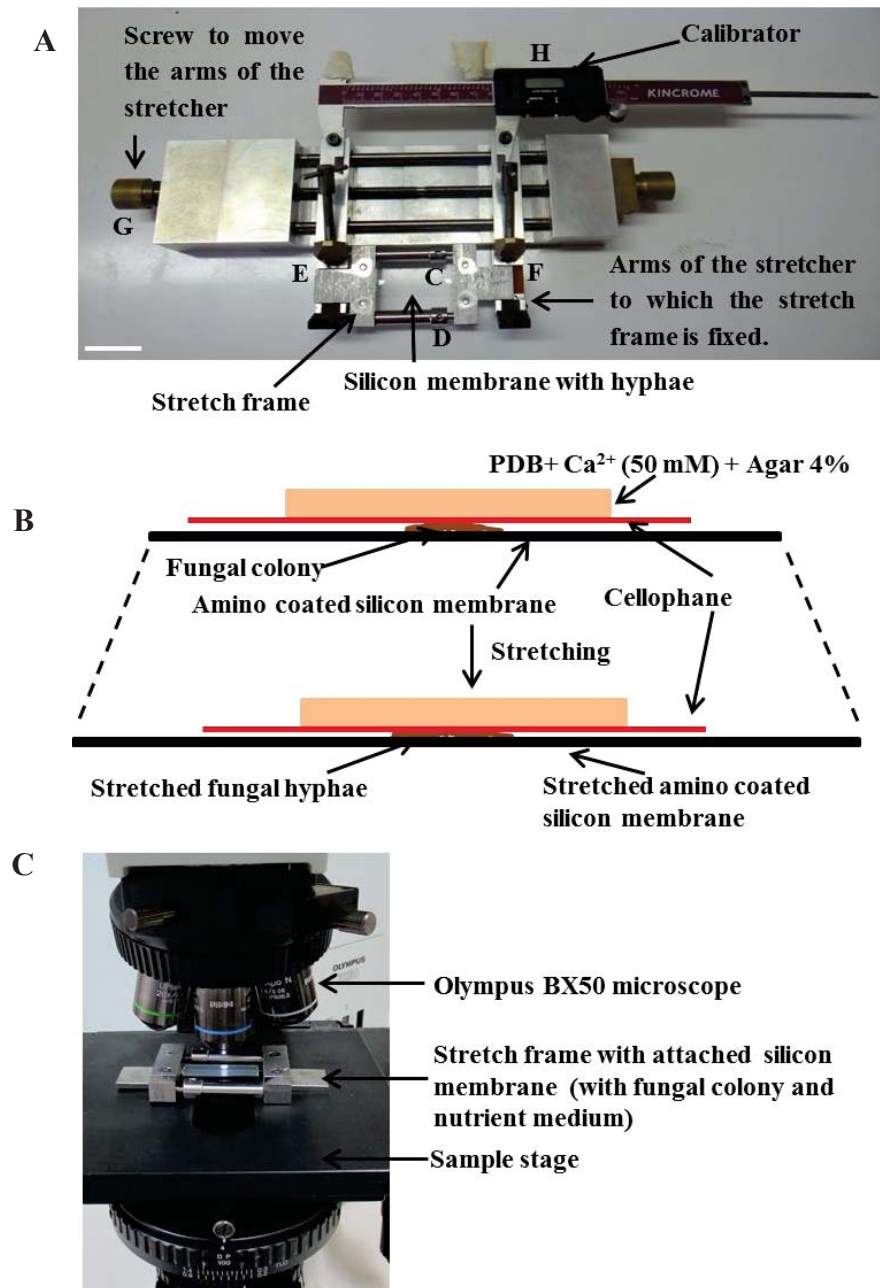


Figure 5.11: Fibre stretcher used to stretch fungal hyphae growing on a silicon membrane.

A – Image showing the apparatus (stretcher) with the loaded stretch frame. The stretch frame was lodged on to the arms (E and F) of the stretcher, and using the screw (G) the stretch frame could be moved apart, thereby stretching the attached silicon membrane. White scale bar = 3 cm

B – A diagrammatic representation showing how the silicon membrane was stretched when the arms of the stretcher were moved apart using the screw G.

C – Image showing how the stretch frame was mounted on to the microscope stage (Olympus BX50) for bright field and fluorescence imaging.

5.3.2 Stretching *E. festucae* hyphae *in vitro*

Subsequent to optimising a method to grow hyphae on a silicon membrane and then devising a technique to stretch the membrane, the next step was to test and confirm whether the hyphae were able to stretch along with the membrane. To investigate this, *E. festucae* hyphae were grown on the membrane attached to the stretch frame for 3 days (Section 5.3.1.4). The stretch frame was mounted onto the stretcher and stretched as mentioned in Section 5.3.1.4. Imaging was performed using an Olympus BX50 microscope. It was revealed that when the silicon membrane was stretched excessively (by an arbitrary 20 mm over the total 4 cm length according to the calibrator), the hyphal strands split at random points (Fig 5.12). This demonstrated that the hyphae stretched with the membranes and proved that this technique could be used to apply mechanical stress.

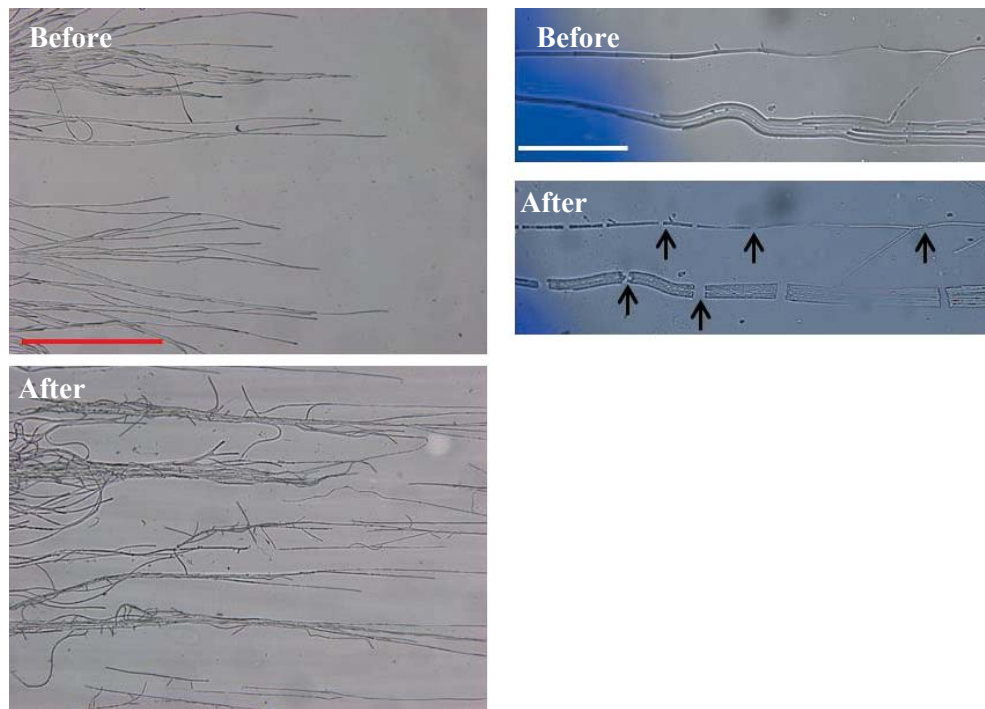


Figure 5.12: Effects of excessive stretching on hyphal integrity.

Microscopy images showing split hyphal segments of *E. festucae* (growing on a silicon membrane) before and after stretching. When the silicon membrane was stretched excessively (20 mm over 4 cm) the hyphae began to split (black arrows) indicating that the hyphae are attached to the membrane and stretch along with the stretching membrane. Red scale bar = 500 μm , white scale bar = 200 μm .

5.3.3 Applied mechanical stretch can increase the length of hyphal compartments

To optimise the amount of stretch to apply, and to determine whether the mechanical stretch is delivered across the colony to a similar extent, *E. festucae* hyphae were grown for 3 days on silicon membranes attached to stretch frames as described above (Section 5.3.1.4). Thereafter, two hyphae parallel to the stretch axis were selected from each colony and imaged using an Olympus BX50 microscope. The stretch frame was inverted onto the microscope stage and imaged through the silicon membranes, while the PDB block remained to prevent the colony from drying (Section 5.3.1.4). This

allowed sufficient clarity in the images to identify septa and the compartments in hyphae. Further, nuclear-labelled *E. festucae* strains (expressing the nuclear-localising H2A/YFP fusion) were used for these experiments. This enabled easy observation of nuclear responses during stretching and also identification of existing compartments and subsequent new compartments formed.

Images were taken of each compartment along the hypha starting from the hyphal tip up to the 11th compartment. After imaging to record the initial state of the hyphae and compartments, the stretch frame was fitted onto the stretcher and the 4 cm silicon membranes were stretched by either 2, 3, 4, 5, 6, 7 or 8 mm. Each stretch level (2, 3, 4, 5, 6, 7 and 8 mm) was applied separately to different colonies (3 replicates for each level of stretch applied). The control treatment consisted of hyphae grown under identical conditions with no stretching applied (the cellophane was nevertheless lifted, as was done for the stretched hyphae, to mimic this potential perturbation). After stretching, the 1st to the 11th compartment of each hypha was imaged as described before. Using the microscopy images, the lengths were measured for each compartment before and immediately after stretching (Fig 5.13-A and B). The percentage length increase for each compartment was calculated from the change in compartment length before and immediately after stretching to confirm that silicon membrane stretch resulted in proportional increases in compartment length.

The results revealed that compartment lengths increased after stretching and that the percentage of increase in compartment length was proportional with the amount of stretch applied (Fig 5.13-B), up to a maximum of 5 mm of stretching. No change in compartment length was observed in the un-stretched hyphae. Excessive stretching of the silicon membrane over 5 mm (over 13% of compartment length increase), at a given

time, damaged the hyphae, as split hyphae and abnormalities in hyphal morphology (even when the cell wall was intact) were observed. It is likely that over-stretching hyphal compartments damaged cellular membranes (although the cell wall was intact) and therefore hyphae lost their viability.

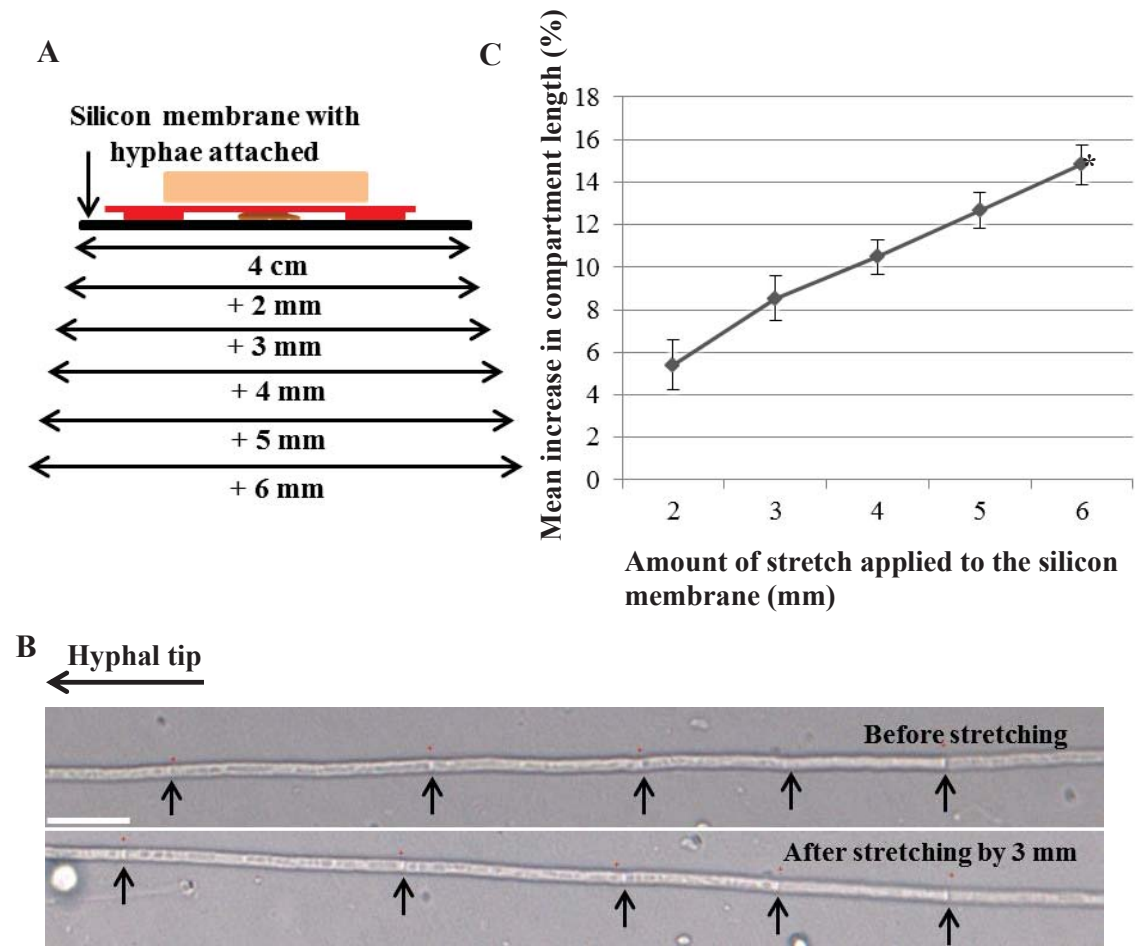


Figure 5.13: Effect of mechanical stretching on compartment lengths in *E. festucae* hyphae.

A- Diagrammatic representation showing the stretch levels applied to the silicon membrane.

B- Bright field images of hyphae growing on silicon membrane before and after stretching. Clearly visible septa (black arrows) were used to measure the compartment lengths at each stage. Scale bar = 20 μ m.

C- Mean percentage increase in compartment length in response to increasing membrane stretch. Mean and SD were calculated from 30 compartments for each level of stretching. Compartment lengths increased proportionally to the degree of stretch applied. * - The compartment length increase was proportional to 6mm but the hyphae showed morphological anomalies indicating damage.

To test the effect of stretching on plasma membrane integrity (and therefore hyphal vitality), un-stretched and stretched hyphae were stained with the lipophilic dye FM[®]4-64 (Invitrogen, USA, stains cellular membranes), and observed using a confocal laser scanning microscope. To stain with FM[®]4-64, silicon membranes with hyphae were mounted in a solution of FM[®]4-64 (2 µg/mL) in standard PDB (Section 2.11.2). Because it was not possible to use the stretch frame under a confocal microscope, stretched membranes were glued on to a glass slide (while maintaining the applied stretch) before mounting specimens in the FM4-64 solution for microscopy. This limited the ability to observe the same hyphae in un-stretched and stretched conditions. Observations were made immediately after staining to prevent the stain penetrating the plasma membrane and entering the cells via endocytosis (within 10 min). If the plasma membrane is damaged, FM[®]4-64 penetrates and stains the whole cell immediately after staining instead of only the plasma membranes. Observations of stretched hyphae revealed that a compartment stretch/length increase of over 10% of its original length at a given time was detrimental to the integrity of the membranes as evidence of membrane damage was observed in hyphae stretched beyond this limit (Fig 5.14).

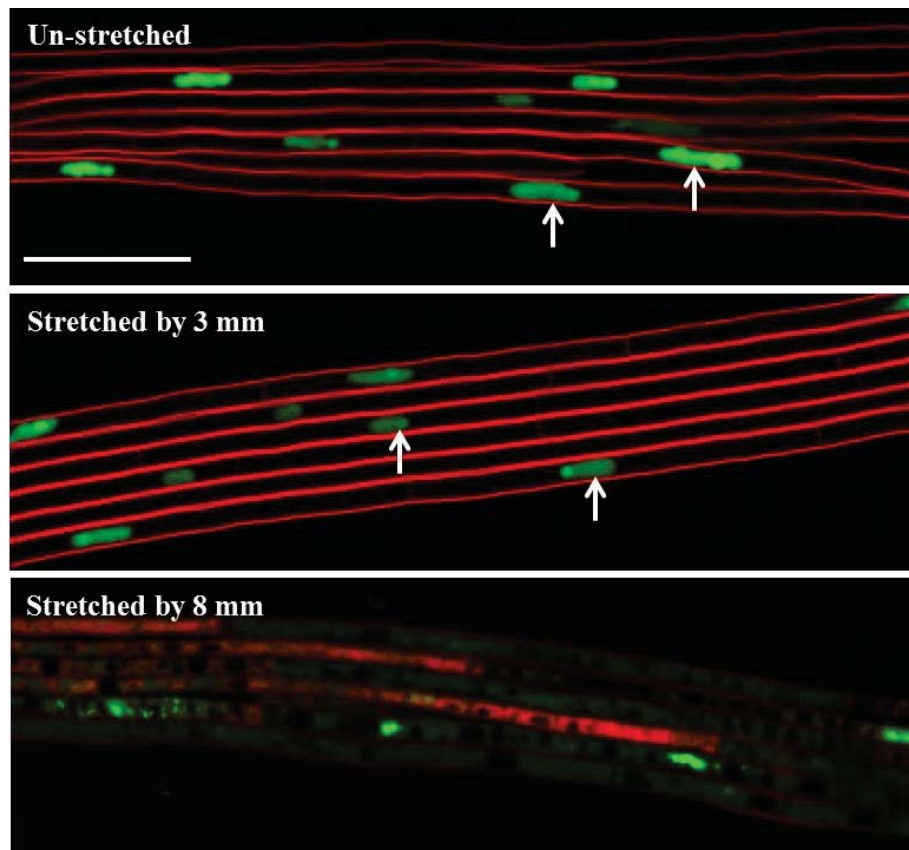


Figure 5.14: Effect of mechanical stretching on the integrity of plasma membranes in nuclear tagged (H2A/YFP) *E. festucae* hyphae. FM[®]4-64 stained the plasma membrane (red lines) and did not penetrate the cells in un-stretched hyphae and hyphae on silicon membrane stretched by 3 mm (7% compartment length increase). Further, the nuclei seemed intact (white arrows). In contrast, hyphae on silicon membranes stretched by 8 mm showed stain penetration, rupture of nuclei and cell membrane damage. Scale bar = 20 μ m.

5.4 Mechanical stretching applied in intervals can increase overall length of hyphae while maintaining viability

The experiments outlined in Section 5.3.3 demonstrated that hyphal compartment lengths can be increased by mechanical stretching without damaging cell integrity as long as excessive stretching is avoided at a given time. This technique was therefore deemed to be suitable for testing the hypothesis that mechanical stretching of

E. festucae hyphae is sufficient to induce sustained intercalary growth, with additional compartmentation. The intention was to simulate the assumed mechanical stretching applied by rapidly elongating leaf cells in the expansion zone of the developing leaf. Although it was not possible to apply continuous stretching over a prolonged period using this method (the stretcher is not motorised), as would be occurring in a developing leaf, the system allowed for manual application of mechanical stretch at intervals over a 9 h time period. Hence, I believed that, as an initial step, this would be sufficient to test whether *E. festucae* hyphae can tolerate applied mechanical stretching (while remaining viable), and undergo sub-apical compartment elongation with compartmentalization equating to intercalary growth under *in vitro* conditions. Depending on the outcome, a mechanism could be designed in future to apply continuous stretching that would more accurately simulate the mechanical stress assumed to be applied within the developing leaf.

Taking previous stretching results into consideration (Section 5.3.3 and Figs 5.13 & 5.14), three consecutive stretches of 3 mm each, equivalent to a 7-8 % compartment length increase, were applied at 3 h intervals to each colony. Nuclear YFP-tagged *E. festucae* hyphae (Section 5.1.1) were used to facilitate easy identification of nuclei by fluorescence microscopy, and hygromycin was used to prevent contamination during the course of the experiment (the nutrient block was infused with 100 mg/mL hygromycin). Hyphae were grown on silicon membranes attached to stretch frames for 3 days (Section 5.3.3) and 1 to 2 hyphae situated parallel to the stretch axis were selected and imaged as described previously (Section 5.3.3). Each hyphal compartment, from the 1st to the 11th was imaged independently using bright field and fluorescence microscopy. Thereafter, the stretch frame was loaded into the stretcher and the silicon membrane was stretched by 3 mm (which represented an approximate 7% increase in

compartment length, see Section 5.3.1.4). Immediately after stretching, the same hyphae were imaged again (from 1st to the 11th) and transferred to a plastic box and incubated at 22°C. After 3 h of incubation, the same hyphae were imaged again, stretched by 3 mm and immediately imaged again and transferred to the box for incubation. This was repeated once more after 3 h of incubation, stretching the hyphae by a total of 9 mm (3 X 3 mm) within a time period of 6 h (at T = 0, 3 & 6 h.). The stretched hyphae were further incubated for 3 h after the 3rd stretch and imaged (after 9 h since the 1st stretch) for the final time. As the control, all the steps mentioned above were followed (including imaging twice at each time interval) except for the stretching steps.

The bright field and fluorescent images of compartments obtained before and after stretching at each step were used to measure the length of individual compartments and position of nuclei at each stage. To identify an individual compartment, the position of septa (using bright field images) and the presence of nuclei (using corresponding fluorescence images) were used as markers. Each compartment was tracked from the beginning (T0 h) to the end of the experiment (T9 h), noting down any nuclear division or septation that occurred in individual compartments during the period. For analysis purposes, the first compartment (compartment 1) at T0 h was considered to be the apical compartment throughout the experiment, irrespective of whether new compartments formed at the tip during the experiment. The 10 compartments behind the apical compartment from 2 to 11 at the start of the experiment were considered to be sub-apical compartments. New compartments formed due to sub-division of existing sub-apical compartments (via new septa formation) within the 9 h period were recorded and assigned a number related to the parent compartment. Thus, if compartment 2 divided, the new compartments were labelled compartments 2A and 2B. This allowed changes in

each sub-apical compartment in terms of length, nuclear division and septation to be tracked (Fig 5.15 and Table 5.2).

As expected, the apical compartments continued to grow in length via apical growth, and to undergo nuclear division and septation forming new compartments at the tip, both in control (un-stretched) and the stretched hyphae. However I did not measure the fate of these compartments as the main objective was to investigate intercalary growth occurring in the original sub-apical compartments.

Measurements of sub-apical compartment lengths at each step of stretching revealed that the mean percentage increase in compartment length at each stretch (by 3 mm) was 7.3 ± 0.91 % (mean \pm SD, n = 204). Further, it showed that the percentage increase in the length of a compartment was consistent at each stretch and evenly distributed among all the sub-apical compartments (sub-apical compartments increased in length by the same proportion) along a hypha (Table 5.2 & Fig 5.16). Hence, collectively at the end of the 3 stretching events (T9 h) the cumulative mean increase in length of a compartment was on average 30% (n = 204) of its original length at T0 h. This resulted in a cumulative length increase (total length from 2nd to the 11th compartment) of the hypha by a similar percentage subsequent to stretching. In comparison, in the un-stretched control, the sub-apical compartment lengths (2nd to the 11th compartment) did not change, and the slight variations in length are attributed to measurement errors. Thus no increase in cumulative length was observed in the sub-apical regions of the control treatments (Table 5.2 & Fig 5.16).

De novo septation/compartmentalization in existing subapical compartments was observed both in un-stretched (control) and stretched hyphae (Fig 5.15) within the 9 h period. Each new sub-apical compartment formed contained a single nucleus which is

consistent with expectation in this largely mono-nucleate species. This indicates that the compartmentalization process (mitosis followed by septation) is not confined to the apical compartment, but continues in the sub-apical compartments in both the unstretched and stretched hyphae. This result also indicated that *E. festucae* hyphae can tolerate stretching within certain limits and that this does not result in damage or loss of viability in compartments, as such damage would be expected to halt any further compartmentalization. The order of septation (compartmentalization) seemed to follow the same size-dependent hierarchy described earlier (Section 5.1.2) where larger compartments divided first, followed by the next larger compartments. Thus, these observations collectively establish the fact that *E. festucae* hyphae can be mechanically stretched, increasing compartment lengths (hence cumulative hyphal length) and that the elongated compartments continue to undergo mitosis and septation.

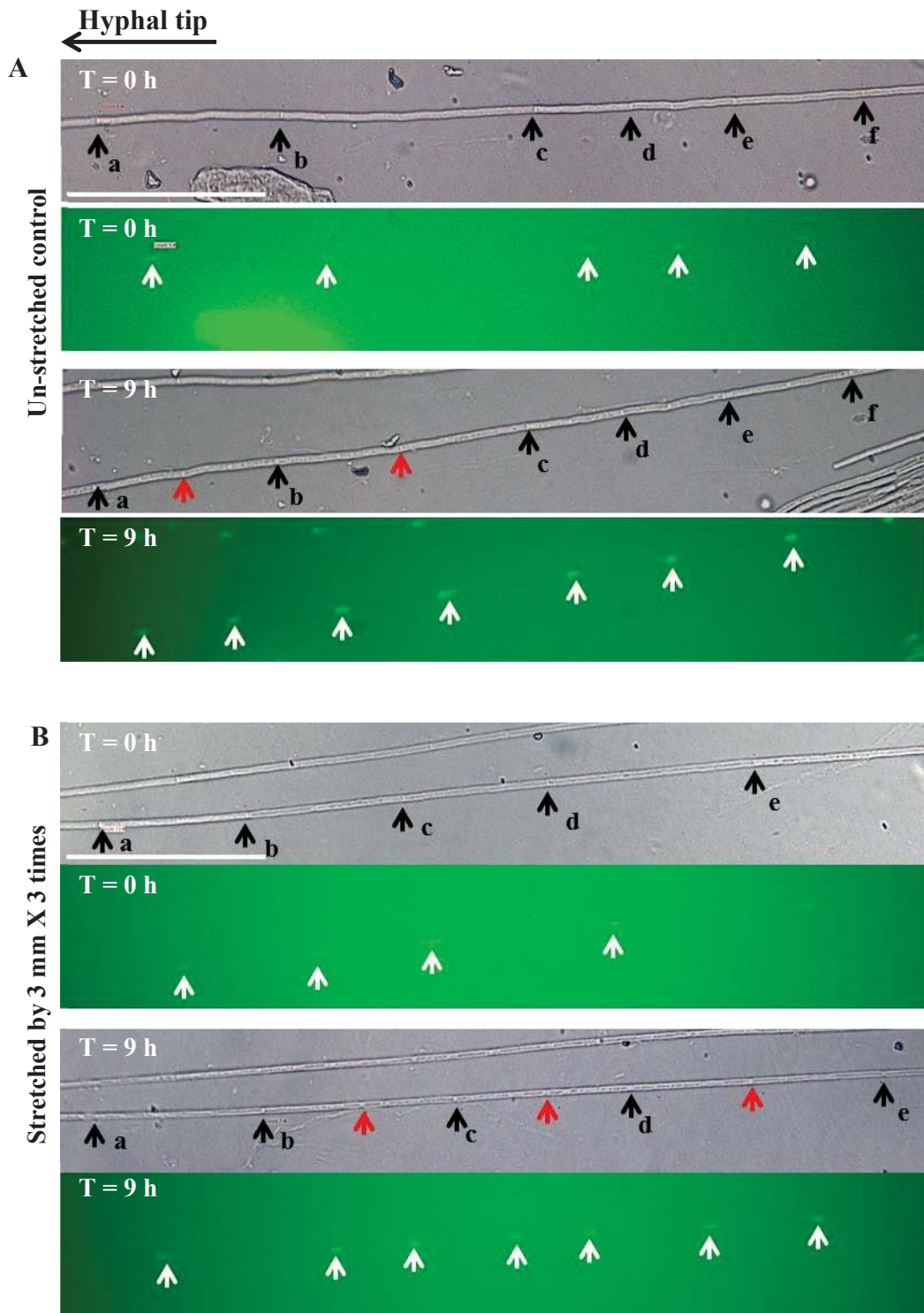


Figure 5.15: Mitosis and septation in sub-apical compartments of un-stretched and stretched hyphae.

Images are representative bright field and corresponding fluorescence images of sub-apical compartments (compartments 3, 4, 5, 6 and 7 from tip at T = 0 h) with septa and nuclei in a hyphal segment at T = 0 h and the same segment of hypha at T = 9 h. Black arrows represent the septa that were present at T = 0 h and red arrows represent new septa formed within the 9 h period. Letters (a to f) denote septa and a similar letter at T = 0 and T = 9 h represent the same septa. White arrows show the nuclei present in each compartment.


A- The status of the sub-apical compartments in a segment of a control un-stretched hypha at the beginning (T = 0 h) and end (T = 9 h) of the incubation period. Sub-apical compartment lengths did not change within the 9 h period. Longer compartments present at T = 0 h underwent septation. A nucleus was visible in each new compartment.

B - The status of sub-apical compartments in a segment of a stretched hypha (stretched by 3 mm every 3 h) at the beginning (T = 0 h) and end (T = 9 h) of the incubation period (this approximately results in 7% compartment length increase at each stretch). Compartment lengths increased compared to their original length at T = 0 h, followed by mitosis and septation.

Table 5.2: Compartment length and compartmentalization in sub-apical compartments of un-stretched and stretched *E. festucae* hyphae.

A- Un-stretched hypha

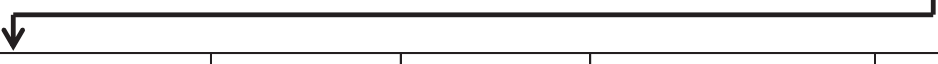
Stretch stage & time ^b	Imaging ^b	Comp-2 ^a				Comp-3	Comp-4			
1 st round, T=0 h	Before	276.9				48.1	123.1			
	After	277.6				47.9	123.0			
2 nd round, T=3 h	Before	125.8	152.0			48.4	33.1	57.6	32.1	
	After	125.4	151.8			48.2	33.1	57.9	32.1	
3 rd round, T=6 h	Before	67.3	58.7	59.6	90.8	48.1	33.9	57.2	31.3	
	After	66.9	58.1	59.7	92.2	48.9	33.3	57.6	30.7	
T=9 h		66.9	58.7	59.2	49.5	42.3	48.1	33.4	56.4	29.4



Comp-5	Comp-6	Comp-7		Comp-8	Comp-9		Comp-10	Comp-11
56.8	28.5	60.8		27.9	73.3		45.4	44.7
57.2	28.8	60.7		28.2	72.6		46.0	44.6
57.5	28.4	60.2		28.0	73.6		46.5	44.6
57.5	28.4	60.3		286.0	72.9		46.0	44.6
57.0	28.7	59.6		29.1	73.6		46.0	44.6
58.5	28.6	60.6		28.8	39.6	34.6	46.1	44.3
58.1	28.7	29.5	30.9	28.5	39.0	34.2	46.3	44.7

B-Stretched hypha

Stretch stage & time ^c	Imaging ^c	Comp-2 ^a						Comp-3		
1 st stretch, T=0 h	Before	242.2						104.1		
	After	263.4						55.7	58.6	
2 nd stretch, T=3 h	Before	98.3	165.4				56.0	58.3		
	After	105.7	178.1				60.4	62.5		
3 rd stretch, T=6 h	Before	56.0	48.7	35.8	28.7	53.1	59.2	60.0	32.5	30.0
	After	60.0	53.0	39.0	30.8	56.2	63.2	64.4	34.7	32.2
T=9 h		59.5	53.5	38.8	30.8	56.2	63.5	64.2	34.7	32.2



Comp-4		Comp-5		Comp-6		Comp-7		Comp-8			
159.8		87.4		62.9		95.7		49.2			
172.7		95.0		68.8		103.1		54.5			
72.6	99.4	44.4	49.9	69.3	45.2	57.4	55.6				
78.3	106.4	47.9	54.3	74.3	49.2	61.8	58.9				
41.7	35.9	67.2	38.1	47.6	54.1	73.8	49.1	62.0	58.0		
45.4	38.5	72.8	42.2	50.8	58.0	79.0	52.5	65.7	62.9		
45.4	38.4	72.4	42.4	50.9	57.9	39.0	40.2	52.3	32.7	33.0	63.0

Comp-9		Comp-10		Comp-11	
58.4		56.6		49.7	
63.6		61.8		54.2	
63.4		61.7		54.1	
67.7		66.7		55.4	
67.0		66.2		55.6	
72.1		70.7		59.9	
35.5	36.1	36.4	34.7	27.7	32.0

^aCompartment lengths of the 2nd to the 11th compartment at each time interval (T = 0, 3, 6 and 9 h); values for one representative hypha are shown. Septation/compartmentalization of existing compartments is shown as vertical divisions in the table and attributed to the original compartment measured at T = 0 h. Comp = Compartment position from the tip.

^bFor the un-stretched control (**A**), imaging was performed twice at each time interval and compartment lengths measured (represented as ‘before’ and ‘after’ in the table). Sub-apical compartment lengths did not change with time, but exhibited ongoing septation of existing compartments.

^cFor the stretched hyphae (**B**), the silicon membrane was stretched by 3 mm at each time interval and imaged before stretching (‘before’) as well as immediately after stretching (‘after’). Compartment lengths increased after each stretch while continuing to undergo compartmentalization.

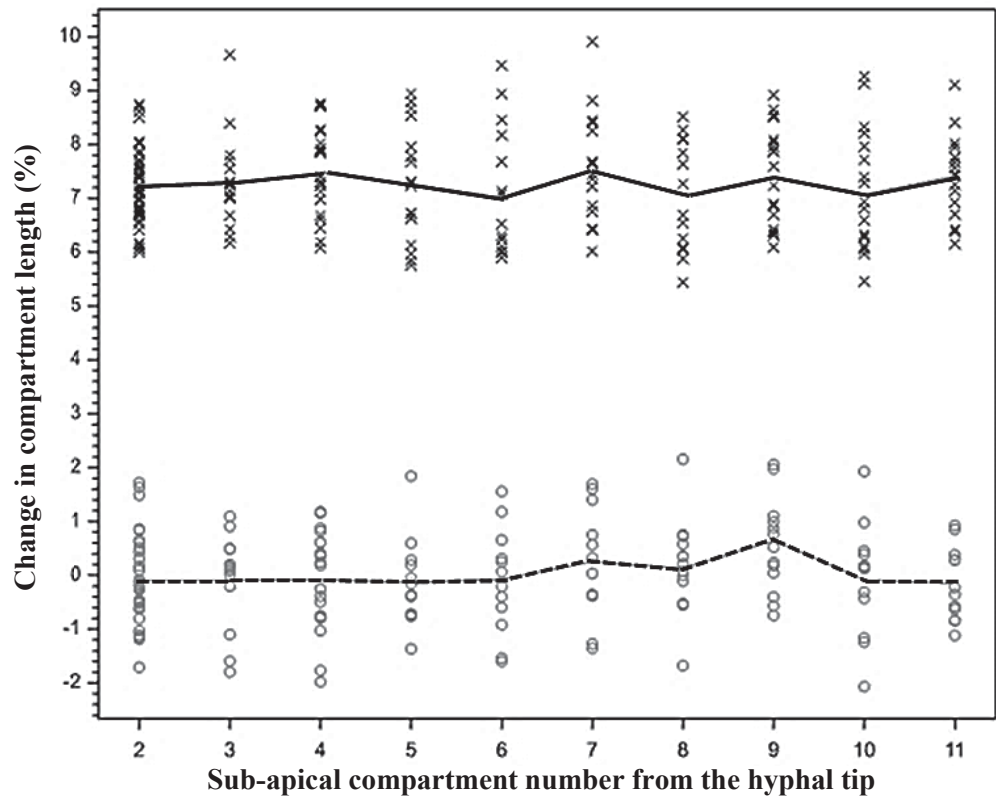


Figure 5.16: Change in length of each sub-apical compartment (2nd to the 11th) in stretched and un-stretched *E. festucae* hyphae.

× - Compartment length increase in stretched hyphae of all replicates at each time point over the 9 h period (T = 0, 3, 6 h). The solid line shows mean length increase in compartment number after stretching.

○ - Compartment length change in un-stretched control hyphae of all replicates at each time point over the 9 h period (T = 0, 3, 6 h).

Compartments lengths at each time point over the 9 h period (T = 0, 3, 6 h) before stretching and immediately after stretching (by 3 mm X 3 time, see Table 5.2) were used to calculate the percentage change in compartment length. The graph represents data from 5 trials each for stretched and un-stretched controls. In stretched hyphae, the sub-apical compartment lengths increased at a fixed percentage at each stretch, and elongation of compartments was uniform across all compartments measured (2nd to the 11th from the apex). In un-stretched control hyphae, compartment length remained un-changed throughout the experiment.

5.5 *E. festucae* hyphae increase the rate of compartmentalization as a response to sub-apical compartment elongation caused by mechanical stretching

Although septation in sub-apical compartments was observed both in un-stretched and stretched hyphae as mentioned previously, a noticeable difference was observed in the septation /compartment formation rate in sub-apical compartments between the two. The number of new compartments formed in sub-apical compartments (2nd to the 11th) over a given period was calculated as the percentage increase in numbers of compartments per 100 μm of hyphal length above that at T = 0 h (see formula below). As mentioned previously, the order of compartmentalization is dependent on the initial volume/lengths of the existing compartments, with more frequent compartmentation observed in the longest compartment within a given period. Hyphal compartment lengths differ between hyphae and therefore have different potentials for sub-apical septation/compartment formation. Therefore, to normalise the effect of initial compartment lengths of hyphae (at T = 0 h.) between treatments, it was decided to divide the number of compartments formed between compartments number 2 and 11 (inclusive) within a given period, by the cumulative length of the original compartments present at T = 0 h. The formula used for this purpose is given below.

$$\text{Number of new compartments formed within a period per } 100 \mu\text{m of hyphal length at } T = 0 \text{ h} = \left[\frac{\text{Number of new compartments formed within the period}}{(\# \text{ comp at } T = X \text{ h} - \# \text{ comp at } T = 0 \text{ h})} \right] \times 100 \mu\text{m} \\ \left[\frac{\text{Cumulative length of the compartments at } T = 0 \text{ h}}{\text{Cumulative length of the compartments at } T = 0 \text{ h}} \right]$$

$$X = 3/6/9 \text{ h}$$

Calculation of the number of new compartments formed within a period of 9 h per 100 μm of hyphal length (at $T = 0$ h) using the formula above, revealed a significant ($p < 0.05$) increase in the number of sub-apical compartments formed in stretched hyphae compared to the un-stretched controls (Table 5.3, Fig 5.17). Together these data indicate that mechanical stretching increases the length (and presumably the volume) of sub-apical compartments, which then induces septation (and therefore compartmentalization) over and above that which would be observed in hyphae where no mechanical stretch had taken place. Mechanical stretching therefore seems to stimulate intercalary hyphal growth in *E. festucae* in culture.

Table 5.3: Sample calculation of the number of new sub-apical compartments formed per 100 μm of control and stretched hyphae within a period of 9 h (from $T = 0$ to $T = 9$ h).

Treatment	Cumulative length at $T = 0$ h (μm) ^a	No. of compartments		Increase in no. of compartments	Increase in no. of compartments per 100 μm length
		$T = 0$ h	$T = 9$ h		
Control ^b	730	10	16	6	0.8219
Stretched ^c	810	10	26	16	1.9753

^aFrom the 2nd to the 11th compartment at $T = 0$ h.

^bUn-stretched hypha

^cStretched hypha (stretched by 3 mm at $T = 0, 3$ & 6 h).

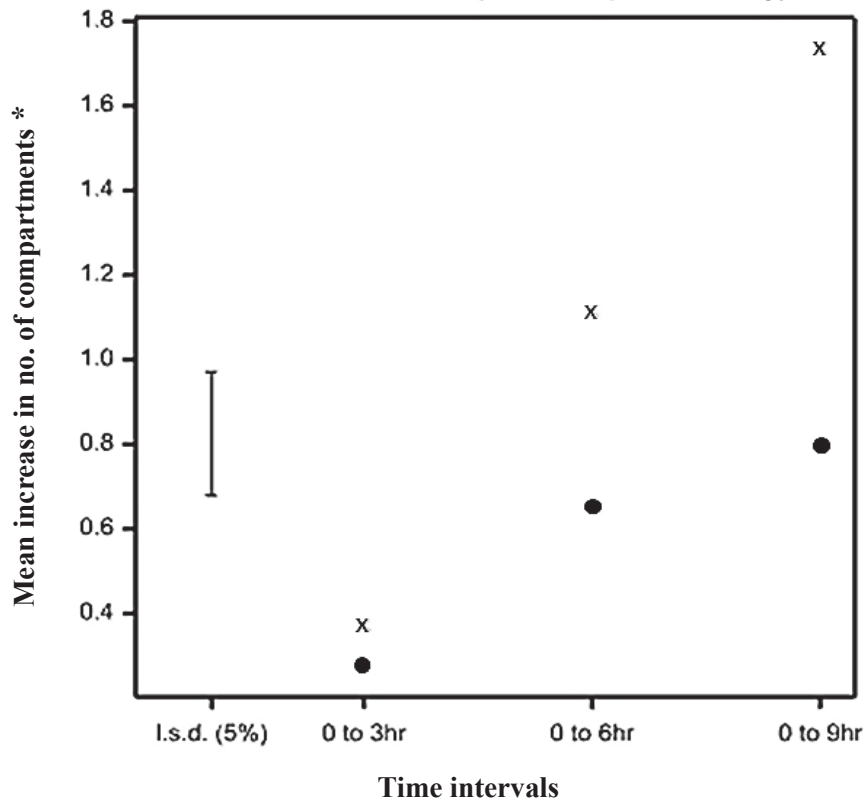


Figure 5.17: Septation (new compartment formation) rate in sub-apical compartments of stretched and un-stretched hyphae.

X - Stretched hyphae ● - Un-stretched control hyphae

*Mean increase in no. of compartments per 100 μm of sub-apical hyphal length at $T = 0$ h within each 3 h time interval

The mean number of new compartments formed in the 2nd to the 11th compartment (at $T = 0$ h) over three time intervals within a total period of 9 h in stretched (see Section 5.4 and Table 5.2) and un-stretched hyphae in 5 independent trials. The number of sub-apical compartments increased with time in both un-stretched and stretched hyphae. In stretched hyphae, the increase exceeded that of un-stretched hyphae, and with time (as more stretching is applied) the increase becomes significant within 5 % least significant difference.

5.6 A possible role for calcium in sensing mechanical stress in *E. festucae*?

Having established that mechanical stretching can increase compartment lengths and the rate of septation/compartmentalization in intercalary compartments, the next steps were to investigate which signalling cascades respond to mechanical stress in this species, and to determine the associated molecular changes that result in intercalary growth. This was outside the scope of this PhD, nevertheless initial experiments were undertaken to test whether the calcium signalling is involved in sensing mechanical stress in hyphal membranes.

Given the potential role of Mid1 as a sensor of mechanical stress in yeast, my first aim was to determine whether application of mechanical stress alone to the plasma membranes of *E. festucae* hyphae was sufficient to induce changes in cytosolic calcium concentration. In order to isolate the endophyte from other plant factors with potential to induce calcium changes, preliminary experiments were conducted *in vitro*. Since the confocal microscope (Olympus Fluoview FV10i–LIV) can only be operated with the lid closed over the stage, the instrumentation required to conduct a test whereby resting hyphae are imaged and then placed under strain requires engineering to retrofit the stretching unit with a remote-controlled motor. The aim of these pilot experiments was to determine whether the stretching unit could be modified, and to conduct preliminary uncontrolled experiments as described below.

5.6.1 Mechanical disturbance of *E. festucae in vitro* induces Ca²⁺ pulses

As a preliminary approach to understanding the involvement of Ca²⁺ in mechanical stretching, *E. festucae* F11 hyphae expressing the calcium sensor GCaMP5 (kindly supplied by Professor Nick Read, University of Manchester) and the nuclear-localised protein YH2A were grown on a silicon membrane as shown in Fig 5.18, using PDA as

the nutrient medium. Nuclear-tagged hyphae were used for easy identification of hyphal compartments on the membrane. The hyphae on the silicon membranes were placed inside petri-plates and incubated for 3 days at 22°C.

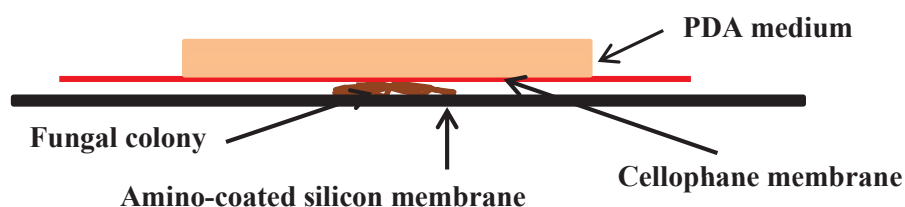


Figure 5.18: Diagrammatic representation showing the arrangement of components used to grow *E. festucae* hyphae on amino-coated silicon membranes (see Section 5.3.1.3). Once assembled the colony was placed in a petri plate and incubated for 3 days to allow hyphae to grow between the two membranes.

After incubation, the nutrient block with the cellophane membrane was removed and the silicon membranes with hyphae were mounted in PDB, a coverslip applied and then inverted onto the stage of an Olympus Fluoview FV10i-LIV confocal laser scanning microscope. A section of the colony was scanned and time lapse imaging was conducted (for microscopy settings and parameters see Section 4.5) to record the pattern of Ca^{2+} pulses occurring within a maximum period of 5 min. To apply mechanical stretch to the plasma membranes of the attached hyphae, the silicon membrane was lightly disturbed by placing pressure (using a glass rod) directly onto the silicon surface adjacent to where the hyphal colony was located. It was assumed that the pressure applied would be sufficient to cause localised distortions/stretching to hyphae on the membrane, however the amount applied could not be verified using this method. Immediately after applying pressure, time lapse imaging was again performed on the same region for a maximum period of 5 min. There was a delay of approximately 30 sec

between the time the pressure was applied and the start of imaging due to the need to refocus the microscope. In spite of this a visible increase in Ca^{2+} pulses in the apical and sub-apical regions of hyphae was observed after hyphae were disturbed (in 5 out of 8 trails conducted). The pulses occurred at seemingly random points in sub-apical regions and did not show a particular pattern in frequency. See supplementary movies in Power Point presentation ‘Calcium pulses when disturbed’ in attached CD for impact of mechanical stress on calcium influx in *E. festucae*. These preliminary analyses indicated that mechanical disturbances of *E. festucae* can cause an alteration in the Ca^{2+} dynamics of the apical and sub-apical compartments of hyphae, and that calcium signalling may be important in mediating growth responses to mechanical stretch. Further analyses using an automated stretching device are required to confirm this finding, including (but not limited to) testing of $\Delta midA$ deletion strains for calcium influx in response to mechanical stretch, and their ability thereafter to undergo intercalary growth. Sequestration of calcium by BAPTA supplementation of the medium will also confirm whether the pulses observed are due to release of calcium from cellular stores or due to influx from the growth medium.

5.7 Discussion

The primary objective of this section of the study was to test the hypothesis that mechanical stretching can trigger intercalary growth in *E. festucae*. Intercalary growth in *E. festucae* hyphae is defined as the increase in sub-apical compartment lengths while undergoing nuclear division and compartmentalization (dividing existing sub-apical compartments through septation) (Christensen et al., 2008). Accordingly, a technique was developed to mechanically stretch fungal hyphae and thereafter conduct preliminary investigations to study the effect of mechanical stretching on hyphae and

intercalary growth. Before investigating the influence of mechanical stretching on intercalary growth, nuclear division and septation in sub-apical compartments in unstretched hyphae (growing in culture) were investigated initially to understand general hyphal growth and compartmentalization in *E. festucae*. Previous studies have shown that fungal filamentous growth is associated with the cell cycle to ensure balanced growth under varying conditions (Veses et al., 2009).

Based on the observations made so far, a sequence of events in nuclear division and septation during hyphal growth can be deduced for *E. festucae* hyphae in culture. *E. festucae* hyphal compartments were almost entirely uni-nuclear, except when there was branching or compartmentalization (Fig 5.1 and 5.2). During apical growth, the hyphal tip grows forward, elongating the uni-nuclear apical compartment. As the length/volume increases, at a particular point, nuclear division occurs and a septum is laid down in the apical compartment giving rise to a uni-nucleate apical compartment and a uni-nuclear *de novo* sub-apical compartment (second compartment from the apex). The positioning of the septum seems arbitrary as it is laid at the distal or proximal end to the hyphal tip in different hyphae. While the apical compartment continues to grow the sub-apical compartment undergoes further division (nuclear division followed by septation) in a compartment length-dependent hierarchy until the compartments reach a minimum length where no further division occurs (Fig 5.4 and 5.5). Except at the very apex, the hyphal diameter in a given hypha is generally constant and therefore the volume of sub-apical compartments can be considered directly proportional to the length of that compartment. At the same time, longer sub-apical compartments behind the newly formed second compartment, with potential for further division, still undergo compartmentalization in a length-dependent hierarchy. The length-dependent hierarchy of sub-apical compartmentalization appears to apply to

the whole hypha, as the longest compartment in the hypha divides first followed by the next longest irrespective of the compartment position (within the observed limit) (Fig 5.19).

Nuclear division and septation pattern observed in *E. festucae* can be compared with that of *A. nidulans*, in which nuclear division and septation have been studied extensively, to further understand the volume-based initiation of nuclear division and septation. In *A. nidulans*, during vegetative growth in the apical compartment, successive parasynchronous waves of nuclear division occur, followed by rounds of septation (Clutterbuck, 1970; Fiddy et al., 1976; Trinci et al., 1979; Wolkow et al., 1996). The mean time between two successive cycles is the same as the organism's doubling time and septa are usually formed sequentially in groups with the septum nearest to the tip formed last (Fiddy et al., 1976). Septation is triggered when the apical compartment grows and reaches a critical ratio of cytoplasm per nucleus/genome and the value for *A. nidulans* had been calculated as $57 \mu\text{m}^3$ (Clutterbuck, 1969; Fiddy et al., 1976).

Although sufficient data on apical growth was not collected to deduce a similar threshold limit for *E. festucae* during this study, observations implied volume-based nuclear division and septation, and the possibility of the existence of a similar threshold in *E. festucae*. For sub-apical compartments it was difficult to define a threshold for cytoplasm volume that triggers further compartmentalization as the compartments underwent division until they reached a minimum length. However, in *E. festucae* growing in culture, sub-apical compartments lengths varied substantially, with the smallest compartments approximately 18-20 μm in length, and report of compartments as small as 4 μm observed *in planta*. In contrast, intercalary compartments in *A.*

nidulans had a constant length of 38 -39 μm (Trinci et al., 1979; Wolkow et al., 1996). The influence of organelle volume on nuclear division and septation has been reported in the filamentous phase of the dimorphic yeast *C. albicans* (Veses et al., 2009), and in *Basidiobolus ranarum*, it has been shown that nuclear division occurs every time the apical cell volume doubles (Robinow, 1963). In addition it has been shown that in *A. nidulans* septum formation fails when mitosis is blocked, indicating that for septation to occur both nuclear division and the critical ratio of cytoplasm to nuclei needs to be achieved (Harris et al., 1994; Wolkow et al., 1996).

The observed correlation between compartment length and nuclear length agrees well with the compartment length-dependent hierarchy seen during sub-apical compartmentalization, as compartments undergoing further division contain elongated nuclei. Observance of elongated nuclei in hyphae in the elongation zone of developing host leaves also aligns with the proposed intercalary growth taking place in this region (Christensen et al., 2008). The average nuclear length in compartments in the host meristematic region is shorter than those in the elongation zone, but longer than those in the mature zone (Fig 5.6 and 5.7). In the meristematic region, where hyphae are extending predominantly through apical growth, further division of intercalary compartments may still be occurring (as longer compartments divide) but this is likely to be at a lower rate than the elongation zone where intercalary extension is occurring. Hyphal compartments in the mature leaf are no longer extending, and in this region nuclei are mostly spherical.

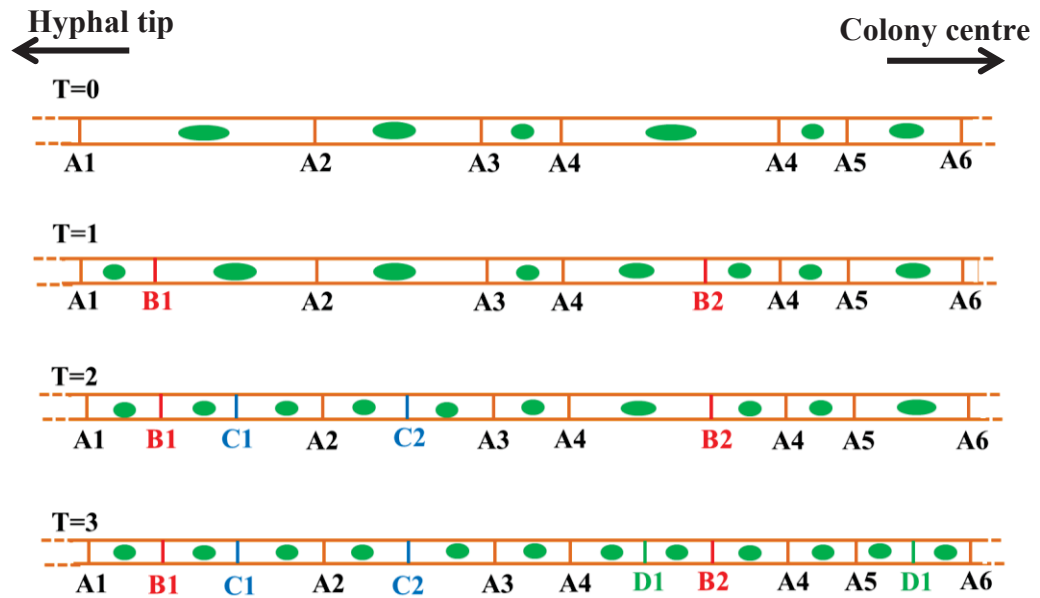


Figure 5.19: A model showing compartment length-dependent nuclear division and septation in sub-apical compartments of *E. festucae* hyphae.

Sub-apical compartments undergo further compartmentalization based on a compartment length/volume-dependent hierarchy where, at a given time, the longest compartment in the hypha divide first followed by the next until they reach a minimum length. The septation pattern shown is a model derived from interpretations of experimental data. A, B, C and D represent new septa appearing at each time point T0, T1, T2 and T3 respectively. The hyphae and compartments are not drawn to scale.

Having an understanding of how nuclear division and septation occur in *E. festucae* hyphae in culture under un-stretched conditions, *E. festucae* hyphae were next subjected to mechanical stretch to investigate its effect on sub-apical hyphal growth. As hypothesised, in the elongation zone of a developing leaf, the host cells will be elongating continuously (during the elongation period) and therefore the attached fungal hyphae will be under continuous mechanical stretch (Schnyder et al., 1990; Durand et al., 1999). The optimised stretching technique did not allow for mechanical stretch to be

applied continuously for prolonged periods as the system was not motorised. However, as an initial approach, the technique was able to test whether endophyte hyphae could be stretched by applying mechanical strain, and if so, whether hyphae could tolerate mechanical stress and respond accordingly.

Experiments conducted using the stretch apparatus under *in vitro* conditions have revealed that compartment length can be increased by around 10% through mechanical stretching at a given time and cumulatively by about 30% of its original length within a period of 9 h with stretch applied in intervals, while maintaining compartment viability (Fig 5.15 and 5.16). To maintain integrity under these conditions, cell walls and membranes of sub-apical compartments need to be, or become, flexible enough to stretch, and thereafter able to synthesise new cell wall material to strengthen the cell walls. Although no studies have been conducted on these aspects in *E. festucae*, studies in other fungi provide evidence to support that cell walls of sub-apical compartments can have special structural arrangements of chitin fibres (arranged as helices and positioned parallel and transverse to the axis of the elongating stipe cells) to increase flexibility and synthesise cell wall during intercalary extensions (Kamada et al., 1977b; Kamada et al., 1977a; Kamada et al., 1991). In addition, recent studies have demonstrated that endocytosis occurs in sub-apical compartments, indicating new cell wall and membrane synthesis is ongoing away from the hyphal tip (Hayakawa et al., 2011; Read, 2011). The implications of these features in mechanical stretch-induced intercalary growth have been discussed in detail in the Introduction (Chapter 1, Section 1.3.4). Future research is required to investigate whether endocytosis also plays a role in intercalary growth in *E. festucae*.

Within the elongation zone of the host (*L. perenne*) developing leaf endophyte hyphae are tightly attached to the surrounding host cells from all sides (Christensen et al., 2008). Therefore, we assume that stretching forces are exerted on the endophyte hyphae in proportion to the spatial and temporal behaviour of the elongation zone of the host developing leaf. Studies on *L. perenne* leaf development show that the leaf elongation zone is confined to the basal 20-30 mm of the leaf with growth stage dependent maximum leaf elongation rate (LER) of 1.39 mmh^{-1} and the minimum of 0.51 mmh^{-1} (Schnyder et al., 1990). Within the elongation zone, the length of epidermal cells had increased from $12 \text{ }\mu\text{m}$ at the leaf base to a maximum of $550 \text{ }\mu\text{m}$ at the distal end. The maximum epidermal cell elongation rate of $28 \text{ }\mu\text{m cell}^{-1} \text{ h}^{-1}$ has been observed close to the centre of the elongation zone, 13-18 mm from the base (Schnyder et al., 1990). Due to the extremely varying cell elongation rates epidermal cell elongation could occur for days until the final length is reached. Accordingly, it is clear that attached endophyte hyphae can be subjected to extreme elongation (considering the epidermal cell length increase of 12-550 μm) under varying degrees of stretch that change with time and the position of the elongation zone. The stretch applied at a given time during this study increased compartment lengths by 10% of their original length (while maintaining viability), exceeding the overall leaf elongation rate (the elongation zone of 30 mm increase at 1.39 mmh^{-1} , about 4.6% of original length per hour) reported for the host. Therefore this clearly indicates that the endophyte hyphae can handle the maximum level of stretch that can be exerted by elongating host cells. However, the maximum length a compartment can be elongated through mechanical stretching is not certain at this stage (so far a cumulative 30% increase in length has been achieved by applying stretch three fold in 3 h intervals). Applying mechanical stretch continuously (mimicking the elongation zone) for a prolong period, as planned as the next step in this

study, will give a better indication of the maximum length hyphal compartments can be elongated to match the maximum individual epidermal cell length increase seen in the host (12 to 550 μm).

Observation of stretched hyphae under *in vitro* conditions (where compartment lengths increased) clearly indicated that, similar to un-stretched hyphae, the sub-apical compartments undergo mitosis and septation based on a compartment length-dependent hierarchy. The only difference observed was an increase in the rate of septation/compartmentalization in sub-apical compartments of stretched hyphae compared to un-stretched hyphae under similar conditions (Fig 5.17). As explained in previous sections, compartment volume plays a crucial role in initiating nuclear division and subsequent septation in filamentous fungi (Fiddy et al., 1976; Veses et al., 2009). In stretched hyphae increases in compartment length imply that compartment volumes are higher than un-stretched hyphae under similar conditions. Compartments can be considered as functionally distinct, separate units or cells with respect to nuclear division and septation (Rosenberger et al., 1967) and it has been well established that in eukaryotic cells, the cell cycle is initiated when the cells reach a critical cell size or threshold (Rupeš, 2002; Cook et al., 2007). Therefore the observed increase in nuclear division and septation rate in stretched hyphae (compared to un-stretched hyphae) may be a direct response to the increased volume in individual compartments caused by mechanical stretch, or alternative mechanisms associated with other responses to compartment stretch.

Mechanically-stretched *E. festucae* hyphae under *in vitro* conditions during this study demonstrated all the basic features of intercalary growth, including increases in sub-apical compartment length (hence a cumulative increase in the hyphal segment) and

compartmentalization (mitosis and division of compartments). Stretching increased compartment lengths and cumulative hyphal length (by 30% of its original length from experiments carried out so far), while not affecting viability, and elongated compartments divided further giving rise to new compartments. Therefore it is rational to conclude that the hypothesis has been proven and that mechanical stretching alone is able to induce intercalary growth in *E. festucae* hyphae. Based on these outcomes a model for mechanical stretch induced intercalary growth is shown in figure 5.20.

A preliminary experiment conducted using genetically encoded calcium sensors showed that mechanical disturbance of *E. festucae* hyphae can trigger a change in Ca^{2+} pulses at the tip and in sub-apical compartments. In addition, during this study, characterization of stretch-activated calcium channel MidA revealed its importance in apical growth and influx of calcium in *E. festucae*. Hence we could hypothesise that MidA is activated during mechanical stretching to trigger an influx of Ca^{2+} in sub-apical compartments to facilitate intercalary growth associated processes such as nuclear division, septation and new cell wall synthesis. Investigations are continuing to test this hypothesis.

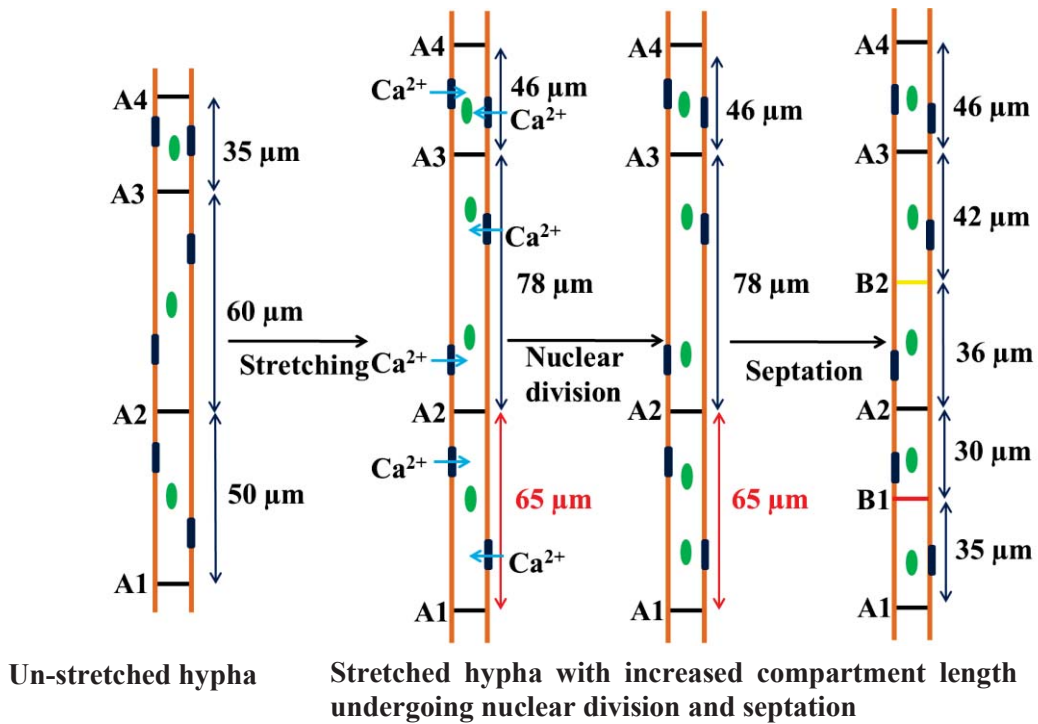
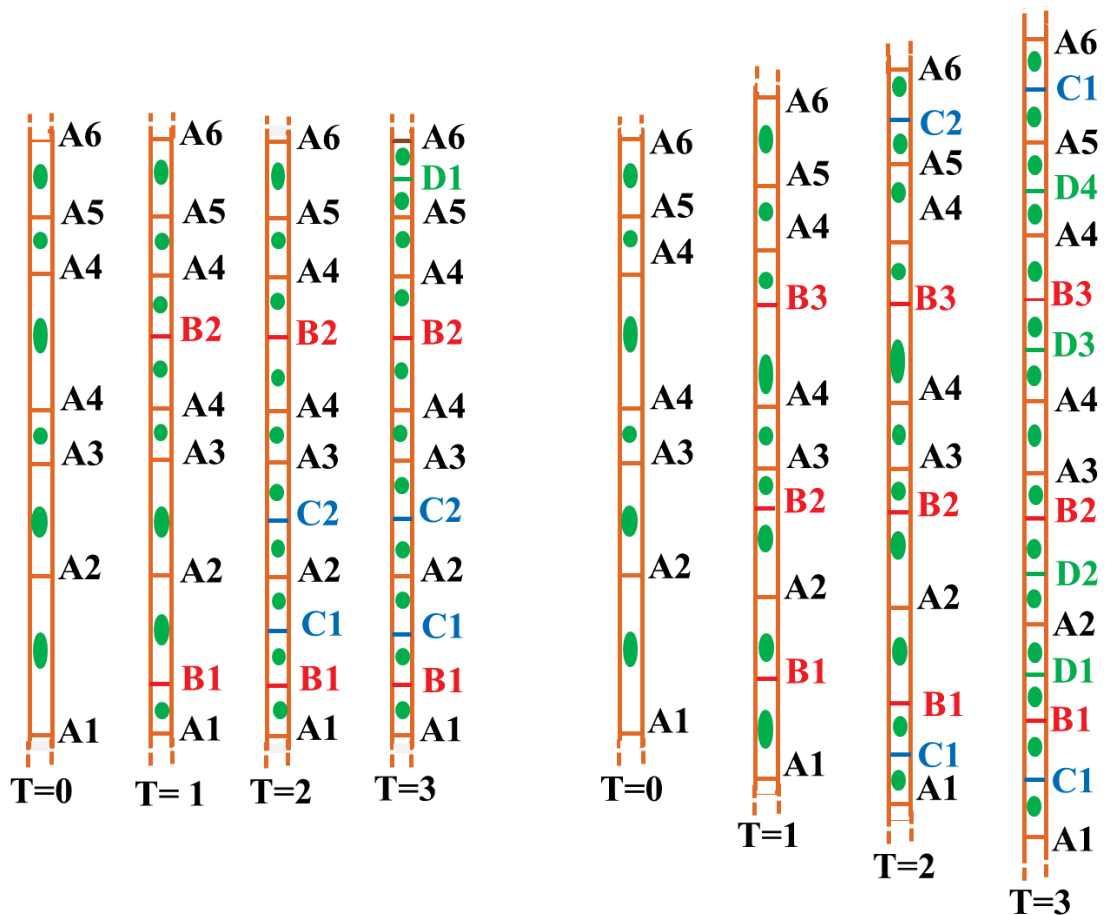


Figure 5.20: A sketch of the proposed model for mechanical stretch induced intercalary growth in sub-apical compartments of *E. festucae* hyphae.

Mechanical stretch increases the compartment length/volume, stretching the membranes and triggering an influx of calcium through the stretch-activated calcium channel MidA. The increased compartment volume results in an increase in compartmentalization (nuclear division and septation) compared to an un-stretched hypha, facilitated by Ca^{2+} signalling. Yellow septum – Septum that would be formed under both un-stretched and stretched conditions (as compartment is large), Red septum - Septum formed only due to increased compartment length at the same time point (as compartment expansion increases beyond the minimum threshold for division), A & B - septa present at each time point, Blue rectangles – stretch-activated calcium channel MidA. The hyphae and compartments are not drawn to scale.



Compartmentalisation in an un-stretched hypha at 4 time points

Compartmentalisation in the same hypha at 4 time points under stretched conditions

Figure 5.21: A representative sketch comparing nuclear division and septation at 4 time points between an un-stretched hypha and a stretched hypha.

When *E. festucae* hyphae are mechanically stretched within tolerable limits, the compartments length/volume increases proportionally to the amount of stretch applied. The stretched compartments undergo compartmentalization similar to un-stretched hyphae, however at a higher rate to accommodate the increased compartment length/volume due to stretching. Compartmentalization is based on a length-dependent hierarchy. The septation pattern shown is a model based on interpretations of experimental data. A, B, C and D represent septa present at each time point T0, T1, T2 and T3 respectively. The hyphae and compartments are not drawn to scale.

The same model can also be applied to intercalary hyphal growth in the elongation zone of the developing leaf. Plant cells in the meristematic zone undergo rapid elongation in the elongation zone. At the same time hyphae attached to host cells are subjected to mechanical stretch as the host cells elongate. As a result, as seen *in vitro*, the sub-apical compartments of attached hyphae increase in length in proportion to host cell elongation, and start to undergo compartmentalization (at higher rate than un-stretched hyphae), accommodating the added length. When host cell elongation ceases (in the mature zones of the leaf) no further mechanical stretching occurs and therefore intercalary growth too will cease. However it is possible that compartmentalization will continue to occur (but no compartment elongation) in the mature zone for some time until the compartments reach a minimum volume that stops further compartmentalization.

The conditions in the apoplast of the elongation zone of the host developing leaf are more complex than the *in vitro* conditions used during this study to demonstrate intercalary growth in *E. festucae* hyphae. Potato dextrose in water was used as the basic nutrient medium during this study. The apoplast environment in the elongation zone of the developing leaf can have different levels of pH, reactive oxygen species (ROS), Ca^{2+} , sugars and other nutrients that may have a significant influence on intercalary growth (Rayle et al., 1992; Cosgrove, 2000; Rodríguez et al., 2002). In grass species such as *Zea mays* high levels of ROS have been found in the apoplast of the expansion zone and shown to be necessary for cell wall loosening during leaf elongation (Schweikert et al., 2000; Rodríguez et al., 2002). In addition, disruption of ROS production via gene deletion in *E. festucae* results in breakdown of the usual symbiotic, synchronised growth seen with the host *L. perenne*, indicating a possible role for ROS in intercalary growth (Tanaka et al., 2006). According to the acid-growth hypothesis of

plant cell expansion, the activity of the plasma membrane-located proton pump reduces the cell wall from pH 7.0 to as low as 4.5 (Rayle et al., 1970; Hager et al., 1991). Whether similar conditions exist in the apoplast of the elongation zone of developing grass leaves has not been reported. Although the influence of these factors have not been tested during this study due to time constraints, the techniques developed will allow the *in vitro* growth medium to be modified easily before or during the stretching experiments (by replacing the growth medium above the cellophane membrane) to test the effect of these factors in future.

This study is the first attempt to investigate intercalary growth under *in vitro* conditions in fungi and examine the effect of mechanical stretching on fungal hyphae. Work so far has managed to successfully optimise a technique to mechanically stretch *E. festucae* fungal hyphae under *in vitro* conditions and demonstrate that hyphae can undergo intercalary growth when subjected to mechanical stretch. This work provides the basis for a broader investigation on intercalary growth and its associated phenomena. The scope of the apparatus to stretch fungal hyphae developed during this study can be further enhanced by motorising the stretch frame and replacing the impermeable silicon membrane with a permeable membrane for nutrient and water. This will enable applying mechanical stretch continuously with high degree of control to mimic the exact conditions in the leaf elongation zone.

As mentioned earlier the plant apoplast is a complex environment, and the impact on intercalary growth of some conditions (e.g. pH, ROS etc) could be tested *in vitro* using this technique by changing the growth medium. Other important avenues that warrant further research during mechanical stretch-driven intercalary growth are changes to the cell wall, cell membranes and nuclear behaviour. Although intercalary growth has been

experimentally shown only in *E. festucae*, it is possible that it may be common phenomenon in other filamentous fungi as well. The technique developed here could be used to test this hypothesis on most filamentous fungi that grow well in culture. The involvement of putative mechanosensors (WscA and MidA) in sensing mechanical stress and intercalary growth has been only partially investigated during this study (chapters 3 and 4) due to time constraints. In future, the mutant strains ($\Delta midA$ and $\Delta wscA$) will be subjected to mechanical stretching using the stretch technique to test their roles in mechanosensing and intercalary growth.

6. Summary, conclusions and future work

The aim of this PhD project was to determine whether mechanical stress was sufficient to induce intercalary extension in *E. festucae* endophytes of grasses, and to identify the proteins that sense and transduce the signal to initiate growth.

6.1 Stimulation of intercalary growth in *E. festucae* through mechanical stress

Colonisation of developing grass leaves by *E. festucae* hyphae requires a change in development from a highly branched mycelium with lots of hyphal tips (in hyphae colonising the host meristem), to long straight hyphae (in the intercalary growth zone) that are seldom branched and grow primarily through intercalary extension. The major objective of this project was to address whether intercalary extension in *E. festucae* is initiated and sustained through mechanical stress which is placed on hyphae by expansion of the host cells to which they are attached.

To test this hypothesis, a technique was developed to stretch fungal hyphae *in vitro*, away from other plant factors that may be involved in stimulating hyphal intercalary extension. Indirect evidence obtained previously suggested that intercalary growth in *E. festucae* in plants is accompanied by mitosis and formation of septa. Therefore, the first objective was to determine whether nuclear division and septation also occur in sub-apical compartments of *E. festucae* under stretch. The following conclusions were derived from the investigations conducted.

***De novo* compartmentalization in relaxed sub-apical compartments of *E. festucae* hyphae occurs according to a compartment length-dependent hierarchy.**

E. festucae hyphae are, for the most part, uni-nucleate. Examination of division in apical and sub-apical compartments of control hyphae extending at the tip during growth in

culture revealed that mitosis and septation occur in all compartments observed (10-15 compartments behind the apex) until a final compartment length of between 20-30 μm is reached. Once at this length, compartments appeared to go into cell cycle arrest. Whether this was permanent or temporary could not be discerned as other hyphae rapidly overgrew these compartments. As in other fungi, it was clear that compartment expansion was strictly confined to the apical compartment. Furthermore, the order of division in sub-apical compartments was not related to their position from the apex, but was dependent on compartment length. There was a hierarchy in compartment division, with longest compartments dividing first.

A positive correlation exists between compartment length and longitudinal length of the corresponding nuclei in a hypha.

Observations of fluorescent nuclei in hyphae growing in axenic culture indicated that longer compartments appeared to have longitudinally elongated nuclei while, shorter compartments contained more globular shaped nuclei. Since these longer compartments divided first, the presence of elongated nuclei in long compartments was a sign of imminent compartmentalization, possibly due to rearrangements of the cytoskeleton prior to nuclear division.

***E. festucae* hyphal compartment lengths can be increased through mechanical stretching while maintaining viability, provided that the stretch is within tolerable limits.**

Experiments that were conducted using the stretch apparatus under *in vitro* conditions revealed that *E. festucae* compartment length can be increased by around 10% through mechanical stretching at a given time, and cumulatively by about 30% of its original length within a period of 9 h with stretch applied in intervals, while maintaining

compartment viability. All compartments along the lengths of hyphae examined increased in length proportionally. *E. festucae* hyphae therefore tolerate quite significant mechanical stress. This is clearly an important attribute, given their biotrophic life cycle and requirement to colonise developing leaves (being seed-transmitted). Whether this is an adaptation that is confined to *Epichloë* endophytes or is present in other biotrophs or fungi in general is not known, as no attempts to stretch other fungi have yet been made. This result therefore represents an important development in our understanding of how *Epichloë* fungi grow, with possible broad implications for fungal growth in general depending on the outcomes of future stretching experiments in other species.

The rate of septation/ compartmentalization in sub-apical compartments of stretched hyphae is significantly higher than that of un-stretched hyphae under similar conditions.

In mechanically-stretched hyphae (within tolerable limits) the sub-apical compartments continue to undergo nuclear division and septation, demonstrating that the compartments are still viable. As found in relaxed hyphae, division occurred according to a compartment length-dependent hierarchy. Notably, the rate of new compartment formation in stretched hyphae was significantly higher than that of the un-stretched hyphae. This indicates that mechanical stretch, apart from increasing compartment length, also stimulates the cell cycle. How this occurs is not yet known, but the simplest explanation is that an increase in the length of shorter compartments (due to mechanical stretching) tips these compartments over the minimum threshold for division, and this stimulates the cell cycle in the same manner as is observed in control un-stretched hyphae.

6.2 Putative sensors of mechanical stress in *E. festucae*

Investigations on WscA and MidA of *E. festucae* were undertaken with the main objective of understanding their role in stimulating intercalary growth. However, as the genes have not been characterised in *E. festucae* before, experiments were also conducted to understand their primary functions as a basis to better understand their possible roles in intercalary growth. The following conclusions were derived from the investigations conducted.

***E. festucae* WscA is essential for hyphal apical growth and cell wall construction during growth in culture.**

Identification of the *E. festucae* orthologue of *wsc1* of *S. cerevisiae* via bioinformatics approaches was not straight forward as there is little homology between the cell wall integrity Wsc proteins of yeast and filamentous fungi. The *E. festucae* *wscA* gene identified here is the presumed orthologue of *S. cerevisiae* *wsc1* at this time, but further characterisation of the role of this protein is still required. Nevertheless, *E. festucae* $\Delta wscA$ mutants exhibited reduced radial colony growth rate and hyphal apical growth, but more cell wall aberrations and hyphal tip lysis compared to WT when growing in standard PDA. This indicated an important role for WscA in *E. festucae* hyphal growth in general and in cell wall construction. The ability of osmotic stabilisers to restore all observed $\Delta wscA$ phenotypes to the WT further supports the argument that *wscA* deletion results in an alterations in cell wall structure and composition, weakening the cell wall. These results suggest a role for WscA in regulating cell wall synthesis, particularly under hypo-osmotic conditions. The signalling pathway through which WscA exerts its effects has not been elucidated in this study, but is likely to be through Rho1 and the cell wall integrity MAP kinase pathway. In addition, the ability of osmotic stabilisers to

restore $\Delta wscA$ phenotypes suggests that another pathway (such as the HOG pathway) may take over under hyper-osmotic conditions, making the CWI MAP kinase pathway redundant under these conditions.

WscA is important in sensing and responding to cell wall perturbation.

E. festucae $\Delta wscA$ mutants exhibited significantly greater sensitivity than the WT in response to the presence of cell wall perturbing agents such as CW and CR, even under osmotically stabilised conditions. Inability of $\Delta wscA$ mutants to sense cell wall stress and respond by inducing cell wall synthesis is the likely factor behind their enhanced sensitivity to cell wall stress. These data lend support to the importance of the putative *E. festucae* WscA in cell wall integrity, particularly when the cell wall is under stress.

WscA alone is not essential in infection and colonization of the host, *L. perenne*.

E. festucae $\Delta wscA$ mutants were able to infect and colonise host plants in a similar manner to WT strains. Hyphal colonization patterns and hyphal densities within the meristematic tissue, expansion zone and mature leaf showed no difference to that of plants inoculated with the WT.

WscA alone is not essential for *E. festucae* hyphal intercalary growth *in planta*.

The ability of *E. festucae* $\Delta wscA$ mutants to colonise and form long parallel hyphae within the expansion zone of the developing leaf indicated that $\Delta wscA$ mutants can undergo intercalary growth. It is possible that the overlapping functions of other sensory proteins in the CWI MAP kinase pathway can complement the loss of WscA under these conditions. Future studies are required to confirm whether $\Delta wscA$ mutants are able to undergo intercalary growth in response to mechanical stretching under *in vitro*

conditions, and to delete further genes in the pathway that may be able to complement its role as a sensor. Complementation of the *S. cerevisiae wsc1* deletion mutant is also required to verify this gene as the yeast orthologue.

MidA is essential in *E. festucae* cell wall construction during hyphal growth under regular or low exogenous Ca²⁺ levels, but not essential to maintain normal hyphal apical growth rate.

Hyphae of the *E. festucae* $\Delta midA$ mutants exhibited cell wall aberrations, hyphal tip branching and frequent hyphal tip lysis, indicating defective and weakened cell walls. Osmotic stabilisers were able to restore these phenotypes, demonstrating that *midA* deletion causes a major structural weakness in the cell walls. Under depleted Ca²⁺ levels (in the presence of EGTA) these phenotypes were exacerbated. Despite defective cell wall synthesis, the apical growth rate of individual $\Delta midA$ hyphae was similar to that of the WT. Therefore the reduced colony growth seen in $\Delta midA$ colonies was attributed to frequent hyphal tip lysis and tip branching, caused by weakened cell walls. In *E. festucae*, Ca²⁺ influx through MidA appears to be essential for proper cell wall synthesis (possibly through the activation of the transcription factor Crz1, as shown in other fungi) under regular and low exogenous Ca²⁺ conditions.

***E. festucae* has alternative uptake systems, other than MidA, that uptake Ca²⁺ in high exogenous Ca²⁺ environments.**

High exogenous Ca²⁺ was able to restore *E. festucae* $\Delta midA$ phenotypes, including reduced radial colony growth and cell wall defects (as observed through Calcofluor White staining). This is likely partly due to the osmotic stability provided by high concentrations of CaCl₂ in the growth medium, and also through the activation of

alternative Ca²⁺ uptake systems such as Fig1 of the LACS under high exogenous Ca²⁺ concentrations.

MidA is essential in sensing and responding to cell wall perturbation.

Cell wall perturbing agents such as CW and CR induced a more profound effect on colony growth of the *ΔmidA* mutants than on WT, both in standard PDA and in the presence of an osmotic stabiliser. *E. festucae* *ΔmidA* mutants were also impaired in their ability to strengthen and repair cell walls under conditions of cell wall stress, suggesting that MidA and calcium influx, as in other fungi, is important in cell wall synthesis and repair in *E. festucae*.

MidA is required for *E. festucae* to make the transition from apical to intercalary growth that occurs during host colonization of developing leaves.

E. festucae *ΔmidA* mutants were fully functional in their ability to colonise host meristematic tissues of the SAM, and colonisation patterns appeared similar to WT hyphae. However, the same strains were impaired in their ability to enter the expansion zone of the developing leaf. Hyphal density was low and appeared to be patchy in transverse sections of leaves. This contrasted with the WT which colonised leaves relatively uniformly. Longitudinal sections of the expansion zone of developing leaves infected with *ΔmidA* mutants showed that those hyphae that made it into the intercalary growth zone appeared capable of intercalary growth. These provide tantalising evidence supporting a role of MidA in sensing and stimulating intercalary growth, possibly supported by other calcium channels or unrelated sensors. The leaf expansion zone is a complex environment, and the possible involvement of other calcium influx channels under these conditions makes it difficult to interpret the exact role of MidA in intercalary growth within the leaf expansion zone. Mechanical stretching of *ΔmidA*

hyphae under *in vitro* conditions is suggested in order to exclude other plant factors and provide a conclusive understanding of the role of MidA alone, with and without exogenous calcium in sensing mechanical stress and triggering intercalary growth.

Calcium concentration at the hyphal tips of *E. festucae* has a pulsatile nature with unique spatial and temporal signatures.

Given the role of MidA in cell wall synthesis and host colonisation, we hypothesised that calcium has a prominent role in hyphal growth in *E. festucae*. Hence a study was undertaken to optimise a technique to study calcium distribution and signalling in *E. festucae* with the intention of extending the study to intercalary growth.

Time lapse imaging of *E. festucae* hyphae transformed with the genetically encoded calcium sensor GCaMP5 revealed frequent Ca^{2+} pulses at the hyphal tip. Each hypha of the same strain under similar conditions displayed unique signatures of temporal and spatial calcium dynamics (amplitude, distribution area and the frequency). The pulses were mostly confined to the hyphal tips, although single Ca^{2+} pulses were occasionally observed in sub-apical regions. Use of the calcium chelating agent EGTA in the medium attenuated Ca^{2+} pulses at the hyphal tip, indicating that the Ca^{2+} pulses were due to influx of external calcium, and not to calcium released from calcium stores.

MidA is responsible for generating the Ca^{2+} pulsatile signatures at the hyphal tip.

Gene replacement studies of *midA* in *E. festucae* indicated that the regular Ca^{2+} pulses present in most WT hyphae were not visible in the mutants. These calcium oscillations are therefore mediated through MidA activity. However an alternative pulse, at times higher than the WT pulses in terms of amplitude and distance from tip, was still

detectable. This indicates that there is either another channel through which calcium is able to enter the hyphal tip or that the CchA channel is activated by more than one regulator. This alternative entry mechanism for calcium has a different periodicity to the MidA-regulated process, and may complement the MidA deletion to a certain extent, possibly explaining the partial intercalary growth phenotype observed in $\Delta midA$ mutants in plants. The FigA of LACS provides a further mechanism which may explain the residual calcium oscillation in the mutants. Complementing the $\Delta midA$ mutant with full length *midA* gene restored the Ca^{2+} pulsatile signature as seen in WT hyphae, confirming that the primary calcium oscillations observed are due to MidA activity.

Ca²⁺ influx and a tip high gradient of Ca²⁺ may not be essential to maintain E. festucae apical growth rate in culture.

Although Ca^{2+} pulses were a frequent occurrence in WT hyphae, there were hyphae that did not show any visible pulses at the tip. Furthermore, the $\Delta midA$ hyphae did not display the frequent pulsatile nature of the WT hyphae, except for the occasional pulses described above. The steep tip-high $[Ca^{2+}]_c$ gradient was also not clearly visible in the $\Delta midA$ hyphae. However, measurements of hyphal apical growth rate in $\Delta midA$ mutant hyphae, or in WT hyphae that were not fluorescing, were not significantly different to that of WT hyphae that demonstrated frequent Ca^{2+} pulses at the tip. This indicates that hyphal tip extension can occur in the absence of rapid periodicity calcium pulses. Nevertheless, the hyphae of the mutants were fragile as a result of cell wall weakness. The reason behind the absence of calcium pulses in some growing WT hyphae is not known.

Ca²⁺ uptake systems are active in sub-apical regions of *E. festucae* hyphae.

Calcium pulses were occasionally observed in sub-apical regions of hyphae at seemingly random positions along a hypha, and appeared to be due to influx of Ca²⁺, as the presence of EGTA eliminated these pulses. Interestingly, mechanical perturbation of hyphae resulted in a visible increase in Ca²⁺ pulses in apical as well as sub-apical regions, which confirmed the presence of active calcium uptake systems away from the hyphal tip, and showed that the channels could be activated through mechanical perturbations. These results provide preliminary evidence to support the possible involvement of Ca²⁺ signalling in intercalary growth.

6.3 General conclusion

To conclude, mechanical stretching of hyphae increases *E. festucae* compartment length, and the elongated compartments remain viable and undergo nuclear division and septation, fulfilling the three basic requirements for intercalary growth. These results indicate that mechanical stretching alone is sufficient to trigger intercalary growth and that hyphae respond to increased compartment lengths by inducing nuclear division and septation in sub-apical compartments. The first step in intercalary growth of endophytes in plants is therefore likely to be the sensing of mechanical stress by proteins in the *Epichloë* plasma membrane when compartments are subjected to strain during host cell expansion. Compartment expansion is likely to be driven by host cell expansion and may simply be a physical process of cell wall stretch. We cannot however rule out that other plant factors are also involved. Nevertheless, expansion in compartments then results in *de novo* cell division and new compartment formation.

Once mechanical stretch has occurred, we propose that sensors in fungal cell membranes are stimulated to initiate cell wall synthesis. Deletion of the *E. festucae*

MidA orthologue suggests that calcium uptake is important for cell wall synthesis and full colonisation of the intercalary growth zone. Redundancy in calcium uptake mechanisms may be masking the role of MidA in intercalary growth. Further experimentation *in vitro* using the mechanical stretcher should resolve this. Deletion of the proposed WscA orthologue had no effect on endophyte intercalary growth in the host indicating that the cell wall integrity MAP kinase pathway may not be involved; however given that there are several redundant Wsc proteins in yeast, the role of this pathway in response to mechanical stress has not yet been adequately explained.

This project has conclusively demonstrated that mechanical stress induces intercalary growth in *E. festucae* hyphae. Taken together these data can be used to develop a model for intercalary growth that involves all the processes that normally occur at the tip in *Epichloë* hyphae. In this model I propose that mechanical stress stimulates sensors in intercalary cell membranes in a similar manner to the turgor pressure at the hyphal tip. This initiates calcium influx, cell wall growth and nuclear division in intercalary compartments, in much the same way as at the tip.

7. References

- Adamíková, L. U., Straube, A., Schulz, I. & Steinberg, G. 2004. Calcium signaling is involved in dynein-dependent microtubule organization. *Molecular biology of the cell*, 15, 1969-1980.
- Akerboom, J., Chen, T.-W., Wardill, T. J., Tian, L., Marvin, J. S., Mutlu, S., Calderón, N. C., Esposti, F., Borghuis, B. G., Sun, X. R., Gordus, A., Orger, M. B., Portugues, R., Engert, F., Macklin, J. J., Filosa, A., Aggarwal, A., Kerr, R. A., Takagi, R., Kracun, S., Shigetomi, E., Khakh, B. S., Baier, H., Lagnado, L., Wang, S. S.-H., Bargmann, C. I., Kimmel, B. E., Jayaraman, V., Svoboda, K., Kim, D. S., Schreiter, E. R. & Looger, L. L. 2012. Optimization of a GCaMP Calcium Indicator for Neural Activity Imaging. *The Journal of Neuroscience*, 32, 13819-13840.
- Altschul, S. F., Gish, W., Miller, W., Myers, E. W. & Lipman, D. J. 1990. Basic local alignment search tool. *Journal of Molecular Biology*, 215, 403-410.
- Altschul, S. F., Madden, T. L., Schaffer, A. A., Zhang, J., Zhang, Z., Miller, W. & Lipman, D. J. 1997. Gapped BLAST and PSI-BLAST: a new generation of protein database search programs. *Nucleic Acids Res*, 25, 3389-402.
- Antebi, A. & Fink, G. R. 1992. The yeast Ca (2+)-ATPase homologue, PMR1, is required for normal Golgi function and localizes in a novel Golgi-like distribution. *Molecular biology of the cell*, 3, 633-654.
- Bartnicki-Garcia, S., Bartnicki, D. D., Gierz, G., López-Franco, R. A. & Bracker, C. E. 1995. Evidence That Spitzenkörper Behavior Determines the Shape of a Fungal Hypha: A Test of the Hyphoid Model. *Experimental Mycology*, 19, 153-159.
- Bartnicki-Garcia, S., Hergert, F. & Gierz, G. 1989. Computer simulation of fungal morphogenesis and the mathematical basis for hyphal (tip) growth. *Protoplasma*, 153, 46-57.
- Bartnicki-Garcia, S. & Lippman, E. 1969. Fungal Morphogenesis: Cell Wall Construction in *Mucor rouxii*. *Science*, 165, 302-304.
- Becker, Y., Eaton, C. J., Brasell, E., May, K. J., Becker, M., Hassing, B., Cartwright, G. M., Reinhold, L. & Scott, B. 2014. The Fungal Cell-Wall Integrity MAPK Cascade Is Crucial for Hyphal Network Formation and Maintenance of Restrictive Growth of *Epichloë festucae* in Symbiosis With *Lolium perenne*. *Molecular Plant-Microbe Interactions*, 28, 69-85.
- Benčina, M., Bagar, T., Lah, L. & Kraševc, N. 2009. A comparative genomic analysis of calcium and proton signaling/homeostasis in *Aspergillus* species. *Fungal Genetics and Biology*, 46, S93-S104.
- Bonilla, M. & Cunningham, K. W. 2003. Mitogen-activated Protein Kinase Stimulation of Ca²⁺ Signaling Is Required for Survival of Endoplasmic Reticulum Stress in Yeast. *Molecular Biology of the Cell*, 14, 4296-4305.
- Bormann, J. & Tudzynski, P. 2009. Deletion of Mid1, a putative stretch-activated calcium channel in *Claviceps purpurea*, affects vegetative growth, cell wall synthesis and virulence. *Microbiology*, 155, 3922-3933.
- Bowman, B. J., Abreu, S., Johl, J. K. & Bowman, E. J. 2012. The *pmr* Gene, Encoding a Ca²⁺-ATPase, Is Required for Calcium and Manganese Homeostasis and Normal Development of Hyphae and Conidia in *Neurospora crassa*. *Eukaryotic Cell*, 11, 1362-1370.
- Bowman, B. J., Abreu, S., Margolles-Clark, E., Draskovic, M. & Bowman, E. J. 2011. Role of Four Calcium Transport Proteins, Encoded by *nca-1*, *nca-2*, *nca-3*, and

- cax*, in Maintaining Intracellular Calcium Levels in *Neurospora crassa*. *Eukaryotic Cell*, 10, 654-661.
- Bowman, B. J., Draskovic, M., Freitag, M. & Bowman, E. J. 2009. Structure and distribution of organelles and cellular location of calcium transporters in *Neurospora crassa*. *Eukaryotic cell*, 8, 1845-1855.
- Brand, A. & Gow, N. a. R. 2009. Mechanisms of hypha orientation of fungi. *Current Opinion in Microbiology*, 12, 350-357.
- Brand, A., Shanks, S., Duncan, V. M. S., Yang, M., Mackenzie, K. & Gow, N. 2007. Hyphal Orientation of *Candida albicans* Is Regulated by a Calcium-Dependent Mechanism. *Current Biology*, 17, 347-352.
- Brem, D. & Leuchtmann, A. 1999. High prevalence of horizontal transmission of the fungal endophyte *Epichloë sylvatica*. *Bull. Geobot. Inst. ETH*, 65, 3-12.
- Buehrer, B. M. & Errede, B. 1997. Coordination of the mating and cell integrity mitogen-activated protein kinase pathways in *Saccharomyces cerevisiae*. *Molecular and cellular biology*, 17, 6517-6525.
- Carnero, E., Ribas, J. C., García, B., Durán, A. & Sánchez, Y. 2000. *Schizosaccharomyces pombe* ehs1p is involved in maintaining cell wall integrity and in calcium uptake. *Molecular and General Genetics MGG*, 264, 173-183.
- Cavinder, B., Hamam, A., Lew, R. R. & Trail, F. 2011. Mid1, a Mechanosensitive Calcium Ion Channel, Affects Growth, Development, and Ascospore Discharge in the Filamentous Fungus *Gibberella zeae*. *Eukaryotic Cell*, 10, 832-841.
- Cavinder, B. & Trail, F. 2012. Role of Fig1, a Component of the Low-Affinity Calcium Uptake System, in Growth and Sexual Development of Filamentous Fungi. *Eukaryotic Cell*, 11, 978-988.
- Chenevert, J., Corrado, K., Bender, A., Pringle, J. & Herskowitz, I. 1992. A Yeast Gene (*bem1*) Necessary For Cell Polarization Whose Product Contains 2 Sh3 Domains.
- Chin, D. & Means, A. R. 2000. Calmodulin: a prototypical calcium sensor. *Trends in Cell Biology*, 10, 322-328.
- Christensen, M., Ball, O.-P., Bennett, R. & Schardl, C. 1997. Fungal and host genotype effects on compatibility and vascular colonization by *Epichloë festucae*. *Mycological research*, 101, 493-501.
- Christensen, M. J., Bennett, R. J., Ansari, H. A., Koga, H., Johnson, R. D., Bryan, G. T., Simpson, W. R., Koolaard, J. P., Nickless, E. M. & Voisey, C. R. 2008. *Epichloë* endophytes grow by intercalary hyphal extension in elongating grass leaves. *Fungal Genetics and Biology*, 45, 84-93.
- Christensen, M. J., Bennett, R. J. & Schmid, J. 2002. Growth of *Epichloë/Neotyphodium* and p-endophytes in leaves of *Lolium* and *Festuca* grasses. *Mycological Research*, 106, 93-106.
- Chung, K.-R. & Schardl, C. 1997. Sexual cycle and horizontal transmission of the grass symbiont, *Epichloë typhina*. *Mycological Research*, 101, 295-301.
- Cid, V. J., Durán, A., Del Rey, F., Snyder, M. P., Nombela, C. & Sánchez, M. 1995. Molecular basis of cell integrity and morphogenesis in *Saccharomyces cerevisiae*. *Microbiological Reviews*, 59, 345-86.
- Cleary, A., Youatt, J. & O'brien, T. 1986. Hyphal emergence and outgrowth of *Allomyces macrogynus* in aerated cultures. *Australian Journal of Biological Sciences*, 39, 241-254.
- Clutterbuck, A. 1969. Cell volume per nucleus in haploid and diploid strains of *Aspergillus nidulans*. *Journal of general microbiology*, 55, 291-299.

- Clutterbuck, A. 1970. Synchronous nuclear division and septation in *Aspergillus nidulans*. *Journal of general microbiology*, 60, 133-135.
- Cook, M. & Tyers, M. 2007. Size control goes global. *Current Opinion in Biotechnology*, 18, 341-350.
- Cornelius, G. & Nakashima, H. 1987. Vacuoles play a decisive role in calcium homeostasis in *Neurospora crassa*. *Journal of general microbiology*, 133, 2341-2347.
- Cosgrove, D. J. 2000. Loosening of plant cell walls by expansins. *Nature*, 407, 321-326.
- Craig, G. D., Gull, K. & Wood, D. A. 1977. Stipe Elongation in *Agaricus bisporus*. *Journal of General Microbiology*, 102, 337-347.
- Craven, K., Hsiau, P., Leuchtmann, A., Hollin, W. & Schardl, C. 2001. Multigene phylogeny of *Epichloë* species, fungal symbionts of grasses. *Annals of the Missouri Botanical Garden*, 14-34.
- Cunningham, K. W. & Fink, G. R. 1994a. Ca²⁺ transport in *Saccharomyces cerevisiae*. *Journal of Experimental Biology*, 196, 157-66.
- Cunningham, K. W. & Fink, G. R. 1994b. Calcineurin-dependent growth control in *Saccharomyces cerevisiae* mutants lacking PMC1, a homolog of plasma membrane Ca²⁺ ATPases. *The Journal of Cell Biology*, 124, 351-363.
- Cunningham, K. W. & Fink, G. R. 1996. Calcineurin inhibits VCX1-dependent H⁺/Ca²⁺ exchange and induces Ca²⁺ ATPases in *Saccharomyces cerevisiae*. *Molecular and Cellular Biology*, 16, 2226-37.
- Cyert, M. S. 2003. Calcineurin signaling in *Saccharomyces cerevisiae*: how yeast go crazy in response to stress. *Biochemical and Biophysical Research Communications*, 311, 1143-1150.
- Davenport, K. R., Sohaskey, M., Kamada, Y., Levin, D. E. & Gustin, M. C. 1995. A second osmosensing signal transduction pathway in yeast hypotonic shock activates the PKC1 protein kinase-regulated cell integrity pathway. *Journal of Biological Chemistry*, 270, 30157-30161.
- De Castro, P. A., Chiaratto, J., Winkelströter, L. K., Bom, V. L. P., Ramalho, L. N. Z., Goldman, M. H. S., Brown, N. A. & Goldman, G. H. 2014. The Involvement of the Mid1/Cch1/Yvc1 Calcium Channels in *Aspergillus fumigatus* Virulence. *PLoS ONE*, 9, e103957.
- Denis, V. & Cyert, M. S. 2002. Internal Ca²⁺ release in yeast is triggered by hypertonic shock and mediated by a TRP channel homologue. *The Journal of Cell Biology*, 156, 29-34.
- Dichtl, K., Helmschrott, C., Dirr, F. & Wagener, J. 2012. Deciphering cell wall integrity signalling in *Aspergillus fumigatus*: identification and functional characterization of cell wall stress sensors and relevant Rho GTPases. *Molecular Microbiology*, 83, 506-519.
- Ding, X., Yu, Q., Xu, N., Wang, Y., Cheng, X., Qian, K., Zhao, Q., Zhang, B., Xing, L. & Li, M. 2013. Ecm7, a regulator of HACS, functions in calcium homeostasis maintenance, oxidative stress response and hyphal development in *Candida albicans*. *Fungal Genetics and Biology*, 57, 23-32.
- Dirr, F., Echtenacher, B., Heesemann, J., Hoffmann, P., Ebel, F. & Wagener, J. 2010. AfMkk2 is required for cell wall integrity signaling, adhesion, and full virulence of the human pathogen *Aspergillus fumigatus*. *International Journal of Medical Microbiology*, 300, 496-502.
- Drgonová, J., Tomás, D., Tanaka, K., Kollár, R., Chen, G.-C., Ford, R. A., Chan, C. S. M., Takai, Y. & Cabib, E. 1996. Rho1p, a Yeast Protein at the Interface Between Cell Polarization and Morphogenesis. *Science*, 272, 277-279.

- Dunn, T., Gable, K. & Beeler, T. 1994. Regulation of cellular Ca²⁺ by yeast vacuoles. *Journal of Biological Chemistry*, 269, 7273-7278.
- Dupres, V., Alsteens, D., Wilk, S., Hansen, B., Heinisch, J. J. & Dufrene, Y. F. 2009. The yeast Wsc1 cell surface sensor behaves like a nanospring in vivo. *Nat Chem Biol*, 5, 857-862.
- Durand, J.-L., Schaufele, R. & Gastal, F. 1999. Grass leaf elongation rate as a function of developmental stage and temperature: morphological analysis and modelling. *Annals of Botany*, 83, 577-588.
- Eaton, C. J., Cox, M. P., Ambrose, B., Becker, M., Hesse, U., Schardl, C. L. & Scott, B. 2010. Disruption of signaling in a fungal-grass symbiosis leads to pathogenesis. *Plant Physiology*, 153, 1780-1794.
- Eaton, C. J., Cox, M. P. & Scott, B. 2011. What triggers grass endophytes to switch from mutualism to pathogenesis? *Plant science*, 180, 190-195.
- Eilam, Y., Lavi, H. & Grossowicz, N. 1985. Cytoplasmic Ca²⁺ homeostasis maintained by a vacuolar Ca²⁺ transport system in the yeast *Saccharomyces cerevisiae*. *Journal of general microbiology*, 131, 623-629.
- Eilers, F. I. 1974. Growth regulation in *Coprinus radiatus*. *Archives of Microbiology*, 96, 353-364.
- Elorza, M. V., Rico, H. & Sentandreu, R. 1983. Calcofluor white alters the assembly of chitin fibrils in *Saccharomyces cerevisiae* and *Candida albicans* cells. *Journal of general microbiology*, 129, 1577-1582.
- Fairhead, C., Llorente, B., Denis, F., Soler, M. & Dujon, B. 1996. New vectors for combinatorial deletions in yeast chromosomes and for gap-repair cloning using 'split-marker' recombination. *Yeast*, 12, 1439-1457.
- Fiddy, C. & Trinci, A. 1976. Mitosis, septation, branching and the duplication cycle in *Aspergillus nidulans*. *Journal of general microbiology*, 97, 169-184.
- Fischer, M., Schnell, N., Chattaway, J., Davies, P., Dixon, G. & Sanders, D. 1997. The *Saccharomyces cerevisiae* CCH1 gene is involved in calcium influx and mating. *FEBS Letters*, 419, 259-262.
- Fuchs, B. B. & Mylonakis, E. 2009. Our Paths Might Cross: the Role of the Fungal Cell Wall Integrity Pathway in Stress Response and Cross Talk with Other Stress Response Pathways. *Eukaryotic Cell*, 8, 1616-1625.
- Fuchs, U., Manns, I. & Steinberg, G. 2005. Microtubules Are Dispensable for the Initial Pathogenic Development but Required for Long-Distance Hyphal Growth in the Corn Smut Fungus *Ustilago maydis*. *Molecular Biology of the Cell*, 16, 2746-2758.
- Fujiwara, T., Tanaka, K., Mino, A., Kikyo, M., Takahashi, K., Shimizu, K. & Takai, Y. 1998. Rho1p-Bni1p-Spa2p Interactions: Implication in Localization of Bni1p at the Bud Site and Regulation of the Actin Cytoskeleton in *Saccharomyces cerevisiae*. *Molecular Biology of the Cell*, 9, 1221-1233.
- Futagami, T., Nakao, S., Kido, Y., Oka, T., Kajiwara, Y., Takashita, H., Omori, T., Furukawa, K. & Goto, M. 2011. Putative Stress Sensors WscA and WscB Are Involved in Hypo-Osmotic and Acidic pH Stress Tolerance in *Aspergillus nidulans*. *Eukaryotic Cell*, 10, 1504-1515.
- García-Rodríguez, L. J., Valle, R., Durán, Á. & Roncero, C. 2005. Cell integrity signaling activation in response to hyperosmotic shock in yeast. *FEBS letters*, 579, 6186-6190.
- Garrill, A., Jackson, S., Lew, R. & Heath, I. 1993. Ion channel activity and tip growth: tip-localized stretch-activated channels generate an essential Ca²⁺ gradient in the oomycete *Saprolegnia ferax*. *European journal of cell biology*, 60, 358-365.

- Gentzsch, M. & Tanner, W. 1996. The PMT gene family: protein O-glycosylation in *Saccharomyces cerevisiae* is vital. *The EMBO Journal*, 15, 5752.
- Glenn, A. E., Bacon, C. W., Price, R. & Hanlin, R. T. 1996. Molecular Phylogeny of *Acremonium* and Its Taxonomic Implications. *Mycologia*, 88, 369-383.
- Gong, X., Hurtado, O., Wang, B., Wu, C., Yi, M., Giraldo, M., Valent, B., Goodin, M. & Farman, M. 2015. pFPL Vectors for High-Throughput Protein Localization in Fungi: Detecting Cytoplasmic Accumulation of Putative Effector Proteins. *Molecular Plant-Microbe Interactions*, 28, 107-121.
- Gooday, G. W. 1971. An Autoradiographic Study of Hyphal Growth of Some Fungi. *Microbiology*, 67, 125-133.
- Gooday, G. W. 1973. Activity of chitin synthase during the development of fruit bodies of the toadstool *Coprinus cinereus*. *Biochem Soc Trans* 1, 1105-1107.
- Gooday, G. W. 1982. Metabolic control of fruitbody morphogenesis in *Coprinus cinereus*. *Basidium and Basidiocarp*, 157-173
- Gooday, G. W. 1995. The dynamics of hyphal growth. *Mycological Research*, 99, 385-394.
- Gooday, G. W. & De Rousset-Hall, A. 1975. Properties of Chitin Synthetase from *Coprinus cinereus*. *Journal of General Microbiology*, 89, 137-145.
- Gooday, G. W., De Rousset-Hall, A. & Hunsley, D. 1976. Effect of polyoxin D on chitin synthesis in *Coprinus cinereus*. *Transactions of the British Mycological Society*, 67, 193-200.
- Grove, S. N. & Bracker, C. E. 1970. Protoplasmic Organization of Hyphal Tips Among Fungi: Vesicles and Spitzenkörper. *Journal of Bacteriology*, 104, 989-1009.
- Guest, G. M., Lin, X. & Momany, M. 2004. *Aspergillus nidulans* RhoA is involved in polar growth, branching, and cell wall synthesis. *Fungal Genetics and Biology*, 41, 13-22.
- Hager, A., Debus, G., Edel, H., Stransky, H. & Serrano, R. 1991. Auxin induces exocytosis and the rapid synthesis of a high-turnover pool of plasma-membrane H⁺-ATPase. *Planta*, 185, 527-537.
- Hahn, H., Huth, W., Schöberlein, W., Diepenbrock, W. & Weber, W. 2003. Detection of endophytic fungi in *Festuca* spp. by means of tissue print immunoassay. *Plant Breeding*, 122, 217-222.
- Hammad, F., Ji, J., Watling, R. & Moore, D. 1993. Cell population dynamics in *Coprinus cinereus*: co-ordination of cell inflation throughout the maturing basidiome. *Mycological Research*, 97, 269-274.
- Harold, F. M. 1997. How hyphae grow: Morphogenesis explained? *Protoplasma*, 197, 137-147.
- Harren, K. & Tudzynski, B. 2013. Cch1 and Mid1 Are Functionally Required for Vegetative Growth under Low-Calcium Conditions in the Phytopathogenic Ascomycete *Botrytis cinerea*. *Eukaryotic Cell*, 12, 712-724.
- Harris, S. D. 2006. Cell Polarity in Filamentous Fungi: Shaping the Mold. In: Kwang, W. J. (ed.) *International Review of Cytology*. Academic Press.
- Harris, S. D. 2008. Branching of fungal hyphae: regulation, mechanisms and comparison with other branching systems. *Mycologia*, 100, 823-832.
- Harris, S. D. & Momany, M. 2004. Polarity in filamentous fungi: moving beyond the yeast paradigm. *Fungal Genetics and Biology*, 41, 391-400.
- Harris, S. D., Morrell, J. L. & Hamer, J. E. 1994. Identification and characterization of *Aspergillus nidulans* mutants defective in cytokinesis. *Genetics*, 136, 517.

- Harris, S. D., Read, N. D., Roberson, R. W., Shaw, B., Seiler, S., Plamann, M. & Momany, M. 2005. Polarisome Meets Spitzenkörper: Microscopy, Genetics, and Genomics Converge. *Eukaryotic Cell*, 4, 225-229.
- Hartley, J. L., Temple, G. F. & Brasch, M. A. 2000. DNA cloning using *in vitro* site-specific recombination. *Genome research*, 10, 1788-1795.
- Hayakawa, Y., Ishikawa, E., Shoji, J.-Y., Nakano, H. & Kitamoto, K. 2011. Septum-directed secretion in the filamentous fungus *Aspergillus oryzae*. *Molecular Microbiology*, 81, 40-55.
- Heinisch, J. J., Dupres, V., Wilk, S., Jendretzki, A. & Dufrêne, Y. F. 2010. Single-Molecule Atomic Force Microscopy Reveals Clustering of the Yeast Plasma-Membrane Sensor Wsc1. *PLoS ONE*, 5, e11104.
- Hestmark, G. 1997. Growth from the centre in an umbilicate lichen. *The Lichenologist*, 29, 379-383.
- Hickey, P. C., Swift, S. R., Roca, M. G. & Read, N. D. 2005. Live-cell imaging of filamentous fungi using vital fluorescent dyes and confocal microscopy. *Methods Microbiol*, 34, 63-87.
- Hofman, K. 1993. TMbase-A database of membrane spanning protein segments. *Biol. Chem. Hoppe-Seyler*, 374, 166.
- Hong, M.-P., Vu, K., Bautos, J. & Gelli, A. 2010. Cch1 Restores Intracellular Ca²⁺ in Fungal Cells during Endoplasmic Reticulum Stress. *Journal of Biological Chemistry*, 285, 10951-10958.
- Hong, M.-P., Vu, K., Bautos, J. M., Tham, R., Jamklang, M., Uhrig, J. P. & Gelli, A. 2013. Activity of the Calcium Channel Pore Cch1 Is Dependent on a Modulatory Region of the Subunit Mid1 in *Cryptococcus neoformans*. *Eukaryotic Cell*, 12, 142-150.
- Horton, P., Park, K. J., Obayashi, T., Fujita, N., Harada, H., Adams-Collier, C. J. & Nakai, K. 2007. WoLF PSORT: protein localization predictor. *Nucleic Acids Res*, 35, W585-7.
- Howard, R. J. 1981. Ultrastructural analysis of hyphal tip cell growth in fungi: Spitzenkörper, cytoskeleton and endomembranes after freeze-substitution. *Journal of Cell Science*, 48, 89-103.
- Howard, R. J. & Aist, J. R. 1979. Hyphal tip cell ultrastructure of the fungus *Fusarium*: Improved preservation by freeze-substitution. *Journal of Ultrastructure Research*, 66, 224-234.
- Iida, H., Nakamura, H., Ono, T., Okumura, M. S. & Anraku, Y. 1994. MID1, a novel *Saccharomyces cerevisiae* gene encoding a plasma membrane protein, is required for Ca²⁺ influx and mating. *Mol Cell Biol*, 14, 8259-71.
- Irie, K., Takase, M., Lee, K., Levin, D., Araki, H., Matsumoto, K. & Oshima, Y. 1993. MKK1 and MKK2, which encode *Saccharomyces cerevisiae* mitogen-activated protein kinase-kinase homologs, function in the pathway mediated by protein kinase C. *Molecular and Cellular Biology*, 13, 3076-3083.
- Jackson, S. L. & Heath, I. B. 1993. Roles of calcium ions in hyphal tip growth. *Microbiological Reviews*, 57, 367-382.
- Jiang, H., Shen, Y., Liu, W. & Lu, L. 2014. Deletion of the putative stretch-activated ion channel Mid1 is hypervirulent in *Aspergillus fumigatus*. *Fungal Genet Biol*, 62, 62-70.
- Johnson, D. I. & Pringle, J. R. 1990. Molecular characterization of CDC42, a *Saccharomyces cerevisiae* gene involved in the development of cell polarity. *The Journal of cell biology*, 111, 143-152.

- Jung, U. S. & Levin, D. E. 1999. Genome-wide analysis of gene expression regulated by the yeast cell wall integrity signalling pathway. *Molecular microbiology*, 34, 1049-1057.
- Jung, U. S., Sobering, A. K., Romeo, M. J. & Levin, D. E. 2002. Regulation of the yeast Rlm1 transcription factor by the Mpk1 cell wall integrity MAP kinase. *Molecular microbiology*, 46, 781-789.
- Kamada, T. 1994. Stipe elongation in fruit bodies. *Growth, Differentiation and Sexuality*. Springer, 367-379.
- Kamada, T., Fujii, T., Nakagawa, T. & Takemaru, T. 1985. Changes in (1→3)- β -glucanase activities during stipe elongation in *Coprinus cinereus*. *Current Microbiology*, 12, 257-259.
- Kamada, T., Hamada, Y. & Takemaru, T. 1982. Autolysis *in vitro* of the stipe cell wall in *Coprinus macrorhizus*. *Journal of General Microbiology*, 128, 1041-1046.
- Kamada, T. & Takemaru, T. 1977a. Stipe elongation during basidiocarp maturation in *Coprinus macrorhizus*: changes in polysaccharide composition of stipe cell wall during elongation. *Plant and Cell Physiology*, 18, 1291-1300.
- Kamada, T. & Takemaru, T. 1977b. Stipe elongation during basidiocarp maturation in *Coprinus macrorhizus*: mechanical properties of stipe cell wall. *Plant and cell physiology*, 18, 831-840.
- Kamada, T., Takemaru, T., Prosser, J. & Gooday, G. 1991. Right and left handed helicity of chitin microfibrils in stipe cells in *Coprinus cinereus*. *Protoplasma*, 165, 64-70.
- Kamada, T. & Tsuru, M. 1993. The onset of the helical arrangement of chitin microfibrils in fruit-body development of *Coprinus cinereus*. *Mycological research*, 97, 884-888.
- Kamada, Y., Jung, U. S., Piotrowski, J. & Levin, D. E. 1995. The protein kinase C-activated MAP kinase pathway of *Saccharomyces cerevisiae* mediates a novel aspect of the heat shock response. *Genes & Development*, 9, 1559-1571.
- Kanzaki, M., Nagasawa, M., Kojima, I., Sato, C., Naruse, K., Sokabe, M. & Iida, H. 1999. Molecular identification of a eukaryotic, stretch-activated nonselective cation channel. *Science*, 285, 882-886.
- Kayano, Y., Tanaka, A., Akano, F., Scott, B. & Takemoto, D. 2013. Differential roles of NADPH oxidases and associated regulators in polarized growth, conidiation and hyphal fusion in the symbiotic fungus *Epichloë festucae*. *Fungal Genetics and Biology*, 56, 87-97.
- Ketela, T., Green, R. & Bussey, H. 1999. *Saccharomyces cerevisiae* Mid2p Is a Potential Cell Wall Stress Sensor and Upstream Activator of the PKC1-MPK1 Cell Integrity Pathway. *Journal of bacteriology*, 181, 3330-3340.
- Kim, H.-S., Czymmek, K. J., Patel, A., Modla, S., Nohe, A., Duncan, R., Gilroy, S. & Kang, S. 2012. Expression of the Cameleon calcium biosensor in fungi reveals distinct Ca^{2+} signatures associated with polarized growth, development, and pathogenesis. *Fungal Genetics and Biology*, 49, 589-601.
- Klis, F. M., Boorsma, A. & De Groot, P. W. J. 2006. Cell wall construction in *Saccharomyces cerevisiae*. *Yeast*, 23, 185-202.
- Klis, F. M., Ram, A. F. J. & De Groot, P. W. J. 2007. A Molecular and Genomic View of the Fungal Cell Wall. In: Howard, R. & Gow, N. R. (eds.) *Biology of the Fungal Cell*. Springer Berlin Heidelberg.
- Kloda, A., Petrov, E., Meyer, G. R., Nguyen, T., Hurst, A. C., Hool, L. & Martinac, B. 2008. Mechanosensitive channel of large conductance. *The International Journal of Biochemistry & Cell Biology*, 40, 164-169.

- Kriangkripiat, T. & Momany, M. 2009. *Aspergillus nidulans* Protein O-Mannosyltransferases Play Roles in Cell Wall Integrity and Developmental Patterning. *Eukaryotic Cell*, 8, 1475-1485.
- Krogh, A., Larsson, B., Von Heijne, G. & Sonnhammer, E. L. 2001. Predicting transmembrane protein topology with a hidden Markov model: application to complete genomes. *Journal of molecular biology*, 305, 567-580.
- Kües, U. 2000. Life History and Developmental Processes in the Basidiomycete *Coprinus cinereus*. *Microbiology and Molecular Biology Reviews*, 64, 316-353.
- Kües, U. & Liu, Y. 2000. Fruiting body production in basidiomycetes. *Applied microbiology and biotechnology*, 54, 141-152.
- Kuldau, G. A., Liu, J.-S., White Jr, J. F., Siegel, M. R. & Schardl, C. L. 1997. Molecular systematics of Clavicipitaceae supporting monophyly of genus *Epichloë* and form genus *Ephelis*. *Mycologia*, 431-441.
- Kumamoto, C. A. 2008. Molecular mechanisms of mechanosensing and their roles in fungal contact sensing. *Nature Reviews Microbiology*, 6, 667-673.
- Landy, A. 1989. Dynamic, structural, and regulatory aspects of lambda site-specific recombination. *Annual review of biochemistry*, 58, 913-941.
- Langer, R. H. M. 1979. How grasses grow. *How grasses grow*.
- Larkin, M. A., Blackshields, G., Brown, N. P., Chenna, R., Mcgettigan, P. A., McWilliam, H., Valentin, F., Wallace, I. M., Wilm, A., Lopez, R., Thompson, J. D., Gibson, T. J. & Higgins, D. G. 2007. Clustal W and Clustal X version 2.0. *Bioinformatics*, 23, 2947-2948.
- Lee, K. S., Irie, K., Gotoh, Y., Watanabe, Y., Araki, H., Nishida, E., Matsumoto, K. & Levin, D. 1993. A yeast mitogen-activated protein kinase homolog (Mpk1p) mediates signalling by protein kinase C. *Molecular and Cellular Biology*, 13, 3067-3075.
- Lee, K. S. & Levin, D. E. 1992. Dominant mutations in a gene encoding a putative protein kinase (BCK1) bypass the requirement for a *Saccharomyces cerevisiae* protein kinase C homolog. *Molecular and Cellular Biology*, 12, 172-182.
- Lengeler, K. B., Wasserstrom, L., Walther, A. & Wendland, J. 2013. Analysis of the cell wall integrity pathway of *Ashbya gossypii*. *Microbiological Research*, 168, 607-614.
- Leuchtmann, A., Bacon, C. W., Schardl, C. L., White, J. F. & Tadych, M. 2014. Nomenclatural realignment of *Neotyphodium* species with genus *Epichloë*. *Mycologia*, 106, 202-215.
- Leuchtmann, A., Schardl, C. L. & Siegel, M. R. 1994. Sexual compatibility and taxonomy of a new species of *Epichloë* symbiotic with fine fescue grasses. *Mycologia*, 802-812.
- Levin, D., Bowers, B., Chen, C., Kamada, Y. & Watanabe, M. 1993. Dissecting the protein kinase C/MAP kinase signalling pathway of *Saccharomyces cerevisiae*. *Cellular & molecular biology research*, 40, 229-239.
- Levin, D. E. 2005. Cell Wall Integrity Signaling in *Saccharomyces cerevisiae*. *Microbiology and Molecular Biology Reviews*, 69, 262-291.
- Levin, D. E. 2011. Regulation of Cell Wall Biogenesis in *Saccharomyces cerevisiae*: The Cell Wall Integrity Signaling Pathway. *Genetics*, 189, 1145-1175.
- Lew, R. R., Abbas, Z., Anderca, M. I. & Free, S. J. 2008. Phenotype of a Mechanosensitive Channel Mutant, *mid-1*, in a Filamentous Fungus, *Neurospora crassa*. *Eukaryotic Cell*, 7, 647-655.

- Liu, M., Du, P., Heinrich, G., Cox, G. M. & Gelli, A. 2006. Cch1 Mediates Calcium Entry in *Cryptococcus neoformans* and Is Essential in Low-Calcium Environments. *Eukaryotic Cell*, 5, 1788-1796.
- Locke, E. G., Bonilla, M., Liang, L., Takita, Y. & Cunningham, K. W. 2000. A homolog of voltage-gated Ca²⁺ channels stimulated by depletion of secretory Ca²⁺ in yeast. *Molecular and Cellular Biology*, 20, 6686-6694.
- Lodder, A. L., Lee, T. K. & Ballester, R. 1999. Characterization of the Wsc1 protein, a putative receptor in the stress response of *Saccharomyces cerevisiae*. *Genetics*, 152, 1487-1499.
- Lohaus, G., Pennewiss, K., Sattelmacher, B., Hussmann, M. & Hermann Muehling, K. 2001. Is the infiltration-centrifugation technique appropriate for the isolation of apoplastic fluid? A critical evaluation with different plant species. *Physiologia Plantarum*, 111, 457-465.
- Lommel, M., Bagnat, M. & Strahl, S. 2004. Aberrant Processing of the WSC Family and Mid2p Cell Surface Sensors Results in Cell Death of *Saccharomyces cerevisiae* O-Mannosylation Mutants. *Molecular and Cellular Biology*, 24, 46-57.
- Macadam, J. W., Volenec, J. J. & Nelson, C. J. 1989. Effects of nitrogen on mesophyll cell division and epidermal cell elongation in tall fescue leaf blades. *Plant Physiology*, 89, 549-556.
- Maddi, A., Dettman, A., Fu, C., Seiler, S. & Free, S. J. 2012. WSC-1 and HAM-7 Are MAK-1 MAP Kinase Pathway Sensors Required for Cell Wall Integrity and Hyphal Fusion in *Neurospora crassa*. *PLoS ONE*, 7, e42374.
- Martin, D. C., Kim, H., Mackin, N. A., Maldonado-Báez, L., Evangelista, C. C., Beaudry, V. G., Dudgeon, D. D., Naiman, D. Q., Erdman, S. E. & Cunningham, K. W. 2011. New regulators of a high affinity Ca²⁺ influx system revealed through a genome-wide screen in yeast. *Journal of Biological Chemistry*, 286, 10744-10754.
- Maruoka, T., Nagasoe, Y., Inoue, S., Mori, Y., Goto, J., Ikeda, M. & Iida, H. 2002. Essential hydrophilic carboxyl-terminal regions including cysteine residues of the yeast stretch-activated calcium-permeable channel Mid1. *Journal of Biological Chemistry*, 277, 11645-11652.
- Matheos, D. P., Kingsbury, T. J., Ahsan, U. S. & Cunningham, K. W. 1997. Tcn1p/Crz1p, a calcineurin-dependent transcription factor that differentially regulates gene expression in *Saccharomyces cerevisiae*. *Genes & Development*, 11, 3445-3458.
- Matthews, T. R. & Niederpruem, D. J. 1972. Differentiation in *Coprinus lagopus*. *Archiv für Mikrobiologie*, 87, 257-268.
- Miller, A. J., Vogg, G. & Sanders, D. 1990. Cytosolic calcium homeostasis in fungi: roles of plasma membrane transport and intracellular sequestration of calcium. *Proceedings of the National Academy of Sciences*, 87, 9348-9352.
- Momany, M. 2002. Polarity in filamentous fungi: establishment, maintenance and new axes. *Current Opinion in Microbiology*, 5, 580-585.
- Moore, D. 1984. Developmental biology of the *Coprinus cinereus* carpophore: Metabolic regulation in relation to cap morphogenesis. *Experimental Mycology*, 8, 283-297.
- Moore, D. 1996. Inside the developing mushroom—cells, tissues and tissue patterns. *Patterns in fungal development*, 1-36.

- Mouriño-Pérez, R. R., Roberson, R. W. & Bartnicki-García, S. 2006. Microtubule dynamics and organization during hyphal growth and branching in *Neurospora crassa*. *Fungal Genetics and Biology*, 43, 389-400.
- Muller, E. M., Locke, E. G. & Cunningham, K. W. 2001. Differential regulation of two Ca²⁺ influx systems by pheromone signaling in *Saccharomyces cerevisiae*. *Genetics*, 159, 1527-1538.
- Muller, E. M., Mackin, N. A., Erdman, S. E. & Cunningham, K. W. 2003. Fig1p Facilitates Ca²⁺ Influx and Cell Fusion during Mating of *Saccharomyces cerevisiae*. *Journal of Biological Chemistry*, 278, 38461-38469.
- Nakai, J., Ohkura, M. & Imoto, K. 2001. A high signal-to-noise Ca²⁺ probe composed of a single green fluorescent protein. *Nat Biotech*, 19, 137-141.
- Namiki, F., Matsunaga, M., Okuda, M., Inoue, I., Nishi, K., Fujita, Y. & Tsuge, T. 2001. Mutation of an arginine biosynthesis gene causes reduced pathogenicity in *Fusarium oxysporum* f. sp. *melonis*. *Molecular Plant-Microbe Interactions*, 14, 580-584.
- Nelson, G., Kozlova-Zwinderman, O., Collis, A. J., Knight, M. R., Fincham, J. R. S., Stanger, C. P., Renwick, A., Hessing, J. G. M., Punt, P. J., Van Den Hondel, C. a. M. J. J. & Read, N. D. 2004. Calcium measurement in living filamentous fungi expressing codon-optimized aequorin. *Molecular Microbiology*, 52, 1437-1450.
- Nguyen, Q. B., Kadotani, N., Kasahara, S., Tosa, Y., Mayama, S. & Nakayashiki, H. 2008. Systematic functional analysis of calcium-signalling proteins in the genome of the rice-blast fungus, *Magnaporthe oryzae*, using a high-throughput RNA-silencing system. *Molecular microbiology*, 68, 1348-1365.
- Nonaka, H., Tanaka, K., Hirano, H., Fujiwara, T., Kohno, H., Umikawa, M., Mino, A. & Takai, Y. 1995. A downstream target of RHO1 small GTP-binding protein is PKC1, a homolog of protein kinase C, which leads to activation of the MAP kinase cascade in *Saccharomyces cerevisiae*. *The EMBO Journal*, 14, 5931-5938.
- Oliver, R. P., Roberts, I. N., Harling, R., Kenyon, L., Punt, P. J., Dingemans, M. A. & Hondel, C. a. M. J. J. 1987. Transformation of *Fulvia fulva*; a fungal pathogen of tomato, to hygromycin B resistance. *Current Genetics*, 12, 231-233.
- Ozaki, K., Tanaka, K., Imamura, H., Hihara, T., Kameyama, T., Nonaka, H., Hirano, H., Matsuura, Y. & Takai, Y. 1996. Rom1p and Rom2p are GDP/GTP exchange proteins (GEPs) for the Rho1p small GTP binding protein in *Saccharomyces cerevisiae*. *The EMBO journal*, 15, 2196.
- Ozeki-Miyawaki, C., Moriya, Y., Tatsumi, H., Iida, H. & Sokabe, M. 2005. Identification of functional domains of Mid1, a stretch-activated channel component, necessary for localization to the plasma membrane and Ca²⁺ permeation. *Experimental Cell Research*, 311, 84-95.
- Paidhungat, M. & Garrett, S. 1997. A homolog of mammalian, voltage-gated calcium channels mediates yeast pheromone-stimulated Ca²⁺ uptake and exacerbates the *cdc1(Ts)* growth defect. *Molecular and Cellular Biology*, 17, 6339-47.
- Palmer, C. P., Zhou, X.-L., Lin, J., Loukin, S. H., Kung, C. & Saimi, Y. 2001. A TRP homolog in *Saccharomyces cerevisiae* forms an intracellular Ca²⁺-permeable channel in the yeast vacuolar membrane. *Proceedings of the National Academy of Sciences*, 98, 7801-7805.
- Park, G., Pan, S. & Borkovich, K. A. 2008. Mitogen-Activated Protein Kinase Cascade Required for Regulation of Development and Secondary Metabolism in *Neurospora crassa*. *Eukaryotic Cell*, 7, 2113-2122.

- Pei, J. & Grishin, N. V. 2012. Cysteine-rich domains related to Frizzled receptors and Hedgehog-interacting proteins. *Protein Science*, 21, 1172-1184.
- Petersen, T. N., Brunak, S., Von Heijne, G. & Nielsen, H. 2011. SignalP 4.0: discriminating signal peptides from transmembrane regions. *Nature methods*, 8, 785-786.
- Philip, B. & Levin, D. E. 2001. Wsc1 and Mid2 Are Cell Surface Sensors for Cell Wall Integrity Signaling That Act through Rom2, a Guanine Nucleotide Exchange Factor for Rho1. *Molecular and Cellular Biology*, 21, 271-280.
- Philipson, M. N. & Christey, M. C. 1986. The relationship of host and endophyte during flowering, seed formation, and germination of *Lolium perenne*. *New Zealand Journal of Botany*, 24, 125-134.
- Pringle, J. R., Bi, E., Harkins, H. A., Zahner, J. E., De Virgilio, C., Chant, J., Corrado, K. & Fares, H. 1995. Establishment of Cell Polarity in Yeast. *Cold Spring Harbor Symposia on Quantitative Biology*, 60, 729-744.
- Pruyne, D. & Bretscher, A. 2000. Polarization of cell growth in yeast. *Journal of Cell Science*, 113, 571-585.
- Putney Jr, J. W. 1990. Capacitative calcium entry revisited: Review article. *Cell Calcium*, 11, 611-624.
- Qadota, H., Python, C. P., Inoue, S. B., Arisawa, M., Anraku, Y., Zheng, Y., Watanabe, T., Levin, D. E. & Ohya, Y. 1996. Identification of Yeast Rho1p GTPase as a Regulatory Subunit of 1,3- β -Glucan Synthase. *Science*, 272, 279-281.
- Qi, M. & Elion, E. A. 2005. MAP kinase pathways. *Journal of cell science*, 118, 3569-3572.
- Rajavel, M., Philip, B., Buehrer, B. M., Errede, B. & Levin, D. E. 1999. Mid2 is a putative sensor for cell integrity signaling in *Saccharomyces cerevisiae*. *Molecular and Cellular Biology*, 19, 3969-3976.
- Rayle, D. L. & Cleland, R. 1970. Enhancement of wall loosening and elongation by acid solutions. *Plant Physiology*, 46, 250-253.
- Rayle, D. L. & Cleland, R. E. 1992. The Acid Growth Theory of auxin-induced cell elongation is alive and well. *Plant physiology*, 99, 1271-1274.
- Read, N., Allan, W., Knight, H., Knight, M., Malho, R., Russell, A., Shacklock, P. & Trewavas, A. 1992. Imaging and measurement of cytosolic free calcium in plant and fungal cells. *Journal of Microscopy*, 166, 57-86.
- Read, N. D. 2011. Exocytosis and growth do not occur only at hyphal tips. *Molecular Microbiology*, 81, 4-7.
- Read, N. D. & Roca, M. G. 2006. Vegetative hyphal fusion in filamentous fungi. *Cell-Cell Channels*. Springer.
- Rech, C., Engh, I. & Kück, U. 2007. Detection of hyphal fusion in filamentous fungi using differently fluorescence-labeled histones. *Current Genetics*, 52, 259-266.
- Reinoso-Martín, C., Schüller, C., Schuetzer-Muehlbauer, M. & Kuchler, K. 2003. The Yeast Protein Kinase C Cell Integrity Pathway Mediates Tolerance to the Antifungal Drug Caspofungin through Activation of Slt2p Mitogen-Activated Protein Kinase Signaling. *Eukaryotic Cell*, 2, 1200-1210.
- Riquelme, M. & Bartnicki-Garcia, S. 2004. Key differences between lateral and apical branching in hyphae of *Neurospora crassa*. *Fungal Genetics and Biology*, 41, 842-851.
- Rispail, N., Soanes, D. M., Ant, C., Czajkowski, R., Grünler, A., Huguet, R., Perez-Nadales, E., Poli, A., Sartorel, E. & Valiante, V. 2009. Comparative genomics of MAP kinase and calcium-calcineurin signalling components in plant and human pathogenic fungi. *Fungal Genetics and Biology*, 46, 287-298.

- Robinow, C. 1963. Observations on cell growth, mitosis, and division in the fungus *Basidiobolus ranarum*. *The Journal of cell biology*, 17, 123-152.
- Rodicio, R. & Heinisch, J. J. 2010. Together we are strong—cell wall integrity sensors in yeasts. *Yeast*, 27, 531-540.
- Rodríguez, A. A., Grunberg, K. A. & Taleisnik, E. L. 2002. Reactive oxygen species in the elongation zone of maize leaves are necessary for leaf extension. *Plant Physiology*, 129, 1627-1632.
- Rosenberger, R. F. & Kessel, M. 1967. Synchrony of Nuclear Replication in Individual Hyphae of *Aspergillus nidulans*. *Journal of Bacteriology*, 94, 1464-1469.
- Rudolph, H. K., Antebi, A., Fink, G. R., Buckley, C. M., Dorman, T. E., Levitre, J., Davidow, L. S., Mao, J.-I. & Moir, D. T. 1989. The yeast secretory pathway is perturbed by mutations in PMR1, a member of a Ca²⁺ ATPase family. *Cell*, 58, 133-145.
- Rupeš, I. 2002. Checking cell size in yeast. *Trends in Genetics*, 18, 479-485.
- Sanders, W. B. 2001. Lichens: The Interface between Mycology and Plant Morphology Whereas most other fungi live as an absorptive mycelium inside their food substrate, the lichen fungi construct a plant-like body within which photosynthetic algal symbionts are cultivated. *Bioscience*, 51, 1025-1035.
- Sanders, W. B. & Ascaso, C. 1995. Reiterative Production and Deformation of Cell Walls in Expanding Thallus Nets of the Lichen *Ramalina menziesii* (Lecanorales, Ascomycetes). *American journal of botany*, 1358-1366.
- Schardl, C., Scott, B., Young, C., Aiken, G., McCulley, R. & Strickland, J. Recommendations for gene nomenclature for Epichloë species and related Clavicipitaceae. Epichloae, endophytes of cool season grasses: implications, utilization and biology. Proceedings of the 7th International Symposium on Fungal Endophytes of Grasses, Lexington, Kentucky, USA, 28 June to 1 July 2010., 2012. Samuel Roberts Noble Foundation, 84-87.
- Schardl, C. L., Grossman, R. B., Nagabhyru, P., Faulkner, J. R. & Mallik, U. P. 2007. Loline alkaloids: Currencies of mutualism. *Phytochemistry*, 68, 980-996.
- Schardl, C. L., Leuchtman, A. & Spiering, M. J. 2004. Symbioses of grasses with seedborne fungal endophytes. *Annu. Rev. Plant Biol.*, 55, 315-340.
- Schardl, C. L. & Phillips, T. D. 1997. Protective grass endophytes: where are they from and where are they going? *Plant Disease*, 81, 430-438.
- Schardl, C. L., Young, C. A., Hesse, U., Amyotte, S. G., Andreeva, K., Calie, P. J., Fleetwood, D. J., Haws, D. C., Moore, N., Oeser, B., Panaccione, D. G., Schweri, K. K., Voisey, C. R., Farman, M. L., Jaromczyk, J. W., Roe, B. A., O'sullivan, D. M., Scott, B., Tudzynski, P., An, Z., Arnaoudova, E. G., Bullock, C. T., Charlton, N. D., Chen, L., Cox, M., Dinkins, R. D., Florea, S., Glenn, A. E., Gordon, A., Güldener, U., Harris, D. R., Hollin, W., Jaromczyk, J., Johnson, R. D., Khan, A. K., Leistner, E., Leuchtman, A., Li, C., Liu, J., Liu, J., Liu, M., Mace, W., Machado, C., Nagabhyru, P., Pan, J., Schmid, J., Sugawara, K., Steiner, U., Takach, J. E., Tanaka, E., Webb, J. S., Wilson, E. V., Wiseman, J. L., Yoshida, R. & Zeng, Z. 2013. Plant-Symbiotic Fungi as Chemical Engineers: Multi-Genome Analysis of the Clavicipitaceae Reveals Dynamics of Alkaloid Loci. *PLoS Genet*, 9, e1003323.
- Schäufele, R. & Schnyder, H. 2000. Cell growth analysis during steady and non-steady growth in leaves of perennial ryegrass (*Lolium perenne* L.) subject to defoliation. *Plant, Cell & Environment*, 23, 185-194.

- Schmid, J., Spiering, M. J. & Christensen, M. J. 2000. Metabolic activity, distribution, and propagation of grass endophytes in planta: investigations using the GUS reporter gene system. *Microbial Endophytes*, 295-322.
- Schnyder, H., Seo, S., Rademacher, I. F. & Kühbauch, W. 1990. Spatial distribution of growth rates and of epidermal cell lengths in the elongation zone during leaf development in *Lolium perenne* L. *Planta*, 181, 423-431.
- Schuchardt, I., Abmann, D., Thines, E., Schuberth, C. & Steinberg, G. 2005. Myosin-V, Kinesin-1, and Kinesin-3 Cooperate in Hyphal Growth of the Fungus *Ustilago maydis*. *Molecular Biology of the Cell*, 16, 5191-5201.
- Schweikert, C., Liskay, A. & Schopfer, P. 2000. Scission of polysaccharides by peroxidase-generated hydroxyl radicals. *Phytochemistry*, 53, 565-570.
- Scott, B., Becker, Y., Becker, M. & Cartwright, G. 2012. Morphogenesis, Growth, and Development of the Grass Symbiont *Epichloe festucae*. *Morphogenesis and Pathogenicity in Fungi*. Springer.
- Scott, B. & Schardl, C. 1993. Fungal symbionts of grasses: evolutionary insights and agricultural potential. *Trends in microbiology*, 1, 196-200.
- Sharpless, K. E. & Harris, S. D. 2002. Functional Characterization and Localization of the *Aspergillus nidulans* Formin SEPA. *Molecular Biology of the Cell*, 13, 469-479.
- Sietsma, J. & Wessels, J. 2006. Apical wall biogenesis. *Growth, Differentiation and Sexuality*. Springer, 53-72
- Silverman-Gavrila, L. B. & Lew, R. R. 2002. An IP₃-activated Ca²⁺ channel regulates fungal tip growth. *Journal of Cell Science*, 115, 5013-5025.
- Silverman-Gavrila, L. B. & Lew, R. R. 2003. Calcium gradient dependence of *Neurospora crassa* hyphal growth. *Microbiology*, 149, 2475-2485.
- Smith, S. E., Csank, C., Reyes, G., Ghannoum, M. A. & Berlin, V. 2002. *Candida albicans* RHO1 is required for cell viability in vitro and in vivo. *FEMS yeast research*, 2, 103-111.
- Sonnhammer, E. L., Von Heijne, G. & Krogh, A. A hidden Markov model for predicting transmembrane helices in protein sequences. *Ismb*, 1998. 175-182.
- Steinberg, G. 2007. Hyphal Growth: a Tale of Motors, Lipids, and the Spitzenkörper. *Eukaryotic Cell*, 6, 351-360.
- Stephenson, N. & Gooday, G. 1984. Nuclear numbers in the stipe cells of *Coprinus cinereus*. *Transactions of the British Mycological Society*, 82, 531-534.
- Straede, A. & Heinisch, J. J. 2007. Functional analyses of the extra-and intracellular domains of the yeast cell wall integrity sensors Mid2 and Wsc1. *FEBS letters*, 581, 4495-4500.
- Sung, G.-H., Hywel-Jones, N. L., Sung, J.-M., Luangsa-Ard, J. J., Shrestha, B. & Spatafora, J. W. 2007. Phylogenetic classification of *Cordyceps* and the clavicipitaceous fungi. *Studies in mycology*, 57, 5-59.
- Takemoto, D., Kamakura, S., Saikia, S., Becker, Y., Wrenn, R., Tanaka, A., Sumimoto, H. & Scott, B. 2011. Polarity proteins Bem1 and Cdc24 are components of the filamentous fungal NADPH oxidase complex. *Proceedings of the National Academy of Sciences*, 108, 2861-2866.
- Takemoto, D., Tanaka, A. & Scott, B. 2006. A p67Phox-like regulator is recruited to control hyphal branching in a fungal-grass mutualistic symbiosis. *The Plant Cell Online*, 18, 2807-2821.
- Tan, Y. Y., Spiering, M. J., Scott, V., Lane, G. A., Christensen, M. J. & Schmid, J. 2001. In *Planta Regulation of Extension of an Endophytic Fungus and*

- Maintenance of High Metabolic Rates in Its Mycelium in the Absence of Apical Extension. *Applied and Environmental Microbiology*, 67, 5377-5383.
- Tanaka, A., Cartwright, G. M., Saikia, S., Kayano, Y., Takemoto, D., Kato, M., Tsuge, T. & Scott, B. 2013. ProA, a transcriptional regulator of fungal fruiting body development, regulates leaf hyphal network development in the *Epichloë festucae*–*Lolium perenne* symbiosis. *Molecular microbiology*, 90, 551-568.
- Tanaka, A., Christensen, M. J., Takemoto, D., Park, P. & Scott, B. 2006. Reactive Oxygen Species Play a Role in Regulating a Fungus–Perennial Ryegrass Mutualistic Interaction. *The Plant Cell Online*, 18, 1052-1066.
- Tanaka, A., Takemoto, D., Hyon, G. S., Park, P. & Scott, B. 2008. NoxA activation by the small GTPase RacA is required to maintain a mutualistic symbiotic association between *Epichloë festucae* and perennial ryegrass. *Molecular microbiology*, 68, 1165-1178.
- Tanaka, A., Tapper, B. A., Popay, A., Parker, E. J. & Scott, B. 2005. A symbiosis expressed non-ribosomal peptide synthetase from a mutualistic fungal endophyte of perennial ryegrass confers protection to the symbiotum from insect herbivory. *Molecular Microbiology*, 57, 1036-1050.
- Tian, L., Hires, S. A., Mao, T., Huber, D., Chiappe, M. E., Chalasani, S. H., Petreanu, L., Akerboom, J., McKinney, S. A., Schreier, E. R., Bargmann, C. I., Jayaraman, V., Svoboda, K. & Looger, L. L. 2009. Imaging neural activity in worms, flies and mice with improved GCaMP calcium indicators. *Nat Meth*, 6, 875-881.
- Torralba, S. & Heath, I. B. 2001. Cytoskeletal and Ca²⁺ regulation of hyphal tip growth and initiation. *Current Topics in Developmental Biology*. Academic Press, 135-187.
- Trinci, A. & Morris, N. 1979. Morphology and growth of a temperature-sensitive mutant of *Aspergillus nidulans* which forms aseptate mycelia at non-permissive temperatures. *Journal of General Microbiology*, 114, 53-59.
- Valiante, V., Jain, R., Heinekamp, T. & Brakhage, A. A. 2009. The MpkA MAP kinase module regulates cell wall integrity signaling and pyomelanin formation in *Aspergillus fumigatus*. *Fungal Genetics and Biology*, 46, 909-918.
- Valkonen, M., Kalkman, E. R., Saloheimo, M., Penttilä, M., Read, N. D. & Duncan, R. R. 2007. Spatially Segregated SNARE Protein Interactions in Living Fungal Cells. *Journal of Biological Chemistry*, 282, 22775-22785.
- Vanden, W. A., Cullen, D., Spear, R., Schoenike, B. & Andrews, J. 1997. Expression of green fluorescent protein in *Aureobasidium pullulans* and quantification of the fungus on leaf surfaces. *Biotechniques*, 23, 686-690.
- Vay, H. A., Philip, B. & Levin, D. E. 2004. Mutational analysis of the cytoplasmic domain of the Wsc1 cell wall stress sensor. *Microbiology*, 150, 3281-3288.
- Vermeulen, C. & Wessels, J. 1984. Ultrastructural differences between wall apices of growing and non-growing hyphae of *Schizophyllum commune*. *Protoplasma*, 120, 123-131.
- Verna, J., Lodder, A., Lee, K., Vagts, A. & Ballester, R. 1997. A family of genes required for maintenance of cell wall integrity and for the stress response in *Saccharomyces cerevisiae*. *Proceedings of the National Academy of Sciences*, 94, 13804-13809.
- Veses, V., Richards, A. & Gow, N. A. 2009. Vacuole inheritance regulates cell size and branching frequency of *Candida albicans* hyphae. *Molecular microbiology*, 71, 505-519.

- Viladevall, L., Serrano, R., Ruiz, A., Domenech, G., Giraldo, J., Barceló, A. & Ariño, J. 2004. Characterization of the calcium-mediated response to alkaline stress in *Saccharomyces cerevisiae*. *Journal of Biological Chemistry*, 279, 43614-43624.
- Voisey, C. R. 2010. Intercalary growth in hyphae of filamentous fungi. *Fungal Biology Reviews*, 24, 123-131.
- Vollmer, S. J. & Yanofsky, C. 1986. Efficient cloning of genes of *Neurospora crassa*. *Proceedings of the National Academy of Sciences*, 83, 4869-4873.
- Walker, L. A., Gow, N. a. R. & Munro, C. A. 2013. Elevated Chitin Content Reduces the Susceptibility of *Candida* Species to Caspofungin. *Antimicrobial Agents and Chemotherapy*, 57, 146-154.
- Wang, S., Cao, J., Liu, X., Hu, H., Shi, J., Zhang, S., Keller, N. P. & Lu, L. 2012. Putative Calcium Channels CchA and MidA Play the Important Roles in Conidiation, Hyphal Polarity and Cell Wall Components in *Aspergillus nidulans*. *PLoS ONE*, 7, e46564.
- Ward, H. M. & Marshall-Ward, H. 1888. A lily-disease. *Annals of Botany*, 319-382.
- Watanabe, Y., Irie, K. & Matsumoto, K. 1995. Yeast RLM1 encodes a serum response factor-like protein that may function downstream of the Mpk1 (Slf2) mitogen-activated protein kinase pathway. *Molecular and Cellular Biology*, 15, 5740-5749.
- Watts, H., Veacute, A.-A., Perera, T., Davies, J. & Gow, N. 1998. Thigmotropism and stretch-activated channels in the pathogenic fungus *Candida albicans*. *Microbiology*, 144, 689-695.
- Wessels, J. 1986. Cell wall synthesis in apical hyphal growth. *Int. Rev. Cytol*, 104, 37-79.
- White Jr, J. F., Reddy, P. V. & Bacon, C. W. 2000. Biotrophic endophytes of grasses: a systematic appraisal. *Microbial endophytes*. New York: Marcel Dekker, Inc. p, 49-62.
- Wilkinson, H. H., Siegel, M. R., Blankenship, J. D., Mallory, A. C., Bush, L. P. & Schardl, C. L. 2000. Contribution of Fungal Loline Alkaloids to Protection from Aphids in a Grass-Endophyte Mutualism. *Molecular Plant-Microbe Interactions*, 13, 1027-1033.
- Wolkow, T. D., Harris, S. D. & Hamer, J. E. 1996. Cytokinesis in *Aspergillus nidulans* is controlled by cell size, nuclear positioning and mitosis. *J Cell Sci*, 109 (Pt 8), 2179-88.
- Wösten, H. a. B., Moukha, S. M., Sietsma, J. H. & Wessels, J. G. H. 1991. Localization of growth and secretion of proteins in *Aspergillus niger*. *Journal of General Microbiology*, 137, 2017-2023.
- Yafetto, L., Davis, D. J. & Money, N. P. 2009. Biomechanics of invasive growth by *Armillaria rhizomorphs*. *Fungal Genetics and Biology*, 46, 688-694.
- Yoshimoto, H., Saltsman, K., Gasch, A. P., Li, H. X., Ogawa, N., Botstein, D., Brown, P. O. & Cyert, M. S. 2002. Genome-wide analysis of gene expression regulated by the calcineurin/Crz1p signaling pathway in *Saccharomyces cerevisiae*. *Journal of Biological Chemistry*, 277, 31079-31088.
- Yoshimura, H., Tada, T. & Iida, H. 2004. Subcellular localization and oligomeric structure of the yeast putative stretch-activated Ca²⁺ channel component Mid1. *Experimental Cell Research*, 293, 185-195.
- Youatt, J. 1986. Oxygen and morphological changes in *Allomyces macrogynus*. *Australian Journal of Biological Sciences*, 39, 233-240.
- Youatt, J., Gow, N. & Gooday, G. 1988. Bioelectric and biosynthetic aspects of cell polarity in *Allomyces macrogynus*. *Protoplasma*, 146, 118-126.

- Young, C., Bryant, M., Christensen, M., Tapper, B., Bryan, G. & Scott, B. 2005. Molecular cloning and genetic analysis of a symbiosis-expressed gene cluster for lolitrem biosynthesis from a mutualistic endophyte of perennial ryegrass. *Molecular Genetics and Genomics*, 274, 13-29.
- Young, C., Itoh, Y., Johnson, R., Garthwaite, I., Miles, C. O., Munday-Finch, S. C. & Scott, B. 1998. Paxilline-negative mutants of *Penicillium paxilli* generated by heterologous and homologous plasmid integration. *Curr Genet*, 33, 368-77.
- Yu, Q., Wang, H., Cheng, X., Xu, N., Ding, X., Xing, L. & Li, M. 2012. Roles of Cch1 and Mid1 in Morphogenesis, Oxidative Stress Response and Virulence in *Candida albicans*. *Mycopathologia*, 174, 359-369.
- Zdobnov, E. M. & Apweiler, R. 2001. InterProScan--an integration platform for the signature-recognition methods in InterPro. *Bioinformatics (Oxford, England)*, 17, 847-848.
- Zelter, A., Bencina, M., Bowman, B. J., Yarden, O. & Read, N. D. 2004. A comparative genomic analysis of the calcium signaling machinery in *Neurospora crassa*, *Magnaporthe grisea*, and *Saccharomyces cerevisiae*. *Fungal Genetics and Biology*, 41, 827-841.
- Zheng, Y., Bender, A. & Cerione, R. A. 1995. Interactions among Proteins Involved in Bud-site Selection and Bud-site Assembly in *Saccharomyces cerevisiae*. *Journal of Biological Chemistry*, 270, 626-630.
- Zu, T., Verna, J. & Ballester, R. 2001. Mutations in WSC genes for putative stress receptors result in sensitivity to multiple stress conditions and impairment of Rlm1-dependent gene expression in *Saccharomyces cerevisiae*. *Molecular Genetics and Genomics*, 266, 142-155.

8. Appendices

8.1 Appendix 1: Buffers used in this study

TAE buffer

Stock solution (50x)

Tris base	242.0 g
Glacial acetic acid	57.1 mL
EDTA (pH 8.0)	100.0 mL from 0.5 M stock
Total	<u>1000 mL</u>

Working solution (1x) - Dilute stock solution 50:1

TE buffer pH 8.0

Stock solution (10x)

Tris-HCl pH 7.5	100 mL from 1 M stock
EDTA pH 8.0	20 mL from 500 mM stock
Total	<u>1000 mL</u>

Working solution (1x) - Dilute stock solution 10:1

Loading dye

Stock solution (6x)

Bromophenol blue	25 mg
Xylene cyanol FF	25 mg
Glycerol	3.3 mL
H ₂ O	<u>6.7 mL</u>
Total	10.0 MI

OM buffer

MgSO ₄ ·7H ₂ O (1.2 M)	88.8 g
Na ₂ HPO ₄ (10 mM)	<u>30.0 mL from 1M stock</u>
Total	300 mL

Add 100 mL of sterile water to dissolve the MgSO₄ and heat if necessary. Add a few drops of 100 mM NaH₂PO₄·H₂O until the pH reaches 5.8 (1.56 g/100 mL). Top up to final volume (pH raises to ~6.3). Filter sterilized.

ST buffer

Sorbitol (0.6 M)	10.93 g
Tris-HCl (100 mM), pH 8.0	<u>10.0 mL from 1 M stock</u>
Total	100 mL

STC buffer

Sorbitol (1 M)	72.8 g
Tris-HCl (50 mM) pH 8.0	20.0 mL of 1M stock
CaCl ₂ ·6H ₂ O	<u>4.38 g</u>
Total	400 mL

2x SSC, 0.1% (w/v) SDS

NaCl (3 M)	175.3 g
Na ₃ C ₆ H ₅ O ₇ ·2H ₂ O (300 mM)	<u>88.2 g</u>
Total	1000 mL (with deionized water), Adjust the pH to 7.0, add SDS 0.1% (w/v).

8.2 Appendix 2: PCR and restriction enzyme reaction mixtures and conditions

BigDye® Terminator v3.1 cycle sequencing reaction mix

ABI buffer	1.75 μ L
Primer (2 μ M)	0.80 μ L
3.1 Big Dye	0.50 μ L
PCR product/Plasmid	1.00 μ L
Deionized water	5.95 μ L
Total volume	<u>10.00 μL</u>

Cycle sequencing conditions for BigDye® Terminator v3.1

95°C	2 min X 1	
95°C	30 sec	} X 30
53.5-54°C	30 sec	
72 °C	32 sec	
72 °C	7 min X 1	

Restriction digestion of genomic DNA for southern blot

Buffer (10X)	10 μ L
Genomic DNA (140 ng/ μ L)	30 μ L
RE enzyme (10 U/ μ L)	6 μ L (added in two steps)
Deionized water	54 μ L
Total	<u>100 μL</u>

Digested overnight at 37°C

8.3 Appendix 3: Plasmid vector physical maps

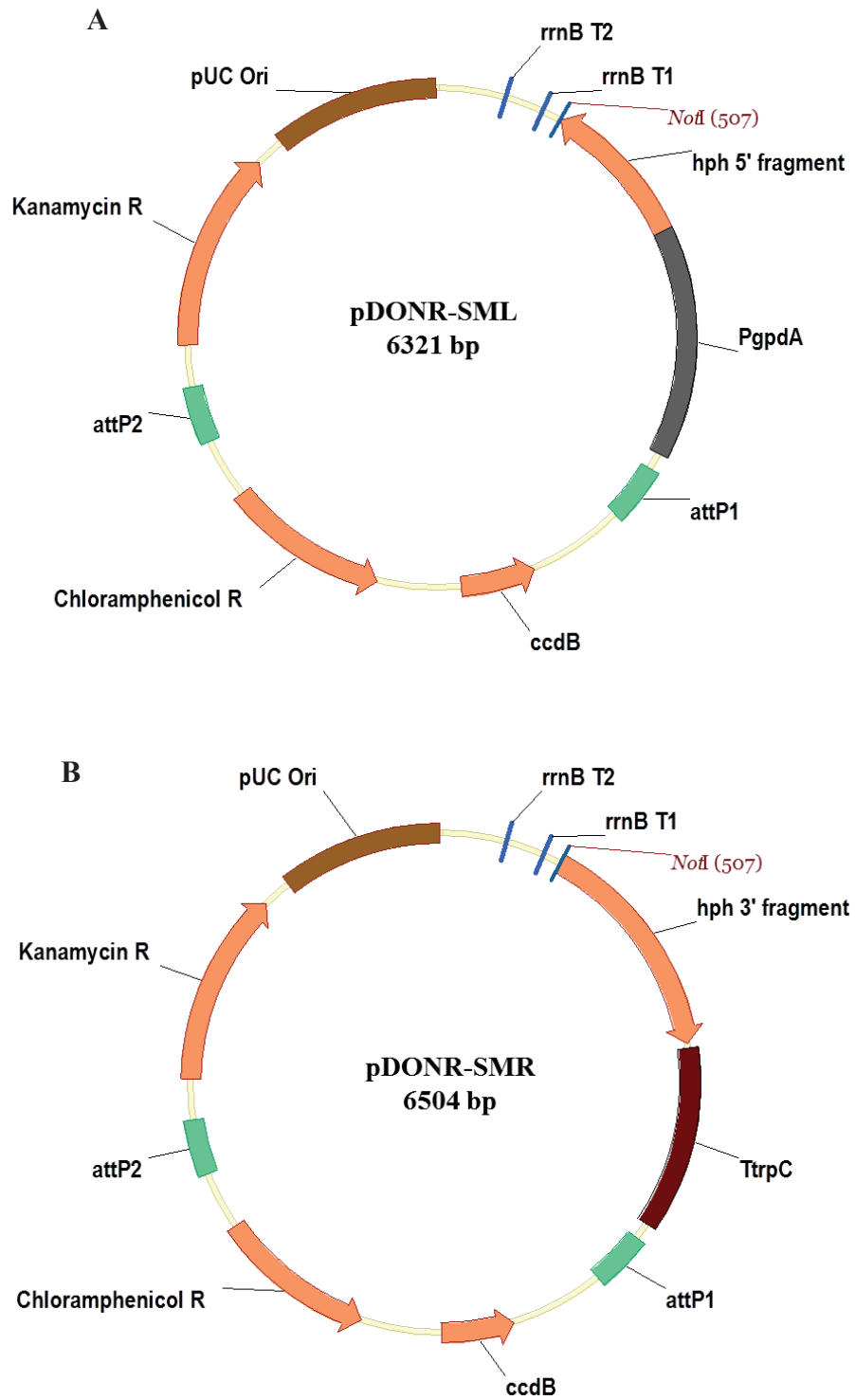


Figure 8.1: Donor vectors pDONR-SML (A) and pDONR-SMR (B) (Invitrogen™) used to construct gene replacement vectors.

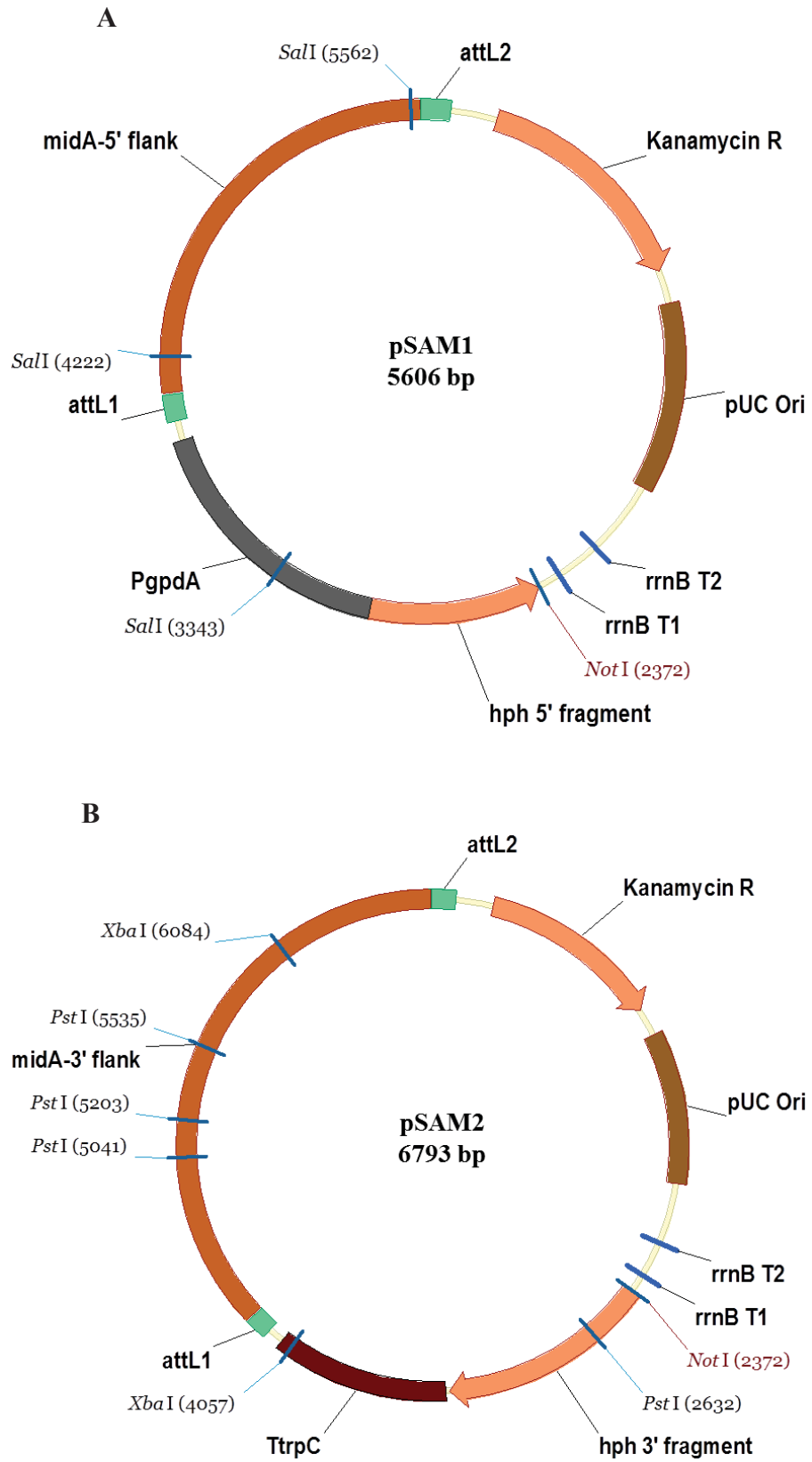


Figure 8.2: Replacement vectors for *midA* harbouring the 5' flank pSAM1 (A) and 3' flank pSAM2 (B).

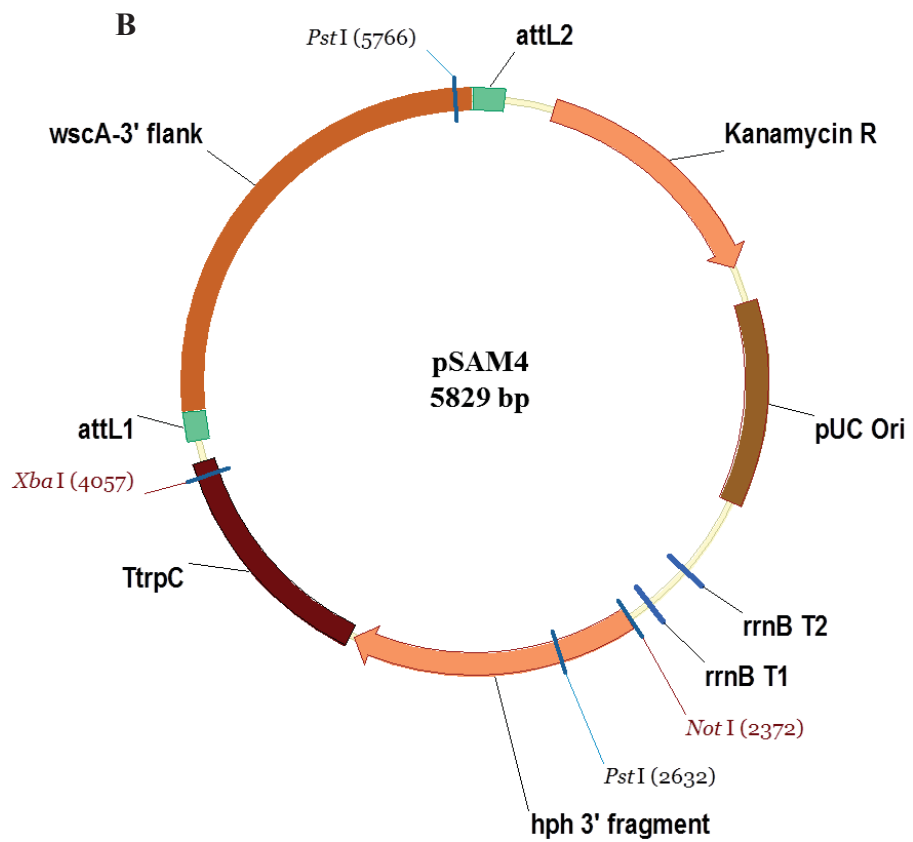
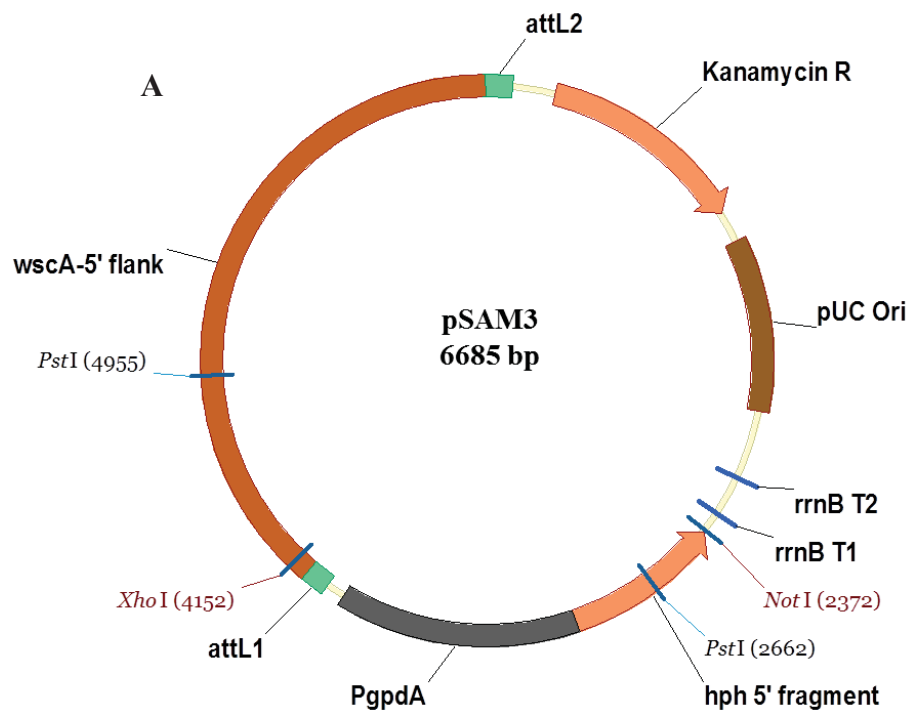


Figure 8.3: Replacement vectors for *wscA* harbouring the 5' flank pSAM3 (A) and 3' flank pSAM4 (B).

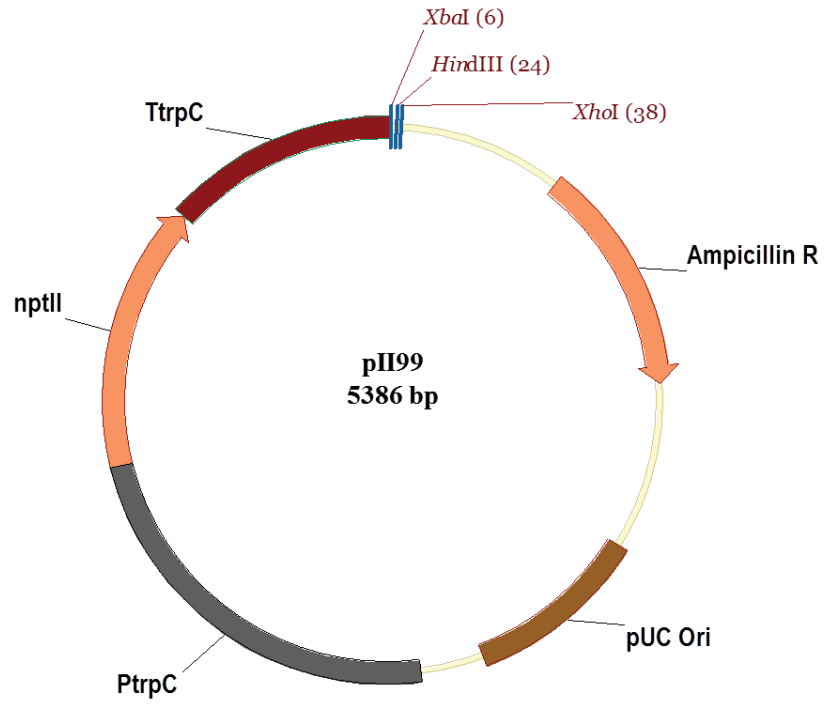


Figure 8.4: Vector pII99 used for complementation vector construction.

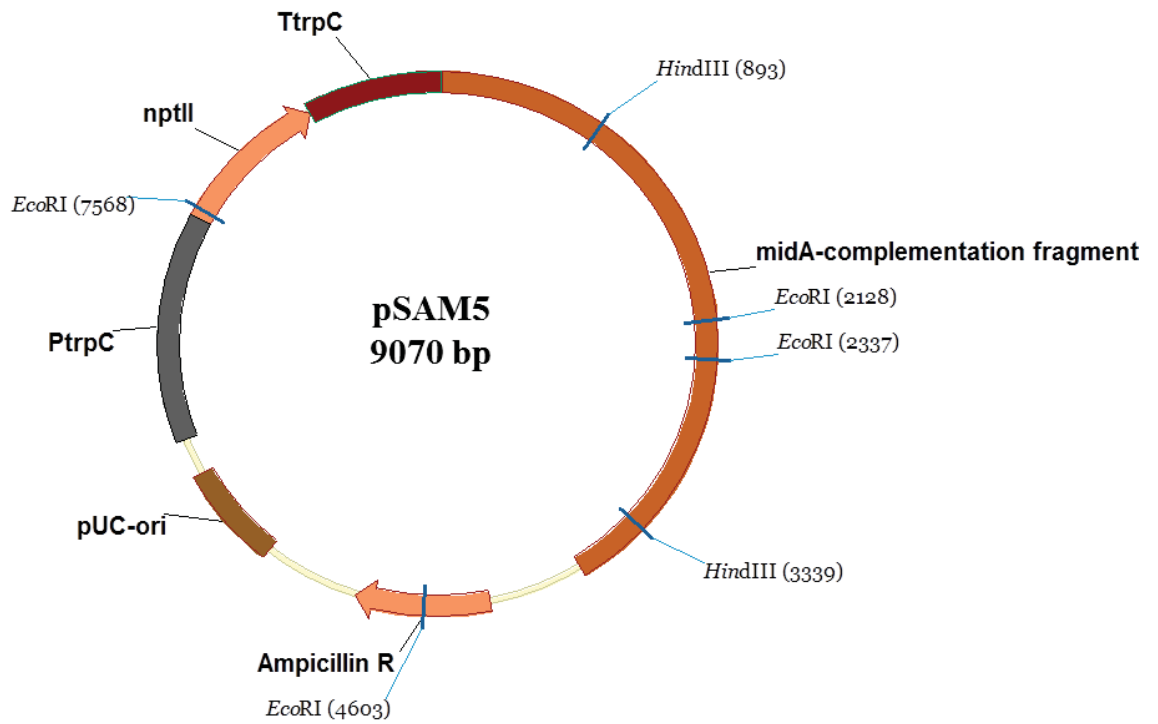


Figure 8.5: Vector pSAM5 for $\Delta midA$ complementation.

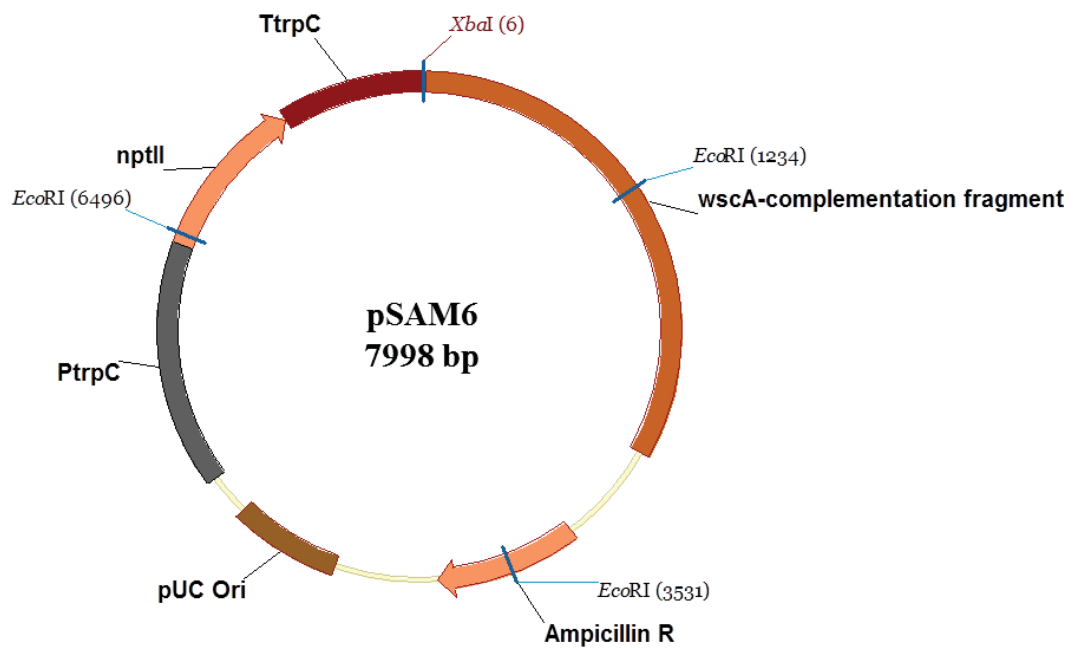


Figure 8.6: Vector pSAM6 for $\Delta wscA$ complementation.

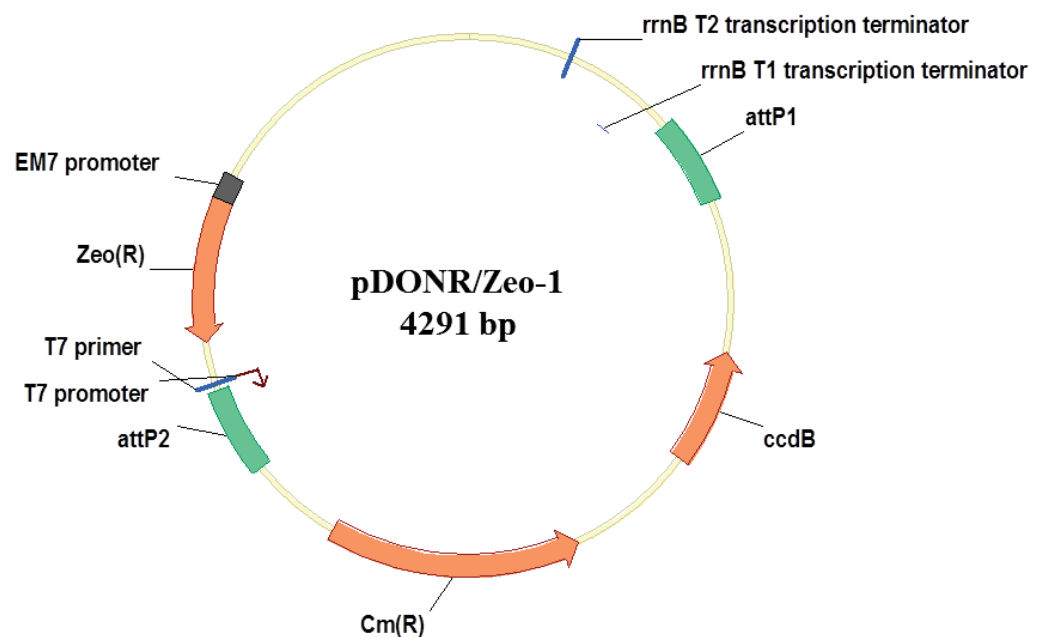


Figure 8.7: Donor vector pDONR/Zeo (Invitrogen™) used for *wscA:egfp* expression vector construction.

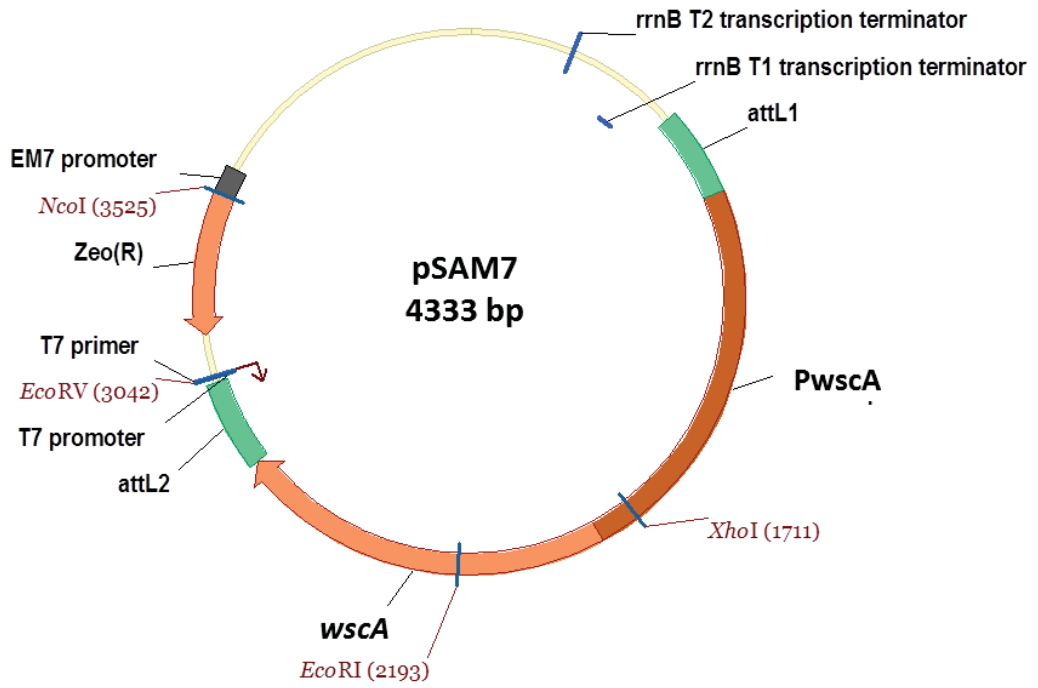


Figure 8.8: Entry vector pSAM7 harbouring *wscA* with native promoter.

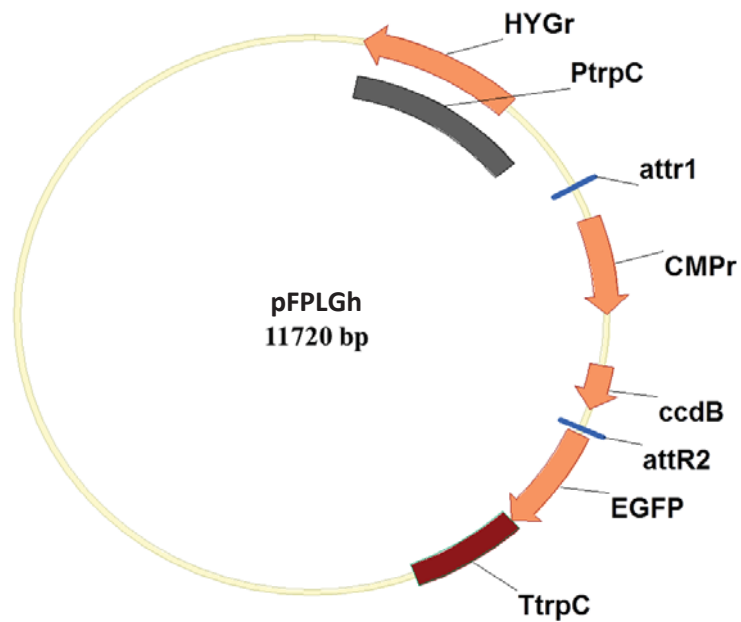


Figure 8.9: Destination vector pFPLGh used for *wscA:egfp* expression vector construction.

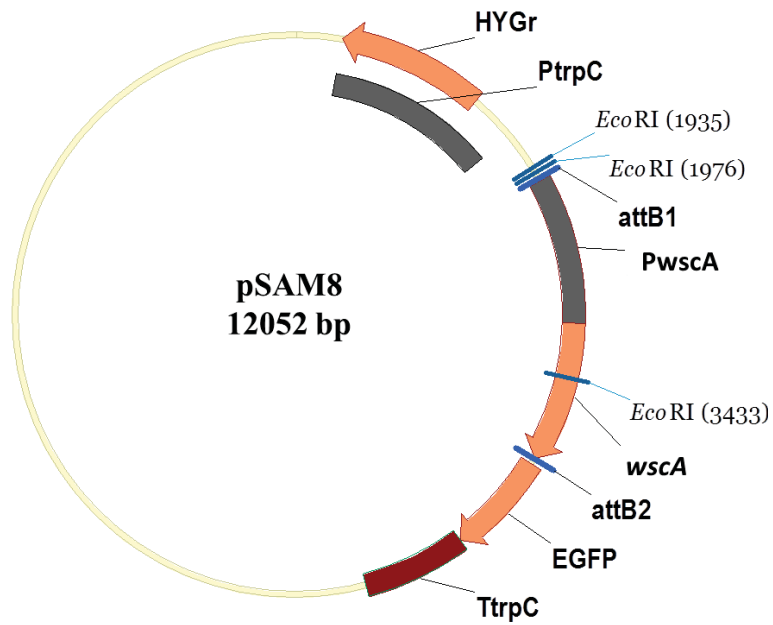


Figure 8.10: Expression vector pSAM8 with *wscA:egfp*.

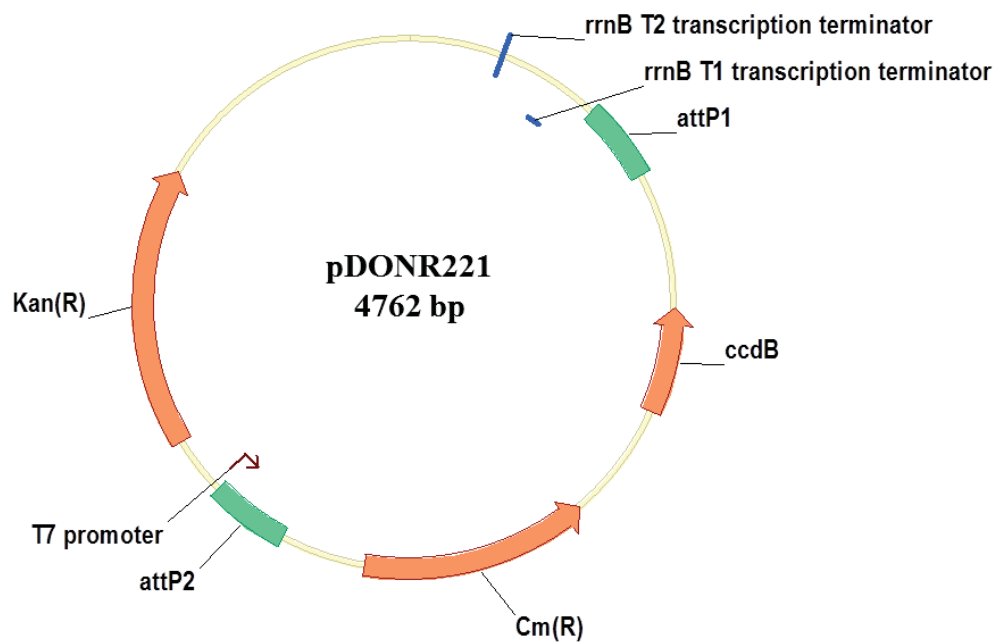


Figure 8.11: Donor vector pDONR221 used for *Ptef:wscA:egfp* expression vector construction.

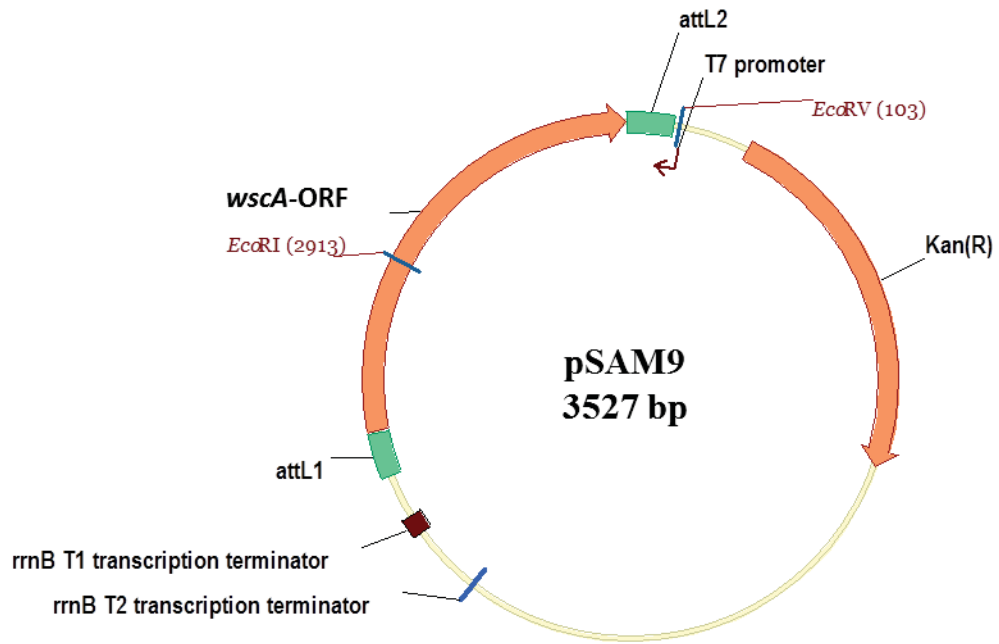


Figure 8.12: Entry vector pSAM7 harbouring *wscA*.

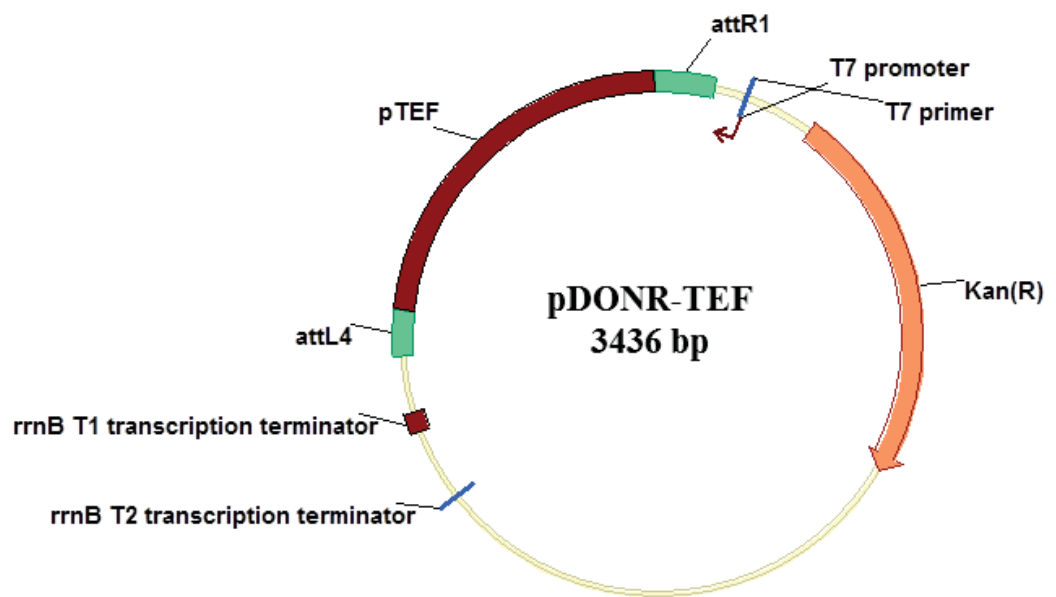


Figure 8.13: Entry vector pDONR-TEF harbouring *tef2* promoter.

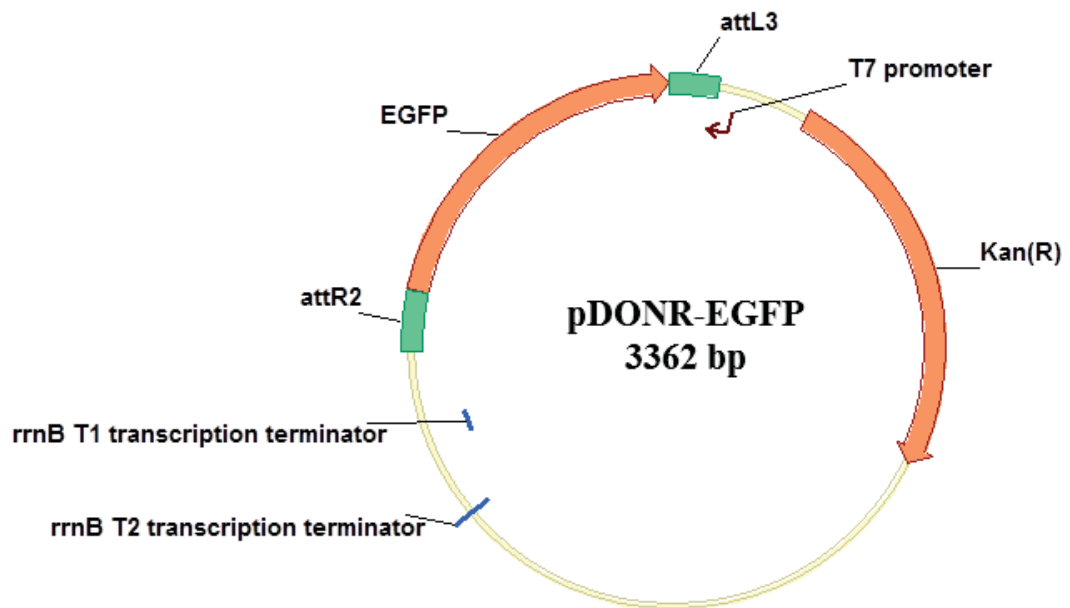


Figure 8.14: Entry vector pDONR-EGFP harbouring *egfp*.

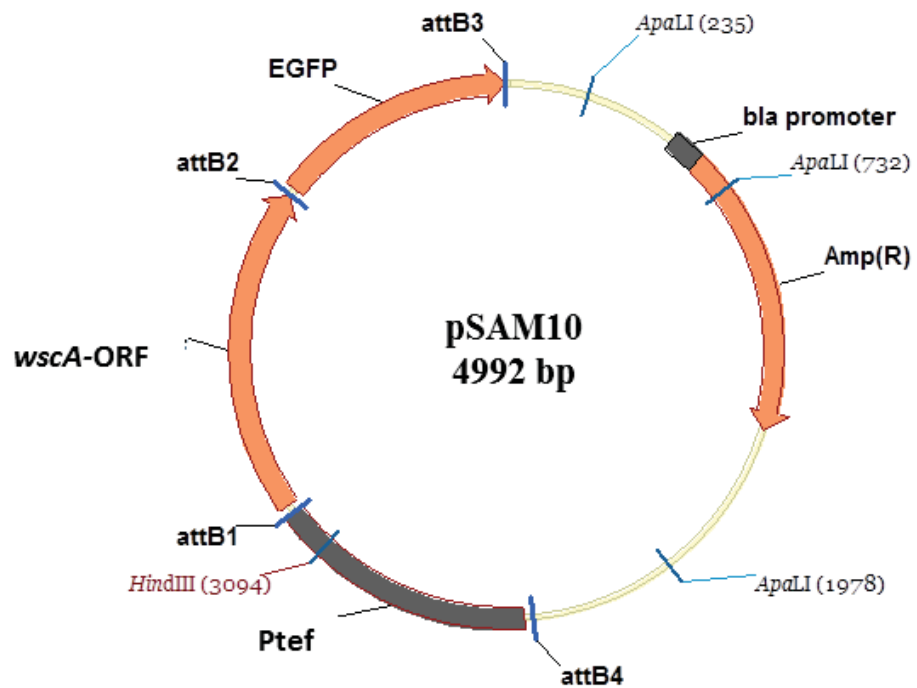


Figure 8.15: Expression vector pSAM10 harbouring *Ptef:wscA:egfp*.

Appendix 4: MidA and WscA protein sequences

E. festucae MidA protein sequence

> **MidA, *E. festucae*, fgenesh_masked-contig_726-abinit-gene-0.103(computed protein)**
MQLSPLQSRLVASLAATFCLLVLFSLLLVPKGAVAHEFLHESFLTSSSTRPDLASFEEDGHSPDS
QISSYEPILNFLGRSILGRAGDTIPLNDKPLAFNIQPGGAPICYIHKKSLGNSTSQGKQVQPRQ
TDDDNERTGQEVKNATIYISANTCLQPIVQSGGKRSKPPQLILFLSNGTEAGCPQVTSNPKG
HLARGFTSHTFEEGAVRVSANATSDIYIGLYAPNITDSFEGSYDYQVAASSTEYFHQYQSNET
EGAKLLWMSDSTAALLITRNLTEASEARRIWSEDPPYQLYVSGQDWPMLDGLHHSACGL
ERNALVGANKEGTAKNNGMVKTSMTLRGPGGMPKQQFYVGLNATTSYSGVVLVQPANVT
VNSKRQANGGGQSLRKPGSVVFQGTTFQTNAAPNCKVVTDLEFCDEIQYAVPGNDGKFNNT
ELAKVYDKQAKTVYDNFLKVMQQIQCEADRTSKYSLARTCEDCKRAYKRWLCTVSFPRCE
DFLDGSRFSVLRNVNQAFPNGTLLPTEIRQELAKVPAQNASRNSFIDETIQPGPYKEIMPCEDIC
YQVVQSCPAMIKFNCPPQPGMYGFNVTYGRRNADNTVVSCNFPGEARTRTSAGHDTIPNLAL
LTCIMSVFSILVMAR

E. festucae WscA protein sequence

> **WscA, *E. festucae*, maker-contig_1037-snap-gene-0.47(computed protein)**
MRLSTIAFGAIMAATGVHAQTPKPKQPALQIPVDGISTSSGCYGSYGNMTMHKPISADKMST
AACNNACKADGFWLAAMHGGQCLCGYALPPKKDLVEDSECNQPCPAYPPEACGGIDSYSIY
NVTGIQLQINRYEPSSSSTTGGSKTSAASPTPTDTSSTNTGGNNNNNHSNNNNNHSNNNNGGG
GGTTVTQTSVPTETPKPEKSGPNVAGIAAGVVVGVFAAAAAIAGVFFYVRRKRNSEIEEEHRR
NAAVNAFISGSKPSSSHGSISMTDSRLDPVMAHRRMSDGSADNEDYSRRILRVNTA

Appendix 5: Multiple sequence alignments for MidA and WscA proteins with the respective orthologues of *S. cerevisiae*.

```

E. festucae      MQLSPLQSR LVASLAATFCLLVLFSLLLL PKGAVAHEFLHES--FLTSS-TRPDLASFEE 57
C. purpurea     MQLSPLQSR LAAASLAATVCLFLLYLLLL LAPQGA VAFELPLDS--LSRSSSSWTDLASIEG 58
G. zeae         MLPN ASISRLPISRKY I LTLVLSLFLCAF GNAHAS ELLHDS--IFDAE-----THIER 52
N. crassa       MHLGPLHLRFAASFIALSLLVVF NITL FSLDCALAAELEDAPPILLDDVDSDLDVDSQGS 60
S. cerevisiae   -----MIVWQALFVVYCLF TTSIHGLFQDFN PFA----- 29
                .       . . . :       .       .       .       .       .       .

E. festucae      DGHSPDSQISSYEPILNFLGRS ILGRA--GDTI PLENDKPLAFNIQPGGAPIC YIIKKGS 115
C. purpurea     N-DDLGSHTPFYEPILNFLGRS ILGRA--GDTI PLGDEAPLAFNLQPGNAPIC YIIKKGS 115
G. zeae         S----DASNL IYEPDFGAFDRS ILGRAP-AEQSLL TNNGPDSRKLSPG-ATVCYVVDKKT 106
N. crassa       VSDLGSPLDQMYEPEFAAFDRS I IGRDQVRD TNALINNEAFQLNVRQGDTERFVFKLSQL 120
S. cerevisiae   ----NKNISLKYPSLNRWEKNVMATG---QQT I INSDSIYEWTPILS----- 69
                .       *       :       . . . .       :       .       .       .

E. festucae      -----LGN STSQGKQVQPRQTDD DNN----- 136
C. purpurea     -----LGN STDPASRKRDDDDDDDDDPDDT----- 140
G. zeae         L-----FGKDKRDDDGHEPRNAEDDPG----- 128
N. crassa       SERELEVVQLELRDEEHTWEDI DEDEDEDEAEDEK DENNDL SGKGLDRDSDVLNLASA 180
S. cerevisiae   -----NITAGKKDSFVFTIDAEASG----- 89
                .       .       .       .       .

E. festucae      --ERTGQEVKNATIYISANTCLOPIVQSGGKRS-----KPPQLILFLS NGT--EAGC 184
C. purpurea     -ADASVYEGM N TTTYISANTCLOPKIRPKGN DTDKSN KSGPKPPQ LIMFLSN GTDKDVGC 199
G. zeae         --HQNFRAESKTVYISVNTCSRPTMKSKDKDNNPE-----TAPQLSLYTSMSM--KIKC 179
N. crassa       KQKLGKRQQGARRLFLSANTCLOPQAF N ATKKTQ-----PPPQLTYVSTST----- 227
S. cerevisiae   ---YGFAPTYEVL MFI SGNICQMPMN RSDVDLTIYYSFN --ETVLENPNIGQSAVFQDGY 144
                . . . * * * *       . . . .       . . . .

E. festucae      PQVTSNPKGHLARGFTSHTFEEGAVRVS-AN ATSDIYIGLYAP NITDSFEGSYDYQVAAS 243
C. purpurea     PRITN STSGEVTQGF TAHNFEEGAVTVSLINATTDVY IGIYAPNIEDDYEGVYNYQVAAS 259
G. zeae         PDSSNYN--KTNSDLKRI PFDEGAAMVT-V N ATDAIYISVAAP NITKKHGDWEYQIAIS 236
N. crassa       -DNVEPGPGADSNSQVSMVFNEGAIMY N -FTTTT DVYVGVHAPNVAEIFDKPYNIKIAIS 285
S. cerevisiae   IQALAI SPVQSSSS N ATSTYSNLVVAELVN STTEQPLSSSD-----ASENWEYRLSIS 198
                .       . . .       . : *       . .       . : : : *

E. festucae      STEYFHQYQSN ETEGAKLLWMSDSTAALLITRN LTTEASE-ARRIWSEDPPYQLYVS-- 300
C. purpurea     STDYFHQYQSN AEDGAELLWMSDSTAALLMTRNL TDDASE-TREVWSEDPPYQLYVS-- 316
G. zeae         FDEYYHNYDS- QNGTARLLLMDTDSTALLVTSNL TEDSSE-TQQIMKRPPYQLFVFG-- 292
N. crassa       TDGYYYSYNV--DDDADLIWVSDSDSQGALLITHNL TDSNDEKEQQRIMNTPPYVMFAQ-- 341
S. cerevisiae   ENDLVFQWDVR---PWVEVLDTDMNSALLSTGNVTADAKVYH NYSIYDPSLYDLVYYSY 254
                . . . :       . :       . : * * * * * * * * * .       . * : : .

E. festucae      GQDWPMLDGLHHSACGLERNALVGANKEGT-----AKNNGMVKTSMTLR----GPGGMP 350
C. purpurea     GQDWPVLDGLRRSACGLENNAPIGSNHGHT-----AKNNEMVRTSMTLR----GPGGLP 366
G. zeae         DEKLRSIDGLRHSACGLKQSAEIWANS NRT-----GRHNDLVTGVTR----GPGQLP 342
N. crassa       DKS N PSINGVRYSF CGLEQNAQIATTKD-----GKYSNMVQTMKTR----GQGNFP 389
S. cerevisiae   EDSVQLNQNY NLSLCAVKNGPYLVSSQNTS N ATVTS N STNPLERTDLAIQKKITEYGGSV314
                . .       . . * * . : : . .       . :       . * : : :       *

E. festucae      KQQFYVVLGNATTSYSGVLVQPAN VTVNSKRQANGGQSLRKP GSVVFQGTTFQTNAAP- 409
C. purpurea     KQQFYVVLGN ATTSYSGMLVLPAN TTVNVKRQDDASG-SSRKRGSIVFEGTTFQTNAAP- 424
G. zeae         KQQFLIAGL NHSSSYLGILVKMP--EGNGKRAETTGG-----GGTVYRATSFETSSSS- 393
N. crassa       KQQFFFSGLPSTSYLGILAKT N VTDTGSPNLVGGGG-----HVFKATNFQTKSDHG 441
S. cerevisiae   TEMFYVTGLNASTTYVAYLTKKLIS---NGDGLSSVGG-----ILFSHVYFTTRSTD- 362
                . : * . * : : : * . * .       . *       . :       . * * :

E. festucae      NCKVVTDFEFCDEIQYAVPGNDG-KFN NTELAKVYDKQAKTVYDNFLKVMQQIQCEADRT 468
C. purpurea     NCKVVTDFEFCDEIQYAVPGNDG-KFN NTELAKTYDKQAKSIYDNFLKVMQQIQCEADRT 483
G. zeae         NCKMVTNLDFCNETQYAVPGNDK-KFN N TALAKHYDDYARKMYANFEKVMQMPCETTFPE 452
N. crassa       NCNIVLN LTFCDQVAYSVPSNPN-FGNASVLAKFYDDYAAEAWGYFKKALAQVACEAPVT 500
S. cerevisiae   AC SLIFGLDFCSDVAYSVPTSSFSVGN KTLMAQTYDHI AEALYAN FSKALQLISCDADK D 422
                * . : : * * * . : * * * .       * : : : * * * *       . : * * . : : * :

```

```

E. festucae      SKYSLARTCEDCKRAYKRWLCTVSFPRCEDFLDGSRFSVLRNVNQAFPNG-----TL 520
C. purpurea     SRYSLARTCEDCKRAYKRWLCTVSLPRCEDFLSGSPFSVVRNVNQAFPNG-----TF 535
G. zeae         SLYSLVRNCDECRAAYKRWLCTVTIPRCEDEVMGSSRFSVVRNAFQAFPNG-----TT 504
N. crassa       QRYSLTRNCSDCEAAAYKDWLCSVTIPRCEDFSNNASYLHPRAMSQFPDPGERLDNATMSL 560
S. cerevisiae   ARYSPVMTCDCCAAYRDWVCAVSIPRCSTTS--SQYYIHR----- 461
                ** . .*.:* **:*:***:***. : : *

E. festucae     LPTEIRQELAKVPAQNASRNSFIDETIQP-GPYKEIMPCEDI CYQVVQSC PAMIKFNC P- 578
C. purpurea     LPTDIRQELAKLPSQNASRNASRIDQTIQP-GPYNELMPCEDI CYQVVQSC PAAIQFKCP- 593
G. zeae        LPDNFRKGLNSS-ANSSRNAWIDETVKP-GPYKELLPQDICYDVVQSC PSAIGFTCP- 561
N. crassa       YAENYGDGKVLGKAFQSRSSRIDEFIKP-GPYKEVLP CDYLCYRLVQSC PSSMGFGCP- 618
S. cerevisiae   -----DKSHNRNDYLNKFIKPLDDYYEILP CIDM CYTLVRNCP SDFQFSCP N 508
                .*. :*: :*: . * *:*:* :** :*:** : : * **

E. festucae     QPGMYGFNVTYGRRNADNTVVS CNFPGEARTRTSAGHDTIPNLALLTCIMSVFSILVMAR 638
C. purpurea     QPGMYGFNMTYGVRVANSTVVS CNFPGEARTPT SAGVTMPGLALVAWVALFLFGLLVVW 653
G. zeae        QPGFPSFDVSYGERNSDTSSITCNYPGEARTKISAARVIRPGTFMLGTVSMMWLVAV--- 618
N. crassa       LPGQKGFNSSYYIKNETNGEVVCNYPGSAHIFSGSSKDAVSVGLTIIVLVLVSLLLAC-- 676
S. cerevisiae   -LTTEDLLYQSYNFYMDTDYSTCN YIGNSSLMVIHPLDDT----- 548
                .: . **:*:

```

Figure 4.1: Multiple sequence alignment between Mid1 of *S. cerevisiae* (AKB00818.1) and orthologues of *E. festucae*, *C. purpurea* (CAU66903.1), *N. crassa* (EAA31782.3) and *G. zeae* (ESU13681). Underline – Signal peptide. Red letters – Conserved cysteine residues. Highlighted red - Conserved cysteine domains shown to be essential in *S. cerevisiae*. Highlighted green – GPI anchor sites. Highlighted blue – potential N-glycosylation sites. Highlighted grey – Transmembrane domains (according to TMpred). The multiple sequence alignment was performed using ClustalW2 from <http://www.ebi.ac.uk>.